brain sciences

MDPI

Article

Effects of Dizocilpine, Midazolam and Their Co-Application on the Trimethyltin (TMT)-Induced Rat Model of Cognitive Deficit

Marketa Chvojkova [1,2,3,*], Hana Kubova [1] and Karel Vales [1,2]

[1] Institute of Physiology of the Czech Academy of Sciences, Videnska 1083, 142 20 Prague 4, Czech Republic; Hana.Kubova@fgu.cas.cz (H.K.); Karel.Vales@nudz.cz (K.V.)
[2] National Institute of Mental Health, Topolova 748, 250 67 Klecany, Czech Republic
[3] 2nd Faculty of Medicine, Charles University, V Uvalu 84, 150 06 Prague 5, Czech Republic
* Correspondence: Marketa.Chvojkova@nudz.cz

Abstract: Research of treatment options addressing the cognitive deficit associated with neurodegenerative disorders is of particular importance. Application of trimethyltin (TMT) to rats represents a promising model replicating multiple relevant features of such disorders. N-methyl-D-aspartate (NMDA) receptor antagonists and gamma-aminobutyric acid type A ($GABA_A$) receptor potentiators have been reported to alleviate the TMT-induced cognitive deficit. These compounds may provide synergistic interactions in other models. The aim of this study was to investigate, whether co-application of NMDA receptor antagonist dizocilpine (MK-801) and $GABA_A$ receptor potentiator midazolam would be associated with an improved effect on the TMT-induced model of cognitive deficit. Wistar rats injected with TMT were repeatedly (12 days) treated with MK-801, midazolam, or both. Subsequently, cognitive performance was assessed. Finally, after a 17-day drug-free period, hippocampal neurodegeneration (neuronal density in CA2/3 subfield in the dorsal hippocampus, dentate gyrus morphometry) were analyzed. All three protective treatments induced similar degree of therapeutic effect in Morris water maze. The results of histological analyses were suggestive of minor protective effect of the combined treatment (MK-801 and midazolam), while these compounds alone were largely ineffective at this time point. Therefore, in terms of mitigation of cognitive deficit, the combined treatment was not associated with improved effect.

Keywords: cognitive function; trimethyltin; hippocampus; NMDA receptor; GABA A receptor; dementia; combination therapy; Alzheimer's disease; neurodegeneration; neuroprotection

Citation: Chvojkova, M.; Kubova, H.; Vales, K. Effects of Dizocilpine, Midazolam and Their Co-Application on the Trimethyltin (TMT)-Induced Rat Model of Cognitive Deficit. *Brain Sci.* **2021**, *11*, 400. https://doi.org/10.3390/brainsci11030400

Academic Editors: Basavaraj S. Balapal and Pilar Gonzalez-Cabo

Received: 7 February 2021
Accepted: 18 March 2021
Published: 22 March 2021

1. Introduction

Dementias, exemplified mainly by Alzheimer's disease, represent a serious worldwide problem. The rising numbers of patients, significant socioeconomic burden, and limited treatment options necessitate research into treatments targeting the disabling cognitive deficit. Amyloid beta is assumed to play a pivotal role in the pathogenesis of the disease. Besides other detrimental effects, amyloid beta seems to contribute to disturbance of the balance between excitation and inhibition in limbic structures, including hippocampus. These alterations of neurotransmitter systems may contribute to the cognitive deficit. Therefore, pharmacological approaches aiming at restoration of the neurotransmission balance by modulation of glutamatergic and GABAergic systems seem reasonable (reviewed in [1]).

A representative of antagonists of the glutamate receptor of the N-methyl-D-aspartate (NMDA) type, memantine, is already clinically used and is capable of reducing the worsening of clinical symptoms in patients with Alzheimer's disease [2]. It was also proven to decrease the levels of Alzheimer's disease associated proteins amyloid beta and tau in a triple transgenic mouse model, suggesting its disease-modifying potential [3]. Multiple publications corroborate promising effects of NMDA receptor antagonists on cognitive functions in genetic and non-genetic rodent models of Alzheimer's disease [4–6], and neuroprotective effects in other animal models [7–9]. Generally, the neuroprotective effect

lies in mitigation of glutamate excitotoxicity [9]. However, as NMDA receptors are necessary for physiological neurotransmission, many NMDA receptor antagonists can induce undesirable side effects [9,10].

The role of the modulation of the GABAergic system by various compounds including benzodiazepines in the treatment of dementias did not receive bigger attention until the last decade [1,11]. Benzodiazepines acts as positive allosteric modulators of $GABA_A$ receptors, therefore facilitating the inhibitory effect of GABA [12]. Such action may possibly help to restore the balance between excitation and inhibition. Besides, $GABA_A$ receptor potentiators, including benzodiazepines, possess beneficial neuroprotective properties in animal and in vitro models [13–17]. On the other hand, side effects may limit the use of these compounds [18].

Among animal models of neurodegenerative diseases associated with cognitive deficit, one possible approach is a systemic administration of trimethyltin (TMT), an organometallic compound inducing neurodegeneration in the limbic system, particularly in the hippocampus [19–21], and behavioral alterations, including cognitive deficit in various tasks [22–26] in laboratory rats. The effect of TMT is age-dependent, affecting older animals more profoundly [27]. Moreover, the model shares other typical features of neurodegenerative disorders, such as oxidative stress [25], microglia activation [28], mitochondrial dysfunction [29], progressive pattern of action [22], altered neurotransmission [23,30–32], and altered expression of multiple gene groups, including those relevant to Alzheimer's disease, such as presenilin 1, presenilin 2, amyloid precursor protein, and tau [33,34]. These properties make the TMT model a promising tool for testing of treatment options targeting the disabling cognitive deficit associated with neurodegenerative disorders, particularly Alzheimer's disease.

The precise mechanisms of the selective neurotoxicity of TMT are complex and not yet fully elucidated. Oxidative stress, calcium overload, and mitochondrial damage are most probably involved, although other phenomena like glutamate excitotoxicity are also considered, as reviewed by Geloso et al. [35]. Among other pathologies, alterations of neurotransmitter systems [32] involving increased extracellular levels of glutamate [30,31] and decreased levels of GABA in hippocampus [23] seem to be present. Correspondingly, therapeutic effects of drugs with various mechanisms of action (anti-inflammatory agents, antioxidants, or agents correcting altered neurotransmission) were described (for review see [36]).

NMDA receptor antagonists [37] or positive modulators of $GABA_A$ receptors [38] are able to accomplish the desired alleviation of the TMT-induced cognitive deficit. The precise underlying mechanism is difficult to specify due to the complex nature of TMT action. It is supposed to lie mainly in correction of altered neurotransmission [36], since the neuroprotective potential of these compounds in the TMT model appears rather limited [39–41].

Due to the complex nature of Alzheimer's disease, combined treatment is expected to represent a more suitable approach than monotherapy [1,42]. Such an approach may lead to increased therapeutic effects and an improved side effect profile [42], which would be of great benefit. Furthermore, given the current interest in so-called multi-target directed ligands, these findings can represent a potential basis for future drug development. It seems reasonable to suppose that co-application of NMDA receptor antagonists and $GABA_A$ receptor potentiators might, by complementary mechanisms, help to restore the excitatory/inhibitory balance and lead to an increased effect. The evidence from models of different central nervous system disorders suggests that co-application of NMDA receptor antagonists with $GABA_A$ potentiators may be associated with beneficial synergistic interactions [15,43–45].

To our knowledge, it remains to be elucidated whether similar beneficial interactions may also occur in the TMT model. Therefore, the purpose of this study was to investigate whether co-application of an NMDA receptor antagonist and $GABA_A$ receptor potentiator would increase the intended anti-amnestic therapeutic effect in the TMT model. As a selective NMDA receptor antagonist, we used MK-801 [46], as a representative of $GABA_A$

receptor potentiators of the benzodiazepine class, we chose midazolam; its advantage over other benzodiazepines lies in its water-solubility [47]. MK-801, midazolam, or their combination were repeatedly administered to the TMT-injected rats. Subsequently, we focused on the cognitive performance of the animals in Morris water maze (a hippocampus-dependent task [48]) and contextual fear conditioning (task involving hippocampus- and amygdala-associated processes [49,50]). We hypothesized that the co-application would be associated with increased cognitive effect. In addition, the neurodegeneration in dorsal hippocampus was histologically assessed.

2. Materials and Methods

2.1. Animals

Thirty-two adult male Wistar rats (10–11 weeks old, 380–490 g) purchased from the Institute of Physiology of the Czech Academy of Sciences (accredited breeding colony) were used. After one week acclimatization period, the experiment has been initiated. As TMT may induce aggression [22,25], the animals were single housed since the day of TMT administration in transparent plastic cages (20 × 25 × 40 cm). The cages were located in an air-conditioned animal room with constant temperature (22 °C), humidity (50–60%), and 12 h light/dark cycle (lights on: 06:00–18:00 h). Water and food were available ad libitum. All experiments were conducted in accordance with the guidelines of the European Union directive 2010/63/EU and Act No 246/1992 Coll., on the protection of animals against cruelty, and were approved by the Animal Care and Use Committee of the Institute of Physiology of the Czech Academy of Sciences and by the Central Committee of the Czech Academy of Sciences (approval number 136/2013, approved 3 October 2013). All efforts were made to reduce the number of animals and minimize suffering.

2.2. Drugs and Experimental Design

The rats were pseudorandomly allocated to five groups: Saline, TMT, TMT + MK-801, TMT + midazolam, and TMT + MK-801 + midazolam. On Day 0, animals were intraperitoneally injected with a single dose of TMT (trimethyltin chloride, #146498, Sigma-Aldrich, St. Louis, MO, USA; 8 mg/kg body weight, TMT weight expressed as total salt, 8 mg/mL, dissolved in 0.9% saline). Control animals (group saline) received a corresponding volume of saline. MK-801 at a dose of 0.1 mg/kg ((+)-MK-801 hydrogen maleate, #M107, Sigma-Aldrich, 0.1 mg/mL, dissolved in 0.9% saline), midazolam at a dose of 5 mg/kg (midazolam hydrochloride, 5 mg/mL, Dormicum, Roche, Prague, Czech Republic), or both MK-801 and midazolam were applied to animals from corresponding groups 30 min before the application of TMT on Day 0 and then on a daily basis until Day 11, while animals from groups saline and TMT received 0.9% saline. All drugs were administered intraperitoneally.

The timeline of the experiment is shown in Figure 1. After finishing the treatment, a battery of behavioral tests was conducted. Ethical aspects were considered in the experimental design. The same animals were used for behavioral tests and histological assessment, enabling reduction of the number of animals. Perfusion was performed on Day 28 (therefore, after a 17-day drug-free period).

The number of animals in groups was: 7 animals in saline, 8 animals in TMT, 6 animals in TMT + MK-801, 6 animals in TMT + midazolam, and 5 animals in TMT + MK-801 + midazolam group.

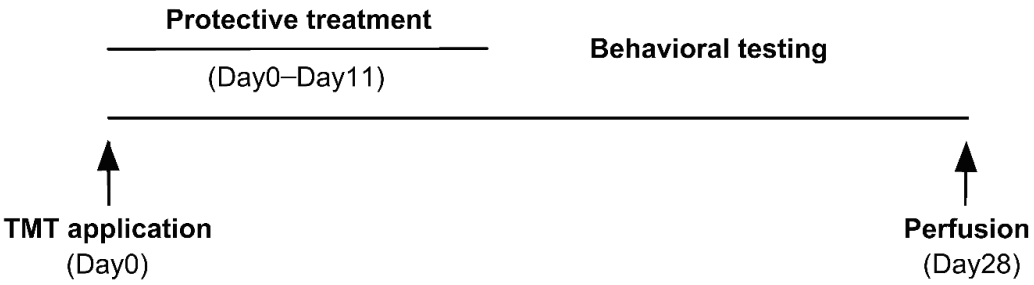

Figure 1. Timeline of the experiment.

2.3. Morris Water Maze

Morris water maze (MWM) was performed to assess cognitive performance. The apparatus consisted of a blue plastic circular pool (180 cm in diameter) with a circular platform (10 cm in diameter, transparent plastic, submerged 1 cm below the water surface). The position of the platform was constant (in the center of SW quadrant). The pool was filled with water (21–22 °C, 28 cm deep) colored by a small amount of non-toxic grey dye. The position of the rat was recorded every 40 ms by an overhead camera connected to a digital tracking system (Tracker, Biosignal Group, New York, NY, USA). The data was later analyzed using software Carousel Maze Manager 0.4.0 [51].

The MWM testing was initiated on Day 12 of the experiment and it was conducted during four consecutive days (MWM Day 1–4) in the light phase of the day. The rats were trained to find the hidden platform. Each day the rats underwent 8 swims from different starting points located on the periphery of the pool (in pseudorandom order). Animals were released into the water facing the inner wall of the pool. If the rat did not find the platform in 60 s, it was guided to the platform by the experimenter. On the MWM Day 4, after finishing the MWM sessions, the platform was removed, and the rats underwent a 30-s probe trial. Subsequently, the platform was returned to the pool, raised 1 cm above the water surface, and provided with a contrast rim for better visibility. A 60-s visible platform trial was conducted to assess sensorimotor functions and motivation [52].

The dependent variables for training trials were total distance (m) moved by the rat to reach the hidden platform (or total distance moved in the case of unsuccessful trials) and mean distance (cm) from platform (mean of the distances of the animal from the platform, sampled in 40 ms intervals), which represents a sensitive parameter, reflecting not only the ability to locate the platform, but also the search strategy [53]. Mean daily values were calculated for each animal and used for analysis. Latency was also analyzed, but as latency and distance are generally correlated, we report only the distance, which is less sensitive to possible differences in swimming speed. Cumulative latency (sum of all latencies during MWM Day 3 and 4) was calculated to assess the best achieved performance [54]. Days 3–4 were chosen because all groups reached asymptotic performance by MWM Day 3 (within each group, there was no significant difference between MWM Day 3 and Day 4 with respect to the distance moved as well as escape latency [latency data not shown]; two-way repeated measures ANOVA with Bonferroni post hoc test).

The dependent variables for probe trial and visible platform trial were dwell time in target quadrant (=the quadrant where the platform was originally located) and latency to find the platform, respectively.

"The periphery of the pool" refers to an 18-cm wide annulus; the wall of the pool represented the outer border of the annulus.

2.4. Contextual Fear Conditioning

Contextual fear conditioning is a cognitive task based on association of aversive stimulus with the context of its administration. In healthy animals, repeated exposition to the context leads to manifestation of freezing behavior [55]. The experiment was performed during two consecutive days (Day 17–18). An automated apparatus TSE Multi Condi-

tioning System (TSE Systems, Bad Homburg, Germany) with corresponding software (TSE ActiMot) was used. The apparatus consisted of a testing box (44 × 44 cm; the floor was made of a stainless steel grid) and enabled administration of electric stimulus via the grid floor and detection of the animal's activity using infrared sensors. For the first session (learning), the animal was placed into the apparatus and after 3 min, an electric stimulus (1 mA, direct current, 2000 ms) was administered. After 2 min, the stimulus was administered once more. Testing session was performed 24 h later. The animal was placed again into the testing box for 5 min and the cumulative duration of freezing was analyzed. Freezing episode was defined as absence of (other than breathing) body movements for 2 s or more.

2.5. Open Field Tests

The rats were subjected to open field tests to monitor their locomotor activity to exclude any presence of severe malaise or decreased state of well-being, possibly induced by the TMT toxicity and manifested as decreased/absent locomotion. These non-specific effects, if present, may influence the performance of the animals in the cognitive tests. Open field tests (10 min) were performed on Day 0 before TMT administration (baseline activity) and then weekly: on Day 7, Day 14, and Day 21. The TSE Multi Conditioning System (TSE Systems, Germany) apparatus (open field size 44 × 44 cm) with corresponding software (TSE ActiMot) were used. The dependent variable was distance moved by the animal. Due to apparatus error, one animal from the saline group and one animal from the TMT group were excluded from the analysis.

2.6. Histology

On Day 28, the rats were anaesthetized with intraperitoneal injection of ketamine (Narketan, Vétoquinol, Lure, France; 120 mg/kg) and xylazine (Rometar, Bioveta, Ivanovice na Hane, Czech Republic; 6 mg/kg), and transcardially perfused with 0.01 M phosphate buffered saline (pH 7.4) rinse followed by ice cold 4% paraformaldehyde in 0.15 M Na-phosphate buffer and 15% saturated picric acid (pH 7.4). The brains were dissected, postfixed in the paraformaldehyde solution overnight, cryoprotected in buffered 10% and 30% sucrose solution at 4 °C, frozen on dry ice, and stored at −80 °C. The brains were sectioned (coronal plane, 50 µm) using cryostat Leica CM1850. Two series were used for following analyses.

A randomly selected series of sections (every 6th section) was mounted on gelatin-coated slides, stained with cresyl violet, and coverslipped.

Another series of sections (50 µm apart the cresyl violet stained sections) was immunostained with antibodies against neuronal nuclei (NeuN) using the previously described avidin-biotin method [56]. The protocol involved incubation in the solution containing primary antibody (anti-NeuN, mouse monoclonal, clone A60, #MAB377, Chemicon International, Temecula, CA, USA; dilution 1:1000), 1.5% normal horse serum, sodium azide (0.2 mg/mL), and 0.3% Triton-100 in 0.01 M phosphate buffered saline (PBS, pH 7.6) for 72 h at 8 °C. The incubation with secondary antibody was performed using the solution containing biotinylated horse anti-mouse IgG (BA-2001, Vector Laboratories, Burlingame, CA, USA; dilution 1:200), 1.5% normal horse serum, and 0.3% Triton-100 in 0.01 M PBS (1 h incubation at room temperature). After the staining, the sections were mounted on gelatin-coated slides and coverslipped.

2.7. Stereological Estimate of CA2/3 Neuronal Density in a Defined Portion of the Dorsal Hippocampus

Five NeuN-stained sections starting at the level corresponding to −2.92 from Bregma according to rat brain atlas [57] were used for stereological estimation of neuronal density in the cornu Ammonis 2/3 (CA3 together with CA2) subfield in the dorsal hippocampus. Dorsal CA3 was selected as it is known to be susceptible to TMT-induced damage [20,58] and is also necessary for normal MWM performance [59]. As the CA3/CA2 border is not always easily distinguishable, CA2 was included in the region of interest as well. The

region of interest is shown in Figure 2a. Nomenclature (CA3, CA2) is based on Paxinos and Watson [57]. CA3c refers to the portion of CA3 encapsulated by the blades of dentate gyrus, as described in Hunsaker et al. [60].

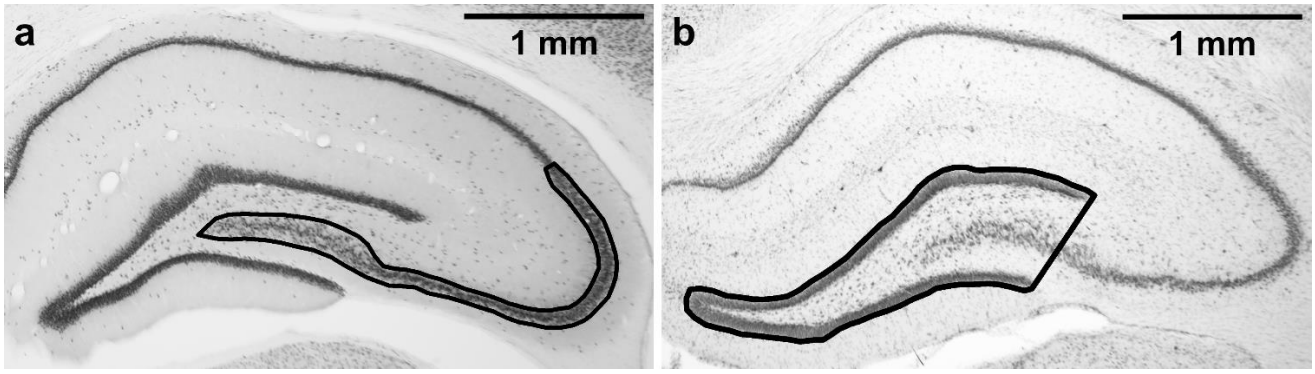

Figure 2. Regions of interest tracing. (**a**) CA2/3 subfield, where the stereological counting was performed; (**b**) area of dentate gyrus. Magnification: 2×. Microphotographs in Figure 2 were acquired using a microscope (Olympus BX53, 2×/0.08 objective lens) connected to a camera (Olympus DP74 for the Olympus BX53 microscope, and Zeiss AxioCam MRm for the Zeiss microscope) and acquisition system in brightfield illumination in grayscale camera mode.

The neuronal density was determined using unbiased stereology approach. The neurons were visualized with Olympus BX51 microscope (100× oil immersion objective lens) and stereologically counted using optical fractionator [61] using the software Stereo Investigator (MBF Bioscience, Williston, VT, USA). Counting was performed with 50 × 50 µm counting frame and the systematic random sampling grid size was 150 × 150 µm. Tissue thickness was measured at every sampling site, dissector height was 7 µm. Guard zones were used to avoid abnormalities of the tissue surface, guard zone distance was 0.6 µm. Subsequently, estimated population using mean section thickness was calculated by the software. The coefficient of error for a single measurement (Gundersen, m = 1) was $\leq$0.07. Analysis was performed in a blinded manner.

The volume of the analyzed area (μm^3) was assessed by the software as well. The neuronal density was then calculated by dividing the estimated neuronal count by the volume of the analyzed area. Right and left hippocampus from each subject was analyzed separately. Subsequently, mean value of neuronal density was calculated for each animal and used for statistical analysis.

2.8. Mean Area of Dentate Gyrus in a Defined Portion of the Dorsal Hippocampus

As excessive neurodegeneration in CA3c may lead to thinning of dentate gyrus [62], five cresyl violet-stained sections (corresponding to the NeuN-stained sections used for the stereological counting) were used for dentate gyrus morphometry. Microphotographs were acquired using a microscope (Olympus BX53; 2× objective lens) connected to a camera (Olympus DP74) and acquisition system (Olympus CellSens Dimension 1.18). Analysis was performed using Fiji (ImageJ 2.0.0) software. A line was drawn around the outer borders of the suprapyramidal and infrapyramidal blades of the granule cell layers, and the shape was closed by drawing a straight line connecting the temporal ends of the dentate gyrus blades, resulting in a triangle-like area, including the granule cell layer, a part of CA3 pyramidal layer, and the hilus (Figure 2b). The area of the dentate gyrus was measured. These measurements were done for the left and right hippocampus in all five sections, and the mean of all the 10 measurements per animal was calculated. Analysis was performed in a blinded manner.

2.9. Statistics

Statistical analysis was performed using GraphPad Prism 5.0 (San Diego, CA, USA). The differences were considered as significant at $p < 0.05$. Asterisks and number signs in graphs denote statistical significance, * $p < 0.05$, ** $p < 0.01$, *** $p < 0.001$.

Distance moved and mean distance from platform in MWM were analyzed using two-way repeated measures ANOVA (treatment and day factor) followed by Bonferroni post hoc test to assess treatment effect (differences between treatment groups within each day). An additional Bonferroni post hoc test was performed for distance moved to assess the day effect (differences between days within each treatment group).

In the probe trial, the percentage of time spent in the target quadrant was compared to 25% (the value corresponding to random preference for quadrants) using one-sample *t*-test.

The data from MWM visible platform, MWM cumulative latency, dorsal CA2/3 neuronal density, and area of dentate gyrus were tested for normality using Kolmogorov–Smirnov test and for equal variances by Bartlett's test. If these assumptions for ANOVA were met, ANOVA followed by Tukey's post hoc test (when appropriate) was used for data analysis (CA2/3 neuronal density, area of dentate gyrus; data are graphically represented as group mean + SEM). If the assumptions for ANOVA were not met (MWM visible platform, MWM cumulative latency), the data were analyzed using Kruskal–Wallis test followed by Dunn's multiple comparison test where appropriate, and graphically represented as median with interquartile range. The data from fear conditioning (cumulative duration of freezing) were analyzed using ANOVA. The distance moved in open field was analyzed using ANOVA (individual days separately) and, if appropriate, Bonferroni post hoc test was performed to compare the groups with the saline group.

3. Results

3.1. Morris Water Maze

Spatial cognition of the animals was tested using MWM. Two-way repeated measures ANOVA of distance moved in MWM revealed a significant effect of treatment ($F_{4,81} = 6.234$, $p = 0.0011$) and day ($F_{3,81} = 60.22$, $p < 0.0001$), with no interaction. Bonferroni post hoc test (treatment effect) showed that the distance moved by the TMT group was significantly longer than that of saline-treated animals on all MWM days ($p < 0.01$, $p < 0.001$, $p < 0.001$, and $p < 0.01$ for MWM Day 1, 2, 3 and 4, respectively), indicating impaired cognitive performance. Conversely, the distance moved by the treated groups (TMT + MK-801, TMT + midazolam, TMT + MK-801 + midazolam) did not differ from saline-treated animals throughout whole experiment. Moreover, the distance moved by animals treated with TMT + MK-801 on MWM Day 2 was significantly shorter than that of the TMT group ($p < 0.05$). Similarly, on Day 2 and 3, the animals from the TMT + midazolam group ($p < 0.01$ for day 2 and $p < 0.05$ for day 3) and animals from the TMT + MK-801 + midazolam group ($p < 0.05$ for both days) travelled shorter distances compared to the TMT group (Figure 3a). These findings suggest alleviation of TMT-induced cognitive deficit.

Analysis of day effect using Bonferroni post hoc test revealed that the distance moved by saline-treated animals as well as by all groups treated with tested drugs (TMT + MK-801, TMT + midazolam, TMT + MK-801 + midazolam) significantly decreased on Day 2 (compared to the same group on day 1; $p < 0.001$, $p < 0.05$, $p < 0.01$, and $p < 0.01$, respectively), indicating successful learning. In contrast, in the TMT group, there was no significant difference between distance moved on Day 1 and 2. The improvement occurred on Day 3 (vs. day 1; $p < 0.001$), indicating a delayed onset of learning. These findings may further corroborate a beneficial effect of both drugs and their combination on cognition.

Two-way repeated measures ANOVA of mean distance from the platform yielded a significant effect of treatment ($F_{4,81} = 5.973$, $p = 0.0014$) and day ($F_{3,81} = 119.1$, $p < 0.0001$). TMT treatment was associated with an increased mean distance from the platform compared to saline on all MWM days (Bonferroni post hoc test, treatment effect, $p < 0.01$, $p < 0.001$, $p < 0.001$, and $p < 0.05$ for Day 1, 2, 3, and 4, respectively). The groups treated with tested drugs did not differ from saline; moreover, they displayed lower mean distance

from the platform than TMT-treated rats on certain days: the TMT + MK-801group differed from TMT on Day 2 ($p < 0.05$), TMT + midazolam on Day 2 ($p < 0.01$), and TMT + MK-801 + midazolam differed from TMT on Days 2, 3, and 4 ($p < 0.05$ for all; Figure 3b).

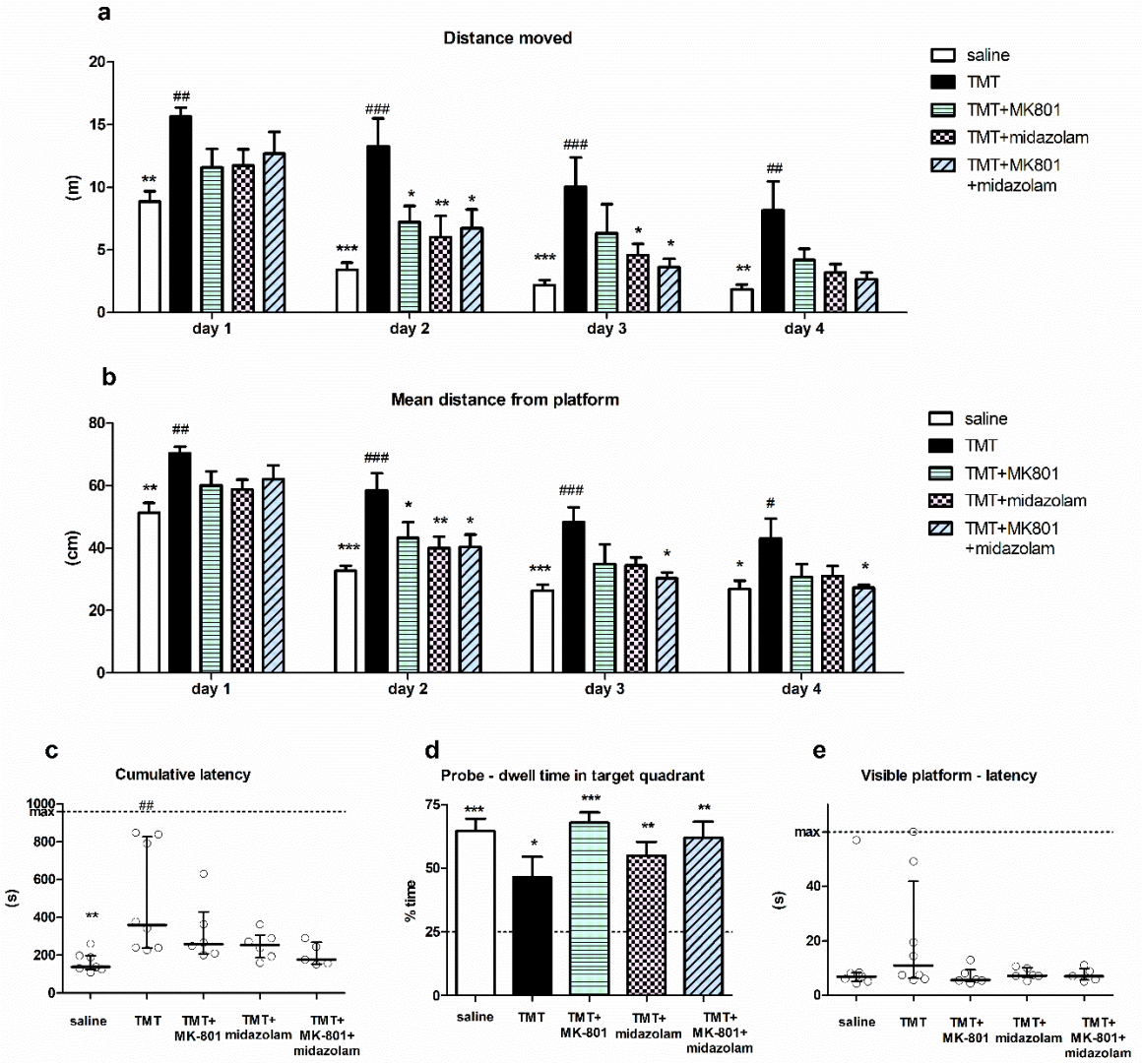

Figure 3. Morris water maze. (**a**) Distance moved. Group mean + SEM, two-way repeated measures ANOVA and Bonferroni post hoc test (treatment effect within day), * $p < 0.05$, ** $p < 0.01$, *** $p < 0.001$ vs. TMT, $^{\#\#}$ $p < 0.01$, $^{\#\#\#}$ $p < 0.001$ vs. saline. (**b**) Mean distance from platform. Group mean + SEM, two-way repeated measures ANOVA and Bonferroni post hoc test (treatment effect within day), * $p < 0.05$, ** $p < 0.01$, *** $p < 0.001$ vs. TMT, $^{\#}$ $p < 0.05$, $^{\#\#}$ $p < 0.01$, $^{\#\#\#}$ $p < 0.001$ vs. saline. (**c**) Cumulative latency. Kruskal–Wallis with Dunn's multiple comparison test, ** $p < 0.01$ vs. TMT, $^{\#\#}$ $p < 0.01$ vs. saline. Median with interquartile range, circles represent values from individual animals. (**d**) Probe trial—dwell time in target quadrant. Group mean + SEM, asterisks denote difference from the quadrant choice equivalent to random chance (25%, indicated by the dashed line) analyzed using one-sample *t*-test, * $p < 0.05$, ** $p < 0.01$, *** $p < 0.001$. (**e**) Visible platform trial—latency to find the platform. Median with interquartile range, circles represent values from individual animals.

Cumulative latencies (sum of latencies from MWM day 3–4) of the treatment groups were significantly different (Kruskal–Wallis test, H = 14.25, $N_1 = 7$, $N_2 = 8$, $N_3 = 6$, $N_4 = 6$, $N_5 = 5$, $p = 0.0065$). TMT-treated animals had higher cumulative latency than saline-treated animals (Dunn's multiple comparison test, $p < 0.01$), indicating impaired performance. Although we observed differences between the group means, with that of saline group being the lowest, followed by TMT + MK-801 + midazolam group, no other statistically significant differences were found (Figure 3c). In the TMT group, three out of eight animals

(37.5%) displayed considerably high cumulative latency. High cumulative latency was associated with an increased time spent in the periphery of the pool in these three animals (time spent in the periphery on Day 3–4 was 66–78%, representing the highest values of all animals), suggesting that they failed to adopt effective strategy. One of the six animals (16.7%) in the TMT + MK-801 group tended to manifest similar deficit; however, other groups (saline, TMT + midazolam, TMT + MK-801 + midazolam) were free of such "poor performers".

Analysis of probe trial showed that despite observed differences in the groups' performance, animals from all treatment groups displayed significant preference for the target quadrant, as one sample *t*-test revealed that time spent in target quadrant was >25%, which corresponds to random choice ($t_6 = 7.929$, $p = 0.0002$ for saline, $t_7 = 2.668$, $p = 0.0321$ for TMT, $t_5 = 10.61$, $p = 0.0001$ for TMT + MK-801, $t_5 = 5.544$, $p = 0.0026$ for TMT + midazolam, $t_4 = 5.728$, $p = 0.0046$ for TMT + MK-801 + midazolam group). Therefore, all groups were able to eventually learn the location of target quadrant (Figure 3d).

Finally, we did not detect any significant differences between groups in the visible platform trial. This suggests a low risk of confounding the MWM results via alterations in sensorimotor functions or motivation (Kruskal–Wallis test; Figure 3e).

3.2. Contextual Fear Conditioning

According to visual observation during the learning phase, control as well as TMT-treated animals exhibited the typical response to the painful stimulus (running, vocalization; not quantified). ANOVA of the cumulative duration of freezing during the testing phase did not find a statistically significant group effect, although we observed differences in the groups' means (Figure 4).

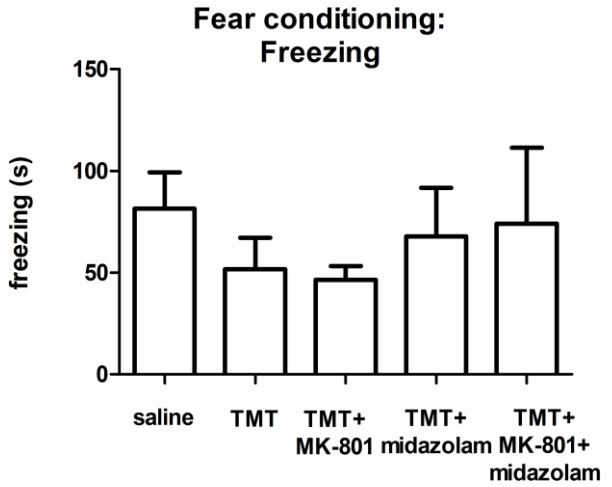

Figure 4. Contextual fear conditioning: Cumulative duration of freezing. Group mean + SEM. No statistically significant differences were found (ANOVA).

3.3. Open Field Tests

Analyses of distance moved in open field (Day 0, Day 14, Day 21) did not reveal significant differences between groups (ANOVA). On Day 7, there was a group effect ($F_{4,25} = 3.426$, $p = 0.0230$), but the post hoc test (Bonferroni) did not find statistically significant differences. Therefore, we failed to detect any significant activity decrease, which would suggest severe impairment of health condition by the toxic effects of TMT (data not shown).

3.4. Stereological Estimate of CA2/3 Neuronal Density in a Defined Portion of the Dorsal Hippocampus

Examination of NeuN-stained sections confirmed that TMT induced pyramidal cell loss in dorsal CA3, which was particularly prominent in the CA3c subfield. Various degrees

of cell loss were observed in individual animals. Representative images of NeuN-stained sections from animals in different treatment groups are shown in Figure 5a1–e2.

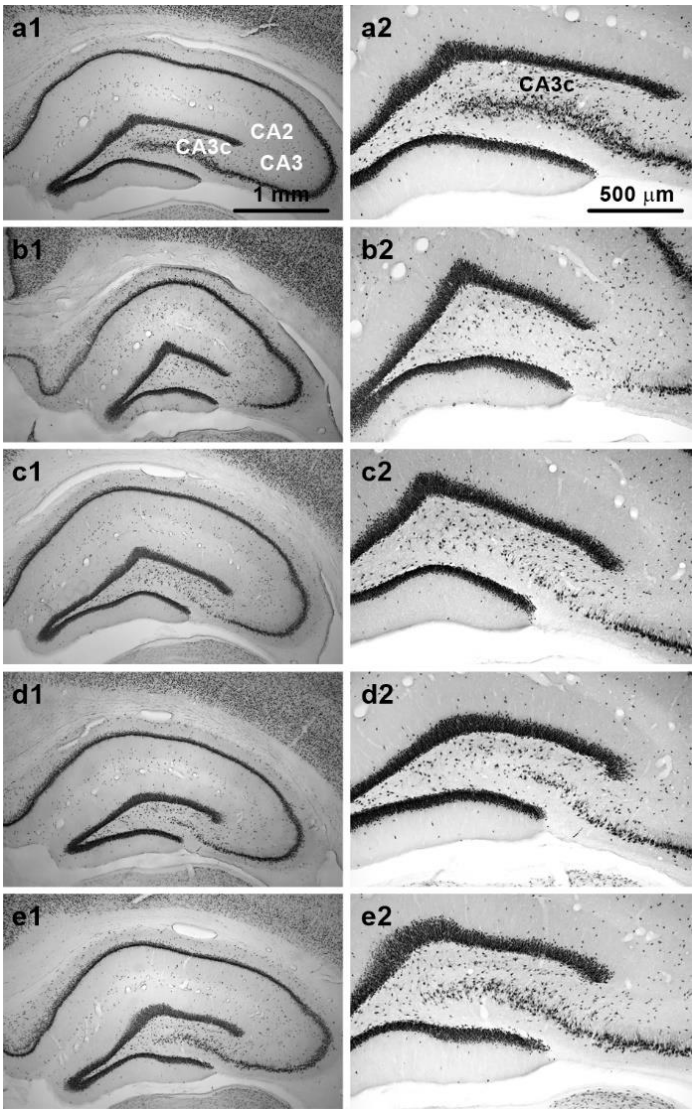

Figure 5. Representative NeuN-stained sections from dorsal hippocampus. Panels show sections from animals treated with: (**a1**,**a2**) Saline (relevant subfields of pyramidal cell layer are marked); (**b1**,**b2**) TMT (note almost complete neuronal loss in CA3c); (**c1**,**c2**) TMT + MK-801; (**d1**,**d2**) TMT + midazolam; (**e1**,**e2**) TMT + MK-801 + midazolam. Note different neuronal densities in CA3c. Sections from animals with neuronal density close to the group mean are depicted. Magnification: 4× (left panels); 10× (right panels). Microphotographs in Figure 5 were acquired using a microscope (left panels: Zeiss Axio Observer D1, 4×/0.1 objective lens; right panels: Olympus BX53, 10×/0.40 dry objective lens) connected to a camera (Olympus DP74 for the Olympus BX53 microscope, and Zeiss AxioCam MRm for the Zeiss microscope) and acquisition system in brightfield illumination in grayscale camera mode.

ANOVA of the stereological estimates of neuronal density in CA2/3 in the defined portion of the dorsal hippocampus found significant effect of treatment ($F_{4,27}$ = 6.772, p = 0.0007). The TMT ($p < 0.001$), TMT + MK-801 ($p < 0.01$), and TMT + midazolam ($p < 0.05$) group displayed significantly lower neuronal densities than the saline-treated group (Tukey's post hoc test). In contrast, the TMT + MK-801 + midazolam group did not differ from the saline or from the TMT group, suggesting mild neuroprotective effect (Figure 6a).

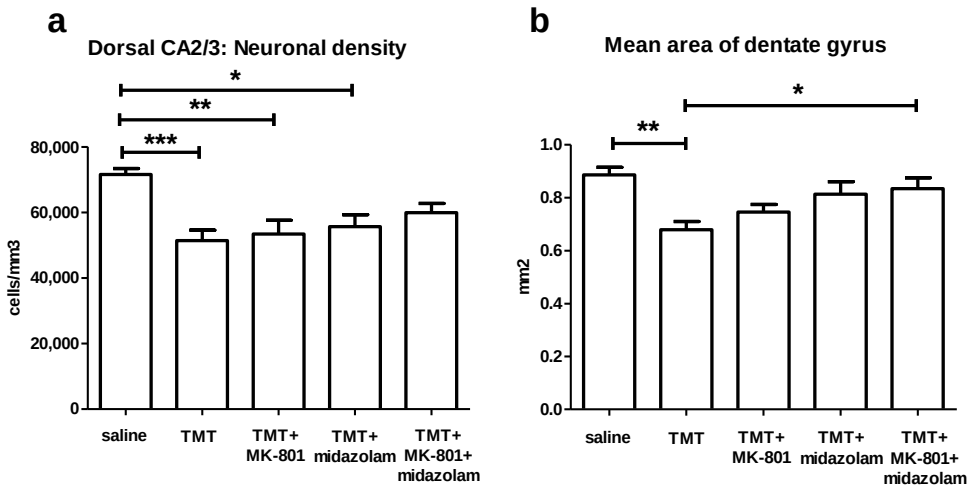

Figure 6. Histology. (**a**) Stereological estimate of neuronal density in CA2/3 in the defined portion of the dorsal hippocampus. Group mean + SEM. ANOVA and Tukey's post hoc test, * $p < 0.05$, ** $p < 0.01$, *** $p < 0.001$. (**b**) Mean area of dentate gyrus (including the hilus, as described in Methods) in the defined portion of the dorsal hippocampus. ANOVA and Tukey's post hoc test, * $p < 0.05$, ** $p < 0.01$.

3.5. Mean Area of Dentate Gyrus in a Defined Portion of the Dorsal Hippocampus

To assess thinning of dentate gyrus, possibly associated with degeneration of CA3c neurons, area of dentate gyrus was measured. ANOVA of the mean area of dentate gyrus revealed significant effect of treatment ($F_{4,27} = 5.978$, $p = 0.0014$). TMT reduced the area of dentate gyrus ($p < 0.01$, compared to saline, Tukey's post hoc test). In contrast, TMT + MK-801 + midazolam treatment was associated with increased area of dentate gyrus compared to TMT group ($p < 0.05$), being suggestive of protective effect. The TMT + MK-801 and TMT + midazolam groups did not differ from saline or from TMT group, which may be interpreted as possible partial protective effect (Figure 6b).

4. Discussion

The research of the treatment options addressing the disabling cognitive deficit accompanying neurodegenerative diseases is of particular importance. One possible approach may be based on restoration of balance in neurotransmitter systems. The administration of TMT to laboratory rats is considered as a promising model of neurodegenerative diseases associated with cognitive deficit, especially Alzheimer's disease [35]. The TMT-induced pathologies may involve increased levels of glutamate [30,31] and decreased levels of GABA [23]. Correspondingly, THIP (gaboxadol), representing an agonist of extrasynaptic $GABA_A$ receptors [38,63], and phencyclidine, acting predominantly but not exclusively as an NMDA receptor antagonist [37], were found to ameliorate the TMT-induced cognitive deficit. Besides, the co-application of NMDA receptor antagonists with positive modulators of $GABA_A$ receptors is associated with beneficial synergistic interactions in other models [15,43–45]. This prompted us to investigate the possible benefit of the co-application of these agents in the TMT-induced model of cognitive deficit in rats. MK-801 was chosen as a selective NMDA receptor antagonist [46]. We selected midazolam as a representative of water-soluble [47] $GABA_A$ receptor potentiators of the benzodiazepine class.

In accordance with existing literature [23,26], TMT induced cognitive deficit in MWM, manifested as increased distance moved and mean distance from platform throughout the experiment. Moreover, the onset of learning was delayed and TMT-treated animals never reached the level of performance of control animals, as indicated by cumulative latency [54]. According to visible platform trial and open field test, the impaired performance was not caused by non-cognitive phenomena (sensorimotor dysfunction or decreased activity/malaise, respectively). Treatment with MK-801, midazolam, as well as a combination

thereof, provided a similar degree of alleviation of manifestations of cognitive impairment in the observed parameters. Our results confirm the protective effects of NMDA receptor inhibition [37] and $GABA_A$ receptor positive modulation [38] against TMT-induced cognitive deficit. However, we failed to bring forward any clear evidence for the superiority of the combined treatment. Interestingly, the combined treatment (TMT + MK-801 + midazolam), but not MK-801 or midazolam alone (TMT + MK-801, TMT + midazolam), improved the search strategy on MWM Day3–4, as indicated by the mean distance from the platform [53]. We also observed mildly improved cumulative latency in animals with the combined (TMT + MK-801 + midazolam) treatment compared to the compounds alone; nonetheless, the difference did not attain statistical significance. It is therefore possible that a subtle difference in cognition was present, but that the basic version of MWM used in our study was not sensitive enough to detect it. Anyway, no statistically significant advantage of the combined treatment over monotherapy was found.

As opposed to MWM, we did not find any statistically significant difference between the performance of the treatment groups in the contextual fear conditioning, although we observed tendency to impaired performance in the groups TMT and TMT + MK-801. Hence, our results do not corroborate the findings of Takahashi, who reported decreased freezing in TMT-treated rats in the testing phase of contextual fear conditioning [64]. However, it is worth noting that the experimental design was not identical.

In addition to cognitive aspects, we assessed the TMT-induced hippocampal neuronal loss. Brain samples were harvested with time delay, after completing the behavioral tests (therefore 17 days after treatment cessation). Neuronal loss in CA3 subfield in dorsal hippocampus, a region highly susceptible to TMT-induced damage [20,58], was evaluated using the unbiased stereology approach. Consistently, TMT induced neuronal loss in dorsal CA2/3. Moreover, as the CA3c subfield in the dorsal hippocampus is extremely vulnerable to TMT-induced neurodegeneration [19,20], possibly leading to dentate gyrus thinning [62], the area of dentate gyrus was measured as well, revealing a shrinkage of dentate gyrus in TMT-treated animals. Combined treatment (TMT + MK-801 + midazolam) was associated with mild mitigation of dorsal CA2/3 neuronal loss as well as of dentate gyrus shrinkage, while the substances were largely ineffective when administered alone (TMT + MK-801, TMT + midazolam), suggesting the possible benefit of the combined treatment. It should be noted that the protective effect of the combined treatment at the selected time point was minor. Nevertheless, the analyzed area included the CA3c, the subfield considered the most sensitive for the toxic effects of TMT [19,20], and the beneficial effect of treatment was present even after the 17-day drug-free period. Therefore, although MK-801 [39] or $GABA_A$ receptor potentiator phenobarbital [41] alone were reported to fail to protect neurons against TMT-induced degeneration, our results seem to suggest that co-application of similar agents may provide some degree of protective effect.

To sum up, we hypothesized that NMDA receptor antagonists and $GABA_A$ receptor potentiators might by complementary mechanisms restore the essential balance between excitation and inhibition in the central nervous system, resulting in desired increase of anti-amnestic effect. However, our results do not support this hypothesis. The behavioral and delayed histological assessments brought different results, with only the latter suggesting possible benefit of combined treatment. It should be emphasized that the benefit of the combined treatment on the histological parameters at selected time point was only minor, and, on the other hand, a non-significant tendency towards improved performance of the group with combined treatment (compared to monotherapy) in Morris water maze was observed.

An insight into the mechanisms underlying the effects of MK-801, midazolam, and their combination in the TMT model is difficult to gain due to the complex and not fully understood mechanisms of action of TMT. In this context, it is challenging to interpret the lack of beneficial interactions of MK-801 and midazolam with respect to the cognitive performance. Moreover, the anti-amnestic and neuroprotective effects of agents interfering with neurotransmitter systems in the TMT model may not be necessarily exerted via

identical mechanisms and their relationship is unclear. In general, similar drugs seem to be effective in terms of mitigation of cognitive deficit, but less effective in preventing TMT-induced neuronal loss [36–39,41]. Addressing the question whether the nature of the anti-amnestic effect is mainly symptomatic or causal is not the objective of the current study and it is also constrained by the design of the experiment, in which, due to ethical reasons, the same animals were used for behavioral and histological assessment (resulting in time gap between them).

Among putative mechanisms underlying the observed mild neuroprotective effect, mitigation of glutamate excitotoxicity seems possible. Excitotoxicity refers to overactivation of glutamate receptors including NMDA receptors by glutamate, enabling calcium influx into neurons, triggering multiple processes including oxidative stress, ultimately resulting in neuronal loss [9]. NMDA receptor antagonists [9,65] and $GABA_A$ receptor potentiators [66,67] can mitigate glutamate excitotoxicity and exert neuroprotective effects in other models, and co-application of these agents may increase these effects [15]. Although TMT does not directly activate glutamate receptors [68], glutamate excitotoxicity has been indeed suggested to participate in its neurotoxic effect. As proposed in the 1980s, degeneration of CA3 pyramidal neurons was ascribed to their putative hyperstimulation caused by disinhibited dentate granule cells [20,69,70]. Proven increased release and reduced uptake of glutamate in the TMT model [30,31] may be consistent with this hypothesis. Nevertheless, the role of glutamate excitotoxicity in the TMT model remains controversial [36,39,40] and if it is involved at all, it most likely represents only one of the factors contributing to the neuronal injury, rather than the exclusive one [35,40]. As opposed to excitotoxicity, involvement of oxidative stress in the mechanism of action of TMT is much more definite [35,36]. Activation of NMDA receptors by glutamate may perhaps only potentiate the oxidative effect induced by distinct mechanisms and accelerate the neuronal degeneration [40]. In this context, the antioxidant effect of midazolam [17] seems especially relevant.

In summary, co-application of MK-801 and midazolam did not significantly improve the pro-cognitive effect. Since the mitigation of behavioral and cognitive symptoms in patients is more important than histological aspects, we consider behavioral outcomes of primary importance. From this perspective, MK-801 and midazolam co-application did not lead to an improved effect in the current experimental setup.

5. Conclusions

In conclusion, MK-801, midazolam, as well as the combination thereof, mitigated cognitive deficit in MWM; however, we failed to detect any significant superiority of the combined treatment. According to the delayed histological assessment of the neuronal loss in the dorsal CA2/3 hippocampal subfield, a minor protective effect of the combined treatment with MK-801 and midazolam was present, while no significant effect of MK-801 or midazolam alone was detected at the selected time point.

Author Contributions: Conceptualization, K.V.; methodology, K.V. and H.K.; formal analysis, M.C.; investigation, M.C.; writing—original draft preparation, M.C.; writing—review and editing, K.V. and H.K.; visualization, M.C.; supervision, K.V.; funding acquisition, K.V. All authors have read and agreed to the published version of the manuscript.

Funding: This research was funded by European Regional Development Fund project "PharmaBrain", grant number CZ.02.1.01/0.0/0.0/16_025/0007444; Grantova Agentura Ceske Republiky, grant numbers P304 18-09296S and P304 14-20613S; Agentura Pro Zdravotnicky Vyzkum Ceske Republiky, grant number NU20-04-00389; by the project "Sustainability for the National Institute of Mental Health", under grant number LO1611, with financial support from the Ministry of Education, Youth and Sports of the Czech Republic under the NPU I program; and Czech Academy of Sciences grant RVO: 67985823.

Institutional Review Board Statement: All experiments were conducted in accordance with the guidelines of the European Union directive 2010/63/EU and Act No 246/1992 Coll., on the protection of animals against cruelty, and were approved by the Animal Care and Use Committee of the Institute of Physiology of the Czech Academy of Sciences and by the Central Committee of the Czech Academy of Sciences (approval number 136/2013, approved 3 October 2013).

Data Availability Statement: The data presented in this study are openly available in Mendeley Data at http://dx.doi.org/10.17632/wn442rdyb3.1 (accessed on 19 March 2021).

Acknowledgments: We thank Blanka Cejkova and Jan Pala, for technical help and advice.

Conflicts of Interest: The authors declare no conflict of interest. The funders had no role in the design of the study; in the collection, analyses, or interpretation of data; in the writing of the manuscript, or in the decision to publish the results.

References

1. Nava-Mesa, M.O.; Jiménez-Díaz, L.; Yajeya, J.; Navarro-Lopez, J.D. GABAergic neurotransmission and new strategies of neuromodulation to compensate synaptic dysfunction in early stages of Alzheimer's disease. *Front. Cell. Neurosci.* **2014**, *8*, 167. [CrossRef]
2. Wilkinson, D.; Andersen, H.F. Analysis of the Effect of Memantine in Reducing the Worsening of Clinical Symptoms in Patients with Moderate to Severe Alzheimer's Disease. *Dement. Geriatr. Cogn. Disord.* **2007**, *24*, 138–145. [CrossRef] [PubMed]
3. Martinez-Coria, H.; Green, K.N.; Billings, L.M.; Kitazawa, M.; Albrecht, M.; Rammes, G.; Parsons, C.G.; Gupta, S.; Banerjee, P.; LaFerla, F.M. Memantine Improves Cognition and Reduces Alzheimer's-Like Neuropathology in Transgenic Mice. *Am. J. Pathol.* **2010**, *176*, 870–880. [CrossRef]
4. Companys-Alemany, J.; Turcu, A.L.; Bellver-Sanchis, A.; Loza, M.I.; Brea, J.M.; Canudas, A.M.; Leiva, R.; Vázquez, S.; Pallàs, M.; Griñán-Ferré, C. A Novel NMDA Receptor Antagonist Protects against Cognitive Decline Presented by Senescent Mice. *Pharmaceutics* **2020**, *12*, 284. [CrossRef]
5. Ponce-Lopez, T.; Liy-Salmeron, G.; Hong, E.; Meneses, A. Lithium, phenserine, memantine and pioglitazone reverse memory deficit and restore phospho-GSK3β decreased in hippocampus in intracerebroventricular streptozotocin induced memory deficit model. *Brain Res.* **2011**, *1426*, 73–85. [CrossRef] [PubMed]
6. Minkeviciene, R.; Banerjee, P.; Tanila, H. Memantine Improves Spatial Learning in a Transgenic Mouse Model of Alzheimer's Disease. *J. Pharmacol. Exp. Ther.* **2004**, *311*, 677–682. [CrossRef]
7. McDonald, J.W.; Silverstein, F.S.; Johnston, M.V. Neuroprotective effects of MK-801, TCP, PCP and CPP against N-methyl-d-aspartate induced neurotoxicity in an in vivo perinatal rat model. *Brain Res.* **1989**, *490*, 33–40. [CrossRef]
8. Schauwecker, P.E. Neuroprotection by glutamate receptor antagonists against seizure-induced excitotoxic cell death in the aging brain. *Exp. Neurol.* **2010**, *224*, 207–218. [CrossRef]
9. Chen, H.-S.V.; Lipton, S.A. The chemical biology of clinically tolerated NMDA receptor antagonists. *J. Neurochem.* **2006**, *97*, 1611–1626. [CrossRef] [PubMed]
10. Muir, K.W.; Lees, K.R. Clinical Experience With Excitatory Amino Acid Antagonist Drugs. *Stroke* **1995**, *26*, 503–513. [CrossRef]
11. Pilipenko, V.; Narbute, K.; Pupure, J.; Rumaks, J.; Jansone, B.; Klusa, V. Neuroprotective action of diazepam at very low and moderate doses in Alzheimer's disease model rats. *Neuropharmacol.* **2019**, *144*, 319–326. [CrossRef]
12. Delorey, T.M.; Olsens, R.W. γ-Aminobutyric Acid A Receptor Structure and Function. *J. Biol. Chem.* **1992**, *267*, 16747–16750. [CrossRef]
13. Ito, H.; Watanabe, Y.; Isshiki, A.; Uchino, H. Neuroprotective properties of propofol and midazolam, but not pentobarbital, on neuronal damage induced by forebrain ischemia, based on the GABAA receptors. *Acta Anaesthesiol. Scand.* **1999**, *43*, 153–162. [CrossRef] [PubMed]
14. Harman, F.; Hasturk, A.E.; Yaman, M.; Arca, T.; Kilinc, K.; Sargon, M.F.; Kaptanoglu, E. Neuroprotective effects of propofol, thiopental, etomidate, and midazolam in fetal rat brain in ischemia-reperfusion model. *Child's Nerv. Syst.* **2012**, *28*, 1055–1062. [CrossRef] [PubMed]
15. Shibuta, S.; Varathan, S.; Mashimo, T. Ketamine and thiopental sodium: Individual and combined neuroprotective effects on cortical cultures exposed to NMDA or nitric oxide. *Br. J. Anaesth.* **2006**, *97*, 517–524. [CrossRef] [PubMed]
16. Sarnowska, A.; Beręsewicz, M.; Zabłocka, B.; Domańska-Janik, K. Diazepam neuroprotection in excitotoxic and oxidative stress involves a mitochondrial mechanism additional to the GABAAR and hypothermic effects. *Neurochem. Int.* **2009**, *55*, 164–173. [CrossRef]
17. Liu, J.-Y.; Guo, F.; Wu, H.-L.; Wang, Y.; Liu, J.-S. Midazolam anesthesia protects neuronal cells from oxidative stress-induced death via activation of the JNK-ERK pathway. *Mol. Med. Rep.* **2016**, *15*, 169–179. [CrossRef]
18. Lanctôt, K.L.; Herrmaan, N.; Mazzotta, P.; Khan, L.R.; Ingber, N. GABAergic function in Alzheimer's disease: Evidence for dysfunction and potential as a therapeutic target for the treatment of behavioral and psychological symptoms of dementia. *Can. J. Psychiatry* **2004**, *49*, 439–453. [CrossRef] [PubMed]
19. Robertson, D.G.; Gray, R.H.; De Laiglesia, F.A. Quantitative Assessment of Trimethyltin Induced Pathology of the Hippocampus. *Toxicol. Pathol.* **1987**, *15*, 7–17. [CrossRef]

20. Whittington, D.L.; Woodruff, M.L.; Baisden, R.H. The time-course of trimethyltin-induced fiber and terminal degeneration in hippocampus. *Neurotoxicol. Teratol.* **1989**, *11*, 21–33. [CrossRef]
21. Balaban, C.; Callaghan, J.; Billingsle, M. Trimethyltin-induced neuronal damage in the rat brain: Comparative studies using silver degeneration stains, immunocytochemistry and immunoassay for neuronotypic and gliotypic proteins. *Neuroscience* **1988**, *26*, 337–361. [CrossRef]
22. Brown, A.W.; Aldridge, W.N.; Street, B.W.; Verschoyle, R.D. The behavioral and neuropathologic sequelae of intoxication by trimethyltin compounds in the rat. *Am. J. Pathol.* **1979**, *97*, 59–82.
23. Earley, B.; Burke, M.; Leonard, B.E. Behavioural, biochemical and histological effects of trimethyltin (TMT) induced brain damage in the rat. *Neurochem. Int.* **1992**, *21*, 351–366. [CrossRef]
24. Ishida, N.; Akaike, M.; Tsutsumi, S.; Kanai, H.; Masui, A.; Sadamatsu, M.; Kuroda, Y.; Watanabe, Y.; McEwen, B.S.; Kato, N. Trimethyltin syndrome as a hippocampal degeneration model: Temporal changes and neurochemical features of seizure susceptibility and learning impairment. *Neuroscience* **1997**, *81*, 1183–1191. [CrossRef]
25. Kaur, S.; Nehru, B. Alteration in Glutathione Homeostasis and Oxidative Stress During the Sequelae of Trimethyltin Syndrome in Rat Brain. *Biol. Trace Element Res.* **2013**, *153*, 299–308. [CrossRef] [PubMed]
26. Lalkovicova, M.; Burda, J.; Nemethova, M.; Burda, R.; Danielisova, V.; Maria, L.; Jozef, B.; Miroslava, N.; Rastislav, B.; Viera, D. Postconditioning Effectively Prevents Trimethyltin Induced Neuronal Damage in the Rat Brain. *Folia Biol.* **2016**, *64*, 97–103. [CrossRef] [PubMed]
27. Scallet, A.C.; Pothuluri, N.; Rountree, R.L.; Matthews, J.C. Quantitating silver-stained neurodegeneration: The neurotoxicity of trimethlytin (TMT) in aged rats. *J. Neurosci. Methods* **2000**, *98*, 69–76. [CrossRef]
28. Brabeck, C.; Michetti, F.; Geloso, M.C.; Corvino, V.; Goezalan, F.; Meyermann, R.; Schluesener, H.J. Expression of EMAP-II by Activated Monocytes/Microglial Cells in Different Regions of the Rat Hippocampus after Trimethyltin-Induced Brain Damage. *Exp. Neurol.* **2002**, *177*, 341–346. [CrossRef]
29. Misiti, F.; Orsini, F.; Clementi, M.E.; Lattanzi, W.; Giardina, B.; Michetti, F. Mitochondrial oxygen consumption inhibition importance for TMT-dependent cell death in undifferentiated PC12 cells. *Neurochem. Int.* **2008**, *52*, 1092–1099. [CrossRef]
30. Dawson, R.; Patterson, T.A.; Eppler, B. Endogenous excitatory amino acid release from brain slices and astrocyte cultures evoked by trimethyltin and other neurotoxic agents. *Neurochem. Res.* **1995**, *20*, 847–858. [CrossRef]
31. Aschner, M.; Gannon, M.; Kimelberg, H. Interactions of trimethyl tin (TMT) with rat primary astrocyte cultures: Altered uptake and efflux of rubidium,l-glutamate andD-aspartate. *Brain Res.* **1992**, *582*, 181–185. [CrossRef]
32. Koczyk, D. How does trimethyltin affect the brain: Facts and hypotheses. *Acta Neurobiol. Exp.* **1996**, *56*, 587–596.
33. Little, A.; Miller, D.; Li, S.; Kashon, M.; O'Callaghan, J.; Little, R. Trimethyltin-induced neurotoxicity: Gene expression pathway analysis, q-RT-PCR and immunoblotting reveal early effects associated with hippocampal damage and gliosis. *Neurotoxicol. Teratol.* **2012**, *34*, 72–82. [CrossRef] [PubMed]
34. Nilsberth, C.; Kostyszyn, B.; Luthman, J. Changes in APP, PS1 and other factors related to Alzheimer's disease pathophysiology after trimethyltin-induced brain lesion in the rat. *Neurotox. Res.* **2002**, *4*, 625–636. [CrossRef]
35. Geloso, M.C.; Corvino, V.; Michetti, F. Trimethyltin-induced hippocampal degeneration as a tool to investigate neurodegenerative processes. *Neurochem. Int.* **2011**, *58*, 729–738. [CrossRef] [PubMed]
36. Corvino, V.; Marchese, E.; Michetti, F.; Geloso, M.C. Neuroprotective Strategies in Hippocampal Neurodegeneration Induced by the Neurotoxicant Trimethyltin. *Neurochem. Res.* **2013**, *38*, 240–253. [CrossRef]
37. Earley, B.; Burke, M.; Leonard, B.; Gouret, C.; Junien, J. A comparison of the psychopharmacological profiles of phencyclidine, ketamine and (+) SKF 10,047 in the trimethyltin rat model. *Neuropharmacology* **1990**, *29*, 695–703. [CrossRef]
38. O'Connell, A.; Earley, B.; Leonard, B.E. Effects of the GABA agonist THIP (gaboxadol) on trimethyltin-induced behavioural neurotoxicity in the rat. *Med. Sci. Res.* **1994**, *22*, 201–202.
39. Shuto, M.; Seko, K.; Kuramoto, N.; Sugiyama, C.; Kawada, K.; Yoneyama, M.; Nagashima, R.; Ogita, K. Activation of c-Jun N-Terminal Kinase Cascades Is Involved in Part of the Neuronal Degeneration Induced by Trimethyltin in Cortical Neurons of Mice. *J. Pharmacol. Sci.* **2009**, *109*, 60–70. [CrossRef]
40. Gunasekar, P.; Li, L.; Prabhakaran, K.; Eybl, V.; Borowitz, J.L.; Isom, G.E. Mechanisms of the Apoptotic and Necrotic Actions of Trimethyltin in Cerebellar Granule Cells. *Toxicol. Sci.* **2001**, *64*, 83–89. [CrossRef]
41. Zimmer, L.; Woolley, D.; Chang, L. Does phenobarbital protect against trimethyltin-induced neuropathology of limbic structures? *Life Sci.* **1985**, *36*, 851–858. [CrossRef]
42. Kabir, T.; Uddin, S.; Al Mamun, A.; Jeandet, P.; Aleya, L.; Mansouri, R.A.; Ashraf, G.M.; Mathew, B.; Bin-Jumah, M.N.; Abdel-Daim, M.M. Combination Drug Therapy for the Management of Alzheimer's Disease. *Int. J. Mol. Sci.* **2020**, *21*, 3272. [CrossRef] [PubMed]
43. Martin, B.S.; Kapur, J. A combination of ketamine and diazepam synergistically controls refractory status epilepticus induced by cholinergic stimulation. *Epilepsia* **2007**, *49*, 248–255. [CrossRef]
44. Niquet, J.; Baldwin, R.; Norman, K.; Suchomelova, L.; Lumley, L.; Wasterlain, C.G. Midazolam-ketamine dual therapy stops cholinergic status epilepticus and reduces Morris water maze deficits. *Epilepsia* **2016**, *57*, 1406–1415. [CrossRef]
45. Shakarjian, M.P.; Ali, M.S.; Velíšková, J.; Stanton, P.K.; Heck, D.E.; Velíšek, L. Combined diazepam and MK-801 therapy provides synergistic protection from tetramethylenedisulfotetramine-induced tonic–clonic seizures and lethality in mice. *NeuroToxicology* **2015**, *48*, 100–108. [CrossRef]

46. Ellison, G. The N-methyl-d-aspartate antagonists phencyclidine, ketamine and dizocilpine as both behavioral and anatomical models of the dementias. *Brain Res. Rev.* **1995**, *20*, 250–267. [CrossRef]
47. Kanto, J.H. Midazolam: The First Water-soluble Benzodiazepine; Pharmacology, Pharmacokinetics and Efficacy in Insomnia and Anesthesia. *Pharmacother. J. Hum. Pharmacol. Drug Ther.* **1985**, *5*, 138–155. [CrossRef] [PubMed]
48. Morris, R.G.M.; Garrud, P.; Rawlins, J.N.P.; O'Keefe, J. Place navigation impaired in rats with hippocampal lesions. *Nat. Cell Biol.* **1982**, *297*, 681–683. [CrossRef] [PubMed]
49. Kochli, D.E.; Thompson, E.C.; Fricke, E.A.; Postle, A.F.; Quinn, J.J. The amygdala is critical for trace, delay, and contextual fear conditioning. *Learn. Mem.* **2015**, *22*, 92–100. [CrossRef] [PubMed]
50. Maren, S.; Fanselow, M.S. Electrolytic Lesions of the Fimbria/Fornix, Dorsal Hippocampus, or Entorhinal Cortex Produce Anterograde Deficits in Contextual Fear Conditioning in Rats. *Neurobiol. Learn. Mem.* **1997**, *67*, 142–149. [CrossRef] [PubMed]
51. Bahník, Š. Carousel Maze Manager (Version 0.4.0) [Software]. 2014. Available online: https://github.com/bahniks/CM_Manager_0_4_0 (accessed on 21 April 2015).
52. Vorhees, C.V.; Williams, M.T. Morris water maze: Procedures for assessing spatial and related forms of learning and memory. *Nat. Protoc.* **2006**, *1*, 848–858. [CrossRef] [PubMed]
53. Whiting, M.D.; Kokiko-Cochran, O.N. Assessment of cognitive function in the water maze task: Maximizing data collection and analysis in animal models of brain injury. In *Injury Models of the Central Nervous System: Methods and Protocols, Methods in Molecular Biology*; Kobeissy, F., Ed.; Springer Science + Business Media: New York, NY, USA, 2016; Volume 1462, pp. 553–571.
54. Mátéffyová, A.; Otáhal, J.; Tsenov, G.; Mareš, P.; Kubová, H. Intrahippocampal injection of endothelin-1 in immature rats results in neuronal death, development of epilepsy and behavioral abnormalities later in life. *Eur. J. Neurosci.* **2006**, *24*, 351–360. [CrossRef] [PubMed]
55. Rustay, N.; Browman, K.; Curzon, P. Cued and Contextual Fear Conditioning for Rodents. In *Methods of Behavior Analysis in Neuroscience*, 2nd ed.; CRC Press/Taylor & Francis: Boca Raton, FL, USA, 2008; pp. 19–37.
56. Krsek, P.; Mikulecká, A.; Druga, R.; Kubová, H.; Hliňák, Z.; Suchomelová, L.; Mareš, P. Long-term behavioral and morphological consequences of nonconvulsive status epilepticus in rats. *Epilepsy Behav.* **2004**, *5*, 180–191. [CrossRef] [PubMed]
57. Paxinos, G.; Watson, C. *The Rat Brain in Stereotaxic Coordinates*, 6th ed.; Academic Press: London, UK, 2007.
58. Latini, L.; Geloso, M.C.; Corvino, V.; Giannetti, S.; Florenzano, F.; Viscomi, M.T.; Michetti, F.; Molinari, M. Trimethyltin intoxication up-regulates nitric oxide synthase in neurons and purinergic ionotropic receptor 2 in astrocytes in the hippocampus. *J. Neurosci. Res.* **2009**, *88*, 500–509. [CrossRef] [PubMed]
59. Florian, C.; Roullet, P. Hippocampal CA3-region is crucial for acquisition and memory consolidation in Morris water maze task in mice. *Behav. Brain Res.* **2004**, *154*, 365–374. [CrossRef]
60. Hunsaker, M.R.; Rosenberg, J.S.; Kesner, R.P. The role of the dentate gyrus, CA3a,b, and CA3c for detecting spatial and environmental novelty. *Hippocampus* **2008**, *18*, 1064–1073. [CrossRef]
61. West, M.J.; Slomianka, L.; Gundersen, H.J.G. Unbiased stereological estimation of the total number of neurons in the subdivisions of the rat hippocampus using the optical fractionator. *Anat. Rec. Adv. Integr. Anat. Evol. Biol.* **1991**, *231*, 482–497. [CrossRef] [PubMed]
62. Dyer, R.S.; Deshields, T.L.; Wonderlin, W.F. Trimethyltin-induced changes in gross morphology of the hippocampus. *Neurobehav. Toxicol. Teratol.* **1982**, *4*, 141–147.
63. Meera, P.; Wallner, M.; Otis, T.S. Molecular basis for the high THIP/gaboxadol sensitivity of extrasynaptic GABAA receptors. *J. Neurophysiol.* **2011**, *106*, 2057–2064. [CrossRef]
64. Takahashi, H. Automated Measurement of Freezing Time to Contextual and Auditory Cues in Fear Conditioning as a Simple Screening Method to Assess Learning and Memory Abilities in Rats. *J. Toxicol. Sci.* **2004**, *29*, 53–61. [CrossRef]
65. Gill, R.; Brazell, C.; Woodruff, G.N.; Kemp, J.A. The neuroprotective action of dizocilpine (MK-801) in the rat middle cerebral artery occlusion model of focal ischaemia. *Br. J. Pharmacol.* **1991**, *103*, 2030–2036. [CrossRef] [PubMed]
66. Mazzone, G.L.; Nistri, A. Modulation of extrasynaptic GABAergic receptor activity influences glutamate release and neuronal survival following excitotoxic damage to mouse spinal cord neurons. *Neurochem. Int.* **2019**, *128*, 175–185. [CrossRef]
67. Nelson, R.M.; Green, A.R.; Lambert, D.G.; Hainsworth, A.H. On the regulation of ischaemia-induced glutamate efflux from rat cortex by GABA;in vitrostudies with GABA, clomethiazole and pentobarbitone. *Br. J. Pharmacol.* **2000**, *130*, 1124–1130. [CrossRef] [PubMed]
68. Krüger, K.; Diepgrond, V.; Ahnefeld, M.; Wackerbeck, C.; Madeja, M.; Binding, N.; Musshoff, U. Blockade of glutamatergic and GABAergic receptor channels by trimethyltin chloride. *Br. J. Pharmacol.* **2005**, *144*, 283–292. [CrossRef] [PubMed]
69. Chang, L.W. Neuropathology of trimethyltin: A proposed pathogenetic mechanism. *Fundam. Appl. Toxicol.* **1986**, *6*, 217–232. [CrossRef]
70. Chang, L.W.; Dyer, R.S. Early effects of trimethyltin on the dentate gyrus basket cells: A morphological study. *J. Toxicol. Environ. Health Part A* **1985**, *16*, 641–653. [CrossRef] [PubMed]

Bioorganic Chemistry 107 (2021) 104596

Contents lists available at ScienceDirect

Bioorganic Chemistry

journal homepage: www.elsevier.com/locate/bioorg

Tacrine – Benzothiazoles: Novel class of potential multitarget anti-Alzheimeŕs drugs dealing with cholinergic, amyloid and mitochondrial systems

Eugenie Nepovimova [a], Lucie Svobodova [b], Rafael Dolezal [a,c], Vendula Hepnarova [c,d], Lucie Junova [d], Daniel Jun [d], Jan Korabecny [c,d], Tomas Kucera [d], Zuzana Gazova [e], Katarina Motykova [e], Jana Kubackova [e], Zuzana Bednarikova [e], Jana Janockova [a,c], Catarina Jesus [f], Luisa Cortes [g], Joao Pina [f], Danijela Rostohar [h], Carlos Serpa [f], Ondrej Soukup [c], Laura Aitken [i], Rebecca E. Hughes [j], Kamil Musilek [a], Lubica Muckova [c,d], Petr Jost [c,d], Marketa Chvojkova [k], Karel Vales [k], Martin Valis [c,l], Zofia Chrienova [a], Katarina Chalupova [a,c], Kamil Kuca [a,*]

[a] Department of Chemistry, Faculty of Science, University of Hradec Kralove, Rokitanskeho 62, 500 03 Hradec Kralove, Czech Republic
[b] Department of Pharmaceutical Chemistry and Pharmaceutical Analysis, Faculty of Pharmacy in Hradec Kralove, Charles University in Prague, Heyrovskeho 1203, 500 05 Hradec Kralove, Czech Republic
[c] Biomedical Research Centre and Department of Neurology, University Hospital Hradec Kralove, Sokolska 581, 500 05 Hradec Kralove, Czech Republic
[d] Department of Toxicology and Military Pharmacy, Faculty of Military Health Sciences, University of Defence, Trebesska 1575, 500 01 Hradec Kralove, Czech Republic
[e] Department of Biophysics, Institute of Experimental Physics, Slovak Academy of Sciences, Watsonova 47, 040 01 Kosice, Slovak Republic
[f] Centro de Quimica de Coimbra, Department of Chemistry, University of Coimbra, 3044-535 Coimbra, Portugal
[g] Center for Neuroscience and Cell Biology, University of Coimbra, 3004-504 Coimbra, Portugal
[h] HiLASE Centre, Institute of Physics, Czech Academy of Sciences, Za Radnici 828, 252 41 Dolni Brezany, Czech Republic
[i] School of Biology, Medical and Biological Sciences Building, University of St. Andrews, North Haugh, St. Andrews KY16 9ST, United Kingdom
[j] Cancer Research UK Edinburgh Centre, MRC Institute of Genetics and Molecular Medicine, Western General Hospital, University of Edinburgh, Edinburgh EH4 2XU, United Kingdom
[k] National Institute of Mental Health, Topolova 748, 250 67 Klecany, Czech Republic
[l] Faculty of Medicine in Hradec Kralove, Charles University in Prague, Simkova 870/13, 500 03 Hradec Kralove, Czech Republic

ARTICLE INFO

Keywords:
Alzheimer's disease
Tacrine
Benzothiazole
Acetylcholinesterase Inhibitors
Amyloid β
ABAD
MTDLs

ABSTRACT

A series of tacrine – benzothiazole hybrids incorporate inhibitors of acetylcholinesterase (AChE), amyloid β (Aβ) aggregation and mitochondrial enzyme ABAD, whose interaction with Aβ leads to mitochondrial dysfunction, into a single molecule. *In vitro*, several of 25 final compounds exerted excellent anti-AChE properties and interesting capabilities to block Aβ aggregation. The best derivative of the series could be considered **10w** that was found to be highly potent and selective towards AChE with the IC_{50} value in nanomolar range. Moreover, the same drug candidate exerted absolutely the best results of the series against ABAD, decreasing its activity by 23% at 100 μM concentration. Regarding the cytotoxicity profile of highlighted compound, it roughly matched that of its parent compound – 6-chlorotacrine. Finally, **10w** was forwarded for *in vivo* scopolamine-induced amnesia

Abbreviations: 7-MEOTA, 7-methoxytacrine; AFM, atomic force microscopy; Aβ, amyloid β; ABAD, amyloid β – binding alcohol dehydrogenase; ACh, acetylcholine; AChE, acetylcholinesterase; AChEIs, acetylcholinesterase inhibitors; AD, Alzheimer's disease; ATC, acetylthiocholine; BBB, blood-brain barrier; BChE, butyrylcholinesterase; BTC, butyrylthiocholine; BTZ, 2-aminobenzothiazole; CAS, catalytic active site; CHO-K1, Chinese hamster ovary cell line; CNS, central nervous system; DIPEA, *N*,*N*-diisopropylethylamine; DMEM, Dulbecco's modified Eagle's medium; DMF, dimethylformamide; DTNB, 5,5́-dithiobis(2-nitrobenzoic acid), Ellmańs reagent; *h*AChE, human acetylcholinesterase; *h*BChE, human butyrylcholinesterase; HepG2, human hepatocellular carcinoma cell line; HRMS, high-resolution mass spectra; i.p., intraperitoneally; MFD, maximum feasible dose; MOPS, 3-(*N*-morpholino)-propanesulfonic acid; MTD, maximum tolerated dose; MTDL, multitarget-directed ligand; MTT, 3-(4,5-dimethylthiazol-2-yl)-2,5-diphenyltetrazolium bromide; MWM, Morris Water Maze; PAMPA-BBB, parallel artificial membrane permeation assay for the BBB; PAS, peripheral anionic site; PBL, polar brain lipid; PBS, phosphate buffer solution; P_e, permeability; ppm, parts per million; scop, scopolamine; SEM, standard error of the mean; SI, selectivity index; THA, tacrine; ThT, thioflavin T; t_{lag}, length of the lag time.

* Corresponding author.
E-mail address: kamil.kuca@uhk.cz (K. Kuca).

https://doi.org/10.1016/j.bioorg.2020.104596
Received 11 October 2020; Received in revised form 30 November 2020; Accepted 22 December 2020
Available online 28 December 2020

experiment consisting of Morris Water Maze test, where it demonstrated mild procognitive effect. Taking into account all *in vitro* and *in vivo* data, highlighted derivative **10w** could be considered as the lead structure worthy of further investigation.

1. Introduction

Alzheimer's disease (AD) is currently incurable neurodegenerative condition and one of the greatest health-care challenges of the 21st century. In 2013, the "Group of Eight" countries stated that dementia should be made a global priority with a presumptuous ambition of discovery of the cure or disease-modifying therapy by 2025 [1]. People suffering from AD usually exert memory impairment, executive dysfunction interfering with the activities of daily living, and finally progressing dependency on others for care. According to the Alzheimer's Association, 13% of people over 65 suffer from this disease in developed countries, where it is the fifth leading cause of death in patients at this age [2]. Pursuant to the World Health Organization estimates, the overall projected prevalence in global population will quadruple in the next decades, reaching 114 million patients by 2050 [3]. Apart from having a significant social impact, this would clearly lead to increased economic burden to healthcare systems worldwide.

In spite of large gains in our understanding of AD pathogenesis and how the disease is conceptualized, there are still striking gaps mainly in diagnosis, ethiology and available therapy. Since the uncompromising trigger of the disease is still elusive, several hypotheses have been put forward based on the various causative factors in order to explain this disorder. Efforts to identify which changes in the CNS play the major role in AD pathogenesis pointed out on pharmacological interference with cholinergic function suggested a strong relationship between acetylcholine-mediated neurotransmission and cognitive function. Following afore-mentioned studies, the cholinergic hypothesis of Alzheimer's disease has been evolved [4]. Seminal work on cholinergic hypothesis of AD by Bartus *et al.* in 1982 was the stimulus for a great deal of effort in experimental pharmacology and in a large number of clinical trials. Such endeavor bore the fruit in the form of approved drugs – tacrine, donepezil, rivastigmine and galantamine [5]. Although aforesaid paragraph has pointed out to a fact that cholinergic neurotransmission is affected by AD, it is no longer widely believed that the cholinergic depletion alone is responsible for causing AD.

The credibility of cholinergic hypothesis as the only theory explaining the ethiopathogenesis of AD was undermined by purification of amyloid β (Aβ) from the neuritic plaques. This discovery set the premise for the amyloid cascade hypothesis, which revolves around an imbalance in Aβ peptide metabolism followed by its aggregation and deposition in plaques as the major cause of neuronal death and dysfunction leading to dementia [6–7]. Additionally, a considerable evidence gained over the past decades has supported the idea that the neurons overexpressing amyloid precursor protein are more vulnerable to oxidative stress, mitochondrial dysfunction and apoptosis [8]. Passing the Aβ-channel in the cytoplasmic membrane, Aβ binds to a specific carrier called amyloid β-binding alcohol dehydrogenase (ABAD, EC 1.1.1.51) to reach mitochondria [9]. Such coupling modifies the permeability of mitochondrial membranes [10]. In mitochondrial matrix Aβ binds again to ABAD and presumably this interaction results in the mitochondrial dysfunction [11]. In healthy brain, ABAD functions as a vital energy regulator within the mitochondria, containing a Rossman fold that acts to oxidize alcohols and reduce aldehydes and ketones [12]. The interaction between Aβ and ABAD inhibits enzymes physiological functions, leading eventually to oxidative burden. The latter information points out to the fact that the original version of amyloid cascade hypothesis, prevailing for the last two decades and having much of experimental support, does not account for the complexity of the disease. Thus, such lack of complexity recognized in basic and clinical trials caused a shift from the simple assumption of linear causality as proposed in the original amyloid cascade hypothesis to the multifactorial nature of the disease that involves multiple biological pathways.

Successful introduction of L-DOPA for Parkinsons disease therapy had a significant impact on the AD therapy research field. Such discovery opened the way for so-called "neurotransmitter replacement" therapies for neurodegenerative diseases and led to development of the leading class of drugs currently approved for AD treatment, i.e. acetylcholinesterase inhibitors (AChEIs) [13]. This concept was additionally supported by the evidence of amnestic effect of anticholinergic drugs, such as scopolamine, in experimental and human studies [14]. AChEIs act by enhancing cholinergic neurotransmission through the inhibition of enzyme acetylcholinesterase (AChE, EC 3.1.1.7), thus decreasing the breakdown of ACh. There have been four, equally effective, AChEIs approved for the symptomatic treatment of AD: tacrine, donepezil, rivastigmine and galantamine [15]. Unfortunately, none of these drugs is capable of reversing the course of AD nor of even appreciably slowing down the rate of disease progression. Their clinical effect is largely palliative, however, their potential use in combination therapy with other disease-modifying compounds should not be excluded [16].

As it has been mentioned above, "one-target, one-molecule" therapeutic strategy is unlikely to help in multifactorial diseases such as AD. Moreover, the cells can often find ways to compensate for a protein whose activity is affected by a drug [17]. Thus, "multitarget-directed ligand" (MTDL) paradigm has been formulated aiming on therapeutics that hit more than one target simultaneously [18]. This approach normally involves the use of two or more different pharmacophore moieties (in most cases, at least one is directly related to AChEIs being a pillar of standard AD therapy) to include into a single framework [19].

2. Design

There exists a long-established relationship between Aβ aggregation and AChE activity [20]. Namely, Aβ-AChE complexes trigger neurodegeneration much more intensively than Aβ alone, acting as a chaperone protein which increases the toxicity of Aβ peptide [21–22]. More recently, many evidences have indicated that the increased neurotoxicity of Aβ-AChE complexes is probably related to a more rapid and non-reversible increase in mitochondrial dysfunction or to some direct effects at a mitochondrial viability level [23].

In the study presented herein, we turned our attention to compounds combining tacrine scaffolds with benzothiazole moieties in order to obtain MTDLs acting as triple inhibitors of AChE activity, Aβ aggregation and mitochondrial dysfunction via ABAD activity modulation (Chart 1). To get at least partial proof-of-concept, several derivatives (**10a**, **10c**, **10e**, **10 g**) have been already tested by our group for their potential to inhibit amyloid aggregation in hen egg white lysozyme [24]. This study pointed out to a significant improvement in inhibitory activity of novel compounds comparing to parent building blocks. Such positive finding pushed our group to extend the series with more derivatives.

The story of tacrine (1,2,3,4-tetrahydroacridin-9-amine, THA, Chart 1) started already in the middle of 20th century, however, only in the 1980s, THA was rediscovered by William Summers who hypothesized that it may be of benefit in treating the early stages of AD [25–27]. Thus, THA became the first of four AChEIs approved for treating this type of dementia. However, due to its clinical shortcomings instigating hepatotoxicity, the use of tacrine was limited soon after its inception in therapeutic application [28]. In this regard, development of tacrine derivatives lacking the aforementioned drawback has drawn significant attention in last three decades [29]. On the other hand, the main trumps

of THA as a relevant lead scaffold in the field of medicinal chemistry include: its easy commercial accessibility, drug-like properties, low molecular weight and cholinesterase inhibitory potential at nanomolar concentration. For design of our compounds we have decided to utilize not only non-substituted tacrine moiety, but also two other tacrine derivatives – 7-methoxytacrine (7-MEOTA, Chart 1) and 6-chlorotacrine (Chart 1). The former represents a class of tacrine-like compounds with safer pharmacological profile, since Phase I of clinical trials with 7-MEOTA did not disclose any sign of hepatotoxicity [30]. The latter analogue – 6-chlorotacrine - belongs among tacrine derivatives with more favorable inhibitory effect on AChE comparing to its parent compound [31].

Benzothiazole scaffold belongs to a class of heterocyclic two-ring systems consisting of benzene ring fused with a thiazole moiety. From the physical–chemical properties point of view, benzothiazole fragment is planar, aromatic lacking rotatable bonds, thus, it is able to interact with various proteins as hydrogen-bond acceptor and at the same time as electron-density acceptor within $\pi - \pi$ non-bonding complexes. This motif takes up its honorary place in medicinal chemistry, since it exhibits various biological activities such as antitumor, antidiabetic, antitubercular, antibacterial etc. [32]. For us, however, the most interesting are those benzothiazole compounds with potential anti-AD application. Due to similarity with Thioflavin T dye, the majority of them are used as diagnostic tools to detect Aβ. Fewer publications are devoted to benzothiazole-containing anti-AD therapeutics: some of them have been designed as ABAD modulators, others as multitarget ligands affecting cholinergic and amyloid pathways simultaneously [33–37].

Several scientific groups have already published tacrine – benzothiazole hybrids with various linkers. Huang and colleagues described such derivatives with a phenyl linker [35]. They tested them towards both cholinesterases and for their potential to inhibit Aβ self-aggregation. Keri *et al.* designed a series of tacrine – benzothiazoles linked by an amide spacer confronting AChE, Aβ aggregation and reactive oxygen species [34]. Finally, Rajeshwari and coworkers synthesized tacrine – phenylbenzothiazole heterodimers in order to obtain dual inhibitors of AChE and Aβ aggregation [36]. Considering moderate to good AChE inhibitory potential and average inhibition of Aβ aggregation exerted by aforementioned compounds we may prioritize our tacrine – benzothiazole hybrids, since they proved better results from both aspects and, moreover, they demonstrated their potential in mitochondrial dysfunction inhibition via ABAD activity modulation.

Within our study, firstly, we have synthesized the 1st generation of tacrine – benzothiazoles (**10a-10v**) in order to ascertain which linker and tacrine moiety are the most appropriate in terms of all three proteins, i.e. AChE, Aβ and ABAD. The results of cytotoxicity and blood–brain barrier penetration have been taken into account as well. Within the 2nd generation (**10v-10y**), the only variable parameter has been substitution on 6-position of benzothiazole ring in order to obtain even more potent representatives than in the 1st generation.

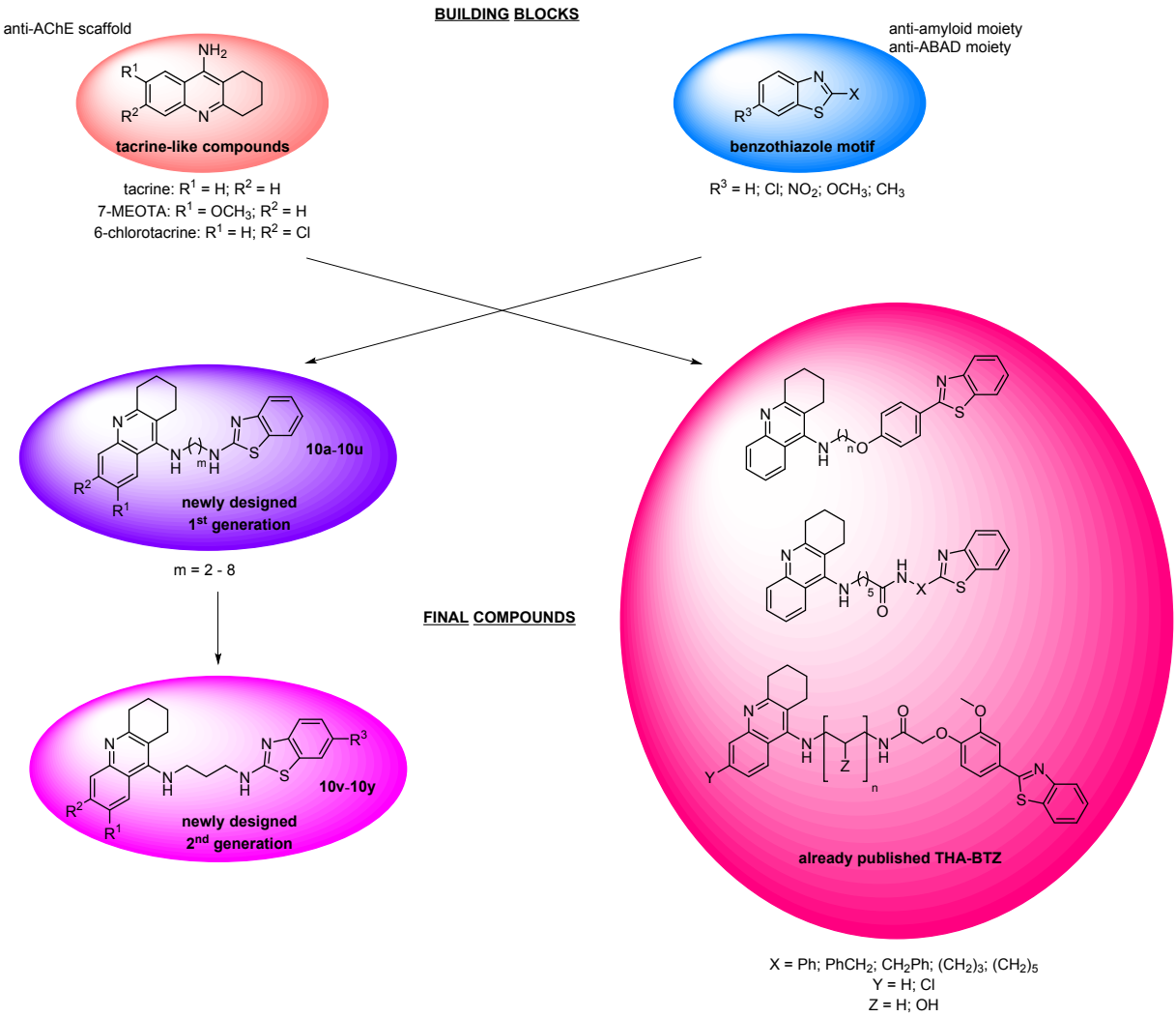

Chart 1. Design strategy toward tacrine – benzothiazoles **10a-10y.**

3. Results and discussion

3.1. Chemistry

Tacrine – benzothiazole hybrids (**10a-10y**) were synthesized via three- or four-step sequence from commercially available 2-chloro-1,3-benzothiazoles (**5**–**9**) and tacrine intermediates (**4a-4u**) (Scheme 1a). 9-Chlorotacrines (**1**–**3**) were obtained as reported in the literature [38]. Subsequent reaction of **1**–**3** with α,ω-diaminoalkanes gave key intermediates (**4a-4u**) in good yields (70 – 90%) [39–40]. Such intermediates were further utilized for the synthesis of final products (**10a-10y**) by coupling with unsubstituted 2-chloro-1,3-benzothiazole (**5**) (1st generation) or 6-position substituted 2-chloro-1,3-benzothiazoles (**6**–**9**) (2nd generation) in the presence of *N*,*N*-diisopropylethylamine (DIPEA) in dimethylformamide (DMF). Finally, novel tacrine – benzothiazoles (**10a-10y**) were characterized in the form of hydrochloride salts through their spectroscopic (^{1}H and ^{13}C NMR), HRMS and melting point data. Hydrochloride salts were also used for the activity profile assessment.

3.2. In vitro inhibition of human cholinesterases

As was mentioned above, the mode of action of the most frequently used drugs against AD is AChE inhibition. However, apart from AChE, butyrylcholinesterase (BChE, EC 3.1.1.8) could also represent a target of interest, inasmuch as this enzyme exerts a compensatory effect in response to a greatly decreased AChE activity in CNS when AD progresses [41]. Due to this fact, all target compounds were evaluated for their potential to inhibit both cholinesterases by following Ellmańs spectrophotometric method using human recombinant AChE (*h*AChE) and human plasma BChE (*h*BChE) [42]. Tacrine, 7-MEOTA and 6-chlorotacrine were used as reference compounds. 2-Aminobenzothiazole (BTZ) was found to be inactive. Experimental results, presented as IC_{50} values, i.e. concentration that reduces cholinesterase activity by 50%, as well as selectivity indexes (SI) are summarized in Table 1.

Regarding the 1st generation of tacrine – benzothiazoles (**10a-10u**), all of them turned out to be potent *h*AChE inhibitors with the IC_{50} values in micromolar to nanomolar range. Considering the general structure variations, two main modifications could be highlighted: 1) substitution on tacrine scaffold and/or 2) spacer length between two pharmacophores. In line with the expected binding mode of prepared molecules along the active site gorge of AChE, [31,39,43] hybrids bearing 7-methoxytacrine moiety (**10a-10 g**) displayed the poorest inhibitory potential towards *h*AChE, heterodimers derived from non-substituted tacrine (**10 h-10n**) showed moderate results, whereas analogues with 6-chlorotacrine core (**10o-10u**) proved to be the best *h*AChE inhibitors of the 1st generation. From the point of view of the second varying parameter – tether length, the results showed no linear relationship

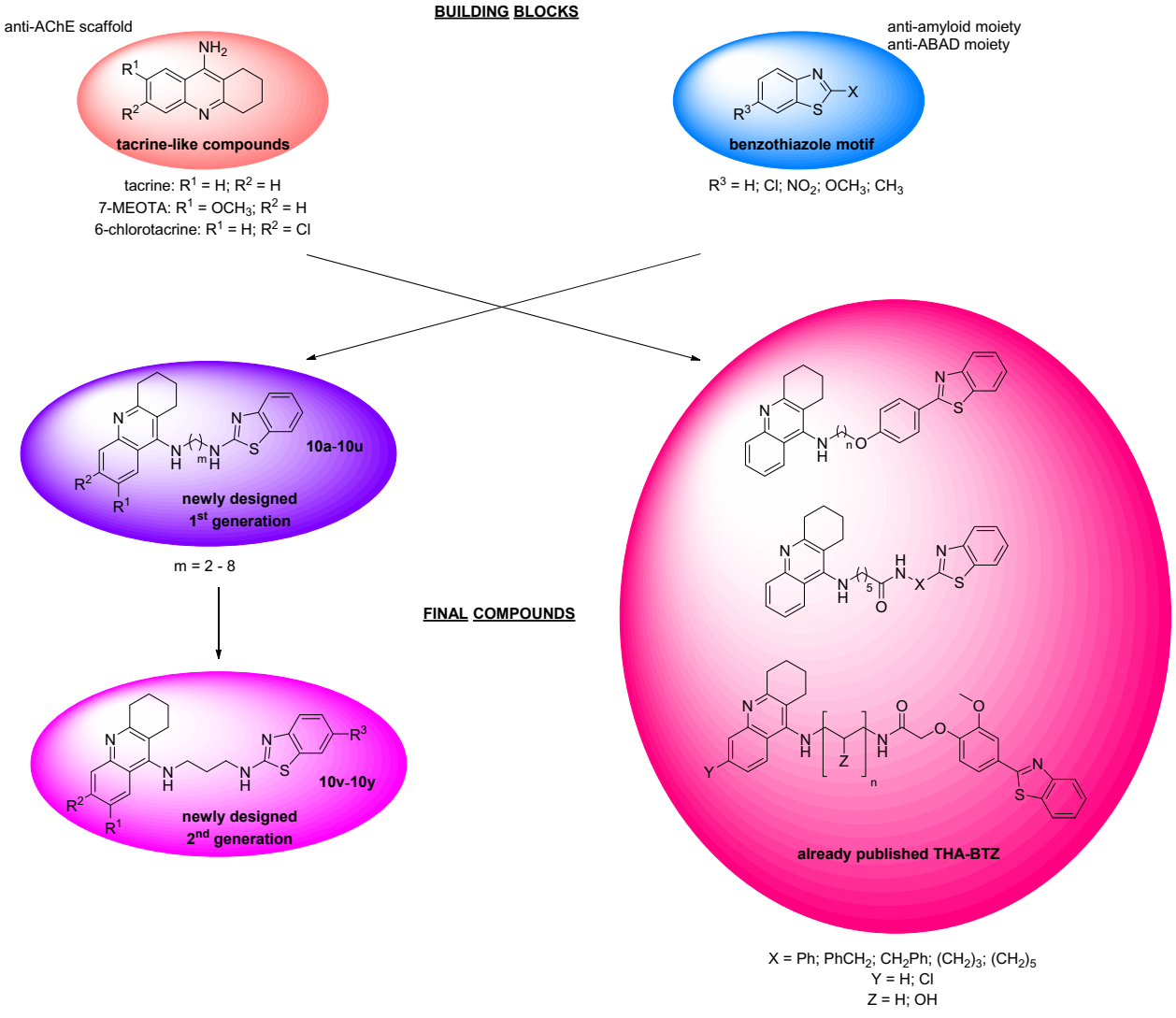

Scheme 1a. Synthesis of tacrine – benzothiazole hybrids **10a-y.**

Table 1
In Vitro results of tacrine – benzothiazole hybrids **10a**-**10y** and reference compounds.

Compound	IC_{50} *h*AChE ± SEM (nM)[a]	IC_{50} *h*BChE ± SEM (nM)[a]	SI (*h*BChE/*h*AChE)[b]	IC_{50} Aβ_{40} (μM)[a]	% of remaining ABAD activity ± SEM (100 μM)[a]	IC_{50} CHO-K1 ± SEM (μM)[a]
10a	34 660 ± 4 330	1 340 ± 55	0.04	161.1	99.44 ± 1.50	33.2 ± 5.06
10b	10 360 ± 929	196 ± 6	0.02	392.4	101.57 ± 2.71	36.7 ± 7.54
10c	12 190 ± 783	462 ± 13	0.04	11.5	103.71 ± 2.55	27.5 ± 2.01
10d	3 918 ± 324	1 595 ± 23	0.41	76.9	102.37 ± 2.11	12.8 ± 3.65
10e	1 265 ± 226	417 ± 20	0.33	28.3	109.32 ± 3.21	8.47 ± 0.54
10f	33 630 ± 17 090	4 188 ± 84	0.12	20.3	107.91 ± 4.01	5.64 ± 0.39
10g	2 823 ± 361	1 608 ± 60	0.57	41.3	110.93 ± 3.75	5.33 ± 0.45
10h	671 ± 34	64 ± 1	0.09	63.1	104.82 ± 3.05	36.9 ± 3.24
10i	1 727 ± 76	8 ± 0.2	0.005	84.2	107.22 ± 3.10	105 ± 3.2
10j	525 ± 22	24 ± 2	0.04	133.4	102.81 ± 4.12	41.5 ± 3.51
10k	854 ± 37	11 ± 1	0.01	46.0	90.90 ± 3.21	27.0 ± 3.59
10l	136 ± 6	20 ± 1	0.14	59.5	83.33 ± 5.95	11.2 ± 1.41
10m	89 ± 2	43 ± 2	0.44	21.8	106.23 ± 3.48	7.87 ± 0.39
10n	68 ± 2	483 ± 10	6.86	40.1	110.27 ± 2.82	6.92 ± 0.46
10o	4 ± 0.3	799 ± 37	200.00	39.3	103.20 ± 2.30	18.4 ± 1.63
10p	55 ± 2	41 ± 3	0.67	50.2	105.13 ± 2.10	42.0 ± 3.29
10q	15 ± 1	382 ± 16	38.00	74.5	106.60 ± 3.68	24.1 ± 0.09
10r	18 ± 0.2	49 ± 1	2.50	117.9	108.09 ± 3.44	18.0 ± 2.87
10s	9 ± 0.4	259 ± 11	28.89	34.3	111.41 ± 3.27	11.4 ± 2.33
10t	16 ± 0.4	270 ± 10	13.50	89.5	110.33 ± 2.11	20.1 ± 0.12
10u	18 ± 1	1 325 ± 41	66.50	44.9	113.79 ± 3.06	31.0 ± 3.89
10v	32 ± 3	1 859 ± 75	58.09	14.3	93.11 ± 3.08	21.4 ± 1.05
10w	18 ± 1	4 657 ± 428	258.72	3.8	77.85 ± 1.03	25.4 ± 4.73
10x	8 ± 1	902 ± 93	112.75	19.0	87.25 ± 3.80	38.5 ± 1.39
10y	25 ± 3	840 ± 57	33.60	24.0	95.02 ± 7.28	15.3 ± 1.70
tacrine	320 ± 13	88 ± 1	0.68	735.1	n.d.	248.0 ± 11.0
7-MEOTA	10 000 ± 975	17 560 ± 795	1.76	454.3	n.d.	63.0 ± 4.12
6-chlorotacrine	18 ± 1	1 727 ± 98	100.68	170.0	n.d.	71.2 ± 2.39
BTZ	167 100 ± 46 120	> 1 000 000	n.d.	n.d.	n.d.	> 1000

n.d. not determined.
[a] Results are expressed as the mean of at least three experiments.
[b] Selectivity for *h*AChE is determined as ratio IC_{50}(*h*BChE)/IC_{50}(*h*AChE).

between the linker length and the inhibitory activity across all tacrine subfamilies was observed. Overall, compound **10o** (IC_{50} = 4 ± 0.3 nM) was highlighted as the most potent *h*AChE inhibitor of the 1st generation. Additionally, **10o** even surpassed the inhibitory potential of its parent compound 6-chlorotacrine (IC_{50} = 18 ± 1 nM) more than four times. However, regardless aforesaid excellent results of **10o** towards *h*AChE, for further derivatization and subsequent synthesis of the compounds of the 2nd generation (**10v-10y**) has been selected derivative **10p** (IC_{50} = 55 ± 2 nM) due to its superiority also in other biological disciplines.

From the perspective of *h*BChE inhibition by target compounds of the 1st generation (**10a-10u**), the inhibitory power remained relatively similar as in the case of AChE ranging from micromolar to nanomolar concentration. Nevertheless, structure–activity relationship analysis revealed quite different findings from those obtained for *h*AChE. Considering tacrine motif modifications, the inhibitory potential towards *h*BChE dropped in case of 7-MEOTA derivatives (**10a-10 g**), slightly increased in 6-chlorotacrine heterodimers (**10o-10u**) and dramatically raised in dimers derived from non-substituted tacrine (**10 h-10n**). Concerning spacer length, no significant changes were observed with the exception of compounds with 3-carbon linker (e.g. **10b**, **10i**, **10p**) that belonged among the most active BChE inhibitors within each subfamily. The highest *h*BChE inhibition was achieved with compound **10i** (IC_{50} = 8 ± 0.2 nM), whose IC_{50} value fell in nanomolar range and overcame thus the inhibitory potential of its parent compound tacrine (IC_{50} = 88.1 ± 1.3 nM).

The importance of selectivity for one of two cholinesterase enzymes by the 1st generation of tacrine – benzothiazoles (**10a-10u**) deserves a comment as well. Considering the fact that the roles played by AChE and BChE in central cholinergic tone modulation vary with the disease progression, it is conceivable that selective AChE inhibitors would be more effective in the early stages of AD, while selective BChE inhibitors may be beneficial rather in moderate to severe forms of the disease. Synthesized tacrine – benzothiazoles (**10a-10u**) exhibited both types of selectivity, namely, compounds bearing 7-MEOTA (**10a-10 g**) and non-substituted tacrine (**10 h-10n**) scaffolds proved to be rather BChE selective inhibitors, whereas 6-chlorotacrine analogues (**10o-10u**) displayed rather AChE selective profile. Such finding is in a strong agreement with the selectivity of parent compounds pointing out to a fact that the decisive motif of prepared hybrids in the interaction with cholinesterases is rather tacrinés one.

Also all representatives of the 2nd generation of tacrine – benzothiazoles (**10v-10y**) were tested for their anti-cholinestesterase potential. These compounds showed an increasing efficacy towards *h*AChE, comparing to the parent compound **10p**, in the following order: -Cl < $–CH_3$ < $–NO_2$ < $–OCH_3$ (Table 1). The most active derivative **10x** with OCH_3 function (IC_{50} = 8 ± 1 nM) exceeded even the inhibitory concentration of 6-chlorotacrine which highlights the fact that chemical modification of the benzothioazole moiety has an important impact on the observed cholinesterase activity as well. Considering *h*BChE inhibition, the situation was found to be completely different in comparison to the parent compound **10p**, when the IC_{50} values of **10v** – **10y** raised pronouncedly. Selectivity, reflecting the results obtained above, pointed out to a strong preference to *h*AChE, similarly to 6-chlorotacrine. In view of excellent anti-cholinesterase selectivity and anti-amyloid profile, compound **10w** with nitro function in the benzothiazole part has been finally forwarded for further biological testing.

3.3. Molecular modeling study of *h*AChE inhibition

To predict the binding mode as well as binding affinity between the ligand and receptor and to gain deeper understanding of the structure–activity relationship for the *h*AChE inhibition by selected compound (**10w**), molecular docking study was conducted on the model of *h*AChE (PDB ID: 4EY7) using AutoDock Vina software [44–45]. Resulted complex of **10w** and *h*AChE is depicted in Fig. 1. In general, **10w** spans throughout the cavity gorge of the enzyme. By all accounts, 6-chlorotacrine moiety occupies the peripheral anionic site (PAS) of *h*AChE. Such finding is in contrast with previously published studies, where 6-chlorotacrine was anchored to the catalytic active site (CAS) of *h*AChE either as a single entity [46] or complexed into the hybrid compounds like pyrano[3,2-*c*]quinoline-6-chlorotacrine, [47] tetrahydrobenzo[*h*][1,6]naphthyridine-6-chlorotacrine series, [48] or tacrine-benzyl quinolone carboxylic acid hybrids [49]. On the other hand, in the scientific literature cases when 6-chlorotacrine-based compounds interact rather with PAS have also been described, e.g. tacrine-trolox hybrids or huprine-tacrine family [39,50–51]. A more detailed view on the PAS of AChE revealed that 1,2,3,4-tetrahydroacridine unit is sandwiched between Tyr122 (3.7 Å) and Trp286 (3.7 Å) via π-π stacking. The latter amino acid residue is considered as a crucial one since it participates on AChE-induced aggregation of Aβ [52]. Accordingly, based on this observation, it can be assumed that tacrine – benzothiazole hybrids by interaction with Trp286 could block Aβ-aggregation process mediated by AChE. Another critical interaction within the PAS region is cation-π formed between Tyr72 and protonated tacrine aromatic nitrogen (3.9 Å). In line with other methylene-tethered dual-binding inhibitors, [53–55] alkyl chain spacer between 2-amino-6-nitrobenzothiazole and 6-chlorotacrine pharmacophores stabilizes ligand anchoring by several

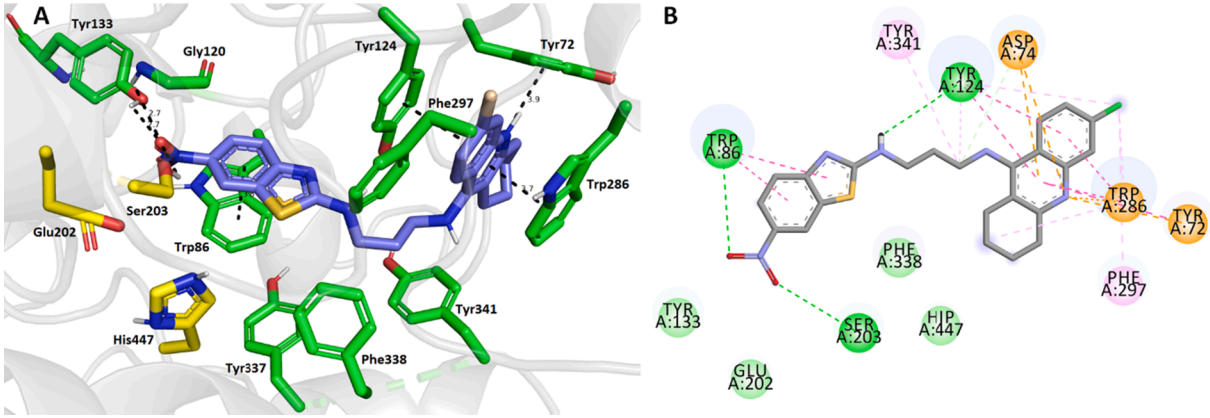

Fig. 1. Top-scored docking pose of **10w** in the *h*AChE active site (PDB ID: 4EY7). Close-up view is displayed either as 3D (A) or 2D (B) representation. In Fig. 1A, 10w is shown in blue, important amino acid residues in green and the catalytic triad in yellow. Dashed lines represent crucial intermolecular interactions of different origin (hydrogen bonds, π-π/π-cation stacking, van der Waal's interactions and other hydrophobic forces). Fig. 1A was created with the PyMOL Molecular Graphics System, Version 2.0 Schrödinger, LLC. Fig. 1B was rendered with Dassault Systèmes BIOVIA, Discovery Studio Visualizer, v 17.2.0.16349, San Diego: Dassault Systèmes, 2016. (For interpretation of the references to colour in this figure legend, the reader is referred to the web version of this article.)

distinct interactions, e.g. with Tyr341 (van der Waals), Tyr124 (hydrogen bond), Phe338 (van der Waals) or Asp74 (hydrogen-carbon bond). Regarding 2-amino-6-nitrobenzothiazole moiety, the study revealed that it is proximally lodged in CAS of AChE. Such accommodation enables face-to-face π-π interaction with Trp86 (3.6 Å). Presumably the most crucial motif being responsible for high inhibition ability of **10w** is nitro group which establishes hydrogen bonds with –OH of Tyr133 (2.7 Å), –NH- of Gly120 (oxyanion hole residue, 2.7 Å) and –OH of Ser203 (catalytic triad residue, 2.9 Å). Even though other catalytic triad residues (Glu202, His447) lie in a close proximity to **10w**, no significant enzyme – ligand interactions have been found.

3.4. Interaction with amyloid peptide

Aβ peptide is composed of 39 – 43 amino acids, 28 of which are extracellular and the remainder constitutes the transmembrane domain. Twelve amino acids are hydrophobic and confer on this molecule the ability to self-aggregate and polymerize into amyloid fibrils [56]. Two main forms of Aβ can be distinguished by electrophoresis, the shorter, 40 amino acid Aβ_{40} species, and the longer, 42 amino acid Aβ_{42} species. The Aβ_{40} form accounts for ~ 90% of all Aβ normally released by cells and it appears to contribute only to later phases of the disease pathology. The Aβ_{42} form accounts only for ~ 10% of secreted Aβ, however, it is the predominant form found in the amyloid plaques of AD. The Aβ_{42} peptide aggregates and polymerizes into amyloid fibrils more readily than the Aβ_{40} species, and these properties are thought to confer the peptides pathogenicity [57].

In the first phase of investigation all hybrids of the 1st generation (**10a-10u**) were screened for their inhibitory potential towards *in vitro* formation of Aβ_{40} fibrils using thioflavin T (ThT) fluorescence assay to assess various structural elements responsible for the inhibitory activity. This assay is based on a specific interaction between the fluorescent dye thioflavin T that binds to the β-sheets of assembled amyloid fibrils leading to a significant increase in fluorescence signal [58–59]. Therefore, the decrease in ThT fluorescence correlates with the activity of studied compounds to inhibit the formation of amyloid aggregates. For quantification of the inhibitory potential of studied compounds, the IC_{50} values (concentration of the compound causing half-maximal inhibition of Aβ_{40} fibrillization) were determined from fitted fluorescence values and are shown in Table 1. To allow a comparison of the results tacrine, 7-MEOTA, 6-chlorotacrine and 2-aminobenzothiazole were used as the reference compounds. Note, that the lack of activity of the reference compound BTZ shows that this scaffold by itself is unable to inhibit Aβ_{40} formation.

The analysis of the results reported in Table 1 revealed that all compounds of the 1st generation (**10a-10u**) effectively inhibited Aβ_{40} fibrillization with the IC_{50} values spanning from 11.5 to 392.4 μM. A subset bearing non-substituted tacrine moiety (**10 h-10n**) exerted the weakest inhibitory properties. Slightly more effective inhibition was obtained for a class represented by 7-methoxytacrine counterparts (**10a-10 g**). Uncompromisingly, the lowest IC_{50} values were calculated for a group of hybrids substituted with a 6-chlorotacrine scaffold (**10o-10u**). The similar fashion in inhibitory potency could be observed also across the reference compounds (tacrine < 7-MEOTA < 6-chlorotacrine). One would expect, the more planar molecule is, the better it prevents protein–protein interaction, however, the opposite is true. The obtained results suggest to rather favorable interactions of either 7-methoxy- or 6-chloro- substituents within the process of inhibition of Aβ_{40} fibrillization. Modification of the spacer length affected the ability of compounds to prevent Aβ_{40} fibril formation quite dramatically. Based on the IC_{50} values it seems that rather longer linkers (six, seven, eight methylene groups) represent an optimal distance between the two pharmacophores. Overall, all the target hybrids displayed better inhibitory profile towards Aβ_{40} fibrillization comparing to the reference compounds, highlighting derivative **10c**, bearing 7-methoxytacrine, 4-carbon linker and BTZ fragment, as the best representative of the 1st generation. Apart from hybrid **10c** also derivative **10p** was forwarded for more detailed investigation since it exerted the best cytotoxic profile of the first generation of tacrine – benzothiazole hybrids.

Within the next phase we focused on the study of the effect of **10c** and **10p** on Aβ_{42} self-aggregation process using steady-state fluorescence and microscopy techniques, since methods using ThT are known for limitations and false results [60]. Obtained results were compared with myricetin, a well-known natural polyphenol, which is widely used as a positive control for Aβ_{42} inhibition experiments [61]. For the purpose of this assay, a novel label-free manner to trigger amyloid formation, following the intrinsic visible autofluorescence of amyloid aggregates, was used [60]. Fig. 2a plots the fluorescence emission intensity at 430 nm followed during 32 h throughout the aggregation process of 25 μM Aβ_{42}, at pH 7.25 and 30 °C. At the excitation wavelength of 390 nm used, the aromatic residues of Aβ_{42} do not absorb and the fluorescence observed is attributed to the amyloid intrinsic fluorescence [62]. This florescence intensity growth over time sets a clear sigmoidal profile (see open squares in Fig. 2a). It is also possible to follow the Aβ_{42} fibril growth taking advantage on the fact that the scattering intensity is highly dependent on the particle size. As a consequence, the scattering properties of aggregates are significantly larger compared to monomers, and the formation of fibrils can be

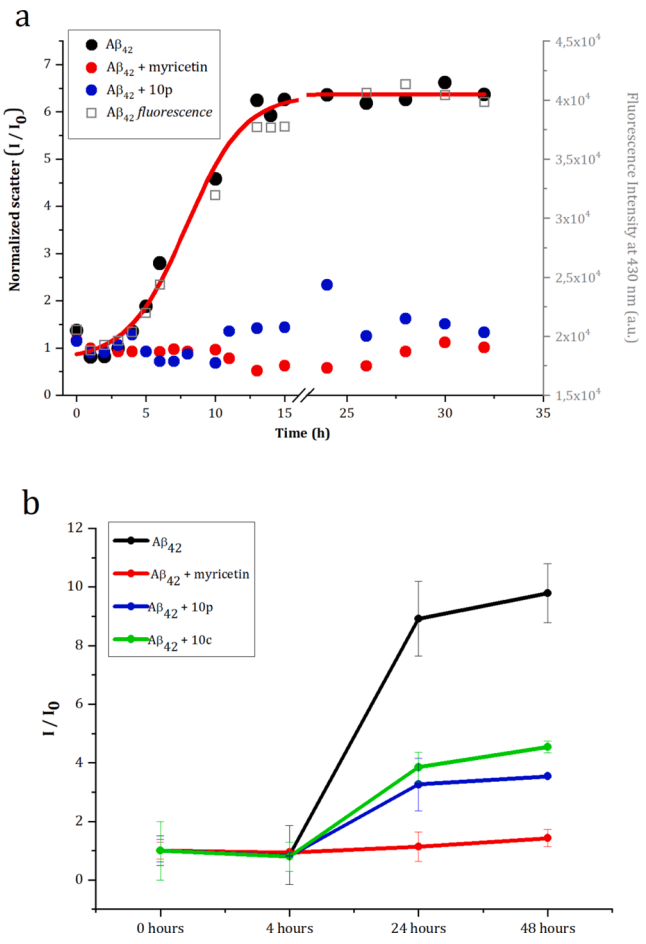

Fig. 2. a) Scatter measurements of Aβ_{42} (25 μM) in absence and in the presence of (10 μM) myricetin and **10p** at several time-points (t = 0–32 h) during the aggregation process. The open squares correspond to (auto)fluorescence measurements of Aβ_{42} (25 μM) at several time-points (t = 0–32 h) during the aggregation process. **b)** Scatter measurements of Aβ_{42} (25 μM) in absence and in the presence of (10 μM) myricetin, **10c** and **10p** at several time-points (t = 0, 4, 24, 48 h); each point corresponds to the average of three independent experiments. λ_{ex} = 550 nm for scatter measurements; λ_{ex} = 390 nm and λ_{em} = 430 nm for fluorescence experiments. Samples were incubated at 30 °C.

detected by following the increase in the scattered intensity during the time. Amyloid intrinsic fluorescence and scattering experiments report a similar aggregation pattern (Fig. 2a). The intrinsic amyloid fluorescence intensity concomitantly increases with the size of the aggregates in solution. An obstacle occurred when we tried to evaluate the inhibitory potential of tacrine – benzothiazole hybrids **10c** and **10p** by following the amyloid intrinsic fluorescence: **10c** and **10p** exhibited not only absorption (Fig. S1) but also intrinsic fluorescence (Fig. S2) in the wavelength range used for monitoring of the enhancement of the intrinsic visible autofluorescence originated from the Aβ_{42} pathogenic aggregation. Nevertheless, it was still possible to take an advantage of changes in the light scattering induced by Aβ_{42} aggregates by exciting and collecting the Rayleigh signal at 550 nm, where no absorption and fluorescence was observed from the aggregates and inhibitors. Fig. 2a and 2b display the measurements of scattered light intensity with time for 25 μM Aβ_{42} in the absence and presence of inhibitors at pH 7.25 and 30 °C. Acquired results show a sigmoidal profile (red curve in Fig. 2a) that is characterized by three kinetic steps: a lag phase, an exponential growth phase and a plateau phase. This trend is in agreement with previously described sigmoid curves obtained by circular dichroism and ThT assays [61,63]. The length of the lag time (t_{lag}) is approximately 7 h, reflecting the nucleation event when the initial size of Aβ_{42} molecules suffers only minor growth.

The second parameter that can be extracted from the kinetic curve is the rate of aggregation k (0.4 h^{-1}) which predicates the kinetics of polymerization event and thus the formation of Aβ_{42} aggregates and has duration of approximately 6 h. Finally, the plateau phase is defined by a beginning of fibril formation at 15 h. The Rayleigh scattering intensity of Aβ_{42} aggregates, in the presence of **10p**, **10c** and myricetin (Fig. 2b) decreased to a different extent. The scattering intensity of Aβ_{42} incubated in the presence of myricetin is relatively constant over time and there is no experimental evidence of an exponential growth phase. The inhibitory potency of myricetin was previously determined by ThT assay, where it was shown that 10 μM myricetin was able to inhibit the increase of ThT fluorescence signal related to 50 μM of Aβ_{42} aggregation almost completely (94%) [61]. Furthermore, the presence of this inhibitor shifted the t_{50} from 12.8 to 78.5 h. In the presence of tacrine – benzothiazole hybrid **10p**, the scattering intensity matched that one observed in the absence of the inhibitor in the first 4 h. Over the following time points the scattering intensity increases, although at a slower rate and reaching a plateau at lower intensities than the scattering intensity for Aβ_{42} alone. The average inhibition potency of **10p** was determined to be approximately 68 ± 9% at 10 μM (Fig. 3, 24 h).

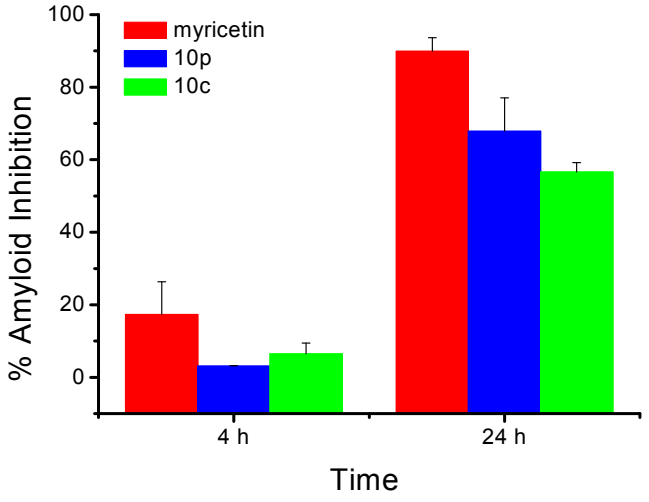

Fig. 3. Percentage of Aβ_{42} inhibition at different time points by tested inhibitors at 10 μM concentration. Note: % inhibition calculations =((I/I$_0$(Aβ_{42}) – I/I$_0$(Aβ_{42} + inhibitor))/ I/I$_0$(Aβ_{42})) × 100.

The second tested inhibitor, **10c**, was also studied from the point of view of inhibition of Aβ_{42} self-aggregation at specific time points. According to obtained results, **10c** is less effective against amyloid formation than **10p**, promoting a decrease in scattering intensity that corresponds to an inhibition percentage of 57 ± 1% at 10 μM (Fig. 3, 24 h).

In order to complement the above-mentioned results, the morphology and dimension of Aβ_{42} aggregates in the absence and in the presence of **10c**, **10p** and myricetin using the spinning-disk confocal microscopy was studied. The advantage of using spinning disk confocal microscopy is that the presence of the Yokogawa disk rejects the out-of-focus light that is emitted by the sample, allowing capturing information only from a reduced depth of focus. Additionally, the selective excitation absorption at 405 nm, contributed to the discriminatory detection of the autofluorescence of Aβ_{42} aggregates, without the interference of the fluorescence emitted by the inhibitors in solution. In order to follow the aggregation process, images were collected every 30 min, for 24 h (data shown for t = 0, 10 and 24 h; Fig. 4). The quantification of the percentage of area occupied by the aggregates over time for the first 10 h (Fig. 5) clearly shows that the overall assembly process is retarded and fibril formation is delayed in the presence of myricetin as well as **10c** and **10p** and that the inhibitory effect of these compounds is observed since the nucleation phase. Obtained results are thus in strong agreement with those gained by light-scattering analysis and validate those obtained from the ThT screening in the way that observed inhibitory potency is not an artefact or a false positive result.

In the last phase of investigation of the interaction between tacrine – benzothiazole hybrids and amyloid peptide, the 2nd generation of compounds (**10v-10y**) was screened for its ability to prevent Aβ_{40} fibril formation in the last phase. The IC_{50} values listed in Table 1 demonstrate that optimization of the prototype structure from the 1st generation brought the fruit. All the representatives of the 2nd generation proved to be more potent inhibitors of Aβ_{40} fibrillization than the 1st generation of hybrids, highlighting derivative **10w** as a compound with absolutely the best results of the series. Additionally, the effect of **10w** on Aβ_{40} fibrillization was examined using atomic force microscopy (AFM). The AFM images of 10 μM of Aβ_{40} fibrils alone (Fig. 6A) and in the presence of studied compound **10w** (Fig. 6B) proved the results obtained within the latter assay, revealing an extensive reduction in a number of fibrillar aggregates caused by tested compound treatment.

3.5. ABAD inhibition

ABAD, also known as 17β-hydroxysteroid dehydrogenase type 10, belongs among the proteins interacting directly with Aβ [64–65]. Such interaction promotes oxidative stress and mitochondrial dysfunction [11]. Furthermore, recent studies have detected elevated ABAD levels in the regions of the hippocampus and cerebral cortex which are generally affected by AD pathology [12,66]. All these and also other findings overwhelmingly confirmed that Aβ-ABAD interaction causes a cascade of events that eventually lead to neuronal damage, evoking a considerable interest in medicinal chemists as a potential target for AD treatment. Frentizole, a non-toxic antiviral and immunosuppressive drug approved by the FDA for rheumatoid arthritis and systemic lupus erythematosus, was identified as an Aβ-ABAD interaction inhibitor (97.9 ± 3.6% of remaining ABAD activity at 25 μM) using an ELISA-based screening assay [67,68]. Interestingly, frentizole bears benzothiazolyl urea moiety. Pursuant to this fact, tacrine – benzothiazole hybrids (**10a-10y**) were screened for their ability to inhibit mitochondrial enzyme ABAD at 100 μM concentration, using modified spectrophotometric assay [64]. The relative percent of remaining ABAD activity after treatment with tested compounds is given in Table 1.

In general, tacrine – benzothiazoles (**10a-10y**) did not significantly inhibit ABAD function, contrary the majority of them potentiated enzymés activity. Within the 1st generation, only compounds **10 k** and **10 l** induced a decrease in ABAD activity by 10% and 17%, respectively. Regarding the 2nd generation, all derivatives showed better inhibitory

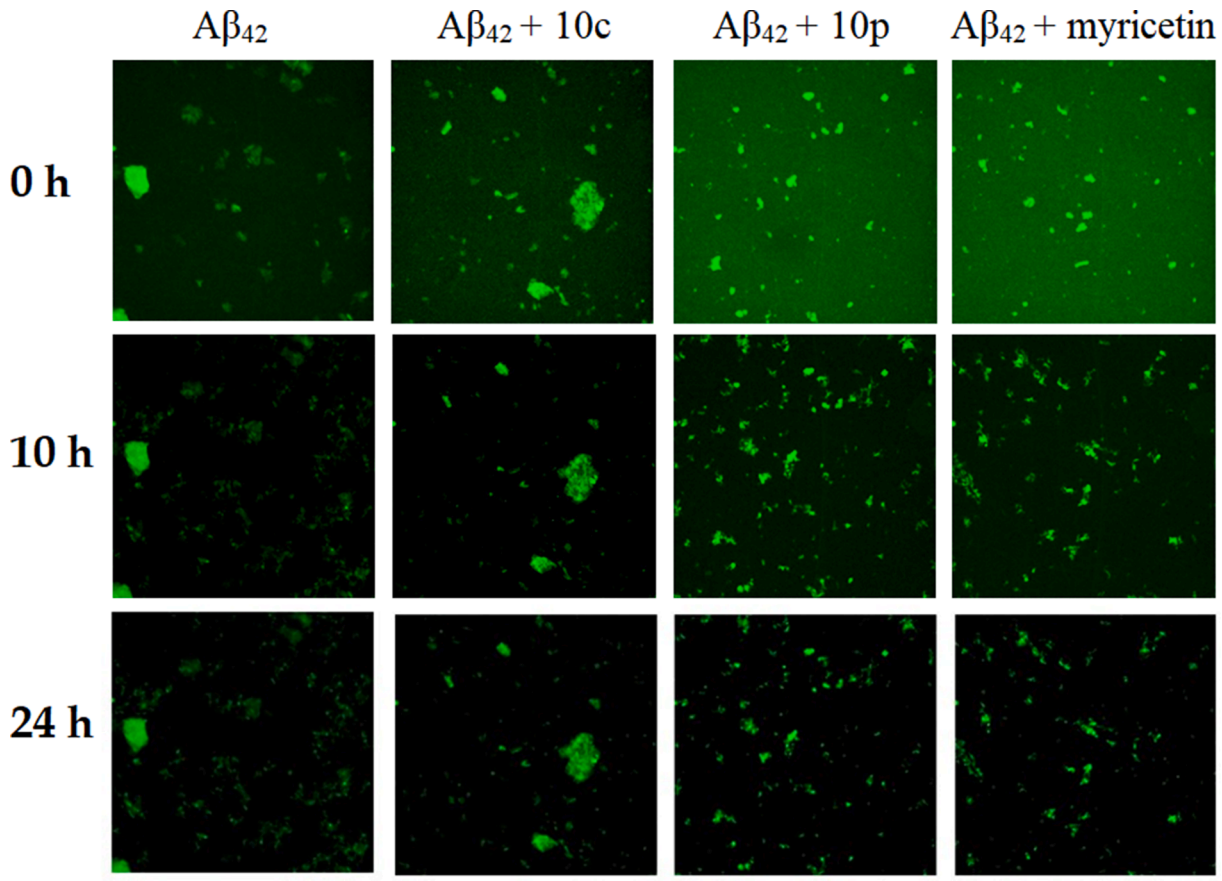

Fig. 4. Fluorescence microscopy images of Aβ_{42} (25 μM), in the absence and in the presence of tacrine – benzothiazole hybrids **10c** (10 μM), **10p** (10 μM) and myricetin at t = 0, 10 and 24 h in PBS at 30 °C.

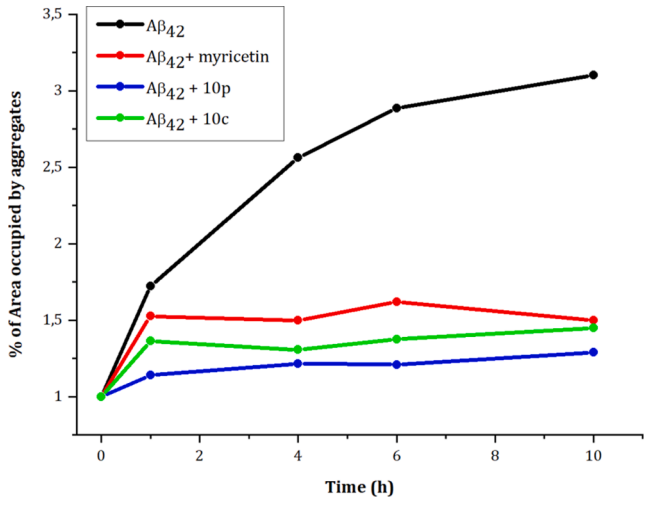

Fig. 5. Quantification of the percentage of the total area occupied by aggregates of Aβ_{42} (25 μM), in the absence and in the presence of tacrine – benzothiazole hybrids **10c** (10 μM), **10p** (10 μM) and myricetin.

potential than the former generation. Derivative **10w** achieved absolutely the best results, decreasing ABAD activity by 23%.

3.6. Cytotoxicity

To assess *in vitro* safety profile of novel hybrids, cell viability assay on various cell lines was performed. Initially, the IC_{50} values (concentration of the compound resulting in 50% decrease in cell viability) of all 25 compounds coming from both generations as well as their building blocks (7-MEOTA, tacrine, 6-chlorotacrine and BTZ) were determined on Chinese hamster ovary cell line (CHO-K1) using standard 3-[4,5-dimethylthiazol-2-yl]-2,5-diphenyltetrazolium bromide (MTT) assay [69]. The results are shown in Table 1. With such data in hand, it is obvious that heterodimers bearing non-substituted tacrine seem to be less toxic comparing to their analogues with 7-MEOTA and 6-chlorotacrine moieties that exerted more pronounced decrease in viability of the cells. The same trend can be observed also in the building blocks forming the final compounds (tacrine < 7-MEOTA, 6-chlorotacrine). Besides, such phenomenon points out to an inferior role of 2-aminobenzothiazole scaffold within current experiment. Another finding that can be deduced from the data obtained is that as the length of the linker increases within each subfamily, so does the cytotoxicity. The plausible explanation of such finding may consist in the general fact that with an increasing lipophilicity also the toxicity rises. The lowest cytotoxicity within each subfamily exerted derivatives bearing propylene linker. Regarding comparison of the prototype (**10p**) and the representatives of the 2nd generation, the latter demonstrated slightly higher toxicity than the former, however, only in terms of absolute numbers.

Hepatotoxicity is one of the most critical biological concerns when dealing with novel tacrine derivatives, since the main reason of tacrinés withdrawal from the market were its side effects associated with liver toxicity [70]. For this reason, derivative **10p**, representatives of the 2nd generation (**10v-10y**) as well as parent compounds were forwarded also for toxicity evaluation on human hepatocellular carcinoma cell line (HepG2). Also for this experiment MTT methodology was used. The results are summarized in Table 2. Looking at obtained IC_{50} values, derivative **10w** could be highlighted as the least toxic compound of the

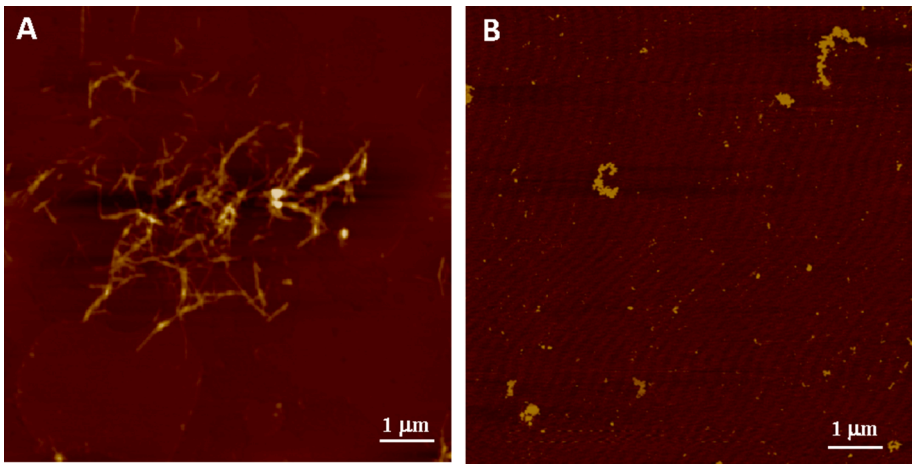

Fig. 6. AFM images of 10 μM of Aβ_{40} fibrils alone (A) and after 7 day treatment with 60 μM of **10w** (B). In all images the xy scale is 10 μm × 10 μm.

Table 2
Advanced *in vitro* results obtained for the prototype of the 1st generation (**10p**), the 2nd generation of tacrine – benzothiazole hybrids (**10v-10y**) and the reference compounds.

Compound	IC_{50} HepG2 ± SEM (μM)[a]	IC_{50} 1321 N1 ± SEM (μM)[a]	P_e ± SEM ($\times 10^{-6}$ cm.s^{-1})	CNS (+/-)
10p	11.18 ± 0.45	28.05 ± 0.56	12.83 ± 3.11	CNS (+)
10v	4.76 ± 0.03	10.43 ± 0.53	13.79 ± 2.69	CNS (+)
10w	20.99 ± 1.19	21.22 ± 1.05	8.31 ± 1.65	CNS (+)
10x	14.29 ± 0.83	31.20 ± 1.21	16.91 ± 0.93	CNS (+)
10y	12.16 ± 0.23	18.34 ± 0.08	13.69 ± 1.04	CNS (+)
tacrine	168.47 ± 3.63	107.90 ± 4.93	5.94 ± 0.67	CNS (+)
7-MEOTA	44.37 ± 1.83	93.92 ± 5.53	8.2 ± 0.6 [72]	CNS (+)
6-chlorotacrine	43.20 ± 1.17	113.43 ± 3.47	11.5 ± 2.7 [72]	CNS (+)
BTZ	> 500	> 500	20.08 ± 0.38	CNS (+)

CNS (+) - high BBB permeation predicted: P_e ($\times 10^{-6}$ cm.s^{-1}) > 4.0.
CNS (-) - low BBB permeation predicted: P_e ($\times 10^{-6}$ cm.s^{-1}) < 2.0.
CNS (+/−) - BBB permeation uncertain: P_e ($\times 10^{-6}$ cm.s^{-1}) from 4.0 to 2.0.
[a] Results are expressed as the mean of at least three experiments.

tested set. However, in relation to reference compounds, drug candidate **10w** proved twice as high hepatotoxicity as its parent compound – 6-chlorotacrine. Notwithstanding, previous studies on multi-target tacrine derivatives have already several times revealed that such assay is only illustrative [39–40]. An example testifying for everything is 7-MEOTA, which according to *in vitro* hepatotoxicity assay exerts higher toxicity comparing to non-substituted tacrine, however, the clinical trials talk about the opposite [30].

Finally, the neurotoxic effect of target compounds (**10p**, **10v-10y**) on human neural astrocytoma 1321 N1 cell line using the MTT assay [69] was determined. The reference compounds were evaluated as well. As given in Table 2, tested tacrine – benzothiazoles exhibited higher toxicity comparing to their building blocks. However, in general, it can be claimed, that cell toxicity profile of the 2nd generation of tacrine – benzothiazole hybrids roughly matched that of their parent compound – 6-chlorotacrine.

3.7. Blood-brain barrier penetration

Successful crossing of the blood–brain barrier (BBB) by a novel drug candidate is a prerequisite for efficient treatment of CNS disorders [71,72]. To explore whether the lead **10p** and the representatives of the 2nd generation of tacrine – benzothiazoles (**10v-10y**) could penetrate into the brain, a parallel artificial membrane permeation assay for the BBB (PAMPA-BBB), described by Di *et al.* [73], was used. The *in vitro* permeabilities (P_e) of newly synthesized compounds **10p**, **10v-10y**, reference compounds and 7 commercially available drugs through a lipid extract of porcine brain were determined (Table 2, Table S1 of Supporting Information). Assay validation was carried out by comparing the experimental permeabilities with the reported values of commercial drugs, which gave a good correlation. According to described limits for BBB permeation, compounds with the P_e values above 4.0 × 10^{-6} cm.s^{-1} could penetrate into the CNS by passive diffusion. All the tested compounds exhibited permeability values over this threshold, pointing out that these compounds could cross the BBB and reach thus their biological targets located in the CNS.

Taking into account all *in vitro* results obtained for the 1st and 2nd generation of tacrine – benzothiazole hybrids, derivative **10w** was selected and forwarded for further *in vivo* evaluation.

3.8. Behavioral study

Given an interesting multipotent activity profile of **10w**, its ability to ameliorate scopolamine-induced cognition impairment in rats was investigated. First of all, the maximum tolerated dose (MTD) assessment upon intraperitoneal (i.p.) administration was performed in Wistar rats. Due to limited compounds solubility, the MTD was replaced by the maximum feasible dose (MFD). The MFD of 10 mg/kg was shown to be relatively safe for **10w**, since only mild to moderate signs of intoxication occurred. They diminished spontaneously in approximately 5 h.

After MFD determination, the therapeutic effect of **10w** on a cognitive impairment model was assessed. Scopolamine-induced amnesia in rodents is an accepted standard model in behavioral pharmacology for evaluation of cholinesterase inhibiting potential of drug candidates to be developed for the anti-AD therapy. Scopolamine (scop) blocks the cholinergic pathway by antagonizing the muscarinic receptors that leads

to impairment of cognitive functions and enables, thus, to test anticholinergic drug candidates preclinically [74]. To evaluate the antiamnesic effect of **10w**, Morris Water Maze (MWM) test was utilized. THA at 2.5 mg/kg was used as a comparator. Tacrine doses were studied for adverse events prior to the study. Therefore, THA was used at a dose of 2.5 mg/kg, since at a higher dose of 5 mg/kg, significant parasympathomimetic side effects are already observed. In contrast, **10w** doses devoid of side effects (e.g. parasympathomimetic effects) were chosen. The rodents were randomly allocated into 4 groups, i) vehicle-injected control, ii) scop, iii) scop + **10w**, and iv) scop + THA. The drugs were applied i.p. each day before MWM. Within the experiment, all rats received 8 swimming sessions per day for 4 consecutive days. One-way ANOVA analysis of the data from day 4 found significant differences between groups in the parameters of distance moved ($F(3, 21) = 4.838$, $p = 0.0103$) and latency ($F(3, 21) = 4.599$, $p = 0.0126$). Tukey's post hoc test showed that the scop group exhibited longer distance moved by the rats ($p < 0.05$) and prolonged escape latency ($p < 0.05$) than the members of the vehicle-treated control group, validating, thus, the experiment (Fig. 7 and Fig. 8, respectively). The rats treated with the combination of **10w** (2 mg/kg) and scopolamine did not differ significantly from vehicle- or scopolamine-treated rats in the parameters of distance moved and latency. These results may hint about mild therapeutic effect of selected dose of **10w**. On the other hand, tacrine (2.5 mg/kg) as well did not exert any therapeutic effect (group scop + tacrine differed significantly from vehicle-treated rats in distance moved ($p < 0.05$) and latency ($p < 0.05$)). Selected dose of THA was apparently too low to reverse scopolamine-induced cognitive deficit. However, it was impossible to use higher doses of tacrine, since these doses may evoke unwanted parasympathomimetic side effects. Taken together, considering the risk of side effects and potential therapeutic effects, **10w** seems to be more promising compared to the comparator.

4. Conclusion

By understanding the multifactorial character of AD, a single molecule acting against multiple disease-relevant targets may offer a potential approach to address successfully the needs for AD therapy. Taking into account the fact, that AChEIs still remain the drugs of choice, anticholinesterase activity has been recognized as a prospective focus point to design MTDLs. Currently, the most accredited hypothesis explaining AD etiology is amyloid-cascade hypothesis. Therefore, searching for multifunctional anti-AD agents combating cholinergic deficiency and amyloid burden could be of high interest.

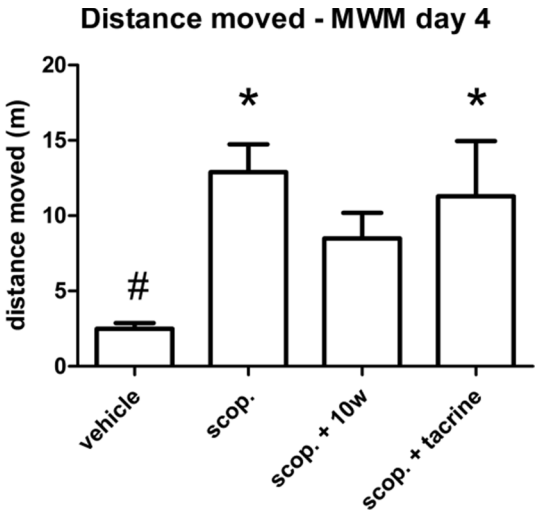

Fig. 7. The distance moved in MWM on day 4. Scopolamine application induced cognitive deficit, which manifested as significant increase in distance moved compared to vehicle-treated rats. The values are shown as group means + SEM. * $p < 0.05$ compared to the vehicle group; # $p < 0.05$ compared to the scopolamine group.

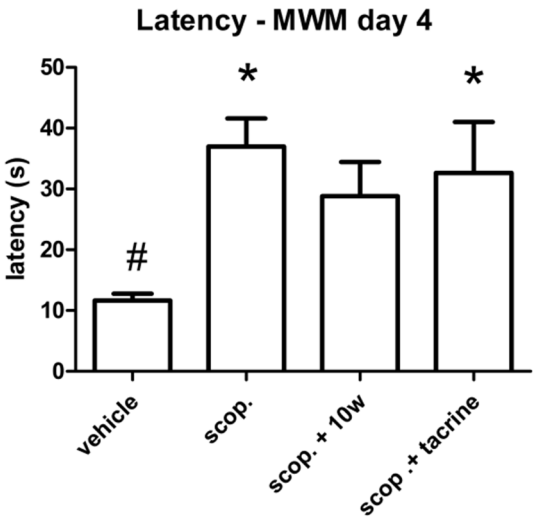

Fig. 8. Escape latency in MWM on day 4. Scopolamine-treated rats exerted significantly longer escape latency compared to vehicle-treated rats. The values are shown as group means + SEM. * $p < 0.05$ compared to the vehicle group; # $p < 0.05$ compared to the scopolamine group.

Presented tacrine – benzothiazole hybrids were designed to exhibit a multitarget profile of interest for the efficient management of AD, which included AChE inhibition, decrease in amyloid aggregation and interaction with mitochondrial enzyme ABAD. These biological properties, along with their ability to penetrate into the CNS and alleviate scopolamine-induced amnesia in AD rodent model similarly to tacrine, highlight this new class of compounds and confirm that the additive approach ("two better than one") to design new multi-acting compounds is a good strategy to confront AD.

5. Experimental section

5.1. Chemistry

5.1.1. General chemical methods

All the chemical reagents used were purchased from Sigma-Aldrich (Czech Republic). Solvents for synthesis were obtained from Penta chemicals Co. The solvents and additives used for LC-UV-MS analyses were purchased from Sigma-Aldrich (Czech Republic) in LC-MS grade purity. The course of the reactions was monitored by thin-layer chromatography on aluminium plates precoated with silica gel 60 F254 (Merck, Czech Republic) and then visualized by UV 254. Melting points were determined on a melting point apparatus M−565 (Büchi, Switzerland) and are uncorrected. Uncalibrated purity at the wavelength of 254 nm was ascertained by a LC-UV system Dionex Ultimate 3000 RS which consisted of a binary high-pressure gradient pump HPG-3400RS connected to a vacuum degasser, a heated column compartment TCC-3000, an autosampler WTS-3000 equipped with a 25 μL injection loop and a VWD-3000 ultraviolet detector. As the stationary phase, a Waters Atlantis dC18 100 Å (2.1 × 100 mm/3 μm) column was used along with a protective in-line filter (Vici Jour) and a frit of 0.5 μm pores. The mobile phase was mixed from two components: ultrapure water (MPA) and acetonitrile (MPB), both acidified by 0.1% (*v/v*) of formic acid. The studied compounds were first properly dissolved in methanol (c ~ 0.1 mg/mL) and then analyzed by the LC-UV-MS system (MS setting is described below). The following ramp-gradient program was used for the elution: 0 – 1 min: 10% MPB, 1 – 4 min: 10% – 100% MPB linearly, 4 – 5 min: 100% MPB, 5 – 7.5 min: 10% MPB. The mobile phase flow-rate in the gradient elution was set to 0.4 mL/min. In the LC-UV analyses, all the synthesized compounds exhibited uncalibrated chromatographic

purity 95 – 99% at a wavelength 254 nm. NMR spectra of target compounds were recorded on Varian S500 spectrometer (operating at 500 MHz for ^{1}H and 126 MHz for ^{13}C; Varian Comp. Palo Alto, USA). Chemical shifts are reported in parts per million (ppm). Spin multiplicities are given as s (singlet), d (doublet), dd (doublet of doublets), t (triplet), p (pentaplet), or m (multiplet). The coupling constants (*J*) are reported in Hertz (Hz). High-resolution mass spectra (HRMS) were determined by Q Exactive Plus hybrid quadrupole-orbitrap spectrometer which was attached to the above-mentioned LC-UV system. Ions for HRMS were generated by a heated electro-spray ionization source (HESI) working in positive mode under the following settings: sheath gas flow rate 40 arbitrary units (a.u.), aux gas flow rate 10 a.u., sweep gas flow rate 2 a.u., spray voltage 3.2 kV, capillary temperature 350 °C, aux gas temperature 300 °C, S-lens RF level 50, microscans 1, maximal injection time 35 ms, automatic gain control 1e6, resolution of the Fourier transformation 140 000. The applied full-scan MS analyses monitored positive ions within *m/z* range of 100 – 1500. In order to increase the accuracy of HRMS, internal lock-mass calibration was employed utilizing polysiloxane traces of *m/z* = 445.12003 ($[M+H]^+$, $[C_2H_6SiO]_6$) present in the mobile phases besides the ordinary MS external calibration system by Pierce™ LTQ ESI Positive Ion Calibration Solution (Sigma-Aldrich, Czech Republic). The chromatograms and HRMS spectra were processed in Chromeleon 6.80 and Xcalibur 3.0.63 software, respectively.

5.2. General procedure for synthesis of tacrine – Benzothiazole hybrids (10a-10y)

Appropriate 2-chlorobenzothiazole (**5**–**9**, 1 eq) was placed in a flask equipped with a stirring bar and septum. The flask was purged with argon and charged with DMF (5 mL). Thereafter, DIPEA (2 eq) was added into the mixture. Finally, appropriate α,ω-diaminotacrine derivative (**4a**-**4u**, 1 eq) were dissolved in a minimal amount of DMF and added via the syringe. The resulting solution was then heated to 110 °C and stirred for 2 h. Subsequently, the mixture was cooled to room temperature and extracted with CH_2Cl_2 (3 × 100 mL) and water (100 mL). Collected organic layers were dried over Na_2SO_4, filtered and evaporated to give crude product. The crude oil was purified by column chromatography using ethyl acetate/MeOH/26% aqueous ammonia solution (60/1/0.2) as eluent to yield a pure base. The pure base was dissolved in MeOH and saturated with gaseous HCl. The solvent was removed and the residue was washed with acetonitrile to afford the final product.

5.2.1. N^2–(1,3-benzothiazol-2-yl)-N^1-(7-methoxy-1,2,3,4-tetrahydroacridin-9-yl)ethane-1,2-diamine Hydrochloride (10a).

Yield 38%. mp 190.4 – 191.6 °C. Purity: 99%. ^{1}H NMR (500 MHz, Methanol-d_4) δ 7.73 (d, J = 8.0 Hz, 1H), 7.68 (d, J = 2.6 Hz, 1H), 7.62 (d, J = 9.2 Hz, 1H), 7.51 – 7.44 (m, 2H), 7.37 – 7.32 (m, 2H), 4.31 (t, J = 5.7 Hz, 2H), 4.00 (t, J = 5.7 Hz, 2H), 3.96 (s, 3H), 3.05 (t, J = 6.3 Hz, 2H), 2.86 (t, J = 6.2 Hz, 2H), 2.00 – 1.89 (m, 4H). ^{13}C NMR (126 MHz, DMSO-d_6) δ 167.01, 163.15, 156.84, 155.33, 150.34, 132.48, 126.79, 124.05, 123.22, 122.31, 120.84, 118.06, 112.37, 103.43, 56.36, 45.55, 28.04, 25.43, 24.81, 21.89, 20.28. HRMS: $[M+H]^+$ 405.1742 (calculated for $[C_{23}H_{25}N_4OS]^+$: 405.1704).

5.2.2. N^3–(1,3-benzothiazol-2-yl)-N^1-(7-methoxy-1,2,3,4-tetrahydroacridin-9-yl)propane-1,3-diamine Hydrochloride (10b).

Yield 25%. mp 157.3 – 158.1 °C. Purity: 99%. ^{1}H NMR (500 MHz, Methanol-d_4) δ 7.77 (d, J = 8.1 Hz, 1H), 7.68 (d, J = 2.6 Hz, 1H), 7.62 (d, J = 9.2 Hz, 1H), 7.54 – 7.47 (m, 2H), 7.43 (dd, J = 9.2, 2.5 Hz, 1H), 7.40 – 7.35 (m, 1H), 4.16 (t, J = 6.7 Hz, 2H), 3.97 (s, 3H), 3.73 (t, J = 6.7 Hz, 2H), 2.99 – 2.94 (m, 2H), 2.86 – 2.81 (m, 2H), 2.31 (p, J = 6.7 Hz, 2H), 1.98 – 1.88 (m, 4H). ^{13}C NMR (126 MHz, Methanol-d_4) δ 158.81, 157.05, 151.12, 139.27, 134.14, 129.20, 126.35, 125.45, 124.43, 123.86, 121.71, 118.82, 115.21, 113.33, 104.67, 56.86, 45.67, 30.41, 29.25, 26.17, 23.17, 21.75. HRMS: $[M+H]^+$ 419.1895 (calculated for $[C_{24}H_{27}N_4OS]^+$: 419.1900).

5.2.3. N^4-(1,3-benzothiazol-2-yl)-N^1-(7-methoxy-1,2,3,4-tetrahydroacridin-9-yl)butane-1,4-diamine Hydrochloride (10c).

Yield 16%. mp 174.9 – 175.1 °C. Purity: 99%. ^{1}H NMR (500 MHz, Methanol-d_4) δ 7.79 (d, J = 7.9 Hz, 1H), 7.70 – 7.63 (m, 2H), 7.58 – 7.48 (m, 2H), 7.45 – 7.35 (m, 2H), 4.02 (t, J = 6.5 Hz, 2H), 3.96 (s, 3H), 3.70 – 3.61 (m, 2H), 3.00 (t, J = 5.4 Hz, 2H), 2.79 (t, J = 5.3 Hz, 2H), 2.04 – 1.85 (m, 8H). ^{13}C NMR (126 MHz, Methanol-d_4) δ 158.74, 157.04, 151.00, 139.40, 134.19, 129.18, 126.29, 125.40, 124.43, 123.92, 121.71, 118.90, 115.20, 113.25, 104.61, 56.77, 47.78, 29.30, 28.99, 26.31, 26.02, 23.18, 21.79. HRMS: $[M+H]^+$ 433.2056 (calculated for $[C_{25}H_{29}N_4OS]^+$: 433.2017).

5.2.4. N^5-(1,3-benzothiazol-2-yl)-N^1-(7-methoxy-1,2,3,4-tetrahydroacridin-9-yl)pentane-1,5-diamine Hydrochloride (10d).

Yield 21%. mp 177.4 – 178.9 °C. Purity: 99%. ^{1}H NMR (500 MHz, Methanol-d_4) δ 7.79 (dd, J = 8.0, 1.1 Hz, 1H), 7.73 – 7.68 (m, 2H), 7.60 – 7.56 (m, 1H), 7.55 – 7.47 (m, 2H), 7.42 – 7.37 (m, 1H), 4.02 – 3.95 (m, 5H), 3.61 (t, J = 7.1 Hz, 2H), 3.04 – 2.99 (m, 2H), 2.82 – 2.76 (m, 2H), 1.98 – 1.91 (m, 6H), 1.90 – 1.82 (m, 2H), 1.67 – 1.57 (m, 2H). ^{13}C NMR (126 MHz, Methanol-d_4) δ 158.79, 157.27, 150.95, 139.55, 134.49, 129.26, 126.33, 125.33, 124.40, 123.86, 121.78, 118.83, 115.28, 113.12, 105.32, 56.75, 48.43, 31.43, 29.30, 28.91, 25.65, 24.87, 23.16, 21.84. HRMS: $[M+H]^+$ 447.2209 (calculated for $[C_{26}H_{31}N_4OS]^+$: 447.2174).

5.2.5. N^6-(1,3-benzothiazol-2-yl)-N^1-(7-methoxy-1,2,3,4-tetrahydroacridin-9-yl)hexane-1,6-diamine Hydrochloride (10e).

Yield 27%. mp 151.7 – 152.6 °C. Purity: 99%. ^{1}H NMR (500 MHz, Methanol-d_4) δ 7.81 (d, J = 8.0 Hz, 1H), 7.73 (d, J = 9.3 Hz, 1H), 7.69 (d, J = 2.6 Hz, 1H), 7.58 (dd, J = 8.1, 1.1 Hz, 1H), 7.55 – 7.49 (m, 2H), 7.41 – 7.36 (m, 1H), 3.99 – 3.94 (m, 5H), 3.58 (t, J = 7.0 Hz, 2H), 3.04 – 2.99 (m, 2H), 2.77 (t, J = 5.8 Hz, 2H), 1.95 (p, J = 3.1 Hz, 4H), 1.92 – 1.85 (m, 2H), 1.85 – 1.78 (m, 2H), 1.61 – 1.50 (m, 4H). ^{13}C NMR (126 MHz, Methanol-d_4) δ 158.65, 157.20, 150.74, 139.48, 134.48, 129.23, 126.29, 125.40, 123.92, 121.75, 118.69, 115.15, 112.92, 105.02, 56.62, 48.52, 31.81, 29.25, 29.14, 27.42, 27.33, 25.66, 23.17, 21.86. HRMS: $[M+H]^+$ 461.2366 (calculated for $[C_{27}H_{33}N_4OS]^+$: 461.2330).

5.2.6. N^7-(1,3-benzothiazol-2-yl)-N^1-(7-methoxy-1,2,3,4-tetrahydroacridin-9-yl)heptane-1,7-diamine Hydrochloride (10f).

Yield 33%. mp 124.6 – 125.1 °C. Purity: 99%. ^{1}H NMR (500 MHz, Methanol-d_4) δ 7.77 (d, J = 8.0 Hz, 1H), 7.72 (d, J = 9.2 Hz, 1H), 7.61 (d, J = 2.6 Hz, 1H), 7.56 (d, J = 8.1 Hz, 1H), 7.51 – 7.44 (m, 1H), 7.42 (dd, J = 9.2, 2.5 Hz, 1H), 7.37 – 7.31 (m, 1H), 3.95 (s, 3H), 3.94 – 3.86 (m, 2H), 3.58 (t, J = 7.1 Hz, 2H), 3.05 – 2.95 (m, 2H), 2.73 (t, J = 5.7 Hz, 2H), 1.96 – 1.89 (m, 4H), 1.89 – 1.82 (m, 2H), 1.82 – 1.74 (m, 2H), 1.56 – 1.43 (m, 6H). ^{13}C NMR (126 MHz, Methanol-d_4) δ 158.40, 156.86, 150.51, 139.30, 134.26, 129.05, 126.14, 125.25, 124.34, 123.84, 121.70, 118.45, 115.11, 112.67, 104.82, 56.73, 48.46, 31.88, 29.78, 29.22, 29.11, 27.54, 25.66, 23.13, 21.80. HRMS: $[M+H]^+$ 475.2520 (calculated for $[C_{28}H_{35}N_4OS]^+$: 475.2487).

5.2.7. N^8-(1,3-benzothiazol-2-yl)-N^1-(7-methoxy-1,2,3,4-tetrahydroacridin-9-yl)octane-1,8-diamine Hydrochloride (10 g).

Yield 15%. mp 146.8 – 147.4 °C. Purity: 99%. ^{1}H NMR (500 MHz, Methanol-d_4) δ 7.78 (d, J = 7.8 Hz, 1H), 7.74 (d, J = 9.2 Hz, 1H), 7.65 (d, J = 2.5 Hz, 1H), 7.60 – 7.54 (m, 1H), 7.52 – 7.44 (m, 2H), 7.38 – 7.31 (m, 1H), 3.96 (s, 3H), 3.95 – 3.88 (m, 2H), 3.57 (t, J = 7.1 Hz, 2H), 3.06 – 2.98 (m, 2H), 2.79 – 2.70 (m, 2H), 1.99 – 1.90 (m, 4H), 1.88 – 1.74 (m, 4H), 1.55 – 1.36 (m, 8H). ^{13}C NMR (126 MHz, Methanol-d_4) δ 158.50, 157.04, 150.57, 139.82, 134.39, 129.05, 126.07, 125.33, 124.59, 123.81, 121.73, 118.54, 115.24, 112.76, 104.93, 56.65, 48.59, 31.95, 30.15, 30.07, 29.22, 27.66, 27.63, 25.62, 23.14, 21.84. HRMS: $[M+H]^+$

489.2682 (calculated for $[C_{29}H_{37}N_4OS]^+$: 489.2683).

5.2.8. N^2–(1,3-benzothiazol-2-yl)-N^1-(1,2,3,4-tetrahydroacridin-9-yl) ethane-1,2-diamine Hydrochloride (10 h).

Yield 16%. mp 152.3 – 153.0 °C. Purity: 99%. ^{1}H NMR (500 MHz, Methanol-d_4) δ 8.44 – 8.41 (m, 1H), 7.80 – 7.72 (m, 3H), 7.58 – 7.54 (m, 1H), 7.54 – 7.46 (m, 2H), 7.38 – 7.33 (m, 1H), 4.38 (t, J = 5.8 Hz, 2H), 4.04 (t, J = 5.8 Hz, 2H), 3.07 – 3.00 (m, 2H), 2.83 – 2.77 (m, 2H), 1.98 – 1.90 (m, 4H). ^{13}C NMR (126 MHz, Methanol-d_4) δ 158.43, 153.00, 140.23, 139.29, 134.11, 129.11, 126.95, 126.20, 125.75, 125.00, 123.75, 120.20, 117.62, 115.61, 114.32, 47.05, 29.42, 25.81, 22.93, 21.65. HRMS: $[M+H]^+$ 375.1636 (calculated for $[C_{22}H_{23}N_4S]^+$: 375.1599).

5.2.9. N^3–(1,3-benzothiazol-2-yl)-N^1-(1,2,3,4-tetrahydroacridin-9-yl) propane-1,3-diamine Hydrochloride (10i).

Yield 23%. mp 158.9 – 159.8 °C. Purity: 99%. ^{1}H NMR (500 MHz, Methanol-d_4) δ 8.43 (d, J = 8.6 Hz, 1H), 7.83 – 7.74 (m, 2H), 7.69 (dd, J = 8.5, 1.1 Hz, 1H), 7.61 – 7.55 (m, 1H), 7.55 – 7.47 (m, 2H), 7.43 – 7.33 (m, 1H), 4.20 (t, J = 6.8 Hz, 2H), 3.75 (t, J = 6.7 Hz, 2H), 3.03 – 2.93 (m, 2H), 2.82 – 2.73 (m, 2H), 2.38 – 2.28 (m, 2H), 2.00 – 1.90 (m, 4H). ^{13}C NMR (126 MHz, Methanol-d_4) δ 157.90, 152.01, 139.47, 139.37, 134.03, 129.18, 126.59, 126.33, 124.46, 123.86, 120.04, 116.97, 115.24, 113.28, 46.21, 30.08, 29.31, 25.29, 22.94, 21.72. HRMS: $[M+H]^+$ 389.1793 (calculated for $[C_{23}H_{25}N_4S]^+$: 389.1794).

5.2.10. N^4-(1,3-benzothiazol-2-yl)-N^1-(1,2,3,4-tetrahydroacridin-9-yl) butane-1,4-diamine hydrochloride (10j).

Yield 36%. mp 147.6 – 148.9 °C. Purity: 97%. ^{1}H NMR (500 MHz, Methanol-d_4) δ 8.42 (d, J = 8.7 Hz, 1H), 7.82 – 7.72 (m, 3H), 7.57 (t, J = 7.7 Hz, 2H), 7.54 – 7.47 (m, 1H), 7.37 (t, J = 7.8 Hz, 1H), 4.06 (t, J = 7.0 Hz, 2H), 3.67 (t, J = 6.9 Hz, 2H), 3.04 – 2.96 (m, 2H), 2.78 – 2.69 (m, 2H), 2.07 – 1.99 (m, 2H), 1.98 – 1.89 (m, 6H). ^{13}C NMR (126 MHz, Methanol-d_4) δ 157.84, 151.88, 139.50, 139.31, 134.00, 129.16, 126.52, 126.35, 126.28, 123.90, 120.05, 117.09, 115.20, 113.08, 48.36, 29.33, 28.63, 26.31, 25.17, 22.96, 21.75. HRMS: $[M+H]^+$ 403.1951 (calculated for $[C_{24}H_{27}N_4S]^+$: 403.1951).

5.2.11. N^5-(1,3-benzothiazol-2-yl)-N^1-(1,2,3,4-tetrahydroacridin-9-yl) pentane-1,5-diamine hydrochloride (10 k).

Yield 38%. mp 226.9 – 227.6 °C. Purity: 98%. ^{1}H NMR (500 MHz, Methanol-d_4) δ 8.42 (d, J = 8.6 Hz, 1H), 7.81 (dd, J = 8.0, 4.7 Hz, 2H), 7.75 (dd, J = 8.5, 1.2 Hz, 1H), 7.58 (dd, J = 8.4, 1.3 Hz, 2H), 7.54 – 7.49 (m, 1H), 7.41 – 7.35 (m, 1H), 4.02 (t, J = 7.2 Hz, 2H), 3.67 – 3.58 (m, 2H), 3.01 (t, J = 5.8 Hz, 2H), 2.73 (t, J = 5.7 Hz, 2H), 2.01 – 1.90 (m, 6H), 1.87 (p, J = 7.1 Hz, 2H), 1.67 – 1.58 (m, 2H). ^{13}C NMR (126 MHz, Methanol-d_4) δ 157.84, 151.68, 139.62, 139.29, 134.01, 129.18, 126.44, 126.40, 126.28, 123.91, 120.06, 116.99, 115.13, 112.89, 48.73, 30.98, 29.31, 28.81, 25.04, 24.79, 22.98, 21.79. HRMS: $[M+H]^+$ 417.2107 (calculated for $[C_{25}H_{29}N_4S]^+$: 417.2107).

5.2.12. N^6-(1,3-benzothiazol-2-yl)-N^1-(1,2,3,4-tetrahydroacridin-9-yl) hexane-1,6-diamine hydrochloride (10 l).

Yield 20%. mp 141.0 – 142.2 °C. Purity: 97%. ^{1}H NMR (500 MHz, Methanol-d_4) δ 8.39 (d, J = 8.7 Hz, 1H), 7.85 – 7.73 (m, 3H), 7.61 – 7.53 (m, 2H), 7.49 (t, J = 7.9 Hz, 1H), 7.36 (t, J = 7.8 Hz, 1H), 4.04 – 3.93 (m, 2H), 3.59 (t, J = 7.2 Hz, 2H), 3.01 (t, J = 5.9 Hz, 2H), 2.71 (t, J = 5.8 Hz, 2H), 2.01 – 1.86 (m, 6H), 1.86 – 1.76 (m, 2H), 1.63 – 1.49 (m, 4H). ^{13}C NMR (126 MHz, Methanol-d_4) δ 157.78, 151.59, 139.59, 139.28, 133.97, 129.12, 126.44, 126.33, 126.21, 123.88, 120.05, 116.94, 115.12, 112.77, 48.91, 31.33, 29.30, 29.09, 27.30, 27.21, 24.97, 22.96, 21.78. HRMS: $[M+H]^+$ 431.2265 (calculated for $[C_{26}H_{31}N_4S]^+$: 431.2264).

5.2.13. N^7-(1,3-benzothiazol-2-yl)-N^1-(1,2,3,4-tetrahydroacridin-9-yl) heptane-1,7-diamine hydrochloride (10 m).

Yield 20%. mp 134.3 – 135.8 °C. Purity: 99%. ^{1}H NMR (300 MHz, Methanol-d_4) δ 8.38 (d, J = 8.6 Hz, 1H), 7.86 – 7.74 (m, 3H), 7.61 – 7.53 (m, 2H), 7.49 (t, J = 8.2 Hz, 1H), 7.35 (dd, J = 8.1, 1.3 Hz, 1H), 4.03 – 3.90 (m, 2H), 3.57 (t, J = 7.0 Hz, 2H), 3.02 (t, J = 5.6 Hz, 2H), 2.69 (t, J = 5.5 Hz, 2H), 2.01 – 1.91 (m, 4H), 1.91 – 1.82 (m, 2H), 1.82 – 1.72 (m, 2H), 1.58 – 1.41 (m, 6H). ^{13}C NMR (75 MHz, Methanol-d_4) δ 157.83, 151.57, 139.66, 139.61, 134.01, 129.11, 126.50, 126.30, 126.15, 124.50, 123.87, 120.07, 116.95, 115.19, 112.76, 31.41, 29.77, 29.29, 29.15, 27.58, 27.53, 24.95, 22.97, 21.82. HRMS: $[M+H]^+$ 445.2417 (calculated for $[C_{27}H_{33}N_4S]^+$: 445.2420).

5.2.14. N^8-(1,3-benzothiazol-2-yl)-N^1-(1,2,3,4-tetrahydroacridin-9-yl) octane-1,8-diamine hydrochloride (10n).

Yield 14%. mp 62.0 – 63.4 °C. Purity: 99%. ^{1}H NMR (500 MHz, Methanol-d_4) δ 8.39 (d, J = 8.7 Hz, 1H), 7.88 – 7.72 (m, 3H), 7.62 – 7.53 (m, 2H), 7.48 (t, J = 7.7 Hz, 1H), 7.33 (t, J = 7.6 Hz, 1H), 3.95 (t, J = 7.2 Hz, 2H), 3.56 (t, J = 7.1 Hz, 2H), 3.03 (t, J = 5.6 Hz, 2H), 2.70 (t, J = 5.5 Hz, 2H), 2.04 – 1.90 (m, 4H), 1.90 – 1.81 (m, 2H), 1.81 – 1.72 (m, 2H), 1.54 – 1.38 (m, 8H). ^{13}C NMR (126 MHz, Methanol-d_4) δ 169.23, 157.88, 151.59, 140.74, 139.68, 134.02, 128.92, 126.48, 126.29, 125.85, 125.02, 123.69, 120.08, 116.97, 115.49, 112.77, 49.10, 47.40, 31.48, 30.10, 30.06, 29.30, 27.64, 27.60, 24.93, 22.97, 21.82. HRMS: $[M+H]^+$ 459.2575 (calculated for $[C_{28}H_{35}N_4S]^+$: 459.2577).

5.2.15. N^2–(1,3-benzothiazol-2-yl)-N^1-(6-chloro-1,2,3,4-tetrahydroacridin-9-yl)ethane-1,2-diamine hydrochloride (10o).

Yield 31%. mp 184.1 – 185.7 °C. Purity: 97%. ^{1}H NMR (500 MHz, DMSO-d_6) δ 10.50 (bs, 1H), 8.48 (d, J = 8.4 Hz, 1H), 8.10 (bs, 1H), 7.99 (s, 1H), 7.78 (d, J = 8.3 Hz, 1H), 7.46 (t, J = 9.9 Hz, 2H), 7.36 (t, J = 7.2 Hz, 1H), 7.20 (t, J = 7.2 Hz, 1H), 4.27 – 4.11 (m, 2H), 4.03 – 3.87 (m, 2H), 2.96 (t, J = 5.7 Hz, 2H), 2.66 (t, J = 5.8 Hz, 2H), 1.85 – 1.65 (m, 4H). ^{13}C NMR (126 MHz, DMSO-d_6) δ 167.22, 156.18, 151.87, 138.43, 137.03, 127.42, 126.97, 125.46, 123.55, 122.53, 117.94, 115.37, 114.70, 112.72, 46.33, 45.07, 28.14, 24.60, 21.51, 20.18. HRMS: $[M+H]^+$ 409.1182 (calculated for $[C_{22}H_{22}ClN_4S]^+$: 409.1248).

5.2.16. N^3–(1,3-benzothiazol-2-yl)-N^1-(6-chloro-1,2,3,4-tetrahydroacridin-9-yl)propane-1,3-diamine hydrochloride (10p).

Yield 30%. mp 217.3 – 218.0 °C. Purity: 95%. ^{1}H NMR (500 MHz, Methanol-d_4) δ 8.40 (d, J = 9.0 Hz, 1H), 7.73 (d, J = 7.9 Hz, 1H), 7.67 – 7.61 (m, 1H), 7.55 – 7.42 (m, 3H), 7.37 – 7.28 (m, 1H), 4.18 (t, J = 5.5 Hz, 2H), 3.84 – 3.63 (m, 2H), 3.06 – 2.86 (m, 2H), 2.82 – 2.65 (m, 2H), 2.43 – 2.22 (m, 2H), 2.06 – 1.81 (m, 4H). ^{13}C NMR (126 MHz, Methanol-d_4) δ 169.17, 157.67, 152.34, 140.71, 140.10, 139.85, 128.91, 128.64, 126.92, 125.94, 125.13, 123.63, 118.97, 115.58, 115.25, 113.70, 46.39, 44.70, 30.10, 29.34, 25.14, 22.81, 21.63. HRMS: $[M+H]^+$ 423.1401 (calculated for $[C_{23}H_{24}ClN_4S]^+$: 423.1405).

5.2.17. N^4-(1,3-benzothiazol-2-yl)-N^1-(6-chloro-1,2,3,4-tetrahydroacridin-9-yl)butane-1,4-diamine hydrochloride (10q).

Yield 30%. mp 194.8 – 195.5 °C. Purity: 95%. ^{1}H NMR (500 MHz, DMSO-d_6) δ 8.45 (dd, J = 9.2, 2.4 Hz, 1H), 8.01 (d, J = 2.3 Hz, 2H), 7.85 (d, J = 8.0 Hz, 1H), 7.63 (d, J = 8.1 Hz, 1H), 7.53 – 7.46 (m, 1H), 7.41 (t, J = 7.7 Hz, 1H), 7.26 (t, J = 7.7 Hz, 1H), 3.95 – 3.84 (m, 2H), 3.72 – 3.60 (m, 2H), 2.96 (t, J = 5.7 Hz, 2H), 2.64 (t, J = 5.6 Hz, 2H), 1.89 (p, J = 7.0 Hz, 2H), 1.82 – 1.69 (m, 6H). ^{13}C NMR (126 MHz, DMSO-d_6) δ 166.84, 155.77, 151.48, 138.93, 137.29, 128.06, 127.63, 125.70, 124.52, 124.41, 123.32, 118.21, 114.69, 114.49, 112.11, 47.00, 45.56, 28.35, 27.22, 25.41, 24.49, 21.77, 20.55. HRMS: $[M+H]^+$ 437.1557 (calculated for $[C_{24}H_{26}ClN_4S]^+$: 437.1561).

5.2.18. N^5-(1,3-benzothiazol-2-yl)-N^1-(6-chloro-1,2,3,4-tetrahydroacridin-9-yl)pentane-1,5-diamine hydrochloride (10r).

Yield 31%. mp 212.5 – 213.1 °C. Purity: 96%. ^{1}H NMR (500 MHz,

DMSO-d_6) δ 8.42 (d, J = 9.3 Hz, 1H), 8.03 (d, J = 2.1 Hz, 1H), 7.96 (bs, 1H), 7.84 (d, J = 7.9 Hz, 1H), 7.59 (d, J = 8.0 Hz, 1H), 7.54 (dd, J = 9.2, 2.1 Hz, 1H), 7.39 (t, J = 7.5 Hz, 1H), 7.24 (t, J = 7.6 Hz, 1H), 3.90 – 3.79 (m, 2H), 3.64 – 3.52 (m, 2H), 2.97 (t, J = 5.9 Hz, 2H), 2.63 (t, J = 5.8 Hz, 2H), 1.87 – 1.73 (m, 6H), 1.69 (p, J = 7.1 Hz, 2H), 1.48 (p, J = 7.2 Hz, 2H). ^{13}C NMR (126 MHz, DMSO-d_6) δ 166.86, 155.75, 151.35, 139.04, 137.33, 128.09, 127.47, 125.65, 124.20, 123.12, 118.27, 115.01, 114.43, 112.00, 47.32, 45.68, 29.53, 28.35, 27.89, 24.38, 23.54, 21.77, 20.59. HRMS: $[M+H]^+$ 451.1715 (calculated for $[C_{25}H_{28}ClN_4S]^+$: 451.1718).

5.2.19. N^6-(1,3-benzothiazol-2-yl)-N^1-(6-chloro-1,2,3,4-tetrahydroacridin-9-yl)hexane-1,6-diamine hydrochloride (10 s).

Yield 23%. mp 228.8 – 230.0 °C. Purity: 99%. ^{1}H NMR (500 MHz, Methanol-d_4) δ 8.40 (d, J = 9.3 Hz, 1H), 7.81 – 7.75 (m, 2H), 7.60 – 7.52 (m, 2H), 7.52 – 7.46 (m, 1H), 7.39 – 7.32 (m, 1H), 4.03 – 3.91 (m, 2H), 3.59 (t, J = 7.0 Hz, 2H), 3.01 (t, J = 5.8 Hz, 2H), 2.69 (t, J = 5.7 Hz, 2H), 2.00 – 1.93 (m, 4H), 1.93 – 1.87 (m, 2H), 1.86 – 1.79 (m, 2H), 1.62 – 1.50 (m, 4H). ^{13}C NMR (126 MHz, Methanol-d_4) δ 169.25, 157.67, 152.06, 140.39, 139.97, 129.06, 128.77, 126.77, 126.06, 124.67, 123.80, 119.09, 115.36, 115.30, 113.31, 47.42, 31.17, 29.32, 29.14, 27.32, 27.23, 24.82, 22.85, 21.72. HRMS: $[M+H]^+$ 465.1873 (calculated for $[C_{26}H_{30}ClN_4S]^+$: 465.1874).

5.2.20. N^7-(1,3-benzothiazol-2-yl)-N^1-(6-chloro-1,2,3,4-tetrahydroacridin-9-yl)heptane-1,7-diamine hydrochloride (10 t).

Yield 26%. mp 69.2 – 70.9 °C. Purity: 97%. ^{1}H NMR (500 MHz, Methanol-d_4) δ 8.40 (d, J = 9.3 Hz, 1H), 7.84 – 7.76 (m, 2H), 7.60 – 7.53 (m, 2H), 7.53 – 7.48 (m, 1H), 7.40 – 7.34 (m, 1H), 4.00 – 3.93 (m, 2H), 3.59 (t, J = 7.0 Hz, 2H), 3.01 (t, J = 5.7 Hz, 2H), 2.69 (t, J = 5.6 Hz, 2H), 2.01 – 1.91 (m, 4H), 1.91 – 1.84 (m, 2H), 1.80 (p, J = 7.1 Hz, 2H), 1.59 – 1.43 (m, 6H). ^{13}C NMR (126 MHz, Methanol-d_4) δ 157.70, 152.05, 140.42, 139.99, 139.49, 129.16, 128.76, 126.74, 126.21, 124.42, 123.88, 119.09, 115.37, 115.14, 113.29, 49.13, 31.26, 29.77, 29.32, 29.14, 27.58, 27.53, 24.80, 22.85, 21.73. HRMS: $[M+H]^+$ 479.2028 (calculated for $[C_{27}H_{32}ClN_4S]^+$: 479.2031).

5.2.21. N^8-(1,3-benzothiazol-2-yl)-N^1-(6-chloro-1,2,3,4-tetrahydroacridin-9-yl)octane-1,8-diamine hydrochloride (10u).

Yield 11%. mp 165.7 – 166.1 °C. Purity: 96%. ^{1}H NMR (500 MHz, Methanol-d_4) δ 8.39 (d, J = 9.3 Hz, 1H), 7.82 – 7.76 (m, 2H), 7.59 – 7.53 (m, 2H), 7.53 – 7.47 (m, 1H), 7.36 (t, J = 7.8 Hz, 1H), 3.99 – 3.91 (m, 2H), 3.57 (t, J = 7.3 Hz, 2H), 3.01 (t, J = 5.8 Hz, 2H), 2.68 (t, J = 5.7 Hz, 2H), 2.01 – 1.91 (m, 4H), 1.86 (p, J = 7.4 Hz, 2H), 1.79 (p, J = 7.3 Hz, 2H), 1.54 – 1.40 (m, 8H). ^{13}C NMR (126 MHz, Methanol-d_4) δ 157.71, 152.04, 140.43, 139.99, 139.89, 129.09, 128.76, 126.72, 126.10, 124.61, 123.83, 119.10, 115.37, 115.24, 113.28, 31.33, 30.12, 30.07, 29.32, 29.24, 27.65, 27.62, 24.78, 22.85, 21.74. HRMS: $[M+H]^+$ 493.2165 (calculated for $[C_{28}H_{34}ClN_4S]^+$: 493.2187).

5.2.22. N^1-(6-chloro-1,2,3,4-tetrahydroacridin-9-yl)–N^3-(6-chlorobenzo[d]thiazol-2-yl)propane-1,3-diamine hydrochloride (10v).

Yield 48%. mp 225.8 – 226.7 °C. Purity: 97%. ^{1}H NMR (500 MHz, Methanol-d_4) δ 8.43 (d, J = 9.3 Hz, 1H), 7.85 (dd, J = 1.8, 0.9 Hz, 1H), 7.68 (d, J = 2.2 Hz, 1H), 7.54 (dd, J = 9.2, 2.1 Hz, 1H), 7.51 – 7.48 (m, 2H), 4.18 (t, J = 6.8 Hz, 2H), 3.73 (t, J = 6.6 Hz, 2H), 3.03 – 2.95 (m, 2H), 2.78 – 2.71 (m, 2H), 2.31 (p, J = 6.7 Hz, 2H), 1.97 – 1.94 (m, 4H). ^{13}C NMR (126 MHz, Methanol-d_4) δ 157.96, 152.55, 140.31, 140.10, 139.42, 131.37, 129.37, 128.64, 127.02, 126.84, 123.62, 119.06, 116.59, 115.43, 113.88, 46.33, 44.74, 30.03, 29.37, 25.10, 22.83, 21.67. HRMS: $[M+H]^+$ 457.1011 (calculated for $[C_{23}H_{23}Cl_2N_4S]^+$: 457.1015).

5.2.23. N^1-(6-chloro-1,2,3,4-tetrahydroacridin-9-yl)–N^3-(6-nitrobenzo[d]thiazol-2-yl)propane-1,3-diamine hydrochloride (10w).

Yield 57%. mp 214.7 – 215.5 °C. Purity: 96%. ^{1}H NMR (500 MHz, DMSO-d_6) δ 14.09 (s, 1H), 9.85 (s, 1H), 8.66 (d, J = 2.5 Hz, 1H), 8.40 (d, J = 9.3 Hz, 1H), 8.08 (dd, J = 8.9, 2.5 Hz, 1H), 7.98 (s, 1H), 7.89 (d, J = 2.3 Hz, 1H), 7.45 (dd, J = 9.2, 2.2 Hz, 1H), 7.30 (d, J = 8.9 Hz, 1H), 4.06 – 3.95 (m, 2H), 3.67 – 3.52 (m, 2H), 2.87 (t, J = 5.1 Hz, 2H), 2.64 (t, J = 5.0 Hz, 2H), 2.11 (p, J = 6.4 Hz, 2H), 1.85 – 1.67 (m, 4H). ^{13}C NMR (126 MHz, DMSO-d_6) δ 155.65, 150.95, 141.51, 138.64, 136.96, 129.84, 127.78, 125.18, 122.49, 118.19, 117.88, 116.27, 114.13, 111.84, 45.10, 42.01, 29.18, 28.00, 24.22, 21.49, 20.30. HRMS: $[M+H]^+$ 468.1252 (calculated for $[C_{23}H_{23}ClN_5O_2S]^+$: 468.1256).

5.2.24. N^1-(6-chloro-1,2,3,4-tetrahydroacridin-9-yl)–N^3-(6-methoxybenzo[d]thiazol-2-yl)propane-1,3-diamine hydrochloride (10x).

Yield 20%. mp 187.6 – 189.0 °C. Purity: 97%. ^{1}H NMR (500 MHz, Methanol-d_4) δ 8.42 (dd, J = 9.3, 2.0 Hz, 1H), 7.67 (d, J = 2.1 Hz, 1H), 7.54 (dd, J = 9.2, 2.1 Hz, 1H), 7.42 (dd, J = 8.9, 2.3 Hz, 1H), 7.38 (d, J = 2.3 Hz, 1H), 7.09 (dd, J = 8.9, 2.4 Hz, 1H), 4.18 (t, J = 6.8 Hz, 2H), 3.86 (s, 3H), 3.71 (t, J = 6.7 Hz, 2H), 2.97 (t, J = 5.7 Hz, 2H), 2.75 (t, J = 5.8 Hz, 2H), 2.31 (p, J = 6.7 Hz, 2H), 2.04 – 1.89 (m, 4H). ^{13}C NMR (126 MHz, Methanol-d_4) δ 157.72, 156.49, 152.16, 138.92, 138.65, 137.89, 131.51, 127.31, 126.20, 125.70, 124.83, 117.77, 115.41, 114.56, 106.67, 55.24, 45.08, 28.72, 27.91, 23.87, 22.30, 21.15, 20.33. HRMS: $[M+H]^+$ 453.1428 (calculated for $[C_{24}H_{26}ClN_4OS]^+$: 453.1510).

5.2.25. N^1-(6-chloro-1,2,3,4-tetrahydroacridin-9-yl)–N^3-(6-methylbenzo[d]thiazol-2-yl)propane-1,3-diamine hydrochloride (10y).

Yield 12%. mp 201.9 – 202.7 °C. Purity: 96%. ^{1}H NMR (500 MHz, Methanol-d_4) δ 8.42 (d, J = 9.3 Hz, 1H), 7.67 (d, J = 2.1 Hz, 1H), 7.59 (d, J = 1.8 Hz, 1H), 7.53 (dd, J = 9.3, 2.2 Hz, 1H), 7.41 (d, J = 8.3 Hz, 1H), 7.34 (dd, J = 8.4, 1.6 Hz, 1H), 4.18 (t, J = 6.8 Hz, 2H), 3.73 (t, J = 6.7 Hz, 2H), 2.98 (t, J = 5.7 Hz, 2H), 2.79 – 2.72 (m, 2H), 2.45 (s, 3H), 2.32 (p, J = 6.7 Hz, 2H), 2.02 – 1.91 (m, 4H). ^{13}C NMR (126 MHz, Methanol-d_4) δ 157.87, 152.53, 140.25, 140.04, 137.03, 130.23, 128.61, 127.01, 123.74, 119.05, 115.36, 114.88, 113.83, 46.30, 44.86, 29.96, 29.35, 25.12, 22.82, 21.65, 21.24. HRMS: $[M+H]^+$ 437.1484 (calculated for $[C_{23}H_{23}ClN_5O_2S]^+$: 437.1561).

5.3. AChE and BChE inhibition assay

AChE and BChE inhibitory potential of tested compounds was determined using modified Ellmańs method and is expressed as IC_{50}.[42] Human recombinant AChE and human plasma BChE, 5,5́-dithiobis(2-nitrobenzoic acid) (Ellmańs reagent, DTNB), phosphate buffer solution (PBS: 0.1 M KH_2PO_4/K_2HPO_4, pH 7.4), acetylthiocholine iodide (ATC) and butyrylthiocholine iodide (BTC) were purchased from Sigma-Aldrich (Prague, Czech Republic). For measuring purposes, polystyrene Nunc 96-well microplates with flat bottom shape (ThermoFisher Scientific, USA) were utilized. The assay medium (100 μL) consisted of 40 μL of PBS, 20 μL of 0.0025 M DTNB, 10 μL of the enzyme, and 20 μL of 0.01 M substrate (ATC or BTC iodide solution).

Compounds were tested in concentration range 10^{-3} – 10^{-11} M. Their solutions were preincubated for 5 min with the enzyme (AChE or BChE). The reaction was initiated by immediate addition of 20 μL of the corresponding substrate. The enzyme activity was determined by measuring the increase in absorbance at 412 nm at 37 °C in 2 min intervals, using Multi-mode microplate reader Synergy 2 (Vermont, USA). Each concentration was assessed in triplicate. Software GraphPad Prism 5 (San Diego, USA) was used for the statistical data evaluation.

5.4. Docking study

Crystal structure of *h*AChE was downloaded from RCSB Protein Data Bank – PDB ID: 4EY7.[45] Receptor structure was prepared by DockPrep function of UCSF Chimera (version 1.4) and converted to pdbqt-files by AutodockTools (v. 1.5.6) [75,76]. Flexible residues selection was based on previous experience with either *h*AChE [51,77,78]. Three-dimensional structures of **10w** were built by Open Babel (v. 2.3.1),

minimized by Avogadro (v 1.1.0) and converted to pdbqt-file format by AutodockTools [79]. The docking calculations were made by Autodock Vina (v. 1.1.2) with the exhaustiveness of 8 [44]. Calculation was repeated 20 times and the best-scored result was selected for manual inspection. The visualization of enzyme – ligand interactions was prepared using The PyMOL Molecular Graphics System, Version 2.0 Schrödinger, LLC, Mannheim, Germany. 2D diagram was created with Dassault Systèmes BIOVIA, Discovery Studio Visualizer, v 17.2.0.16349, San Diego: Dassault Systèmes, 2016.

5.5. Inhibition of $A\beta_{40}$ fibrillization

1 mg of lyophilized powder of $A\beta_{40}$ peptide (LOT # 2061240 T, rPeptide (USA Company)) was dissolved to a final concentration of 665 μM in 10 mM NaOH solution defined by UV–VIS spectroscopy with an extinction coefficient $\varepsilon_{292} = 2300\ M^{-1}.cm^{-1}$ using spectrophotometer Jasco V-630. The stock solution was sonicated for 1 min in a bath sonicator and then 10 min centrifuged at 12 000 g at 4 °C. The supernatant was diluted in 150 mM MOPS (3-(*N*-morpholino)–propanesulfonic acid) buffer solution to a final 10 μM concentration of $A\beta_{40}$ peptide with addition of 0.02% NaN_3 at pH 6.9. $A\beta_{40}$ fibrils were formed after 7-day incubation at 37 °C. All other chemicals used were purchased from Sigma-Aldrich or Fluka and were of analytical reagent grade.

The amount of $A\beta_{40}$ fibrils was quantified using the specific fluorescent dye ThT since a significant enhancement of ThT fluorescence could be observed in the presence of amyloid fibrils. Thioflavin T was added to the 10 μM protein samples to a final ThT concentration of 20 μM. Measurements were performed using a spectrofluorimeter Synergy MX BioTek in a fluorescence 96-well plate. The excitation was set at 440 nm and the emission was recorded at 485 nm. The excitation and emission slits were adjusted to 9.0/9.0 nm and the top probe vertical offset was 6 nm.

Tacrine – benzothiazole hybrids in a concentration range of 100 pM – 500 μM were added to a 10 μM solution of $A\beta_{40}$. The inhibition experiments were carried out after the incubation of $A\beta_{40}$ with studied derivatives for 7 days at 37 °C. The inhibitory effect of derivatives on $A\beta_{40}$ fibrillization was investigated using ThT fluorescence assay. The fluorescence intensities of studied compounds were normalized to the fluorescence intensity of $A\beta_{40}$ fibrils alone. Each experiment was carried out in triplicate and the final values represent the mean of three measurements. The inhibitory curves were obtained by fitting the average fluorescence data by non-linear least-squares method.

5.6. Inhibition of $A\beta_{42}$ self-aggregation

Lyophilized HFIP-pretreated $A\beta_{42}$ was purchased from Bachem (Switzerland). KCl was purchased from PancReac, AppliChem, Spain. NaCl, KH_2PO_4, Na_2HPO_4 and DMSO were supplied by Sigma-Aldrich, Germany.

The stock solution of $A\beta_{42}$ was prepared by dissolving the lyophilized peptide in DMSO, aliquoted and stored at −20 °C. For the measurement of $A\beta_{42}$ self-aggregation and amyloid inhibition studies, $A\beta_{42}$ stock solution was diluted to a final concentration of 25 μM in PBS at pH 7.25 (10 mM PBS, 2.7 mM KCl, 137 mM NaCl) and 10% DMSO.

Amyloid inhibition study was performed by incubating $A\beta_{42}$ peptide (25 μM) in the presence of **10c**, **10p** or myricetin at 30 °C for 48 h, without any stirring. PBS was used as a blank and the inhibitors were used as controls. Steady-state fluorescence spectra and Rayleigh scattering experiments were performed on a FluoroMax-4 spectrofluorometer. The fluorescence spectra were corrected for the wavelength response of the system. The Rayleigh scattering peaks were recorded with excitation at 550 nm using 0.2 mm slits in the excitation and emission monochromators. The reported intensities were corrected for those of buffer/tested inhibitor solutions under similar conditions and normalized with the initial scattering intensity. Fluorescence spectra were recorded in the range of 340 – 600 nm, with an excitation wavelength at 330 nm and slits of 0.5 mm and 2.0 mm for excitation and emission, respectively. All the measurements were performed in 5 mm optical path length cuvettes in a thermostated sample holder, 30 °C.

All spinning-disk confocal microscopy experiments were performed in μ-Slide 8 Well (IBIDI, Germany). Live images were recorded every 30 min for 24 h by spinning disc confocal microscopy (Zeiss Cell Observer SD with Yokogawa CSU-X1 Confocal Spinning Disc unit, Japan, and Evolve 512 EMCCD Camera) with 20×/0.8NA Plan-ApoChromat objective. The temperature of the incubation chamber on the microscope was set to 30 °C. Four conditions were imaged in duplicate: $A\beta_{42}$ peptide (25 μM), $A\beta_{42}$ peptide (25 μM) with myricetin (10 μM), **10c** (10 μM) or **10p** (10 μM). For each time point, the autofluorescence of the aggregates was imaged with excitation wavelength of 405 nm and emission wavelengths of 420–460 nm, together with a brightfield image of the aggregates. Image analysis was performed using Fiji [80]. Aggregates were segmented using Otsu threshold algorithm and selected by the Analyse Particle function, followed by the quantification of the percentage of the area occupied by the aggregates, for each time point, in each condition.

Data analysis was performed with OriginPro 8.0 software. The following empirical sigmoidal function (logistic function) was used to fit the experimental data:

$$y = y_0 + A/[1 + exp(-k(t - -t_{50}))]$$

where y_0 is the pre-transition base line, A the amplitude of the transition, t_{50} its midpoint and k is an apparent growth rate. By this method the lag time is often defined as $t_{lag} = t_{50} - 1/2k$ which is equivalent to the extrapolation from the maximal growth rate.

5.7. Atomic force microscopy

The samples for AFM were prepared by casting aliquots (10 μL) of solution onto freshly cleaved mica, which was left to adsorb for 10 min. Then the samples were 5-times rinsed with ultrapure water and dried in air. The images were recorded by using an atomic force microscope (Veeco di Innova) in a tapping mode under ambient conditions with a rectangular uncoated silicon cantilever NCHV (Bruker AFM Probes) with a specific resistance of 0.01 – 0.025 Wcm@1, antimony (n) doped Si with a typical resonance frequency 320 kHz, and a force constant of 42 Nm^{-1}. All images were unfiltered.

5.8. ABAD inhibition screening assay

Purification of ABAD protein was performed as described in our previous work [81]. Activity assay conditions consisted of ABAD enzyme (0.5 μg/mL), NADH (250 μM), acetoacetyl-CoA (120 μM) and a single compound of interest (25 μM or 100 μM, 1% DMSO (v/v)). Solutions were prepared in assay buffer (10 mM Tris HCl (pH 7.4), 150 mM NaCl, 1 mM DTT, 0.001% Tween and 0.01% BSA at 25 °C). Each compound was weighted in milligrams with maximal 0.1 mg deviation to prepare a 10 mM stock solution in DMSO. The DMSO stock solution was further diluted by assay buffer solution to give a final assay concentration 25 μM 1% DMSO (v/v). Control solutions containing an equivalent concentration of DMSO (1% (v/v)) were also prepared and run concurrently. Reaction progression was measured via a decrease in NADH absorbance at 340 nm using a SpectraMAX M2e spectrophotometer. The reaction period was gated to yield steady state conditions ($R2 > 0.9$).

5.9. Cell viability assay on CHO-K1, HepG2 and 1321 N1 cell lines

To ascertain the cytotoxic effect of studied compounds (**10a**-**10y**), standard MTT assay on the CHO-K1 cell line (Chinese hamster ovary) was used. Tested compounds were dissolved in DMSO and subsequently in the growth medium (Nutrient mixture F-12 Ham) supplemented with 10% PBS and 1% penicillin (10000 U/mL)/streptomycin (10000 μg/

mL), so that the final concentration did not exceed 0.5% (v/v). The cells were seeded in 96-well plates and exposed to the tested compounds in the medium (100 μL) for 24 h at 37 °C, 95% humidity and in an atmosphere of 5% CO_2. Subsequently, this medium was replaced by the medium containing MTT (10 μM) and incubated for another 3–4 h. After that, medium with MTT was removed and formazan crystals were dissolved by an addition of 100 μL DMSO. Viability of the cells was estimated spectrophotometrically by the amount of produced formazan. The absorbance was measured at 570 nm, with 650 nm as a reference wavelength on Synergy HT reader (Biotek, USA). The results were evaluated as IC_{50} from the control substracted triplicates (in comparison with untreated control) using non-linear regression (four parameters) in GraphPad Prism software.

To assess *in vitro* hepatotoxicity human liver hepatocellular carcinoma (HepG2) cell line (ATCC, Mannassas, VA, USA) was used. HepG2 was cultivated in Dubleccós modified Eaglés medium (DMEM, Biosera, Nuaille, France) with 10% foetal bovine serum (Biosera, Nuaille, France) and 1% penicillin–streptomycin antibiotic solution (Sigma-Aldrich, Czech Republic). The cell line was incubated at 37 °C in CO_2 incubator (Binder CO_2 incubator BC 160, Tuttlingen, Germany) and routinely passaged by trypsinization at 75 – 85% confluence. The MTT reduction assay was used for measurement of tested compoundś hepatotoxicity [69,82]. HepG2 cells were plated into 96-well plates in 100 μL volume and density of 15×10^3 per well. The cells were allowed to attach overnight before the treatment. The stock solutions of tested compounds were prepared in DMSO and further serially diluted in DMEM. The cells were treated for 24 h. The final concentration of DMSO was<0.25%. After incubation, the medium was aspirated and replaced by 100 μL of fresh medium containing MTT (0.5 mg/mL). The plates were subsequently incubated at 37 °C in CO_2 incubator for 45 min. The medium containing MTT was aspirated after 45 min incubation and formed purple formazan was dissolved in 100 μL of DMSO. The optical density of each well was measured using Synergy 2 Multi-Mode Microplate Reader (BioTek Instruments, Inc., Winooski, VT, USA) at 570 nm. The cell viability was expressed as the percentage of untreated control. The results were obtained from three independent experiments performed in triplicate. The IC_{50} values were calculated using four parametric non-linear regression by statistic GraphPad Prism software (version 5.04, GraphPad Software Inc., San Diego, CA) by the logarithmic dose–response curve. The IC_{50} values were expressed as a mean ± standard error of the mean (SEM).

For *in vitro* neurototoxicity assessment human neural astrocytoma 1321 N1 cell line (Sigma-Aldrich, St. Louis, MO, USA) was used. 1321 N1 was cultivated in Dubleccós modified Eaglés medium (Biosera, Nuaille, France) with 10% foetal bovine serum (Biosera, Nuaille, France), 1% penicillin–streptomycin antibiotic solution (Sigma-Aldrich, Czech Republic) and 1% non-essential amino acid solution (Sigma-Aldrich, Czech Republic). The cell line was incubated at 37 °C in CO_2 incubator (Binder CO_2 incubator BC 160, Tuttlingen, Germany) and routinely passaged by trypsinization at 75 – 85% confluence. The MTT reduction assay was used for measurement of tested compoundś neurotoxicity [69,82]. 1321 N1 cells were plated into 96-well plates in 100 μL volume and density of 15×10^3 per well. The cells were allowed to attach overnight before the treatment. The stock solutions of tested compounds were prepared in DMSO and further serially diluted in DMEM. The cells were treated for 24 h. The final concentration of DMSO was<0.25%. After incubation, the medium was aspirated and replaced by 100 μL of fresh medium containing MTT (0.5 mg/mL). The plates were subsequently incubated at 37 °C in CO_2 incubator for 45 min. The medium containing MTT was aspirated after 45 min incubation and formed purple formazan was dissolved in 100 μL of DMSO. The optical density of each well was measured using Synergy 2 Multi-Mode Microplate Reader (BioTek Instruments, Inc., Winooski, VT, USA) at 570 nm. The cell viability was expressed as the percentage of untreated control. The results were obtained from three independent experiments performed in triplicate. The IC_{50} values were calculated using four parametric non-linear regression by statistic GraphPad Prism software (version 5.04, GraphPad Software Inc., San Diego, CA) by the logarithmic dose–response curve. The IC_{50} values were expressed as a mean ± SEM.

5.10. PAMPA-BBB assay

Parallel artificial membrane permeability assay is a high-throughput screening tool applied to predict the passive transport of potential drugs across the blood–brain barrier [73]. It was used as a non-cell-based *in vitro* assay carried out in a coated 96-well membrane filter. The filter membrane of the donor plate was coated with polar brain lipid (PBL, Avanti, USA) in dodecane (4 μL of 20 mg/mL PBL in dodecane). The acceptor well was filled with 300 μL of PBS buffer (pH 7.4; V_A). Tested compounds were dissolved first in DMSO and then diluted with PBS (pH 7.4) to reach the final concentration 30 – 50 μM in the donor well. The concentration of DMSO did not exceed 0.5% (v/v) in the donor solution. 300 μL of the donor solution (V_D) was added to the donor wells and the donor filter plate was carefully put on the acceptor plate so that the coated membrane was "in touch" with both donor solution and acceptor buffer. Tested compounds diffused from the donor well through the polar brain lipid membrane (area = 0.28 cm^2) to the acceptor well. The concentration of tested compounds in both donor and acceptor wells was assessed after 3, 4, 5 and 6 h of incubation respectively in quadruplicate using the UV plate reader Synergy HT (Biotek, USA) at the maximum absorption wavelength of each compound. Also solutions at theoretical equilibrium of given compounds (i.e. theoretical concentration if the donor and acceptor compartments were simply combined) were prepared. The concentration of the compounds in the donor and acceptor well and equilibrium concentration were calculated from the standard curve and expressed as the permeability according the equation:

$$\log Pe = \log\left\{ C \times -\ln\left(1 - \frac{[drug]_{acceptor}}{[drug]_{equilibrium}}\right)\right\}$$

$$\text{where } C = \left(\frac{V_D \times V_A}{(V_D + V_A) \times Area \times Time}\right)$$

5.11. Maximum tolerated dose determination

Adult Wistar rats (body weight 409 – 483 g) were randomly assigned to experimental groups consisting of three males per applied dose of **10w**. Several doses were administered to identify the MTD, with a starting dose being of 1 mg/kg according to previously described protocol [83]. **10w** was administered via i.p. injection in standardized volumes of 1 $mL.kg^{-1}$ or 2 $mL.kg^{-1}$ depending on compoundś solubility. Treated rats were extensively observed for signs of toxicity within first five hours; then periodically for 48 h. Clinical signs, such as cardiovascular, respiratory and nervous system disability were monitored according to Laboratory Animal Science Association (UK) guidelines. Severity of symptoms was classified as mild, moderate and substantial [84]. If the category of substantial severity was achieved within 48 h, animals were immediately euthanized by CO_2 and subsequently lower dose was selected for further group. Similarly, if severe adverse effect or death occurred within a few minutes after administration to the first animal in the group, other animals were not treated and lower dose was selected as well. All animals surviving 48 h were euthanized by CO_2. Higher doses than 10 mg/kg was not able to solubilize, therefore the dose 10 mg/kg is considered as the maximum feasible dose.

5.12. Morris water Maze test

The experiments were performed in adult (3 months old, 400 – 550 g) male Wistar rats. The rats were obtained from the breeding colony of the Institute of Physiology, Czech Academy of Sciences. The rats were housed in pairs in transparent plastic cages (20 × 25 × 40 cm) in an

animal room with stable temperature, humidity and a 12-hour light cycle. Water and food were available *ad libitum*. The experiments were performed in the light phase of the day. All experiments were conducted in accordance with the guidelines of the European Union directive 2010/63/EU and approved by the Animal Care and Use Committee of the National Institute of Mental Health (reference number MZDR 51755/2018–4/OVZ). Scopolamine hydrobromide and tacrine hydrochloride were purchased from Sigma-Aldrich (Czech Republic). Scopolamine rodent model was adopted to induce AD-like phenotype, especially amnesia.

Rats were divided into four experimental groups as per the given treatment: (i) vehicle, (ii) scopolamine, (iii) scopolamine + **10w**, and (iv) scopolamine + tacrine. Each group consisted of six animals with the exception of the vehicle group, which consisted of seven animals. Each rat received two i.p. injections. Scopolamine hydrobromide (2.5 mg/kg) was dissolved in saline and administered 20 min before the start of MWM test to all groups except the vehicle-injected control group that received an equal volume of saline only. The suitability of selected scopolamine dose was verified within previous experiments published in the literature [85,86]. Tacrine hydrochloride was dissolved in 5% DMSO in redistilled water and applied at the dose of 2.5 mg/kg 10 min prior to administration of scopolamine. **10w** was dissolved in 5% DMSO in redistilled water and applied at the dose of 2 mg/kg 5 min before the start of MWM test. The timing of **10w** application before the experiment was chosen pursuant to results of the previous experiment dealing with MTD determination, i.e. shorter mild activity decrease and diarrhoea were observed 5 min after **10w** administration. The rats in the vehicle group received an equal volume of 5% DMSO in redistilled water instead of **10w**. All these treatments were applied each day before MWM (4 consecutive days). The volume of i.p. injections was 1 mL/kg. The MWM apparatus consisting of a blue plastic circular pool (180 cm in diameter) was filled with water (23 °C) up to 28 cm depth. The pool was divided into four quadrants and contained an escape platform (circular, 10 cm in diameter, transparent plastic), placed 1 cm below the water surface in the middle of the NW quadrant. The position of the platform was stable during whole experiment. The MWM test was conducted during 4 consecutive days. Every testing day each rat underwent 8 swims from different starting positions (their order was random and different each day). The rats were released into the pool facing the wall. Each trial lasted for 60 s. If the rat did not find the platform during this time, it was guided to the platform by the experimenter. During the experiment the rats were tracked by a camera connected to a tracking system (Tracker, Biosignal Group, New York, USA). Thereafter, the data were analysed using Carousel Maze Manager (https://github.com/bahniks/CM_Manager_0_4_0). The distance moved (m) and escape latency (s) on day 4 were analysed. The mean distance moved and the mean latency were calculated for each rat from all trials performed on day 4. Subsequently, group means were calculated and shown on graphs. Statistical analysis was conducted in GraphPad Prism 5.0 software (San Diego, USA). One-way ANOVA was performed, followed by Tukey's post hoc test. The differences were considered as significant at $p < 0.05$.

Declaration of Competing Interest

The authors declare that they have no known competing financial interests or personal relationships that could have appeared to influence the work reported in this paper.

Acknowledgement

First of all, the authors would like to express their gratitude to laboratory assistants Martina Techlovska, Pavlina Jelinkova, Maria Anna Jancovicova and Lucie Krbalek. Further, this work was supported by the project Excellence UHK, by the ERDF/ESF project "PharmaBrain" (No. CZ.02.1.01/0.0/0.0/16_025/0007444), by MH CZ-DRO (University Hospital Hradec Kralove, No. 00179906), by project PROGRES Q40 (Charles University in Prague, Czech Republic), by Long Term Development Plan of University of Hradec Kralove, by a grant of Ministry of Defence "Long Term Development Plan" Medical Aspects of Weapons of Mass Destruction of the Faculty of Military Health Sciences, University of Defence, by the National Institute of Mental Health (NIMH-CZ) project No. LO1611 with a financial support from the MEYS under the NPU I program and by the project PERSONMED - Center for the Development of Personalized Medicine in Age-Related Diseases (Reg. No. CZ.02.1.01/0.0/0.0/17_048/0007441), co-financed by ERDF and state budget of the Czech Republic, and by the Ministry of Education, Youth and Sports of Czech Republic (project ERDF IT4N No. CZ.02.1.01/0.0/0.0/18_069/0010054). This work was also supported by University of Hradec Kralove (No. SV2105-2020, VT2019-2021). Computational resources were provided by the CESNET LM2015042 and the CERIT Scientific Cloud LM2015085, provided within the programme "Projects of Large Research, Development, and Innovations Infrastructures". This work was also supported by the research grants VEGA 2/0145/17, MVTS COST 083/14 action BM1405, Czech Science Foundation (Project No. 20-29633J) and by the Slovak Research and Development Agency under contract No. APVV – 18-0284. Last but not least, this work received funding from the European Unionś Horizon 2020 research, innovation programme under grant agreement number 654148 Laserlab-Europe, Wellcome Trust (204821/Z/16/Z), The Rosetrees Trust and the RSMacDonald Charitable Trust.

Appendix A. Supplementary data

Supplementary data to this article can be found online at https://doi.org/10.1016/j.bioorg.2020.104596.

References

[1] P. Scheltens, K. Blennow, M.M.B. Breteler, B. de Strooper, G.B. Frisoni, S. Salloway, W.M. Van der Flier, Alzheimer's Disease, Lancet Lond. Engl. 388 (10043) (2016) 505–517, https://doi.org/10.1016/S0140-6736(15)01124-1.
[2] J. Folch, D. Petrov, M. Ettcheto, S. Abad, E. Sánchez-López, M.L. García, J. Olloquequi, C. Beas-Zarate, C. Auladell, A. Camins, Current Research Therapeutic Strategies for Alzheimer's Disease Treatment, Neural Plast. 2016 (2016) 8501693, https://doi.org/10.1155/2016/8501693.
[3] Alzheimer's Association. 2015 Alzheimer's Disease Facts and Figures. Alzheimers Dement. J. Alzheimers Assoc. 2015, 11 (3), 332–384.
[4] R.T. Bartus, R.L. Dean, B. Beer, A.S. Lippa, The Cholinergic Hypothesis of Geriatric Memory Dysfunction, Science 217 (4558) (1982) 408–414.
[5] P. Davies, Challenging the Cholinergic Hypothesis in Alzheimer Disease, JAMA 281 (15) (1999) 1433–1434.
[6] J.A. Hardy, G.A. Higgins, Alzheimer's Disease: The Amyloid Cascade Hypothesis, Science 256 (5054) (1992) 184–185.
[7] J. Hardy, D.J. Selkoe, The Amyloid Hypothesis of Alzheimer's Disease: Progress and Problems on the Road to Therapeutics, Science 297 (5580) (2002) 353–356, https://doi.org/10.1126/science.1072994.
[8] L. Tillement, L. Lecanu, V. Papadopoulos, Alzheimer's Disease: Effects of β-Amyloid on Mitochondria, Mitochondrion 11 (1) (2011) 13–21, https://doi.org/10.1016/j.mito.2010.08.009.
[9] B.L. Kagan, R. Azimov, R. Azimova, Amyloid Peptide Channels, J. Membr. Biol. 202 (1) (2004) 1–10, https://doi.org/10.1007/s00232-004-0709-4.
[10] C.A. Hansson Petersen, N. Alikhani, H. Behbahani, B. Wiehager, P.F. Pavlov, I. Alafuzoff, V. Leinonen, A. Ito, B. Winblad, E. Glaser, M. Ankarcrona, The Amyloid Beta-Peptide Is Imported into Mitochondria via the TOM Import Machinery and Localized to Mitochondrial Cristae, Proc. Natl. Acad. Sci. U. S. A. 105 (35) (2008) 13145–13150, https://doi.org/10.1073/pnas.0806192105.
[11] J.W. Lustbader, M. Cirilli, C. Lin, H.W. Xu, K. Takuma, N. Wang, C. Caspersen, X. Chen, S. Pollak, M. Chaney, F. Trinchese, S. Liu, F. Gunn-Moore, L.-F. Lue, D. G. Walker, P. Kuppusamy, Z.L. Zewier, O. Arancio, D. Stern, S.S. Yan, H. Wu, ABAD Directly Links Abeta to Mitochondrial Toxicity in Alzheimer's Disease, Science 304 (5669) (2004) 448–452, https://doi.org/10.1126/science.1091230.
[12] A. Morsy, P.C. Trippier, Amyloid-Binding Alcohol Dehydrogenase (ABAD) Inhibitors for the Treatment of Alzheimer's Disease, J. Med. Chem. 62 (9) (2019) 4252–4264, https://doi.org/10.1021/acs.jmedchem.8b01530.
[13] S.F. Cappa, The Quest for an Alzheimer Therapy, Front. Neurol. 9 (2018) 108, https://doi.org/10.3389/fneur.2018.00108.
[14] D.A. Drachman, J. Leavitt, Human Memory and the Cholinergic System. A Relationship to Aging? Arch. Neurol. 30 (2) (1974) 113–121, https://doi.org/10.1001/archneur.1974.00490320001001.
[15] F. Zemek, L. Drtinova, E. Nepovimova, V. Sepsova, J. Korabecny, J. Klimes, K. Kuca, Outcomes of Alzheimer's Disease Therapy with Acetylcholinesterase

Inhibitors and Memantine, Expert Opin. Drug Saf. 13 (6) (2014) 759–774, https://doi.org/10.1517/14740338.2014.914168.
[16] K. Kuca, O. Soukup, P. Maresova, J. Korabecny, E. Nepovimova, B. Klimova, J. Honegr, T. Ramalho, T. França, Current Approaches Against Alzheimer's Disease in Clinical Trials, J. Braz. Chem. Soc. 27 (2016), https://doi.org/10.5935/0103-5053.20160048.
[17] R. Morphy, Z. Rankovic, Designing Multiple Ligands - Medicinal Chemistry Strategies and Challenges, Curr. Pharm. Des. 15 (6) (2009) 587–600, https://doi.org/10.2174/138161209787315594.
[18] M.L. Bolognesi, M. Rosini, V. Andrisano, M. Bartolini, A. Minarini, V. Tumiatti, C. Melchiorre, MTDL Design Strategy in the Context of Alzheimer's Disease: From Lipocrine to Memoquin and Beyond, Curr. Pharm. Des. 15 (6) (2009) 601–613, https://doi.org/10.2174/138161209787315585.
[19] A. Rampa, F. Belluti, S. Gobbi, A. Bisi, Hybrid-Based Multi-Target Ligands for the Treatment of Alzheimer's Disease, Curr. Top. Med. Chem. 11 (22) (2011) 2716–2730, https://doi.org/10.2174/156802611798184409.
[20] H. Hampel, M.-M. Mesulam, A.C. Cuello, M.R. Farlow, E. Giacobini, G. T. Grossberg, A.S. Khachaturian, A. Vergallo, E. Cavedo, P.J. Snyder, Z. S. Khachaturian, The Cholinergic System in the Pathophysiology and Treatment of Alzheimer's Disease, Brain J. Neurol. 141 (7) (2018) 1917–1933, https://doi.org/10.1093/brain/awy132.
[21] M.A. Chacón, A.E. Reyes, N.C. Inestrosa, Acetylcholinesterase Induces Neuronal Cell Loss, Astrocyte Hypertrophy and Behavioral Deficits in Mammalian Hippocampus, J. Neurochem. 87 (1) (2003) 195–204, https://doi.org/10.1046/j.1471-4159.2003.01985.x.
[22] A.E. Reyes, M.A. Chacón, M.C. Dinamarca, W. Cerpa, C. Morgan, N.C. Inestrosa, Acetylcholinesterase-Abeta Complexes Are More Toxic than Abeta Fibrils in Rat Hippocampus: Effect on Rat Beta-Amyloid Aggregation, Laminin Expression, Reactive Astrocytosis, and Neuronal Cell Loss, Am. J. Pathol. 164 (6) (2004) 2163–2174, https://doi.org/10.1016/s0002-9440(10)63774-1.
[23] M.C. Dinamarca, J.P. Sagal, R.A. Quintanilla, J.A. Godoy, M.S. Arrázola, N. C. Inestrosa, Amyloid-Beta-Acetylcholinesterase Complexes Potentiate Neurodegenerative Changes Induced by the Abeta Peptide. Implications for the Pathogenesis of Alzheimer's Disease, Mol. Neurodegener. 5 (2010) 4, https://doi.org/10.1186/1750-1326-5-4.
[24] M. Gancar, K. Ho, S.A. Mohid, N.Q. Thai, Z. Bednarikova, H.L. Nguyen, A. Bhunia, E. Nepovimova, M.S. Li, Z. Gazova, 7-Methoxytacrine and 2-Aminobenzothiazole Heterodimers: Structure-Mechanism Relationship of Amyloid Inhibitors Based on Rational Design, ACS Chem. Neurosci. 11 (5) (2020) 715–729, https://doi.org/10.1021/acschemneuro.9b00419.
[25] B. Jarrott, Tacrine. In Vivo Veritas, Pharmacol. Res. 116 (2017) 29–31, https://doi.org/10.1016/j.phrs.2016.12.033.
[26] M. Horak, K. Holubova, E. Nepovimova, J. Krusek, M. Kaniakova, J. Korabecny, L. Vyklicky, K. Kuca, A. Stuchlik, J. Ricny, K. Vales, O. Soukup, The Pharmacology of Tacrine at N-Methyl-d-Aspartate Receptors, Prog. Neuropsychopharmacol. Biol. Psychiatry 75 (2017) 54–62, https://doi.org/10.1016/j.pnpbp.2017.01.003.
[27] W.K. Summers, K.H. Tachiki, A. Kling, Tacrine in the Treatment of Alzheimer's Disease. A Clinical Update and Recent Pharmacologic Studies, Eur. Neurol. 29 (Suppl 3) (1989) 28–32, https://doi.org/10.1159/000116478.
[28] B. Sameem, M. Saeedi, M. Mahdavi, A. Shafiee, A Review on Tacrine-Based Scaffolds as Multi-Target Drugs (MTDLs) for Alzheimer's Disease, Eur. J. Med. Chem. 128 (2017) 332–345, https://doi.org/10.1016/j.ejmech.2016.10.060.
[29] M. Przybyłowska, S. Kowalski, K. Dzierzbicka, I. Inkielewicz-Stepniak, Therapeutic Potential of Multifunctional Tacrine Analogues, Curr. Neuropharmacol. 17 (5) (2019) 472–490, https://doi.org/10.2174/1570159X16666180412091908.
[30] J. Patocka, 9-amino-7-methoxy-1,2,3,4-tetrahydroacridine, a new substance with indirect cholinomimetic effects, Cesk. Farm. 39 (1) (1990) 29–32.
[31] M. Recanatini, A. Cavalli, F. Belluti, L. Piazzi, A. Rampa, A. Bisi, S. Gobbi, P. Valenti, V. Andrisano, M. Bartolini, V. Cavrini, SAR of 9-Amino-1,2,3,4-Tetrahydroacridine-Based Acetylcholinesterase Inhibitors: Synthesis, Enzyme Inhibitory Activity, QSAR, and Structure-Based CoMFA of Tacrine Analogues, J. Med. Chem. 43 (10) (2000) 2007–2018, https://doi.org/10.1021/jm990971t.
[32] L. Hroch, L. Aitken, O. Benek, M. Dolezal, K. Kuca, F. Gunn-Moore, K. Musilek, Benzothiazoles - Scaffold of Interest for CNS Targeted Drugs, Curr. Med. Chem. 22 (6) (2015) 730–747, https://doi.org/10.2174/0929867322666141212120631.
[33] A. Imramovský, V. Pejchal, Š. Štěpánková, K. Vorčáková, J. Jampílek, J. Vančo, P. Šimůnek, K. Královec, L. Brůčková, J. Mandíková, F. Trejtnar, Synthesis and in Vitro Evaluation of New Derivatives of 2-Substituted-6-Fluorobenzo[d]Thiazoles as Cholinesterase Inhibitors, Bioorg. Med. Chem. 21 (7) (2013) 1735–1748, https://doi.org/10.1016/j.bmc.2013.01.052.
[34] R.S. Keri, C. Quintanova, S.M. Marques, A.R. Esteves, S.M. Cardoso, M.A. Santos, Design, Synthesis and Neuroprotective Evaluation of Novel Tacrine-Benzothiazole Hybrids as Multi-Targeted Compounds against Alzheimer's Disease, Bioorg. Med. Chem. 21 (15) (2013) 4559–4569, https://doi.org/10.1016/j.bmc.2013.05.028.
[35] L. Huang, T. Su, W. Shan, Z. Luo, Y. Sun, F. He, X. Li, Inhibition of Cholinesterase Activity and Amyloid Aggregation by Berberine-Phenyl-Benzoheterocyclic and Tacrine-Phenyl-Benzoheterocyclic Hybrids, Bioorg. Med. Chem. 20 (9) (2012) 3038–3048, https://doi.org/10.1016/j.bmc.2012.02.059.
[36] R. Rajeshwari, K. Chand, E. Candeias, S.M. Cardoso, S. Chaves, M.A. Santos, New Multitarget Hybrids Bearing Tacrine and Phenylbenzothiazole Motifs as Potential Drug Candidates for Alzheimer's Disease, Mol. Basel Switz. 24 (3) (2019), https://doi.org/10.3390/molecules24030587.
[37] L. Aitken, O. Benek, B.E. McKelvie, R.E. Hughes, L. Hroch, M. Schmidt, L.L. Major, L. Vinklarova, K. Kuca, T.K. Smith, K. Musilek, F.J. Gunn-Moore, Novel Benzothiazole-Based Ureas as 17β-HSD10 Inhibitors, A Potential Alzheimer's Disease Treatment, Molecules 24 (15) (2019), https://doi.org/10.3390/molecules24152757.
[38] E. Nepovimova, E. Uliassi, J. Korabecny, L.E. Peña-Altamira, S. Samez, A. Pesaresi, G.E. Garcia, M. Bartolini, V. Andrisano, C. Bergamini, R. Fato, D. Lamba, M. Roberti, K. Kuca, B. Monti, M.L. Bolognesi, Multitarget Drug Design Strategy: Quinone-Tacrine Hybrids Designed to Block Amyloid-β Aggregation and to Exert Anticholinesterase and Antioxidant Effects, J. Med. Chem. 57 (20) (2014) 8576–8589, https://doi.org/10.1021/jm5010804.
[39] E. Nepovimova, J. Korabecny, R. Dolezal, K. Babkova, A. Ondrejicek, D. Jun, V. Sepsova, A. Horova, M. Hrabinova, O. Soukup, N. Bukum, P. Jost, L. Muckova, J. Kassa, D. Malinak, M. Andrs, K. Kuca, Tacrine-Trolox Hybrids: A Novel Class of Centrally Active, Nonhepatotoxic Multi-Target-Directed Ligands Exerting Anticholinesterase and Antioxidant Activities with Low In Vivo Toxicity, J. Med. Chem. 58 (22) (2015) 8985–9003, https://doi.org/10.1021/acs.jmedchem.5b01325.
[40] K. Chalupova, J. Korabecny, M. Bartolini, B. Monti, D. Lamba, R. Caliandro, A. Pesaresi, X. Brazzolotto, A.-J. Gastellier, F. Nachon, J. Pejchal, M. Jarosova, V. Hepnarova, D. Jun, M. Hrabinova, R. Dolezal, J. Zdarova Karasova, M. Mzik, Z. Kristofikova, J. Misik, L. Muckova, P. Jost, O. Soukup, M. Benkova, V. Setnicka, L. Habartova, M. Chvojkova, L. Kleteckova, K. Vales, E. Mezeiova, E. Uliassi, M. Valis, E. Nepovimova, M.L. Bolognesi, K. Kuca, Novel Tacrine-Tryptophan Hybrids: Multi-Target Directed Ligands as Potential Treatment for Alzheimer's Disease, Eur. J. Med. Chem. 168 (2019) 491–514, https://doi.org/10.1016/j.ejmech.2019.02.021.
[41] R.M. Lane, S.G. Potkin, A. Enz, Targeting Acetylcholinesterase and Butyrylcholinesterase in Dementia, Int. J. Neuropsychopharmacol. 9 (1) (2006) 101–124, https://doi.org/10.1017/S1461145705005833.
[42] G.L. Ellman, K.D. Courtney, V. Andres, R.M. Feather-Stone, A New and Rapid Colorimetric Determination of Acetylcholinesterase Activity, Biochem. Pharmacol. 7 (1961) 88–95, https://doi.org/10.1016/0006-2952(61)90145-9.
[43] O. Soukup, D. Jun, J. Zdarova-Karasova, J. Patocka, K. Musilek, J. Korabecny, J. Krusek, M. Kaniakova, V. Sepsova, J. Mandikova, F. Trejtnar, M. Pohanka, L. Drtinova, M. Pavlik, G. Tobin, K. Kuca, A Resurrection of 7-MEOTA: A Comparison with Tacrine, Curr. Alzheimer Res. 10 (8) (2013) 893–906.
[44] O. Trott, A.J. Olson, AutoDock Vina: Improving the Speed and Accuracy of Docking with a New Scoring Function, Efficient Optimization, and Multithreading, J. Comput. Chem. 31 (2) (2010) 455–461, https://doi.org/10.1002/jcc.21334.
[45] J. Cheung, M.J. Rudolph, F. Burshteyn, M.S. Cassidy, E.N. Gary, J. Love, M. C. Franklin, J.J. Height, Structures of Human Acetylcholinesterase in Complex with Pharmacologically Important Ligands, J. Med. Chem. 55 (22) (2012) 10282–10286, https://doi.org/10.1021/jm300871x.
[46] S.T. Wlodek, J. Antosiewicz, J.A. McCammon, T.P. Straatsma, M.K. Gilson, J. M. Briggs, C. Humblet, J.L. Sussman, Binding of Tacrine and 6-Chlorotacrine by Acetylcholinesterase, Biopolymers 38 (1) (1996) 109–117, https://doi.org/10.1002/(SICI)1097-0282(199601)38:1%3C109::AID-BIP9%3E3.0.CO;2-#.
[47] P. Camps, X. Formosa, C. Galdeano, D. Muñoz-Torrero, L. Ramírez, E. Gómez, N. Isambert, R. Lavilla, A. Badia, M.V. Clos, M. Bartolini, F. Mancini, V. Andrisano, M.P. Arce, M.I. Rodríguez-Franco, O. Huertas, T. Dafni, F.J. Luque, Pyrano[3,2-c] Quinoline-6-Chlorotacrine Hybrids as a Novel Family of Acetylcholinesterase- and Beta-Amyloid-Directed Anti-Alzheimer Compounds, J. Med. Chem. 52 (17) (2009) 5365–5379, https://doi.org/10.1021/jm900859q.
[48] O. Di Pietro, F.J. Pérez-Areales, J. Juárez-Jiménez, A. Espargaró, M.V. Clos, B. Pérez, R. Lavilla, R. Sabaté, F.J. Luque, D. Muñoz-Torrero, Tetrahydrobenzo[h] [1,6]Naphthyridine-6-Chlorotacrine Hybrids as a New Family of Anti-Alzheimer Agents Targeting β-Amyloid, Tau, and Cholinesterase Pathologies, Eur. J. Med. Chem. 84 (2014) 107–117, https://doi.org/10.1016/j.ejmech.2014.07.021.
[49] V. Hepnarova, J. Korabecny, L. Matouskova, P. Jost, L. Muckova, M. Hrabinova, N. Vykoukalova, M. Kerhartova, T. Kucera, R. Dolezal, E. Nepovimova, K. Spilovska, E. Mezeiova, N.L. Pham, D. Jun, F. Staud, D. Kaping, K. Kuca, O. Soukup, The Concept of Hybrid Molecules of Tacrine and Benzyl Quinolone Carboxylic Acid (BQCA) as Multifunctional Agents for Alzheimer's Disease, Eur. J. Med. Chem. 150 (2018) 292–306, https://doi.org/10.1016/j.ejmech.2018.02.083.
[50] C. Galdeano, E. Viayna, I. Sola, X. Formosa, P. Camps, A. Badia, M.V. Clos, J. Relat, M. Ratia, M. Bartolini, F. Mancini, V. Andrisano, M. Salmona, C. Minguillón, G. C. González-Muñoz, M.I. Rodríguez-Franco, A. Bidon-Chanal, F.J. Luque, D. Muñoz-Torrero, Huprine-Tacrine Heterodimers as Anti-Amyloidogenic Compounds of Potential Interest against Alzheimer's and Prion Diseases, J. Med. Chem. 55 (2) (2012) 661–669, https://doi.org/10.1021/jm200840c.
[51] J. Korabecny, R. Dolezal, P. Cabelova, A. Horova, E. Hruba, J. Ricny, L. Sedlacek, E. Nepovimova, K. Spilovska, M. Andrs, K. Musilek, V. Opletalova, V. Sepsova, D. Ripova, K. Kuca, 7-MEOTA-Donepezil like Compounds as Cholinesterase Inhibitors: Synthesis, Pharmacological Evaluation, Molecular Modeling and QSAR Studies, Eur. J. Med. Chem. 82 (2014) 426–438, https://doi.org/10.1016/j.ejmech.2014.05.066.
[52] N.C. Inestrosa, A. Alvarez, C.A. Pérez, R.D. Moreno, M. Vicente, C. Linker, O. I. Casanueva, C. Soto, J. Garrido, Acetylcholinesterase Accelerates Assembly of Amyloid-Beta-Peptides into Alzheimer's Fibrils: Possible Role of the Peripheral Site of the Enzyme, Neuron 16 (4) (1996) 881–891, https://doi.org/10.1016/s0896-6273(00)80108-7.
[53] K. Spilovska, J. Korabecny, V. Sepsova, D. Jun, M. Hrabinova, P. Jost, L. Muckova, O. Soukup, J. Janockova, T. Kucera, R. Dolezal, E. Mezeiova, D. Kaping, K. Kuca, Novel Tacrine-Scutellarin Hybrids as Multipotent Anti-Alzheimer's Agents: Design, Synthesis and Biological Evaluation, Molecules 22 (6) (2017), https://doi.org/10.3390/molecules22061006.
[54] K. Spilovska, J. Korabecny, J. Kral, A. Horova, K. Musilek, O. Soukup, L. Drtinova, Z. Gazova, K. Siposova, K. Kuca, 7-Methoxytacrine-Adamantylamine Heterodimers

as Cholinesterase Inhibitors in Alzheimer's Disease Treatment-Synthesis, Biological Evaluation and Molecular Modeling Studies, Molecules 18 (2) (2013) 2397–2418, https://doi.org/10.3390/molecules18022397.
[55] G.F. Makhaeva, N.V. Kovaleva, N.P. Boltneva, S.V. Lushchekina, T.Y. Astakhova, E. V. Rudakova, A.N. Proshin, I.V. Serkov, E.V. Radchenko, V.A. Palyulin, S. O. Bachurin, R.J. Richardson, New Hybrids of 4-Amino-2,3-Polymethylene-Quinoline and p-Tolylsulfonamide as Dual Inhibitors of Acetyl- and Butyrylcholinesterase and Potential Multifunctional Agents for Alzheimer's Disease Treatment, Molecules 25 (17) (2020), https://doi.org/10.3390/molecules25173915.
[56] R.N. Martins, P.J. Robinson, J.O. Chleboun, K. Beyreuther, C.L. Masters, The Molecular Pathology of Amyloid Deposition in Alzheimer's Disease, Mol. Neurobiol. 5 (2–4) (1991) 389–398.
[57] G. Verdile, S. Fuller, C.S. Atwood, S.M. Laws, S.E. Gandy, R.N. Martins, The Role of Beta Amyloid in Alzheimer's Disease: Still a Cause of Everything or the Only One Who Got Caught? Pharmacol. Res. 50 (4) (2004) 397–409, https://doi.org/10.1016/j.phrs.2003.12.028.
[58] R. Khurana, C. Coleman, C. Ionescu-Zanetti, S.A. Carter, V. Krishna, R.K. Grover, R. Roy, S. Singh, Mechanism of Thioflavin T Binding to Amyloid Fibrils, J. Struct. Biol. 151 (3) (2005) 229–238, https://doi.org/10.1016/j.jsb.2005.06.006.
[59] M. Biancalana, S. Koide, Molecular Mechanism of Thioflavin-T Binding to Amyloid Fibrils, Biochim. Biophys. Acta 1804 (7) (2010) 1405–1412, https://doi.org/10.1016/j.bbapap.2010.04.001.
[60] F.T.S. Chan, G.S. Kaminski Schierle, J.R. Kumita, C.W. Bertoncini, C.M. Dobson, C. F. Kaminski, Protein Amyloids Develop an Intrinsic Fluorescence Signature during Aggregation, The Analyst 138 (7) (2013) 2156–2162, https://doi.org/10.1039/c3an36798c.
[61] M. Bartolini, M. Naldi, J. Fiori, F. Valle, F. Biscarini, D.V. Nicolau, V. Andrisano, Kinetic Characterization of Amyloid-Beta 1–42 Aggregation with a Multimethodological Approach, Anal. Biochem. 414 (2) (2011) 215–225, https://doi.org/10.1016/j.ab.2011.03.020.
[62] D. Pinotsi, A.K. Buell, C.M. Dobson, G.S. Kaminski Schierle, C.F. Kaminski, A Label-Free, Quantitative Assay of Amyloid Fibril Growth Based on Intrinsic Fluorescence, Chembiochem 14 (7) (2013) 846–850, https://doi.org/10.1002/cbic.201300103.
[63] M. Bartolini, C. Bertucci, M.L. Bolognesi, A. Cavalli, C. Melchiorre, V. Andrisano, Insight into the Kinetic of Amyloid Beta (1–42) Peptide Self-Aggregation: Elucidation of Inhibitors' Mechanism of Action, Chembiochem Eur. J. Chem. Biol. 8 (17) (2007) 2152–2161, https://doi.org/10.1002/cbic.200700427.
[64] S.D. Yan, J. Fu, C. Soto, X. Chen, H. Zhu, F. Al-Mohanna, K. Collison, A. Zhu, E. Stern, T. Saido, M. Tohyama, S. Ogawa, A. Roher, D. Stern, An Intracellular Protein That Binds Amyloid-Beta Peptide and Mediates Neurotoxicity in Alzheimer's Disease, Nature 389 (6652) (1997) 689–695, https://doi.org/10.1038/39522.
[65] S.D. Yan, Y. Shi, A. Zhu, J. Fu, H. Zhu, Y. Zhu, L. Gibson, E. Stern, K. Collison, F. Al-Mohanna, S. Ogawa, A. Roher, S.G. Clarke, D.M. Stern, Role of ERAB/L-3-Hydroxyacyl-Coenzyme A Dehydrogenase Type II Activity in Abeta-Induced Cytotoxicity, J. Biol. Chem. 274 (4) (1999) 2145–2156, https://doi.org/10.1074/jbc.274.4.2145.
[66] X.Y. He, G.Y. Wen, G. Merz, D. Lin, Y.Z. Yang, P. Mehta, H. Schulz, S.Y. Yang, Abundant Type 10 17 Beta-Hydroxysteroid Dehydrogenase in the Hippocampus of Mouse Alzheimer's Disease Model, Brain Res. Mol. Brain Res. 99 (1) (2002) 46–53, https://doi.org/10.1016/s0169-328x(02)00102-x.
[67] Y. Xie, S. Deng, Z. Chen, S. Yan, D.W. Landry, Identification of Small-Molecule Inhibitors of the Abeta-ABAD Interaction, Bioorg. Med. Chem. Lett. 16 (17) (2006) 4657–4660, https://doi.org/10.1016/j.bmcl.2006.05.099.
[68] L. Hroch, O. Benek, P. Guest, L. Aitken, O. Soukup, J. Janockova, K. Musil, V. Dohnal, R. Dolezal, K. Kuca, T.K. Smith, F. Gunn-Moore, K. Musilek, Design, Synthesis and in Vitro Evaluation of Benzothiazole-Based Ureas as Potential ABAD/17β-HSD10 Modulators for Alzheimer's Disease Treatment, Bioorg. Med. Chem. Lett. 26 (15) (2016) 3675–3678, https://doi.org/10.1016/j.bmcl.2016.05.087.
[69] T. Mosmann, Rapid Colorimetric Assay for Cellular Growth and Survival: Application to Proliferation and Cytotoxicity Assays, J. Immunol. Methods 65 (1–2) (1983) 55–63, https://doi.org/10.1016/0022-1759(83)90303-4.
[70] P.B. Watkins, H.J. Zimmerman, M.J. Knapp, S.I. Gracon, K.W. Lewis, Hepatotoxic Effects of Tacrine Administration in Patients with Alzheimer's Disease, JAMA 271 (13) (1994) 992–998.
[71] M. Kaniakova, E. Nepovimova, L. Kleteckova, K. Skrenkova, K. Holubova, Z. Chrienova, V. Hepnarova, T. Kucera, T. Kobrlova, K. Vales, J. Korabecny, O. Soukup, M. Horak, Combination of Memantine and 6-Chlorotacrine as Novel Multi-Target Compound against Alzheimer's Disease, Curr. Alzheimer Res. 16 (9) (2019) 821–833, https://doi.org/10.2174/1567205016666190228122218.
[72] G.L. Perlovich, A.N. Proshin, T.V. Volkova, L.N. Petrova, S.O. Bachurin, Novel 1,2,4-Thiadiazole Derivatives as Potent Neuroprotectors: Approach to Creation of Bioavailable Drugs, Mol. Pharm. 9 (8) (2012) 2156–2167, https://doi.org/10.1021/mp300011r.
[73] L. Di, E.H. Kerns, K. Fan, O.J. McConnell, G.T. Carter, High Throughput Artificial Membrane Permeability Assay for Blood-Brain Barrier, Eur. J. Med. Chem. 38 (3) (2003) 223–232.
[74] R.A. Lenz, J.D. Baker, C. Locke, L.E. Rueter, E.G. Mohler, K. Wesnes, W. Abi-Saab, M.D. Saltarelli, The Scopolamine Model as a Pharmacodynamic Marker in Early Drug Development, Psychopharmacology (Berl.) 220 (1) (2012) 97–107, https://doi.org/10.1007/s00213-011-2456-4.
[75] G.M. Morris, R. Huey, W. Lindstrom, M.F. Sanner, R.K. Belew, D.S. Goodsell, A. J. Olson, AutoDock4 and AutoDockTools4: Automated Docking with Selective Receptor Flexibility, J. Comput. Chem. 30 (16) (2009) 2785–2791, https://doi.org/10.1002/jcc.21256.
[76] E.F. Pettersen, T.D. Goddard, C.C. Huang, G.S. Couch, D.M. Greenblatt, E.C. Meng, T.E. Ferrin, UCSF Chimera–a Visualization System for Exploratory Research and Analysis, J. Comput. Chem. 25 (13) (2004) 1605–1612, https://doi.org/10.1002/jcc.20084.
[77] D. Panek, A. Więckowska, T. Wichur, M. Bajda, J. Godyń, J. Jończyk, K. Mika, J. Janockova, O. Soukup, D. Knez, J. Korabecny, S. Gobec, B. Malawska, Design, Synthesis and Biological Evaluation of New Phthalimide and Saccharin Derivatives with Alicyclic Amines Targeting Cholinesterases, Beta-Secretase and Amyloid Beta Aggregation, Eur. J. Med. Chem. 125 (2017) 676–695, https://doi.org/10.1016/j.ejmech.2016.09.078.
[78] L.F.N. Lemes, G. de Andrade Ramos, A.S. de Oliveira, F.M.R. da Silva, G. de Castro Couto, M. da Silva Boni, M.J.R. Guimarães, I.N.O. Souza, M. Bartolini, V. Andrisano, P.C. do Nascimento Nogueira, E.R. Silveira, G.D. Brand, O. Soukup, J. Korábečný, N.C. Romeiro, N.G. Castro, M.L. Bolognesi, L.A.S. Romeiro, Cardanol-Derived AChE Inhibitors: Towards the Development of Dual Binding Derivatives for Alzheimer's Disease, Eur. J. Med. Chem. 108 (2016) 687–700, https://doi.org/10.1016/j.ejmech.2015.12.024.
[79] N.M. O'Boyle, M. Banck, C.A. James, C. Morley, T. Vandermeersch, G. R. Hutchison, Open Babel: An Open Chemical Toolbox, J. Cheminformatics 3 (2011) 33, https://doi.org/10.1186/1758-2946-3-33.
[80] J. Schindelin, I. Arganda-Carreras, E. Frise, V. Kaynig, M. Longair, T. Pietzsch, S. Preibisch, C. Rueden, S. Saalfeld, B. Schmid, J.-Y. Tinevez, D.J. White, V. Hartenstein, K. Eliceiri, P. Tomancak, A. Cardona, Fiji: An Open-Source Platform for Biological-Image Analysis, Nat. Methods 9 (7) (2012) 676–682, https://doi.org/10.1038/nmeth.2019.
[81] L. Aitken, S.D. Quinn, C. Perez-Gonzalez, I.D.W. Samuel, J.C. Penedo, F.J. Gunn-Moore, Morphology-Specific Inhibition of β-Amyloid Aggregates by 17β-Hydroxysteroid Dehydrogenase Type 10, Chembiochem Eur. J. Chem. Biol. 17 (11) (2016) 1029–1037, https://doi.org/10.1002/cbic.201600081.
[82] L. Muckova, J. Pejchal, P. Jost, N. Vanova, D. Herman, D. Jun, Cytotoxicity of Acetylcholinesterase Reactivators Evaluated in Vitro and Its Relation to Their Structure, Drug Chem. Toxicol. 42 (3) (2019) 252–256, https://doi.org/10.1080/01480545.2018.1432641.
[83] J. Misik, E. Nepovimova, J. Pejchal, J. Kassa, J. Korabecny, O. Soukup, Cholinesterase Inhibitor 6-Chlorotacrine - In Vivo Toxicological Profile and Behavioural Effects, Curr. Alzheimer Res. 15 (6) (2018) 552–560, https://doi.org/10.2174/1567205015666171212105412.
[84] Guidance on Dose Level Selection for Regulatory General Toxicology Studies for Pharmaceuticals, (n.d.). https://norecopa.no/3r-guide/guidance-on-dose-level-selection-for-regulatory-general-toxicology-studies-for-pharmaceuticals (accessed September 22, 2019).
[85] H. Azizi-Malekabadi, M. Hosseini, M. Soukhtanloo, R. Sadeghian, M. Fereidoni, F. Khodabandehloo, Different Effects of Scopolamine on Learning, Memory, and Nitric Oxide Metabolite Levels in Hippocampal Tissues of Ovariectomized and Sham-Operated Rats, Arq. Neuropsiquiatr. 70 (6) (2012) 447–452, https://doi.org/10.1590/s0004-282x2012000600012.
[86] M. Entlerova, V. Lobellova, H. Hatalova, A. Zemanova, K. Vales, A. Stuchlik, Comparison of Long-Evans and Wistar Rats in Sensitivity to Central Cholinergic Blockade with Scopolamine in Two Spatial Tasks: An Active Place Avoidance and the Morris Water Maze, Physiol. Behav. 120 (2013) 11–18, https://doi.org/10.1016/j.physbeh.2013.06.024.

European Journal of Medicinal Chemistry 168 (2019) 491–514

Contents lists available at ScienceDirect

European Journal of Medicinal Chemistry

journal homepage: http://www.elsevier.com/locate/ejmech

Research paper

Novel tacrine-tryptophan hybrids: Multi-target directed ligands as potential treatment for Alzheimer's disease

Katarina Chalupova [a, b, 1], Jan Korabecny [a, c, d, 1], Manuela Bartolini [e], Barbara Monti [e], Doriano Lamba [f], Rosanna Caliandro [f], Alessandro Pesaresi [f], Xavier Brazzolotto [g], Anne-Julie Gastellier [g], Florian Nachon [g], Jaroslav Pejchal [c], Michaela Jarosova [h], Vendula Hepnarova [c, d], Daniel Jun [c, d], Martina Hrabinova [c, d], Rafael Dolezal [b, d], Jana Zdarova Karasova [c, d], Martin Mzik [i], Zdena Kristofikova [a], Jan Misik [c, d], Lubica Muckova [c], Petr Jost [c, d], Ondrej Soukup [a, c, d], Marketa Benkova [d], Vladimir Setnicka [j], Lucie Habartova [j], Marketa Chvojkova [a, k], Lenka Kleteckova [a, k], Karel Vales [a, k], Eva Mezeiova [a, d], Elisa Uliassi [e], Martin Valis [l], Eugenie Nepovimova [b], Maria Laura Bolognesi [e, **], Kamil Kuca [b, d, *]

[a] National Institute of Mental Health, Topolova 748, 250 67, Klecany, Czech Republic
[b] Department of Chemistry, University of Hradec Kralove, Rokitanskeho 62, 500 03, Hradec Kralove, Czech Republic
[c] Department of Toxicology and Military Pharmacy, Faculty of Military Health Sciences, Trebesska 1575, 500 01, Hradec Kralove, Czech Republic
[d] Biomedical Research Centre, University Hospital Hradec Kralove, Sokolska 581, 500 05, Hradec Kralove, Czech Republic
[e] Department of Pharmacy and Biotechnology, Alma Mater Studiorum-University of Bologna, Via Belmeloro 6, I-40126, Bologna, Italy
[f] Istituto di Cristallografia, Consiglio Nazionale delle Ricerche, Area Science Park - Basovizza, S.S. n° 14-Km 163.5, I-34149, Trieste, Italy
[g] Institut de Recherche Biomédicale des Armées, Département de Toxicologie et Risques Chimiques, 1 Place Général Valérie André, 91220, Brétigny-sur-Orge, France
[h] Department of Pharmaceutical Chemistry and Drug Control, Faculty of Pharmacy in Hradec Kralove, Charles University in Prague, Heyrovskeho 1203, 500 05, Hradec Kralove, Czech Republic
[i] Institute of Clinical Biochemistry and Diagnosis, University Hospital, Sokolska 581, 500 05, Hradec Kralove, Czech Republic
[j] Department of Analytical Chemistry, University of Chemistry and Technology Prague, Technicka 5, 166 28, Prague, Czech Republic
[k] Institute of Physiology, Czech Academy of Sciences, Videnska 1083, 142 20, Prague, Czech Republic
[l] Department of Neurology, Charles University in Prague, Faculty of Medicine in Hradec Kralove and University Hospital, Simkova 870, 500 03, Hradec Kralove, Czech Republic

ARTICLE INFO

Article history:
Received 16 December 2018
Received in revised form
7 February 2019
Accepted 7 February 2019
Available online 27 February 2019

Keywords:
Multi-target directed ligands
Alzheimer's disease
Tacrine-tryptophan hybrids
Acetylcholinesterase
Aβ42 self-aggregation
hAChEinduced Aβ40 aggregation
X-ray crystallographic analysis
Blood-brain barrier

ABSTRACT

A combination of tacrine and tryptophan led to the development of a new family of heterodimers as multi-target agents with potential to treat Alzheimer's disease. Based on the *in vitro* biological profile, compound ***S*-K1035** was found to be the most potent inhibitor of human acetylcholinesterase (*h*AChE) and human butyrylcholinesterase (*h*BChE), demonstrating balanced IC_{50} values of 6.3 and 9.1 nM, respectively. For all the tacrine-tryptophan heterodimers, favorable inhibitory effect on *h*AChE as well as on *h*BChE was coined to the optimal spacer length ranging from five to eight carbon atoms between these two pharmacophores. ***S*-K1035** also showed good ability to inhibit $A\beta_{42}$ self-aggregation (58.6 ± 5.1% at 50 μM) as well as *h*AChE-induced $A\beta_{40}$ aggregation (48.3 ± 6.3% at 100 μM). The X-ray crystallographic analysis of *Tc*AChE in complex with ***S*-K1035** pinpointed the utility of the hybridization strategy applied and the structures determined with the two **K1035** enantiomers in complex with *h*BChE could explain the higher inhibition potency of ***S*-K1035**. Other *in vitro* evaluations predicted the ability of ***S*-K1035** to cross blood-brain barrier and to exert a moderate inhibition potency against neuronal nitric oxide

* Corresponding author. Department of Chemistry, University of Hradec Kralove/ University Hospital Hradec Kralove, Rokitanskeho 62, 500 03, Hradec Kralove, Czech Republic.
** Corresponding author. Department of Pharmacy and Biotechnology, Alma Mater Studiorum-University of Bologna, Via Belmeloro 6, I-40126, Bologna, Italy.
E-mail addresses: marialaura.bolognesi@unibo.it (M.L. Bolognesi), kamil.kuca@fnhk.cz (K. Kuca).
[1] Katarina Chalupova and Jan Korabecny contributed equally.

https://doi.org/10.1016/j.ejmech.2019.02.021

synthase. Based on the initial promising biochemical data and a safer *in vivo* toxicity compared to tacrine, ***S*-K1035** was administered to scopolamine-treated rats being able to dose-dependently revert amnesia.

1. Introduction

Alzheimer's disease (AD) is an age-related neurodegenerative disease and the most common cause of dementia associated with selective loss of cognitive ability and behavioral disturbances ultimately leading to death [1]. The progressive impairment of neurological conditions of patients with AD produces devastating problems on the patients themselves and very high economic burden for their families and society [2]. Unfortunately, the etiology of AD is still not fully understood. To date, several factors have been demonstrated to be responsible for AD development and progression, thus playing an eminent role in the pathogenesis of AD [3,4]. These distinct neuropathological hallmarks include depositions of extracellular β-amyloid (Aβ) into plaques and intracellular neurofibrillary tangles composed of hyper-phosphorylated tau protein. Both of them are suspected to be involved in the pathophisology of AD, however, their exact mechanism rather remains unclear. The difference between the plaques and tangles lies in their structure and effect on the nerve cells in the brain tissues [5]. Besides, the most pronounced hypothesis for AD development stems from low levels of acetylcholine (ACh), oxidative stress and bio-metal dyshomeostasis [6–8]. Low levels of ACh resulting from neuronal death are associated with cognitive and memory deterioration. Based on these observations, enhancement of cholinergic neurotransmission and recovery of ACh levels may alleviate AD symptoms [9]. The administration of cholinesterase inhibitors (ChEIs) builds upon the cholinergic hypothesis, and represents the most prominent strategy providing beneficial therapeutic option in AD therapy [10]. Acetylcholinesterase (AChE, E.C. 3.1.1.7) and butyrylcholinesterase (BChE, E.C. 3.1.1.8) are two types of cholinesterase (ChE) enzymes which are able to hydrolyze ACh. BChE is also able to hydrolyze bulkier substrates like butyrylcholine (BCh). AChE has a nearly 20 Å deep and narrow gorge with two major binding sites. At the bottom of the gorge, catalytic anionic site (CAS) resides whereas peripheral anionic site (PAS) is located near the cavity entrance. Experimental evidence showed that AChE inhibitors (AChEIs) able to simultaneously bind CAS and PAS may have a higher beneficial effect in AD therapy by their indirect anti-aggregating action [11]. Indeed, affinity of AChEIs for PAS confers ability against Aβ aggregation by preventing assembly of Aβ monomers into fibrils and other highly toxic complexes with Aβ [12,13].

Increasing evidence on the role of the two types of ChE in the AD brain pointed out a gradual switch of the hydrolyzing activity, from AChE to BChE, along with the disease progression. In fact, AChE levels were reported to gradually decrease, while BChE levels remain unaltered or significantly increased in the hippocampus and temporal cortex [14,15]. Furthermore, cortical BChE accumulation has been shown to be associated with the formation of neuritic plaques and neurofibrillary tangles [16]. Considering all of the above mentioned observations, AChE/BChE inhibitors may provide beneficial therapeutic effects in AD treatment.

In line with the multifactorial nature of this pathology, it is now recognized that several pathological features coexist in AD and play a role in a still undefined cause-effect circle. In this scenario, even if several factors have been hypothesized to contribute to AD pathogenesis, Aβ peptide is one of the most studied therapeutic targets. The pathological processes related to AD correlate well with the misfolded Aβ, which leads to the formation of amyloid oligomers and aggregates [17]. Aβ of variable length (from 39 to 43 residues) is generated by a sequential cleavage of the amyloid precursor protein (APP) by the subsequent action of β- and γ-secretases. Aβ_{42} tends to aggregate more rapidly than Aβ_{40} and displays higher neurotoxicity [18,19]. Aβ aggregates trigger a cascade of biochemical processes, which ultimately lead to neuronal dysfunction [20]. Many efforts are being made to develop appropriate treatment strategies either to decrease the Aβ production or enhance the Aβ clearance [21].

Current therapy of AD is mainly limited to administration of three AChEIs, namely donepezil, rivastigmine and galantamine, and one *N*-methyl-D-aspartate (NMDA) receptor antagonist, memantine. Unfortunately, these drugs do not effectively address the multifactorial nature of AD, exerting only a palliative effect [22,23].

Tacrine (**3**, THA, Fig. 2) was the first ChEI approved in 1993 by the Food and Drug Administration (FDA) for the AD therapy and withdrawn from clinical use in 2003 because of the hepatotoxic and gastrointestinal side effects [24,25]. The ongoing research aiming at finding novel and presumably more potent THA analogues led to the discovery of 7-methoxytacrine (**1**, 7-MEOTA, Fig. 2), a centrally active AChEI endowed with a limited toxicity compared to THA, due to a distinct metabolic fate [26]. Furthermore, the THA derivative 6-chlorotacrine (**2**, 6-Cl-THA, Fig. 2) showed better AChE inhibitory profile and selectivity than THA [27,28]. Thanks to the easy accessibility and the low molecular weight, tacrines are still widely used as starting fragments for the development of hybrid molecules with additional pharmacological properties beyond ChE inhibition [29].

Over the last decades, the field of tacrine-based multi-target directed ligands (MTDLs) has grown enormously [30–33]. Early encouraging results were obtained when THA dimer bis(7)-tacrine (**4**, Fig. 1), was rationally designed to contact both AChE central and peripheral site, thus acting as a dual binding site AChEI. Indeed, **4** showed improved AChE inhibition, as well as a large array of anti-AD activities, including neuroprotection against glutamate-mediated excitotoxicity [34,35]. The latter is presumably associated to **4** inhibition potency of neuronal nitric oxide synthase (nNOS) [36]. Indeed, excessive nitric oxide generated by nNOS mediates the downstream signal transduction of the NMDA receptors thus leading to excitotoxic neuronal cell death [37]. Thus, **4** has spurred the development of several MTDLs featuring either homo- and hetero-dimeric structures and targeting different pathological pathways intertwined to oxidative stress, mitochondrial dysfunction, metal dyshomeostasis, amyloid aggregation and tau protein hyper-phosphorylation [3,38–40].

2. Design of novel tacrine-tryptophan heterodimers

As part of our efforts in identifying MTDLs as drug candidates for AD, we became interested in hybrids obtained by linking THA and tryptophan (Trp) fragments. Our starting point was the biological profile of THA-based [41–45], melatonin-based [46,47] and Trp-

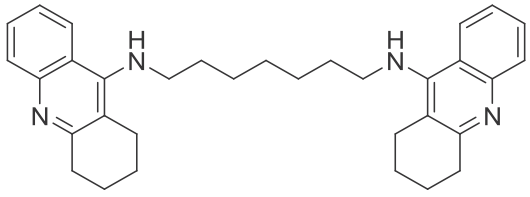

Fig. 1. Chemical structure of bis(7)-tacrine (**4**), first dual binding site AChEI.

based [48–50] hybrids, which are endowed with a wide spectrum of potential disease-modifying activities against AD.

Recently, we have reported on a series of tacrine-naphthoquinone (THA-NQ) hybrids possessing a multifunctional character, which included cholinesterase inhibition related to the THA scaffold, anti-amyloid properties conveyed by the NQ moiety, antioxidant properties, the ability to cross blood-brain barrier (BBB) and, more importantly, lower hepatotoxicity if compared to THA. The most prominent THA-NQ hybrid, in terms of the most balanced and multipotent activity towards all the selected targets, was **5** (Fig. 2) [51] (see Fig. 2).

L-Tryptophan (L-Trp, Fig. 2) is an essential amino acid acting as serotonin (5-HT) precursor. Studies on patients with AD have shown that an acute reduction of L-Trp intake impairs learning and memory [52,53] and that an increased L-Trp intake decreases intraneuronal accumulation of Aβ in the hippocampus in a transgenic mice model of AD [54]. Additionally, thanks to the key involvement of Trp residues in amyloidogenic proteins in the misfolding processes [55], L-Trp possesses strong potential as a fragment for the development of targeted anti-amyloid agents [48]. On this basis, Segal's and Gazit's groups synthesized and investigated 1,4-naphthoquinon-2-yl-L-tryptophan (**6**, L-NQ-Trp, Fig. 2) as a promising inhibitor of Aβ aggregation [56]. **6** was able to inhibit Aβ aggregation, decrease Aβ cytotoxicity, reduce the amount of amyloid brain burden in a transgenic Drosophila model of AD, thereby prolonging lifespan and completely abolishing the defective locomotion [56]. Studies from the same group also showed that the L-NQ-Trp analogue, Cl-1,4-naphthoquinone-2-yl-L-tryptophan (**7**, Cl-L-NQ-Trp, Fig. 2), can inhibit tau aggregation *in vitro* and *in vivo* [49]. Computer simulations investigations have provided further insights into Aβ_{42}/L-NQ-Trp interaction mode [57]. Another reason for linking THA with Trp stems from the structural similarity of the designed molecules **8** and **9** with the THA-melatonin hybrids developed by Rodrigues-Franco et al. as MTDLs against AD. Hybrid **8** showed a multifaceted profile combining cholinergic and antioxidant properties together with low toxicity (Fig. 2) [46]. In 2009, the same group developed 6-Cl-THA-melatonin hybrids [47]. The best-in-class compound **9** (Fig. 2) exhibited good cholinergic inhibitory activity, antioxidant and anti-amyloid properties and excellent neuroprotective effects against Aβ and oxidative stress. Thus, it is plausible that tacrine-tryptophan heterodimers reported herein could similarly span AChE gorge, inhibit Aβ self-aggregation and exert other similar beneficial properties like **8** and **9**.

Based on all aforementioned considerations, herein, we describe the synthesis and biological profile investigation of a novel multitarget hybrids family combining a Trp moiety with a THA scaffold tethered by aliphatic linkers of varying length. The characterization of the biological profile of the synthesized THA-Trp heterodimers includes an *in vitro* evaluation of (i) the inhibitory activity against human AChE (*h*AChE) and human BChE (*h*BChE), (ii) crystallographic analysis of the most promising compound in complex with *Torpedo californica* AChE (*Tc*AChE) and human BChE (*h*BChE), (iii) anti-amyloid properties (inhibition of Aβ_{42} self-aggregation and of AChE-induced Aβ_{40} aggregation), (iv) prediction of BBB penetration using parallel artificial membrane permeation assay (PAMPA), (v) *in vitro* effect on the cell viability, (vi) inhibitory activity against neuronal nitric oxide synthase (nNOS), and (vii) *in vivo* behavioral studies using a scopolamine-induced cognitive deficit rat model.

3. Results and discussion

3.1. Chemistry

The general synthetic procedure for tacrine-tryptophan hybrids ***S*-K1024-K1044** is shown in Scheme 1. The starting 9-chlorotacrines **10**–**12** were prepared according to the previous reports and the spectral data were in good agreement with literature reports [58,59]. The treatment of **10**–**12** with appropriate 1,ω-diaminoalkanes in the presence of phenol yielded the desired intermediates **19**–**39** (70–90%) [60]. *N*-[(*tert*-Butoxy)carbonyl]-L-tryptophan (**16**) was prepared in high yield (87%) from commercially available L-tryptophan (**13**) via protection of the amino group using triethylamine (TEA) and di-*tert*-butyl dicarbonate. Spectral data were in good agreement with literature reports [61]. Finally, the intermediates **19**–**39** with different linker sizes were coupled with Boc-protected L-tryptophan **16** in the presence of TEA and benzotriazol-1-yloxytris(dimethylamino)phosphonium hexafluorophosphate (BOP) to afford Boc-protected tacrine-tryptophan heterodimers **40**–**62** in low-to-excellent yields (15–91%). The deprotection and the final conversion into dihydrochloride salts took place in one pot to obtain the desired tacrine-tryptophan hybrids ***S*-K1024-K1044** in moderate-to-excellent yields (38–99%). Moreover, 6-Cl-THA-containing derivatives bearing an *R*-isomer (***R*-K1035**) and a racemic mixture (**rac-K1035**) from D-tryptophan and DL-tryptophan, respectively, were synthesized for comparative purposes following an analogous procedure. Structural determination and signal assignments of the final compounds were accomplished by the application of standard NMR experiments (^{1}H, ^{13}C, ^{1}H-^{1}H COSY, ^{1}H-^{13}C HSQC, HMBC, DEPT). The structural characterization also involved melting point assessment and liquid chromatography-high-resolution mass spectrometry (LC-HRMS). The absolute configuration of ***S*-K1035,** as the most promising compound in the series, has been validated via electronic circular dichroism (Supporting information).

4. Cholinesterase inhibitory activity

Three series of THA-Trp conjugates underwent initial biological screening for their inhibitory potential against *h*AChE and *h*BChE (Table 1). All data for 7-MEOTA-tryptophan hybrids ***S*-K1024-K1030**, 6-Cl-THA-tryptophan heterodimers ***S*-K1031-K1037** and THA-tryptophan derivatives ***S*-K1038-K1044** were determined using the spectrophotometric method by Ellman et al., using 7-MEOTA, 6-Cl-THA, and THA as reference compounds (Table 1) [62,63].

In each series, the pharmacophores were combined via alkyl chains of different length (n = 2-8). The length of the chain is considered a crucial factor affecting the inhibitory activity against both ChEs as shown in many examples of previously reported THA hybrids [29,41,42,51,59,60,64–66]. This characteristic feature stems from the optimal anchoring of each moiety (THA and Trp) to specific enzyme binding sites, which are located in a spatially defined area of ChE. It has been previously shown that AChE shares 54% homology of BChE [67]. However, some distinct differences between these two α/β hydrolases are present, such as in the gorge dimension; indeed, the bulkier BChE active gorge grants a lower substrate specificity compared to AChE [68]. Hence, it is expected that an optimal chain-length and activity may differ between each THA-containing subset for AChE and BChE. In general, the presence of longer methylene tethers was associated with a favorable inhibitory effect on *h*AChE as well as on *h*BChE, and the optimal length of the spacer was found to lie between five to eight carbon atoms for both ChEs in all the families bearing either THA, 6-Cl-THA or 7-MEOTA scaffolds.

All novel hybrids (except for derivative ***S*-K1026**) turned out to be potent inhibitors of *h*AChE with IC_{50} values ranging from micromoles to nanomoles. Derivative ***S*-K1035** (IC_{50} = 6.3 nM) bearing 6-Cl-THA moiety and a six-methylene spacer showed single digit nanomolar inhibitory potency against *h*AChE. ***S*-K1035** was 1585-, 51- and 3-times more potent *h*AChE inhibitor than 7-MEOTA, THA

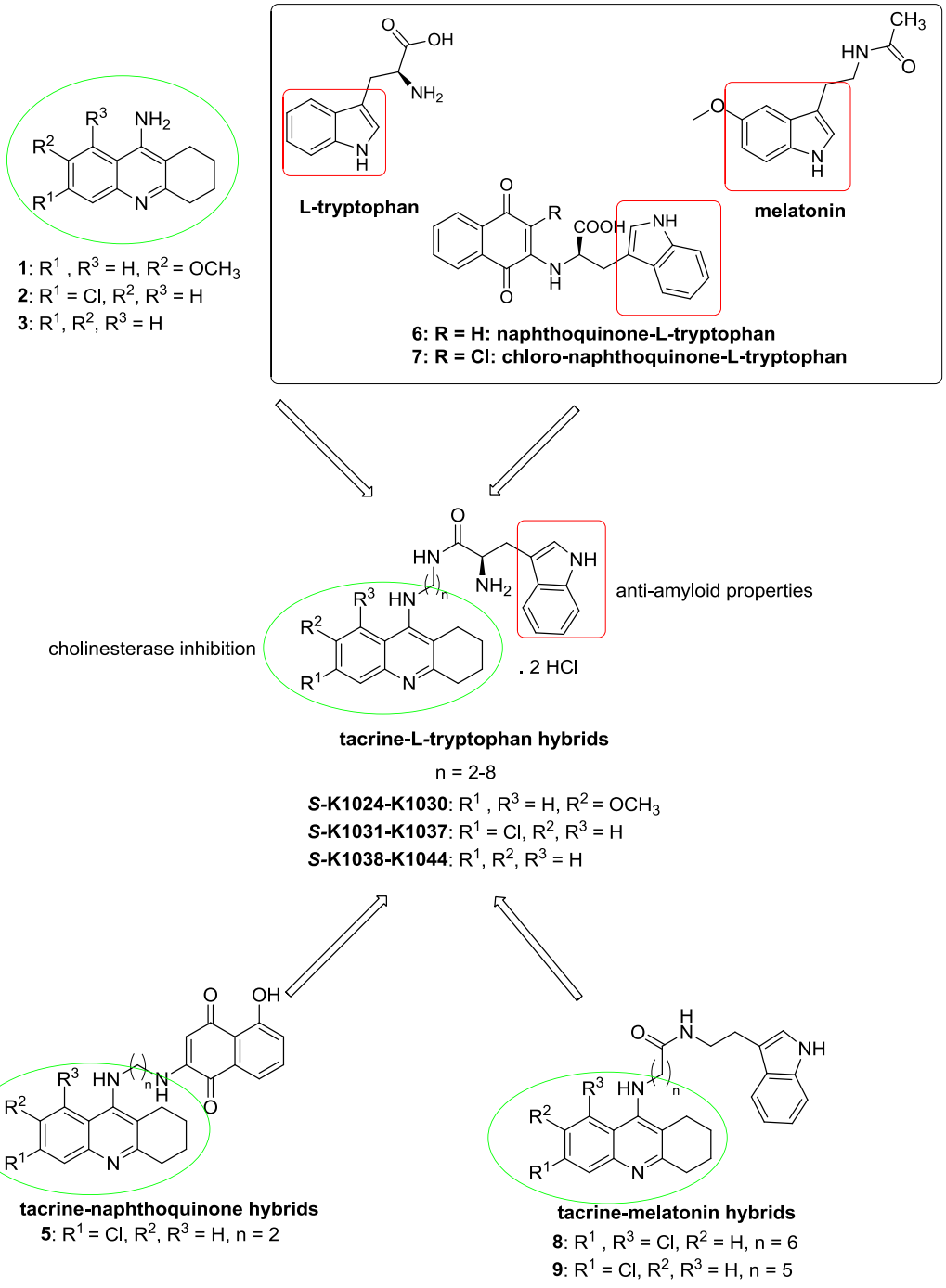

Fig. 2. Design strategy for novel THA-Trp hybrids.

and 6-Cl-THA, respectively. Among hybrids bearing the 7-methoxytacrine fragment, the most promising derivative was ***S*-K1027** ($IC_{50} = 620$ nM), which exhibited a 16.2-fold increased inhibitory activity against *h*AChE with respect to the single fragment 7-MEOTA. All hybrids carrying the 6-Cl-THA (except for hybrid ***S*-K1031**) displayed inhibitory potency towards *h*AChE in the same order of magnitude as the parent compound 6-Cl-THA. These findings are congruent with previous report, unveiling that the hydrogen replacement by chlorine at position 6 of the THA scaffold leads to an enhancement of the binding affinity towards AChE [69]. Similarly to the observations for 6-Cl-THA derivatives, hybrids containing THA (***S*-K1038-K1043**) showed inhibitory activities toward *h*AChE comparable to that of the reference compound THA. The only exception to this trend was hybrid ***S*-K1044,** which exhibited a 4.2-fold higher inhibitory potency compared to that revealed by THA.

Concerning the inhibition of *h*BChE, all 23 hybrids were potent inhibitors with IC_{50} values ranging from the micromoles to nanomoles. All hybrids carrying the 7-methoxytacrine template were better *h*BChE inhibitors than 7-MEOTA with inhibitory activities in the sub-micromolar range. All 6-Cl-THA heterodimers displayed higher inhibitory potency towards *h*BChE than the parent

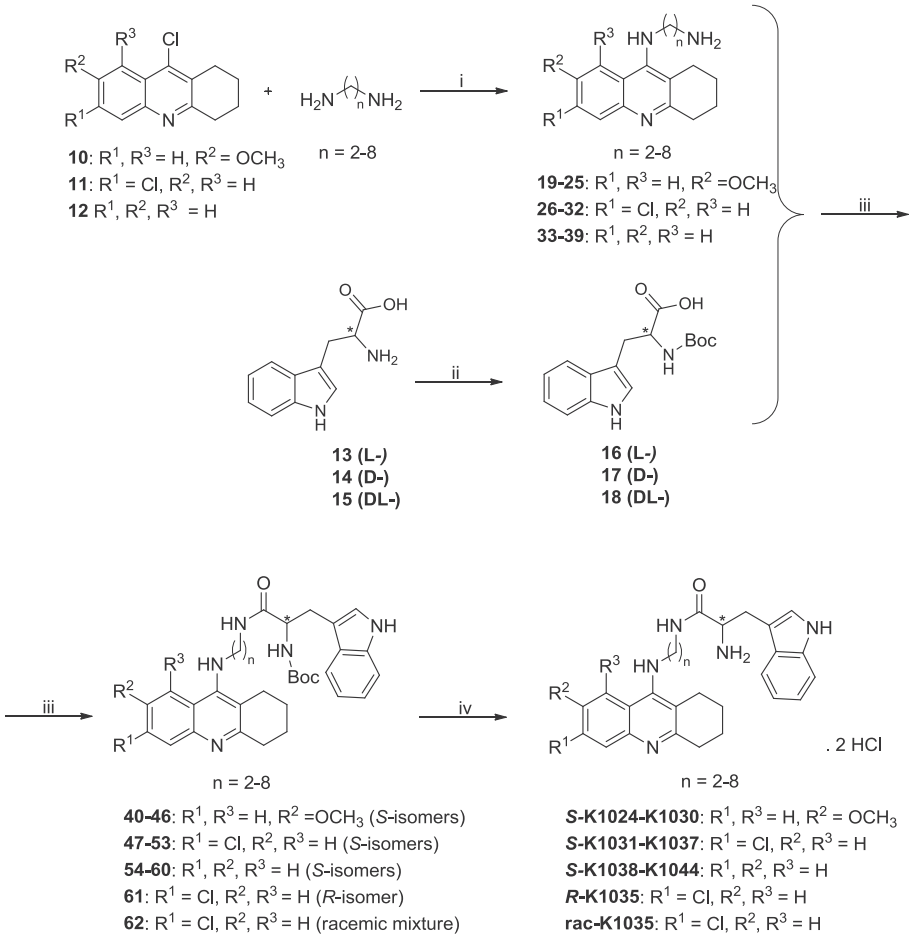

Reagents and conditions: (i) phenol, 130 °C, 4 h; (ii) TEA, MeOH, Boc_2O, RT, 24 h; (iii) TEA, BOP, DMF, RT, 24 h; (iv) 4 M HCl, MeOH, RT, 24 h.

Scheme 1. General Procedure for the Synthesis of Tacrine-Tryptophan Hybrids ***S*-K1024-K1044**, ***R*-K1035** and **rac-K1035**.

compound 6-Cl-THA. Among hybrids from the THA family, the most potent derivative was ***S*-K1042** ($IC_{50} = 3.9$ nM), which exhibited a 20.3-fold increased inhibitory activity compared to THA. Considering all series, the most pronounced inhibitors were the heterodimers bearing a six-methylene linker, namely ***S*-K1035** (bearing a 6-Cl-THA fragment) and ***S*-K1042** (bearing a THA fragment), which were endowed with nanomolar BChE inhibitory potency ($IC_{50} = 9.1$ and 3.9 nM, respectively).

The selectivity index (SI) was calculated for all compounds within the study by comparing the IC_{50} value for *h*BChE inhibition with that achieved for *h*AChE inhibition. Most 7-MEOTA and THA hybrids were *h*BChE-selective (SI $\lesssim$ 1.0) or non-selective (SI $\cong$ 1.0) ChE inhibitors, while 6-Cl-THA hybrids showed a weak preference for AChE. This is in agreement with the selectivity profile of the implemented tacrine core. Hence, whereas all the tacrine hybrids were BChE selective in agreement with the higher affinity for BChE of THA, higher preference for *h*AChE was exhibited by hybrids bearing the 6-Cl-THA fragment. However, if compared with the selectivity profile of 6-Cl-THA (SI = 100.7), all 6-Cl-THA hybrids showed a much smaller SI with values ranging from 0.97 (non-selective) to 2.90 (slightly selective for *h*AChE).

Due to the increasing interest for dual AChE/BChE inhibition [70], this finding makes these hybrids particularly appealing. Indeed, it has been observed that levels of BChE in the brain increase with aging, while those of AChE decrease. This points out the importance of BChE inhibition in moderate to severe stages of AD [71]. The correctness of this idea has already been proved with the development of bisnorcymserine, a BChE-selective inhibitor, which is currently under evaluation in a Phase 1 clinical trial (ClinicalTrials.gov identifier: NCT01747213).

On the basis of anticholinesterase activity results, the best ChE inhibitor ***S*-K1035** was chosen as a prototype for investigating of the importance of the stereochemistry in ChE inhibition. For this purpose, the *R*-isomer (***R*-K1035**) and the racemic mixture (**rac-K1035**) were synthesized. In this regard, we have preserved the 6-Cl-THA scaffold and six-methylene tether and used either D-Trp to yield the *R*-isomer ***R*-K1035**, or the racemic Trp to afford the optically inactive **rac-K1035**. The stereochemistry of the Trp fragment does not seem to have any significant influence on the inhibition of *h*AChE as demonstrated by similar inhibitory activities of ***R*-K1035**, **rac-K1035** and ***S*-K1035**. However, and very surprisingly, a stereoselective interaction was highlighted for *h*BChE, with *S*-enantiomer being 15-fold more potent than the *R*-isomer (9.1 nM *vs.* 140 nM).

In comparison with the previously reported THA-NQ and THA-melatonin derivatives, the THA-Trp hybrids reported herein retained excellent *h*AChE inhibitory potency and showed increased activity towards *h*BChE. This makes them balanced dual AChE/BChE inhibitors, with potentially greater clinical efficacy and fewer side-effects.

5. Propidium displacement studies

The presence of a 6-methylene-tether chain in ***S*-K1035** makes this hybrid in principle able to span the gorge and likely reach the

Table 1
In vitro anticholinesterase activity, inhibition of Aβ_{42} self-aggregation and prediction of BBB crossing for THA-Trp derivatives and reference compounds.

Cmpd	n	R^1	R^2	R^3	*h*AChE $IC_{50} \pm$ SEM (nM)[a]	*h*BChE $IC_{50} \pm$ SEM (nM)[a]	SI for *h*AChE[b]	Inhibition Aβ_{42} self-aggregation % ± SD[c]	BBB assay[e]
***S*-K1024**	2	H	OCH_3	H	5700 ± 370	480 ± 15	0.08	54.7 ± 0.7	CNS-
***S*-K1025**	3	H	OCH_3	H	1300 ± 50	1800 ± 70	1.40	51.6 ± 1.5	CNS-
***S*-K1026**	4	H	OCH_3	H	12000 ± 770	520 ± 22	0.04	47.0 ± 7.0	CNS-
***S*-K1027**	5	H	OCH_3	H	620 ± 21	190 ± 6.7	0.3	51.9 ± 1.4	CNS-
***S*-K1028**	6	H	OCH_3	H	940 ± 61	55 ± 1.2	0.06	58.0 ± 5.7	CNS±
***S*-K1029**	7	H	OCH_3	H	980 ± 47	78 ± 2.7	0.08	57.9 ± 2.3	CNS±
***S*-K1030**	8	H	OCH_3	H	1300 ± 80	130 ± 4	0.10	54.5 ± 6.2	CNS+
***S*-K1031**	2	Cl	H	H	160 ± 8	340 ± 17	2.09	18.7 ± 7.0	CNS±
***S*-K1032**	3	Cl	H	H	70 ± 4	140 ± 6.2	1.99	19.9 ± 2.1	CNS±
***S*-K1033**	4	Cl	H	H	62 ± 2.2	120 ± 3.9	1.95	28.9 ± 1.4	CNS±
***S*-K1034**	5	Cl	H	H	76 ± 1.8	74 ± 1	0.97	50.6 ± 6.6	CNS±
***S*-K1035**	6	Cl	H	H	6.3 ± 0.2	9.1 ± 0.3	1.43	58.6 ± 5.1	CNS+
***R*-K1035**	6	Cl	H	H	6.9 ± 0.3	140 ± 5	19.7	60.7 ± 2.5	CNS+
rac-K1035	6	Cl	H	H	7.4 ± 0.4	13 ± 0.6	1.77	57.2 ± 1.5	CNS+
***S*-K1036**	7	Cl	H	H	19 ± 0.5	52 ± 1.1	2.76	59.0 ± 3.8	CNS+
***S*-K1037**	8	Cl	H	H	50 ± 1.3	140 ± 2.8	2.89	59.4 ± 6.2	CNS+
***S*-K1038**	2	H	H	H	730 ± 32	56 ± 2.1	0.08	44.0 ± 5.3	CNS-
***S*-K1039**	3	H	H	H	580 ± 33	40 ± 1.0	0.07	46.4 ± 6.2	CNS-
***S*-K1040**	4	H	H	H	1300 ± 93	123 ± 2.4	0.10	59.1 ± 2.6	CNS+
***S*-K1041**	5	H	H	H	320 ± 16	23 ± 0.7	0.07	54.3 ± 5.5	CNS-
***S*-K1042**	6	H	H	H	120 ± 3.8	3.9 ± 0.1	0.03	55.5 ± 5.2	CNS-
***S*-K1043**	7	H	H	H	120 ± 3.5	25 ± 1.0	0.22	60.9 ± 4.4	CNS-
***S*-K1044**	8	H	H	H	76 ± 1.1	64 ± 1.7	0.84	63.6 ± 2.1	CNS±
1		H	OCH3	H	10000 ± 97	18000 ± 80	1.76	<5	CNS+
2		Cl	H	H	20 ± 1.0	1800 ± 97	89	<5	CNS+
3		H	H	H	320 ± 13	80 ± 1.0	0.25	<5	CNS+
5 (tacrine- naphthoquinone) [51]	2	Cl	H	H	0.72 ± 0.06	540 ± 16	752.7	37.5 ± 4.9[d]	nd
8 (tacrine-melatonine) [46]	6	Cl	H	Cl	0.008 ± 0.0004	7.8 ± 0.4	975	nd	nd
9 (tacrine-melatonine) [47]	5	Cl	H	H	0.730 ± 0.03	180 ± 5	241	nd	CNS+
D,L-NQ-TRP	–	–	–	–	nd	nd	nd	25.4 ± 3.2	nd
6	–	–	–	–	nd	nd	nd	28.5 ± 3.6	nd

[a] Results are expressed as the mean of at least three experiments.
[b] Selectivity for *h*AChE is determined as a ratio of *h*BChE IC_{50}/*h*AChE IC_{50}.
[c] % Inhibition of Aβ_{42} self-aggregation at [I] = 50 μM. The [Aβ_{42}]/[I] ratio was equal to 1/1. Values are the mean from two to four independent experiments each performed in duplicate ± SD.
[d] Inhibition of Aβ_{42} self-aggregation at [I] = 10 μM.
[e] Prediction of BBB penetration by the PAMPA-BBB assay. "nd" stands for not determined, CNS stands for central nervous.

enzyme's PAS. Hence, to confirm this hypothesis and get deeper understanding of the mechanism of inhibition and to investigate the ability of ***S*-K1035** to interact with PAS, displacement studies using propidium were carried out [72,73]. Propidium, chemically 3,8-diamino-5-{3-[diethyl(methyl)ammonio]propyl}-6-phenylphenanthridinium diiodide, selectively associates with the PAS of AChE exhibiting an eight-fold enhancement of fluorescence [72,74]. Back-titration experiments with an increasing concentration of ***S*-K1035** showed a concentration-dependent decrease in the fluorescence intensity associated with the propidium–AChE complex. Following the method of Taylor and Lappi [73] a dissociation constant of 4.82 μM (Fig. 3 and SI) was calculated. This value shows that the interaction of ***S*-K1035** with PAS is about 6.9-fold weaker than that of propidium [74].

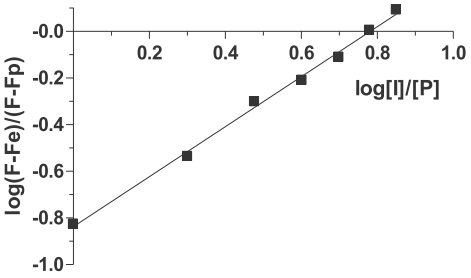

Fig. 3. Determination of K_D value at the PAS for the most active derivative ***S*-K1035** by displacement studies. K_D value is calculated from the antilog of the Y-intercept value. P stands for propidium iodide and I stands for the tested inhibitor; Fe is the initial fluorescence intensity when enzyme sites are saturated with P, F_P is the fluorescence intensity when propidium is completely displaced from the enzyme, and F denotes the fluorescence intensity after adding a determined amount of the displacing agent during the titration experiment.

6. X-ray crystallography of *Tc*AChE – *S*-K1035 complex

In order to gain insights into the molecular determinants responsible for the high AChE inhibitory activity of ***S*-K1035**, the crystal structure of the inhibitor-bound *Tc*AChE (Fig. 4) was determined by X-ray crystallography at a 2.50 Å resolution (summary of Crystallographic Data of the *Tc*AChE – ***S*-K1035** complex in Supporting Information, Table S2).

The position and orientation of ***S*-K1035** with respect to the key residues in the *Tc*AChE active-site gorge confirmed the critical role of the 6-Cl-THA fragment, which binds at the CAS.

The conformation of Phe330 in the *Tc*AChE – ***S*-K1035** complex ($\chi_1 = 145.4°$, $\chi_2 = 63.1°$) was found to be significantly different than those observed in the apo *Tc*AChE structure [75] – PDB ID 1EA5 ($\chi_1 = -126.6°$, $\chi_2 = -48.9°$), in the *Tc*AChE– tacrine-benzofuran hybrid complex [76] – PDB ID 4W63 ($\chi_1 = 92.6°$, $\chi_2 = 110.3°$), and in either of the two alternative conformations observed in the *Tc*AChE – NF595 [(N-(1,2,3,4-tetrahydroacridin-9-yl)-8-[(1,2,3,4-tetrahydroacridin-9-yl)thio]octan-1-amine)] [77] – PDB ID 2CEK complex ($\chi_1 = 76.1°$, $\chi_2 = 83.1°$; $\chi_1 = 96.9°$, $\chi_2 = 80.4°$).

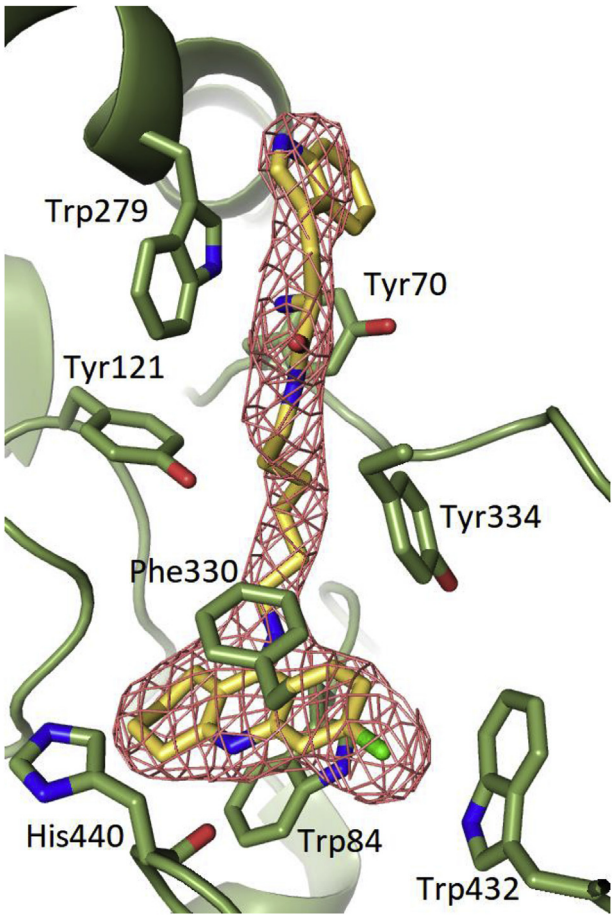

Fig. 4. Close-up view of the active site of *Tc*AChE in complex with ***S*-K1035**. The final $2F_o$ - F_c σ_A-weighted electron density map, carved around ***S*-K1035**, is contoured at 1.0σ. The ***S*-K1035** inhibitor is rendered as a stick model with carbon, oxygen, and nitrogen atoms colored yellow-orange, red, and blue, respectively. Selected key protein residues (with carbon atoms colored in green) in the vicinity of ***S*-K1035** are rendered in stick format and labeled appropriately. The figure was created using PyMOL (http://www.pymol.org). (For interpretation of the references to color in this figure legend, the reader is referred to the Web version of this article.)

In the *Tc*AChE– ***S*-K1035** complex, the swinging gate residue Phe330 closely matches the conformations observed in the *Tc*AChE – tacrine [78] – PDB ID 1ACJ ($\chi_1 = 157.1°$, $\chi_2 = 61.8°$), *Tc*AChE – bis(5)-tacrine [79] – PDB ID 2CMF ($\chi_1 = 160.6°$, $\chi_2 = 67.1°$) and *Tc*AChE – **4** [79], – PDB ID 2CKM ($\chi_1 = 143.9°$, $\chi_2 = 66.1°$) and *Tc*AChE – **5** [51], – PDB ID 4TVK ($\chi_1 = 141.5°$, $\chi_2 = 62.5°$) complexes, respectively.

The 6-chloroquinoline substructure of ***S*-K1035** is embedded in a pocket lined with several aromatic residues (Trp233, Phe288, Phe330, Phe331, and Trp84). The central aromatic ring of the 6-Cl-THA is facing Trp84 while the lateral aromatic ring is facing Phe330.

The endocyclic nitrogen is hydrogen bonded to the main-chain carbonyl oxygen of the catalytic residue His440 (2.89 Å). It can be inferred, from this distance and from the $pK_a = 9.8$ of tacrine [80], that the 6-chloroquinoline moiety of ***S*-K1035** is protonated.

The contribution of the electron withdrawing effect by the chlorine atom to the AChE inhibitory activity of ***S*-K1035** (*h*AChE $IC_{50} = 6.3$ nM) with respect to the un-substituted ligand ***S*-K1042** (*h*AChE $IC_{50} = 120$ nM) may stem from non-specific close spatial contacts with neighboring amino acid residues. Indeed, the chlorine atom of ***S*-K1035** is nested in a hydrophobic pocket delimited by Phe330, Trp432, Met436, Ile439, and Tyr442.

The chlorine atom exhibits the strongest interaction with Trp432 (min. and max. distances of 3.4 Å and 4.3 Å, respectively). Hence, it is plausible that short-range dispersion forces are responsible for the optimal fit of the 6-chloroquinoline fragment in the binding pocket. In principle, the observed increase in affinity conferred by the chlorine atom may be due either to direct interactions with neighboring amino acids, or the modulation of the π–π stacking interaction of the tetrahydroacridine rings of ***S*-K1035**.

Conversely, the presence of the electron donating methoxy group at position 7 of the quinoline fragment in ***S*-K1028**, very significantly reduce the inhibitory activity toward AChE ($IC_{50} = 940$ nM) with respect to the un-substituted ligand ***S*-K1042** ($IC_{50} = 120$ nM). The observed significant drop of the AChE inhibitory activity can likely be attributed to a steric hindrance effect occurring between the methoxy group of ***S*-K1042** and (**1**) and the hydroxyl group of Tyr334. This segment includes *Tc*AChE Asp72, an important residue in the catalytic pathway that is positioned near a constriction, at the boundary between the peripheral and anionic binding sites, and that is primarily engaged in hydrogen bonding with Tyr334 [81].

Interestingly, in the *Tc*AChE–***S*-K1035** complex, the NH_2 group of ***S*-K1035** is not involved in hydrogen bonding with otherwise structurally conserved water molecules belonging to the active site water network. The orientation of the L-Trp moiety is stabilized by a weak hydrogen bonding interaction of 4.4 Å between the indole NH of the L-tryptophan moiety and the CO of Asn280. The likely protonated NH_2 moiety of the L-tryptophan fragment ($pK_a = 9.4$) is, in turn, engaged in a cation-π interaction with Trp279 (distances ranging between 3.2 Å and 4.3 Å) and in a weak hydrogen bonding interaction (4.1 Å) with the OH of Tyr70.

In addition, the positions of the backbone atoms of Trp279 do not significantly differ from their native positions (PDB ID 1EA5), the C_α atom being departed by 0.2 Å.

Likewise, in the structure of the *Tc*AChE–***S*-K1035** complex the side chain of Trp279 adopts a close orientation ($\chi_1 = -64.5°$, $\chi_2 = 87.8°$) with respect to that observed in the native *Tc*AChE structure (PDB ID 1EA5) ($\chi 1 = -62.3°$, $\chi 2 = 96.7°$). Conversely, a dramatic re-orientation of the Trp279 side chain was observed in the crystal structures of *Tc*AChE–tacrine (PDB ID 1 ACJ) ($\chi_1 = -53.6°$, $\chi_2 = 31.2°$), *Tc*AChE–NF595 (PDB ID 2CEK) ($\chi_1 = -118.2°$, $\chi_2 = -131.9°$), *Tc*AChE–bis(5)-tacrine (PDB ID 2CFM) ($\chi_1 = -76.3°$, $\chi_2 = 95.2°$), *Tc*AChE–**4** (PDB ID 2CKM) ($\chi_1 = -121.4°$, $\chi_2 = -132.8°$), *Tc*AChE–tacrine-benzofuran hybrid (PDB ID 4W63) ($\chi_1 = 51.3°$, $\chi_2 = -82.0°$), and *Tc*AChE–**5** (PDB ID 4TVK) ($\chi_1 = -71.4°$, $\chi_2 = 100.7°$), respectively.

7. X-ray crystallography of *h*BChE – *S*-K1035 and *h*BChE – *R*-K1035 complexes

Positions of both ***S*-** and ***R*-K1035** are almost similar in human BChE, mainly stabilized by hydrophobic interactions (Fig. 5 and Fig. S4). The chlorotacrine moiety of ***S*-** and ***R*-K1035** interacts through π-π interactions with Trp82, their centroids being respectively at 3.7 Å and 3.8 Å distances. This interaction is similar to that observed in the structure of human BChE in complex with THA (PDB entry 4BDS). Their endocyclic nitrogen of THA scaffold is hydrogen bonded to the backbone carbonyl oxygen of His438, respectively at 2.8 Å and 2.9 Å distances, for ***S*-** and ***R*-K1035**. The chlorine atom is accommodated in a pocket formed by residues Ala328, Trp430, Met434, Met437 and Tyr440. Surprisingly and contrarily to *Tc*AChE, the tryptophan moiety of both ***S*-** and ***R*-K1035** folds back toward the chlorotacrine moiety in human BChE. This behavior can be explained by the larger active site gorge of BChE compared to AChE (500 vs 300 $Å^3$) and the lack of aromatic residues able to stabilize the indole moiety at the gorge entrance. For

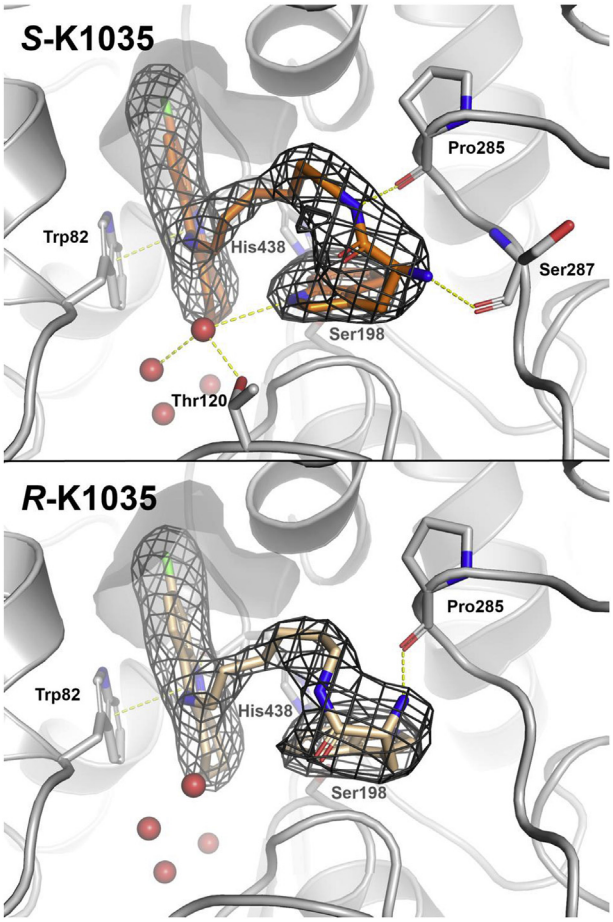

Fig. 5. Comparative binding of the different enantiomers of **K1035** in human BChE. Cartoon representations of human BChE in complex with ***S*-K1035** (top, PDB entry 6I0B) or ***R*-K1035** (bottom, PDB entry 6I0C). Key residues are represented as sticks with carbon atoms in grey. Ligands are represented as stick models with carbon atoms represented in orange for ***S*-K1035** or beige for ***R*-K1035**. Nitrogen, oxygen and chlorine atoms are represented in blue, red and green, respectively. The pocket accommodating the chlorine atom is represented as a grey surface. Water molecules are shown as red spheres. The specific interactions such as hydrogen bonds or π-π interactions are represented as yellow dashed lines. The dark grey meshes represent omit polder maps of each **K1035** ligand contoured at 5 sigmas. The figure was created using PyMOL (http://www.pymol.org). (For interpretation of the references to color in this figure legend, the reader is referred to the Web version of this article.)

example, Trp279 in *Tc*AChE which interacts with the indole moiety (see above) is replaced by the aliphatic residue Ala277 in human BChE. The primary amine of ***S*-K1035** forms a hydrogen-bond with the backbone carbonyl oxygen of Ser287 (2.9 Å), while for the ***R***-enantiomer it forms a similar hydrogen-bond with the backbone carbonyl oxygen of Pro285 (2.4 Å). Additionally, the amide nitrogen of ***S*-K1035** forms a hydrogen bond with the backbone carbonyl oxygen of Pro285 (2.7 Å). More interestingly, the orientation of the indole rings of the tryptophan moiety is the most significant difference between ***S***- and ***R*-K1035** *h*BChE structures. In the ***R***-conformation, the indole group does not make any specific interaction apart from hydrophobic ones with the surrounding residues. On the contrary, in the ***S***- conformation, in addition to similar hydrophobic interactions, the nitrogen atom of the indole group is engaged in a hydrogen bond with a water molecule of the structural water network (3.4 Å), the latter being bridged to Oγ of Thr120 (2.5 Å) and a second water molecule (3.0 Å). These differences and additional interactions specific to the ***S***- enantiomer plausibly account for the lower IC_{50} measured compared to the ***R***-enantiomer.

8. Inhibition of Aβ aggregation

Despite the ongoing debate about the role of Aβ in the onset and progression of AD, new lines of evidence support the concept that accumulation of Aβ and its oligomerization may act as a triggering factor in AD. Therefore, there is a high interest in understanding and inhibiting this process. Amyloid is a nucleation-dependent phenomenon which, is triggered by peptide conformational change [82]. Aromatic residues, including tryptophan, seem to play a role in the self-aggregation process by favoring the stabilization of amyloid structures through the formation of π-stacking interactions [83–86]. Based on this observation, inhibitors bearing aromatic residues capable to target these aromatic recognition residues might reduce amyloid aggregation and act as disease modifying agents. In 2009, the D-tryptophan-α-aminoisobutyric acid dipeptide was shown to be able to interact with low-molecular-weight soluble Aβ oligomers and inhibit their toxicity [87]. Furthermore, D. Segal and E. Gazit research groups have recently shown that **6** was able to strongly reduce both amyloid oligomerization and amyloid fibril formation [56].

Based on these findings, in order to define the structural elements important for amyloid inhibition, all tacrine-tryptophan hybrids were assayed (at an inhibitor/Aβ ratio of 1/1) for their ability to inhibit the spontaneous aggregation of the most amyloidogenic isoform of Aβ, namely $Aβ_{42}$, by using a ThT-based fluorescence assay, which allows the monitoring of amyloid fibril formation [88,89]. Since amyloid aggregation is a very delicate process during which several different oligomeric isoforms are in equilibrium and the *in vitro* inhibitory activity may be strongly influenced by the assay conditions, **6** and its racemate 1,4-naphthoquinon-2-yl-DL-tryptophan (D,L-NQ-Trp) were synthesized and assayed for comparative reasons as reference compounds under the same assay conditions. To the best of our knowledge, the effect of chirality of Trp-containing heterodimers on amyloid recognition has never been studied before.

An analysis of the results listed in Table 1 reveals that all hybrids were able to significantly inhibit $Aβ_{42}$-self-aggregation and that most of them, excluding ***S*-K1031**, ***S*-K1032** and ***S*-K1033**, were endowed with inhibitory potencies in a narrow range, i.e. from 44.0% (***S*-K1038**) to 63.6% (***S*-K1044**). The presence of higher molecular complexity given by the presence of the Trp moiety and the spacer chain seems to be important for the inhibitory activity, since THA and its analogues 7-MEOTA and 6-Cl-THA were not able to significantly inhibit amyloid aggregation.

The length of the spacer chain plays a different role for the three series of hybrids. Indeed, the similar inhibition percentage provided by all of the 7-MEOTA and THA hybrids points to the conclusion that the length of the spacer is not relevant for the inhibitory activity towards $Aβ_{42}$ self-aggregation. Conversely, it seems to influence the inhibitory activity in the case of the 6-Cl-THA derivatives, since an increase in potency was observed when the length between the 6-Cl-THA and Trp fragments was increased from two to six methylene units (from 18.7 to 58.6%). The inhibitory potency remained almost unchanged for a further increase of the spacer length from six (***S*-K1035**) to eight methylene units (***S*-K1037**). Thus, for the 6-Cl-THA-Trp hybrids six/eight methylenes represent the optimal spacer length. This behavior may suggest a possible different mode of interaction for the 6-Cl-THA hybrids compared to the other two series of hybrids and may be beneficial to further investigation. Comparing the inhibitory potencies of hybrids from the three series bearing a space chain with six/eight methylenes, only slight differences can be observed. In the case that the chain length is optimal, the maximum inhibitory activity can be achieved independently from the type of the THA fragment. It might also be further reasoned that the methoxy substituent in position 7 and the

chlorine in position 6 do not significantly influence the inhibitory activity towards amyloid self-aggregation. Finally, the stereocenter of the Trp fragment does not play any critical role (compare inhibition by ***S*-K1035**, ***R*-K1035** and **rac-K1035**).

Weaker inhibition was observed for **6** and its racemate assayed under the same experimental conditions with inhibition percentages (25.4% and 28.5%, respectively) considerably lower than those expected on the basis of the published data ($IC_{50} = 50$ nM) [56]. This difference might be ascribed to the different peptide used for the assay ($A\beta_{42}$ in our study and $A\beta_{40}$ in the study of Scherzer-Attali et al. [56]). Alternatively, since quenching phenomena were excluded and concentration dependence was confirmed, inhibition by **6** might be strongly affected by the type of oligomeric species and kinetics of their formation, which are different under different assay conditions. In the assay conditions used in this work, the newly synthesized tryptophan-tacrine hybrids performed significantly better than **6** and its racemate.

Besides self-aggregation, $A\beta$ aggregation can be also triggered by molecular chaperones. AChE is listed among the „$A\beta$ pathological chaperones“ due to its ability to promote the conformational changes in amyloid monomers and to trigger $A\beta$ oligomerization [13,90]. Furthermore, *in vitro* study showed that AChE was able to form stable complexes with $A\beta$ that were more toxic than $A\beta$ aggregates alone [91]. Due to this non-classical role, AChE has gained much attention in the last decades. The chaperone activity of AChE towards $A\beta$ is thought to be mediated by the PAS, through electrostatic interactions with the cationic area of $A\beta$ [92].

Therefore, as ***S*-K1035** is able to interact with the AChE PAS (shown by X-ray studies on the ***S*-K1035**-AChE complex), we assayed the inhibitory activity of ***S*-K1035**, in comparison with that of ***R*-K1035** and **rac-K1035,** using a previously developed and validated protocol to verify whether the ability of ***S*-K1035** to interact with PAS translates into an inhibition of the molecular chaperone activity of AChE towards $A\beta$ [90] Because of high costs of the assay, only the most promising derivative and its enantiomers were evaluated. The results were compared with those of the known AChEIs THA, donepezil, galantamine, rivastigmine, which were previously tested using the same experimental conditions [90,93]. The achieved data are listed in Table 2. THA was re-assayed as a negative control. It is well known that THA, galantamine, and rivastigmine are not able to significantly inhibit AChE-induced $A\beta$ aggregation, while donepezil acts as a quite weak inhibitor [90] Due to structural similarity and known activity towards AChE-induced amyloid aggregation, **4** was selected as a positive reference compound. Inhibition percentage concurs with previous data [94].

The inhibitory activity of novel compounds at the screening concentration was weaker than that of **4** but significantly higher than reference drugs and **6**. The weaker activity, compared to **4**, is in agreement with results from the crystal structure analysis [79]. The more and the less energetically favored $\pi-\pi$ “sandwich” and “T shaped” stacking configurations between either the outer THA moiety of **4** or the indole ring of ***S*-K1035** and the Trp279 indole ring have been observed in the *Tc*AChE- **4** (PDB ID 2CKM) and *Tc*AChE- ***S*-K1035** complexes, respectively. The average distances and the tilting angles between the planes of the above-mentioned rings are of 4.0 Å and 1.0° in the *Tc*AChE- **4** complex and of 4.9 Å and −49.2° in the *Tc*AChE- ***S*-K1035** complex. These represent key molecular determinants that nicely support the observed lower percentage of *in vitro* inhibition of *h*AChE-induced $A\beta_{40}$ aggregation of 48 ± 6.3% by ***S*-K1035** *vs*. 66.7 ± 4.3% by **4** (Table 2).

Interestingly, the stereochemistry seems to play a role, although to a very limited extent. Indeed, the compounds bearing the L-Trp unit, i.e. ***S*-K1035** and **6**, are slightly more active than those bearing the D-Trp (48.3% *vs*. 36.7% for the *S*- and *R*-enantiomer of the 6-Cl-THA derivative, respectively).

Table 2
In vitro inhibition of $A\beta_{40}$ aggregation induced by *h*AChE.

Cmpd	Inhibition *h*AChE-induced $A\beta_{40}$ aggregation (% ± SEM)[a]
***S*-K1035**	48.3 ± 6.3
***R*-K1035**	36.7 ± 4.7
rac-K1035	45.3 ± 4.0
D,L-NQ-Trp	34.2 ± 3.4
6	29.4 ± 0.6
THA	8.1 ± 2.1
4	66.7 ± 4.3
Donepezil	22[b]
Galantamine	17.9 ± 0.1[c]
Rivastigmine	<5[c]

[a] % inhibition of *h*AChE-induced $A\beta_{40}$ aggregation at [I] = 100 μM. The $A\beta_{40}$/*h*AChE ratio was equal to 100/1. Values are the mean of two experiments each performed in duplicate ± SEM.
[b] Data from Ref. [90].
[c] Data from Ref. [93].

This inhibitory activity toward AChE-induced amyloid aggregation, together with the direct action on amyloid self-aggregation, may have a synergic role in the reduction of the neurotoxic effects of amyloid aggregates in the brain of AD patients.

9. In vitro blood-brain barrier permeation assay

Penetration across the blood-brain barrier (BBB) is an essential property for compounds targeting the central nervous system (CNS). The brain permeability via passive diffusion of the novel THA-Trp hybrids has been predicted through a parallel artificial membrane permeation assay of the BBB (PAMPA-BBB) described by Di et al. [95,96]. The analysis allowed us to obtain preliminary data prior to the administration of the compounds to animals. The permeability is expressed as P_e ($P_e \times 10^{-6}$ cm s^{-1}) with the following limits: $P_e > 4.0$ for compounds with high prediction of BBB permeation (CNS +), $P_e < 2.0$ for compounds with low BBB permeation (CNS -), and $4.0 > P_e > 2.0$ for compounds with uncertain BBB permeation (CNS ±). Based on the results (Table 1), seven tested THA-Trp hybrids exhibited the potential to cross the BBB via passive diffusion. Two basic patterns for BBB permeation can be found. In detail, i) BBB permeability is inferred by tacrine scaffolds with more to less permeable hybrids as follows 6-Cl-THA > 7-MEOTA > THA; ii) chain elongation leads to increased BBB permeability with the exception of the THA subset. It is generally accepted that Log*P* as well as log*D* are important factors for the prediction of passive diffusion. However, it has been reported that donor/acceptor systems better predict the permeability than Log*P* and log*D* values as other factors, such as ionization state, hydrogen bonding, and molecular size influence the permeability. This might explain why analogues with longer alkyl chain, i.e. with higher lipophilicity represented by higher log*D* value showed lower penetration potential than their analogues having shorter alkyl chain in THA subset [97].

10. *In vitro* cell viability

Safety of novel tacrine-tryptophan derivatives and their parent compounds (THA, 7-MEOTA, 6-Cl-THA, L-Trp) was assessed on the Chinese hamster ovary (CHO-K1) and human liver carcinoma (HepG2) cell lines using the standard 3-(4,5-dimethylthiazol-2-yl)-2,5-diphenyltetrazolium bromide (MTT) cell viability assay [98]. HepG2 cell line were purposely selected to investigate the preliminary hepatotoxicity profile. Indeed, it is well-known that hepatotoxicity is a critical issue that needs to be addressed when dealing with THA derivatives. In this regard, while all derivatives were assayed for cytotoxicity on CHO-K1 cells, the hybrids tested on

HepG2 cells were selected on the basis of the anticholinesterase inhibitory activities. Eight hybrids, i.e. ***S*-K1028**, ***S*-K1029**, ***S*-K1035**, ***S*-K1036**, ***S*-K1042**, ***S*-K1044**, ***R*-K1035**, ***rac*-K1035** (two hybrids from each family), were inspected and the results are summarized in Table 3. Using CHO-K1 cell line, THA ranked as the compound with the lowest cytotoxic effect. Only one compound from the novel series, ***S*-K1043** also showed similar cytotoxicity in the same order of magnitude as THA towards the CHO-K1 cell line. However, these data reflect only the direct effect on isolated cell lines omitting the drug metabolism. Accordingly, it has been shown that the metabolism of **3** plays a crucial role on its hepatotoxicity [99]. In a similar way, 7-MEOTA can be considered as a relatively non-hepatotoxic tacrine derivative because of a different metabolic pathway, which further ensures its straight elimination from the organism [26].

Concerning each subset of tacrine-Trp hybrids, some conclusions can be drawn based on the obtained data. The order of toxicity is as follows: THA derivatives < 7-MEOTA analogues < 6-Cl-THA derivatives. 6-Cl-THA hybrids are presumably the most toxic because of the highest lipophilicity and thus easiest cell permeation disturbing cell viability. Furthermore, increasing the number of methylene units in the linker chain exacerbates the cytotoxicity. This feature also correlates well with compound lipophilicity [65]. Reference compounds 7-MEOTA, and 6-Cl-THA were found the least toxic on HepG2 cells, while all novel hybrids were more hepatotoxic than Trp, THA, 7-MEOTA and 6-Cl-THA with the Trp precursor being the least toxic. Interestingly, ***R*-K1035** and **rac-K1035** showed IC_{50} values comparable to that of ***S*-K1035** that allowed us to conclude that chirality is not the key factor for hepatotoxicity.

11. *In vitro* effects of compounds on the activity on neuronal nitric oxide synthase

NMDA receptors are associated with particular NOS isoforms through a postsynaptic density protein. The excessive stimulation of the receptors activates synthesis of nitric oxide (NO) especially via nNOS isoform - NO pathway is involved in the neuropathology of many neurodegenerative diseases, including AD [100]. In addition to NMDA receptor antagonists, such as memantine, the reduction of excessive NO generation by inhibiting the activity of nNOS could be the viable therapeutic approach for AD [101]. Particular attention in this field has been turned to dimeric compound **4** (Fig. 1) acting synergistically *via* the blockade of NMDA receptors and inhibition of nNOS. Besides **4**, other well-known nNOS inhibitors with potential implication in AD treatment, such as N^G-monomethyl-L-arginine (L-NMMA) and 7-nitroindazole (7-NI) (Fig. 6) showed inhibition potency in the same order of magnitude with IC_{50} values in the micromolar concentration [102]. In the *in vitro* experiment, we evaluated all THA-Trp hybrids ***S*-K1024-K1044**, ***R*-K1035** and **rac-K1035** showing moderate inhibition ability against nNOS with IC_{50} values in the range of 18–45 μM (Table 4). Note that all of the reference compound, *i.e.* THA, 6-Cl-THA, 7-MEOTA and **13** were ineffective proposing that nNOS inhibition potency is an unique feature delivered by a combination of different tacrine scaffolds with L-Trp. Our data indicates that the length of aliphatic linkers or chirality (comparison of effects of ***S*-K1035**, ***R*-K1035** and **rac-K1035**) do not play a significant role in the nNOS inhibition. To conclude, all of the new heterodimers resulted to be only slightly less effective inhibitors of nNOS in comparison with bis(7)tacrine, L-NMMA.

12. *In vivo* toxicity and behavioral studies

In order to predict the *in vivo* toxic effect of ***S*-K1035**, the assessment of acute toxicity upon intraperitoneal (i.p.) administration (fixed dose procedure) was performed in adult Wistar rats. The maximum tolerated dose (MTD) of ***S*-K1035** was determined to be 70 mg kg^{-1}. At this dose, only mild to moderate signs of intoxication occurred, including partial piloerection, persistent oculonasal discharge, intermittent abnormal breathing pattern, intermittent tremors and prostration, diminishing spontaneously

Table 3
Cell viability evaluation of tacrine-tryptophan hybrids and reference compounds.

Cmpd	CHO-K1 cytotoxicity IC_{50} (μM) ± SEM[a]	HepG2 cytotoxicity IC_{50} (μM) ± SEM[a]
***S*-K1024**	131 ± 3	nd
***S*-K1025**	95 ± 11	nd
***S*-K1026**	73 ± 18	nd
***S*-K1027**	46 ± 3	nd
***S*-K1028**	23 ± 3	16 ± 0.5
***S*-K1029**	14 ± 1	5.6 ± 0.5
***S*-K1030**	43 ± 12	nd
***S*-K1031**	26 ± 6	nd
***S*-K1032**	29 ± 5	nd
***S*-K1033**	16 ± 1	nd
***S*-K1034**	21 ± 3	nd
***S*-K1035**	21 ± 2	4.9 ± 0.4
***S*-K1036**	24 ± 5	6.0 ± 0.5
***S*-K1037**	65 ± 10	nd
***S*-K1038**	200 ± 20	nd
***S*-K1039**	116 ± 4	nd
***S*-K1040**	34 ± 3	nd
***S*-K1041**	83 ± 1	nd
***S*-K1042**	90 ± 4	26 ± 1.1
***S*-K1043**	248 ± 6	nd
***S*-K1044**	47 ± 3	9.3 ± 1.2
***R*-K1035**	15 ± 2	4.2 ± 0.6
rac-K1035	21 ± 3	5.1 ± 0.3
1	63 ± 4	120 ± 3
2	71 ± 2	71 ± 1.1
3	248 ± 11	190 ± 7.5
13	nd	17000 ± 900

[a] Values are the mean ± SEM of three independent measurements. “nd” stands for not determined.

Table 4
Effect of the compounds on the nNOS activity.

Cmpd	nNOS IC_{50} (μM) ± SEM)[a]
***S*-K1024**	19 ± 1
***S*-K1025**	30 ± 7
***S*-K1026**	27 ± 3
***S*-K1027**	26 ± 9
***S*-K1028**	27 ± 7
***S*-K1029**	26 ± 9
***S*-K1030**	45 ± 10
***S*-K1031**	39 ± 10
***S*-K1032**	31 ± 12
***S*-K1033**	26 ± 8
***S*-K1034**	27 ± 10
***S*-K1035**	26 ± 11
***S*-K1036**	27 ± 4
***S*-K1037**	43 ± 11
***S*-K1038**	33 ± 4
***S*-K1039**	32 ± 10
***S*-K1040**	18 ± 1
***S*-K1041**	26 ± 12
***S*-K1042**	33 ± 2
***S*-K1043**	32 ± 8
***S*-K1044**	37 ± 8
***R*-K1035**	26 ± 4
***rac*-K1035**	33 ± 9
4[b]	2.9 ± 0.21
L-NMMA[b]	4.1 ± 0.17
7-NI[b]	0.7 ± 0.19

[a] Values are the mean ± SEM of three independent measurements.
[b] Data from Ref. [102].

within approximately 2 h. No weight loss was observed in rats administered with the dose corresponding to MTD within 24 and 48 h. For comparative purposes but using intramuscular (i.m.) administration, THA revealed a toxicity expressed at the MTD of 34 mg kg^{-1} [103].

Knowing the tolerated dose, the therapeutic efficacy of tested drugs was assessed in the animal models of the disease. Namely, the effect of ***S*-K1035** in scopolamine-induced model of cognitive deficit in adult Wistar rats was investigated. Scopolamine, a competitive muscarinic ACh receptor antagonist, causes deficits in multiple cognitive domains and it is considered as an appropriate model for assessing the efficacy of various procognitive compounds [104]. Different AChEIs including THA [105], donepezil [104] and phenserine [106], were found to have therapeutic effect in modifications of scopolamine model in rats.

The effect of ***S*-K1035** on cognition was tested in the Morris water maze (MWM; long-term memory version), which represents one of the most common tests of spatial cognition in laboratory rodents. The MWM task designed by Jackson and Soliman was modified and used [105]. The rats underwent 3 days of intact training and on the 4th day before MWM, drugs were applied. The effect of drugs was assessed by comparing the performance of the group on MWM day 3 (group baseline, without drugs) with the performance of the same group on day 4 (with drugs). ***S*-K1035** was applied intracerebroventricularly (i.c.v.; at two concentrations:10 nM and 100 nM), scopolamine (SCOP) was applied intraperitoneally (i.p.; 5 mg kg^{-1}), saline (SAL) was applied i.c.v and i.p. There were five treatment groups: (1) SAL i.c.v. + SAL i.p.; (2) SAL i.c.v. + SCOP i.p.; (3) ***S*-K1035** 100 nM i.c.v. + SAL i.p.; (4) ***S*-K1035** 10 nM i.c.v. + SCOP i.p.; (5) ***S*-K1035** 100 nM i.c.v. + SCOP i.p. (Fig. 7).

In our experiment, ***S*-K1035** was applied i.c.v. and its effect was observed in modified MWM. The MWM design containing only one application of the tested drug and scopolamine was chosen, because it is suitable for the i.c.v. application (in comparison with repeated i.c.v. applications, which can represent an increased risk of the head implant damage by repeated manipulations). This MWM design involving the application of scopolamine after intact training in MWM requires a relatively high dose of scopolamine (5 mg kg^{-1}, used in our study and in the work of Jackson and Soliman [105]).

It should be also mentioned that the lower concentration of ***S*-K1035** administered (10 nM) mimics the administration of ***S*-K1035** at a concentration close to its IC_{50} values towards cholinesterase enzyme, i.e. 6.3 nM for *h*AChE. The higher dose of ***S*-K1035** administered (100 nM) is more than ten-times higher. The need of this high dose is related to the rather high dose of scopolamine used in the experimental set up (as mentioned above). Indeed, it is worth mentioning that in the study of Jackson and Soliman who studied the effect of THA upon scopolamine-induced cognitive impairment in a similar modification of MWM (application of 5 mg kg^{-1} of scopolamine preceded by intact training in MWM), also a high dose of THA (8 mg kg^{-1}) was used to overcome the effect of this dose of scopolamine.

The results showed that there was no significant difference between groups on day 3 (baseline, before the treatment) in any of the four studied parameters (distance moved, escape latency, average distance from platform, time in target sector). In saline-treated animals (SAL i.c.v. + SAL i.p.), no significant difference between day 3 and day 4 performance in any of parameters measured was found, showing that the manipulations during the injections alone had no effect on rat performance.

Administration of scopolamine (SAL i.c.v. + SCOP i.p.) caused a significant increase of distance moved ($p = 0.0043$), escape latency ($p = 0.0194$), average distance from platform ($p = 0.0152$), and a considerable decrease in time spent in the target sector ($p = 0.0411$). These findings indicate cognitive deficit and therefore confirm the validity of the modification of the model used.

In control group of ***S*-K1035** (higher dose) treated animals (***S*-K1035** 100 nM i.c.v. + SAL i.p.) only, no significant change in any of parameters measured was found. The i.c.v. application of ***S*-K1035** alone thus did not have any detrimental effect on rat performance. In addition, in the ***S*-K1035** treated animals, we did not observe any evident cholinergic effects like salivation or tremors.

In the group treated with the lower dose of ***S*-K1035** and with scopolamine (***S*-K1035** 10 nM i.c.v. + SCOP i.p.), there was a significant increase between the distance moved on day 3 and day 4 ($p = 0.0411$), showing that the lower dose of ***S*-K1035** was not sufficient to alleviate the increase of distance moved caused by scopolamine. On the other hand, concerning escape latency, average distance from platform, time in target sector, there were no differences between day 3 and day 4, indicating ***S*-K1035** was able to ameliorate these parameters even at a lower dose. Therefore, the therapeutic effect of the lower dose of ***S*-K1035** was only partial. Most importantly, in the ***S*-K1035** (higher dose) and scopolamine-treated rats (***S*-K1035** 100 nM i.c.v. + SCOP i.p.), we did not find any significant difference between day 3 and day 4 performance in any parameter studied, demonstrating the beneficial effect of ***S*-K1035** in the scopolamine-induced cognitive deficit rat model.

In summary, we proved a dose-dependent beneficial effect of ***S*-**

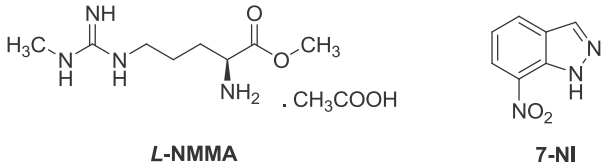

***L*-NMMA** **7-NI**

Fig. 6. Structures of NOS inhibitors N^G-monomethyl-*L*-arginine (*L*-NMMA) and 7-nitroindazole (7-NI).

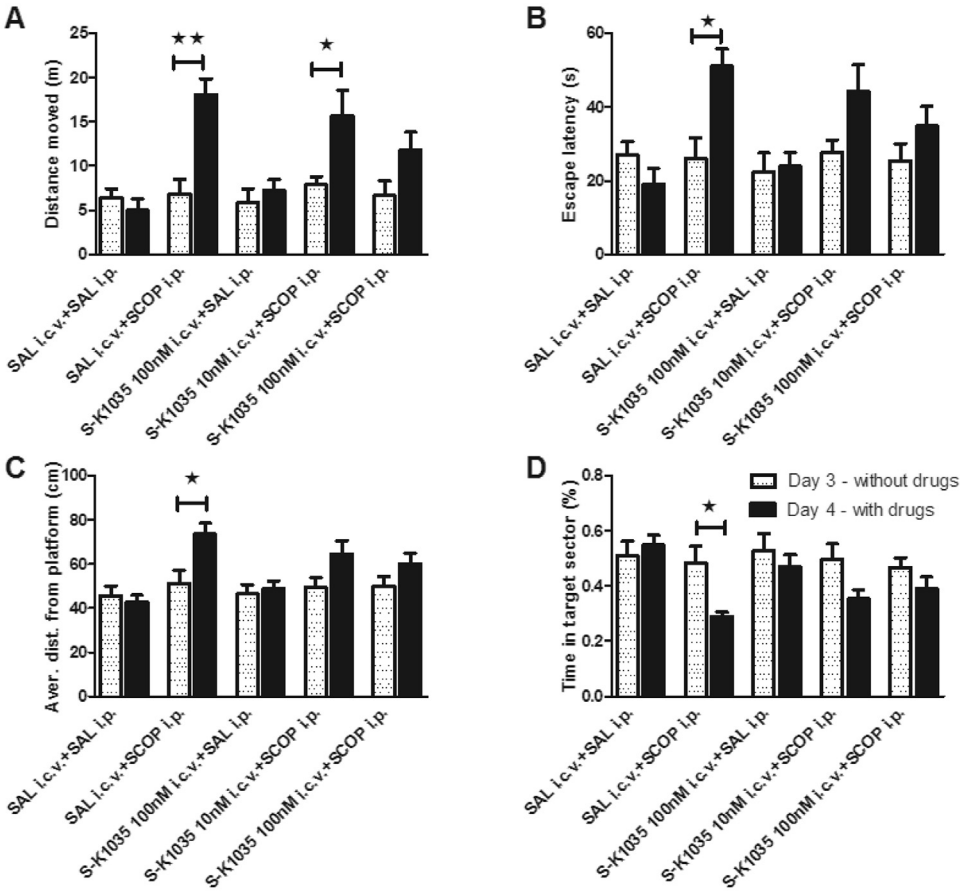

Fig. 7. Effects of ***S*-K1035** in the scopolamine-induced model of cognitive deficit in Morris water maze comparing group performance on days 3 and 4. A **-** distance moved to reach the platform, B – escape latency, C – average distance from the platform, and D – time in the target sector.

K1035 in scopolamine-induced cognitive deficit rat model. This favorable result is consistent with the AChE inhibiting action of ***S*-K1035**, as some other AChEIs were found to be effective in modifications of the scopolamine model in MWM in rats. THA was effective in a similar modification of MWM, in which it completely alleviated escape latency impairment caused by scopolamine. Similar effect on cognitive improvement was observed for THA, however, direct comparison of their action is impossible since THA was administered i.p [105]. Additionally, we are also displaying other beneficial properties of ***S*-K1035**, that are not conveyed to the action of THA, like inhibition of Aβ-self/AChE-induced aggregation and inhibition of nNOS as shown *in vitro*. From a long-term view point of view of AD therapy, ***S*-K1035** may deliver much appreciable effect not only to reduce the symptoms of AD but also to mitigate pathological signs of the disease.

The performance of the group on MWM day 3 (group baseline, without drugs) was compared with the performance of the same group on day 4 (with drugs). In scopolamine treated rats (SAL i.c.v. + SCOP i.p.) the distance moved (Fig. 7 A) was increased ($p = 0.0043$). In rats treated with scopolamine and 10 nM ***S*-K1035** (***S*-K1035** 10 nM i.c.v. + SCOP i.p.), the distance was also increased ($p = 0.0411$), whereas there was no significant change in the distance moved for rats treated with scopolamine and 100 nM ***S*-K1035** (***S*-K1035** 100 nM i.c.v.+SCOP i.p.). This indicate the therapeutic effect of the higher dose of ***S*-K1035** in this parameter. Scopolamine (SAL i.c.v. + SCOP i.p.) caused a significant impairment of rat performance in parameters of escape latency (Fig. 7 B, $p = 0.0194$), average distance from the platform (Fig. 7 C, $p = 0.0152$) and time in the target sector (Fig. 7 D, $p = 0.0411$). Both the lower (***S*-K1035** 10 nM i.c.v. + SCOP i.p.) and higher (***S*-K1035** 100 nM i.c.v. + SCOP i.p.) doses of ***S*-K1035** were able to alleviate the effect of scopolamine in all considered parameters (significant differences between day 3 and day 4 were not found). Saline (SAL i.c.v.+SAL i.p.) or the higher dose of ***S*-K1035** alone (***S*-K1035** 100 nM i.c.v.+SAL i.p.) did not have any detrimental effect on any parameter of the rat performance in MWM. All values represent mean ± SEM, $^{*}p < 0.05$, $^{**}p < 0.01$.

13. Conclusions

This study describes the design, synthesis, *in vitro* and *in vivo* evaluation of new tacrine-tryptophan heterodimers. The synthesis of both ***R*-K1035** and ***rac*-K1035** has allowed to assess differences in potency with respect to the multiple tested biological activities. ***S*-K1035** was found to demonstrate the highest levels of *h*AChE and *h*BChE inhibition if compared to reference standards THA, 7-MEOTA and 6-Cl-THA. Moreover, the crystal structure confirmed the ability of ***S*-K1035** to target both the CAS and PAS of AChE. All the new hybrids also significantly inhibited $A\beta_{42}$ self-aggregation and the *h*AChE-induced $A\beta_{40}$ aggregation. Most of them were predicted to cross BBB via passive diffusion and exhibited moderate inhibitory activity against nNOS. ***S*-K1035** as distinctive *h*AChE/*h*BChE inhibitor was selected in order to determinate its toxic profile. ***S*-K1035** showed higher HepG2 and CHO-K1 cytotoxicity

than tacrine-based analogues, however, these data displayed only the direct effect on isolated cell lines omitting the drug metabolism and behavior under *in vivo* conditions. Assessment of the acute toxicity of ***S*-K1035** was performed on laboratory rats. In agreement with a more complex fate of a drug in a whole body compared to isolated cells, the safety behavior of ***S*-K1035**, compared to THA, was reversed. Indeed, the MTD of ***S*-K1035** was found to be 70 mg kg^{-1}, a value which is two times higher than that found for THA, meaning ***S*-K1035** can be considered safer than THA when administered to rats. Based on these results, the therapeutic effect of ***S*-K1035** in a scopolamine-induced cognitive deficit rat model was investigated using Morris water maze that confirmed pro-cognitive potential.

All of these results suggested that the newly developed tacrine-tryptophan derivatives represent a novel promising MTDLs that deserve further investigation for their potential use against AD.

14. Experimental section

14.1. Chemistry. General methods

All reagents were reagent grade quality and obtained from Sigma-Aldrich (Prague, Czech Republic). Solvents for synthesis of tacrine-tryptophan hybrids were obtained from Penta Chemicals Co. (Czech Republic). All experiments were carried out under nitrogen atmosphere. Thin layer chromatography (TLC) was performed on aluminium sheets precoated with silica gel 60 F254 (Merck, Prague, Czech Republic) and then visualized by UV 254. Column chromatography was performed at normal pressure on silica gel 100 (particle size of 0.063–0.200 mm, 70–230 mesh ASTM, Fluka, Prague, Czech Republic). Mass spectra were recorded using a combination of high performance liquid chromatography and mass spectrometry. The analytical system Dionex Ultimate 3000 LC-MS was connected with a Orbitrap Q Exactive Plus hybrid spectrometer (Thermo Fisher Scientific, Bremen, Germany). ^{1}H NMR and ^{13}C NMR spectra were recorded with a Varian Mercury VX BB 300 (operating at 300 MHz for ^{1}H and 75 MHz for ^{13}C) or on a Varian S500 spectrometer (operating at 500 MHz for ^{1}H and 126 MHz for ^{13}C; Varian Comp., Palo Alto, CA). Chemical shifts are reported in parts per million (ppm, δ) relative to tetramethylsilane (TMS). The assignment of chemical shifts is based on standard NMR experiments (^{1}H, ^{13}C, ^{1}H-^{1}H COSY, ^{1}H-^{13}C HSQC, HMBC, DEPT). All of the final compounds showed ≥95% purity by analytical UHPLC (uncalibrated compound purity was determined at the wavelength of 254 nm as a percent ratio between the peak area of the compound and the total area of all peaks in the chromatogram; see Supporting information). Electronic circular dichroism (ECD), a chiroptical method, was used to determine the absolute configuration of the newly prepared hybrids. Our assumption that the hybrids adopt the same configuration corresponding with L-tryptophan has been confirmed. For more information, see Supporting information. Melting points were measured on a microheating stage PHMK 05 (VEB Kombinant Nagema, Radebeul, Germany) and are presented as uncorrected.

Pan assay interference compounds (PAINS) analysis. We have analyzed ***S*-K1024-K1044, *R*-K1035** and ***rac*-K1035** for known classes of assay interference compounds [107]. These compounds were not recognized as PAINS according to the Free ADME-Tox Filtering Tool (FAF-Drugs4) program (http://fafdrugs4.mti.univ-paris-diderot.fr/) or as aggregators according to the software "Aggregator Advisor" (http://advisor.bkslab.org/).

14.1.1. General Procedure for Synthesis of N-[(tert-butoxy) carbonyl]-L-tryptophan (**16**)

The reaction mixture of L-tryptophan (**13**, 4.89 mmol), triethylamine (9.79 mmol) and di-*tert*-butyl dicarbonate (Boc_2O, 6.36 mmol) was stirred in methanol (10 mL) under the nitrogen at room temperature for 24 h. After the evaporation of methanol under the pressure, the final product was isolated in 87% yield.

14.1.2. General Procedure for Synthesis of N-[(tert-butoxy) carbonyl]-D-tryptophan (**17**)

The reaction mixture of D-tryptophan (**14**, 4.89 mmol), triethylamine (9.79 mmol) and di-*tert*-butyl dicarbonate (Boc_2O, 6.36 mmol) was stirred in methanol (10 mL) under the nitrogen at room temperature for 24 h. After the evaporation of methanol under the pressure, the final product was isolated in 86% yield.

14.1.3. General Procedure for Synthesis of N-[(tert-butoxy) carbonyl]-DL-tryptophan (**18**)

The reaction mixture of DL-tryptophan (**15**, 4.89 mmol), triethylamine (9.79 mmol) and di-*tert*-butyl dicarbonate (Boc_2O, 6.36 mmol) was stirred in methanol (10 mL) under the nitrogen at room temperature for 24 h. After the evaporation of methanol under the pressure, the final product was isolated in 88% yield.

14.1.4. General Procedure for Synthesis of N-(7-methoxy-1,2,3,4-tetrahydroacridin-9-yl)alkane-1,ω-diamines (**19**–**25**)

N-(6-chloro-1,2,3,4-tetrahydroacridin-9-yl)alkane-1,ω-diamines (**26**–**32**) and *N*-(1,2,3,4-tetrahydroacridin-9-yl)alkane-1,ω-diamines (**33**–**39**).

The reaction mixture of phenol (18 mmol) and appropriate 9-chlorotacrine (**10**–**12**, 2.01 mmol) was heated at 90 °C to form a liquid. To this mixture was added appropriate diamine (12 mmol) and refluxed at 130 °C for 4 h. Then, the mixture was cooled to the room temperature and 20% aqueous solution of sodium hydroxide was added. The solution was extracted with dichloromethane. The organic layer was washed with brine and water and dried with sodium sulphate. The appropriate intermediate was purified by column chromatography using mobile phase ethylacetate/methanol/triethylamine (8:1:0.2). Yield: 70–90%.

14.1.5. General Procedure for Synthesis of tacrine-tryptophan hybrids (***S*-K1024-K1044**)

N-[(*tert*-Butoxy)carbonyl]-L-tryptophan (**16**, 0.89 g, 2.95 mmol) was dissolved in dimethylformamide (10 mL) and stirred with triethylamine (1.22 mL, 8.85 mmol) at room temperature under nitrogen. Benzotriazol-1-yloxytris(dimethylamino)phosphonium hexafluorophosphate (BOP, 1.30 g, 2.95 mmol) was added to the reaction mixture after 30 min. Then, appropriate *N*-(1,2,3,4-tetrahydroacridin-9-yl)alkane-1,ω-diamine (**19**–**39**, 0.8 g, 2.95 mmol) was added to the mixture 1 h later. This mixture was stirred at room temperature for 24 h. The solution was extracted with ethylacetate/water (1:1) (3 × 100 mL:100 mL) and organic layer was dried over Na_2SO_4 and then evaporated under the pressure. The crude product was purified by column chromatography using mobile phase chloroform/methanol (50:1). Finally, an intermediate *tert*-butyl 1-(2-(*N*-(1,2,3,4-tetrahydroacridin-9-ylamino) ethylcarbamoyl)-2-(1*H*-indole-3-yl) ethylcarbamate (**40**–**62**) was dissolved in methanol (20 mL). 4 M HCl (20 mL) was added to the mixture. This reaction mixture was stirred at room temperature for 24 h. Then, all the solvents were evaporated under the pressure to obtain required dihydrochloride.

14.1.5.1. Tert-butyl 1-(2-(7-methoxy-1,2,3,4-tetrahydroacridin-9-ylamino)ethylcarbamoyl)-2-(1H-indole-3-yl) ethylcarbamate (**40**).

Yield 44%. ^{1}H NMR (500 MHz, DMSO-d_6) δ 10.77 (m, 1H), 8.08 (t, J = 5.7 Hz, 1H), 7.64 (d, J = 9.1 Hz, 1H), 7.53 (d, J = 7.9 Hz, 1H), 7.40 (d, J = 2.7 Hz, 1H), 7.29 (d, J = 8.0 Hz, 1H), 7.22 (dd, J = 9.1, 2.7 Hz, 1H), 7.09 (d, J = 2.4 Hz, 1H), 6.98 (m, 2H), 6.73 (d, J = 8.1 Hz, 1H), 4.13 (m, 1H), 3.88 (s, 3H), 3.29 (m, 2H), 2.98 (m, 1H), 2.87 (m, 3H), 2.71 (m,

2H), 2.49 (m, 2H), 1.98 (m, 2H), 1.80 (m, 2H), 1.28 (s, 9H). ^{13}C NMR (126 MHz, DMSO-d_6) δ 172.82, 170.52, 155.75, 155.34, 155.17, 149.94, 136.20, 129.10, 127.49, 123.75, 120.97, 120.88, 120.55, 118.60, 118.29, 116.73, 111.40, 110.33, 101.83, 78.16, 59.94, 55.62, 55.41, 47.50, 32.89, 29.17, 28.29, 27.95, 25.23, 22.88, 22.49, 20.94. HRMS [M + H]$^+$: 558.3078 (calculated for $[C_{32}H_{40}N_5O_4]^+$: 558.3075).

*14.1.5.2. Tert-butyl 1-(2-(7-methoxy-1,2,3,4-tetrahydroacridin-9-ylamino)propylcarbamoyl)-2-(1H-indole-3-yl) ethylcarbamate (**41**).* Yield 15%; mp 83.3–87.6 °C. ^{1}H NMR (500 MHz, Methanol-d_4) δ 7.66 (d, J = 9.2 Hz, 1H), 7.53 (d, J = 7.9 Hz, 1H), 7.47 (m, 1H), 7.30 (m, 1H), 7.26 (d, J = 8.1 Hz, 1H), 7.07 (s, 1H), 6.98 (m, 2H), 4.27 (m, 1H), 3.90 (s, 3H), 3.42 (m, 2H), 3.30 (m, 3H), 3.19 (m, 3H), 2.95 (m, 2H), 2.73 (m, 2H), 1.89 (m, 2H), 1.67 (m, 2H), 1.34 (s, 9H). ^{13}C NMR (126 MHz, Methanol-d_4) δ 176.36, 175.37, 158.12, 157.55, 154.47, 154.05, 137.97, 128.76, 126.34, 124.55, 123.41, 122.38, 121.08, 119.73, 119.37, 112.23, 111.38, 110.96, 103.27, 80.64, 61.53, 57.33, 56.35, 45.44, 37.36, 31.75, 29.20, 28.61, 26.22, 23.76, 22.11, 22.07, 20.86. HRMS [M + H]$^+$: 572.3225 (calculated for $[C_{33}H_{42}N_5O_4]^+$: 572.3232).

*14.1.5.3. Tert-butyl 1-(2-(7-methoxy-1,2,3,4-tetrahydroacridin-9-ylamino)butylcarbamoyl)-2-(1H-indole-3-yl) ethylcarbamate (**42**).* Yield 79%. ^{1}H NMR (500 MHz, Methanol-d_4) δ 7.66 (d, J = 9.2 Hz, 1H), 7.53 (d, J = 7.7 Hz, 1H), 7.34 (d, J = 2.7 Hz, 1H), 7.27 (d, J = 8.1 Hz, 1H), 7.23 (dd, J = 9.2, 2.7 Hz, 1H), 7.05 (s, 1H), 7.02 (m, 1H), 6.96 (m, 1H), 4.25 (t, J = 7.1 Hz, 1H), 3.88 (s, 3H), 3.38 (m, 2H), 3.13 (m, 2H), 3.00 (m, 2H), 2.92 (t, J = 6.1 Hz, 2H), 2.70 (t, J = 6.0 Hz, 2H), 1.93 (s, 9H), 1.87 (m, 4H), 1.45 (m, 2H), 1.18 (m, 2H). ^{13}C NMR (126 MHz, Methanol-d_4) δ 176.34, 174.69, 172.96, 157.68, 156.20, 152.70, 142.54, 137.97, 128.69, 124.55, 123.26, 121.30, 119.57, 117.66, 112.19, 110.98, 102.99, 80.59, 61.51, 57.18, 56.13, 48.48, 39.97, 33.40, 29.37, 28.62, 27.63, 26.17, 24.00, 23.53, 22.06, 20.85. HRMS [M + H]$^+$: 586.3380 (calculated for $[C_{34}H_{44}N_5O_4]^+$: 586.3388).

*14.1.5.4. Tert-butyl 1-(2-(7-methoxy-1,2,3,4-tetrahydroacridin-9-ylamino)pentylcarbamoyl)-2-(1H-indole-3-yl) ethylcarbamate (**43**).* Yield 28%; 72.7–75.4 °C. ^{1}H NMR (500 MHz, DMSO-d_6) δ 10.77 (m, 1H), 7.83 (t, J = 5.7 Hz, 1H), 7.63 (d, J = 9.1 Hz, 1H), 7.55 (d, J = 7.9 Hz, 1H), 7.40 (d, J = 2.7 Hz, 1H), 7.30 (d, J = 8.1 Hz, 1H), 7.18 (dd, J = 9.1, 2.7 Hz, 1H), 6.99 (m, 2H), 6.66 (d, J = 8.4 Hz, 2H), 4.12 (m, 1H), 3.85 (s, 3H), 3.00 (m, 2H), 2.86 (t, J = 6.4 Hz, 3H), 2.71 (t, J = 6.2 Hz, 2H), 2.50 (m, 3H), 1.80 (m, 2H), 1.75 (m, 4H), 1.49 (m, 2H), 1.40 (m, 2H), 1.28 (s, 9H). ^{13}C NMR (126 MHz, DMSO-d_6) δ 171.68, 170.53, 155.74, 155.60, 149.61, 142.76, 136.21, 129.93, 127.54, 123.75, 121.39, 120.96, 120.10, 118.67, 118.28, 117.22, 111.40, 110.44, 101.72, 78.10, 59.95, 55.58, 55.36, 47.44, 38.35, 33.37, 28.31, 28.14, 26.76, 25.46, 23.00, 22.71, 22.69, 22.28, 20.95. HRMS [M + H]$^+$: 600.3546 (calculated for $[C_{35}H_{46}N_5O_4]^+$: 600.3545).

*14.1.5.5. Tert-butyl 1-(2-(7-methoxy-1,2,3,4-tetrahydroacridin-9-ylamino)hexylcarbamoyl)-2-(1H-indole-3-yl) ethylcarbamate (**44**).* Yield 74%. ^{1}H NMR (500 MHz, DMSO-d_6) δ 10.79 (m, 1H), 7.78 (t, J = 5.7 Hz, 1H), 7.63 (d, J = 9.1 Hz, 1H), 7.55 (d, J = 7.9 Hz, 1H), 7.41 (d, J = 2.8 Hz, 1H), 7.30 (d, J = 8.0 Hz, 1H), 7.18 (dd, J = 9.1, 2.7 Hz, 1H), 7.10 (d, J = 2.0 Hz, 1H), 6.98 (m, 2H), 6.69 (d, J = 8.3 Hz, 1H), 4.12 (m, 1H), 3.85 (s, 3H), 3.31 (m, 6H), 3.01 (m, 3H), 2.87 (m, 3H), 2.71 (m, 2H), 2.49 (m, 2H), 1.78 (m, 6H), 1.28 (s, 9H). ^{13}C NMR (126 MHz, DMSO-d_6) δ 171.87, 155.76, 155.56, 149.61, 142.86, 136.19, 130.02, 127.52, 126.11, 124.37, 123.73, 121.47, 120.94, 118.64, 117.27, 111.38, 110.42, 101.68, 78.05, 59.93, 55.53, 47.70, 38.57, 33.42, 32.46, 30.81, 30.78, 29.18, 28.29, 26.36, 25.50, 25.11, 23.00, 22.75, 20.93. HRMS [M + H]$^+$: 614.3692 (calculated for $[C_{36}H_{48}N_5O_4]^+$: 614.3701).

*14.1.5.6. Tert-butyl 1-(2-(7-methoxy-1,2,3,4-tetrahydroacridin-9-ylamino)heptylcarbamoyl)-2-(1H-indole-3-yl) ethylcarbamate (**45**).* Yield 86%. ^{1}H NMR (500 MHz, DMSO-d_6) δ 10.79 (s, 1H), 7.77 (t, J = 5.7 Hz, 1H), 7.63 (dd, J = 9.1, 1.6 Hz, 1H), 7.56 (d, J = 7.9 Hz, 1H), 7.41 (d, J = 2.6 Hz, 1H), 7.30 (d, J = 8.0 Hz, 1H), 7.18 (m, 1H), 7.10 (d, J = 2.2 Hz, 1H), 6.99 (m, 2H), 6.68 (d, J = 8.3 Hz, 1H), 4.13 (m, 1H), 3.85 (s, 3H), 3.31 (m, 8H), 3.00 (m, 4H), 2.87 (m, 2H), 2.71 (m, 2H), 2.49 (m, 2H), 1.79 (m, 6H), 1.29 (s, 9H). ^{13}C NMR (126 MHz, DMSO-d_6) δ 171.83, 170.50, 155.70, 149.69, 142.77, 136.19, 129.94, 127.53, 123.72, 121.40, 121.37, 120.93, 120.06, 118.64, 118.26, 117.19, 111.38, 110.42, 101.73, 78.05, 59.93, 55.53, 55.34, 47.73, 38.62, 33.37, 30.81, 29.07, 28.76, 28.30, 28.10, 26.57, 26.42, 25.46, 22.98, 22.73, 20.94. HRMS [M + H]$^+$: 628.3846 (calculated for $[C_{37}H_{50}N_5O_4]^+$: 628.3858).

*14.1.5.7. Tert-butyl 1-(2-(7-methoxy-1,2,3,4-tetrahydroacridin-9-ylamino)octylcarbamoyl)-2-(1H-indole-3-yl) ethylcarbamate (**46**).* Yield 40%. ^{1}H NMR (500 MHz, Methanol-d_4) δ 7.65 (dd, J = 9.2, 1.1 Hz, 1H), 7.60 (d, J = 2.5 Hz, 1H), 7.52 (d, J = 7.9 Hz, 1H), 7.48 (m, 1H), 7.28 (d, J = 8.2 Hz, 1H), 7.04 (s, 1H), 7.01 (d, J = 7.7 Hz, 1H), 6.94 (t, J = 7.5 Hz, 1H), 4.25 (m, 1H), 3.93 (s, 3H), 3.87 (m, 2H), 3.14 (m, 2H), 2.98 (m, 2H), 2.68 (m, 2H), 1.93 (s, 16H), 1.78 (m, 2H), 1.35 (s, 9H). ^{13}C NMR (126 MHz, Methanol-d_4) δ 176.37, 174.61, 158.47, 157.15, 150.50, 137.94, 134.50, 128.72, 125.38, 124.51, 122.31, 121.70, 119.68, 119.32, 118.51, 112.87, 112.22, 110.94, 104.96, 80.62, 57.16, 56.47, 49.28, 48.74, 40.80, 40.26, 31.80, 30.06, 30.00, 29.39, 29.14, 28.60, 27.55, 27.23, 25.28, 23.04, 22.06, 21.79. HRMS [M + H]$^+$: 642.4010 (calculated for $[C_{38}H_{52}N_5O_4]^+$: 642.4014).

*14.1.5.8. Tert-butyl 1-(2-(6-chloro-1,2,3,4-tetrahydroacridin-9-ylamino)ethylcarbamoyl)-2-(1H-indole-3-yl) ethylcarbamate (**47**).* Yield 91%. ^{1}H NMR (500 MHz, Methanol-d_4) δ 8.13 (d, J = 9.2 Hz, 1H), 7.66 (d, J = 2.2 Hz, 1H), 7.47 (dt, J = 7.7, 1.1 Hz, 1H), 7.39 (dd, J = 9.2, 2.2 Hz, 1H), 7.15 (d, J = 8.0 Hz, 1H), 7.07 (s, 1H), 6.84 (m, 2H), 4.29 (t, J = 6.9 Hz, 1H), 3.68 (m, 2H), 3.45 (m, 2H), 2.88 (m, 2H), 2.46 (s, 2H), 1.93 (s, 9H), 1.35 (s, 6H). ^{13}C NMR (126 MHz, Methanol-d_4) δ 176.36, 172.99, 157.20, 155.73, 143.20, 138.22, 137.76, 128.71, 127.99, 125.99, 124.56, 122.25, 121.79, 119.67, 119.17, 116.84, 114.67, 112.11, 110.60, 80.73, 61.52, 57.09, 40.62, 31.12, 29.02, 28.61, 25.02, 23.19, 22.34, 22.06, 20.85. HRMS [M + H]$^+$: 562.2573 (calculated for $[C_{31}H_{37}ClN_5O_3]^+$: 562.2580).

*14.1.5.9. Tert-butyl 1-(2-(6-chloro-1,2,3,4-tetrahydroacridin-9-ylamino)propylcarbamoyl)-2-(1H-indole-3-yl) ethylcarbamate (**48**).* Yield 83%. ^{1}H NMR (300 MHz, Methanol-d_4) δ 8.04 (d, J = 9.2 Hz, 1H), 7.68 (d, J = 2.2 Hz, 1H), 7.53 (m, 1H), 7.32 (dd, J = 9.1, 2.2 Hz, 1H), 7.24 (d, J = 7.9 Hz, 1H), 7.06 (s, 1H), 6.97 (m, 2H), 4.26 (t, J = 7.0 Hz, 1H), 3.37 (m, 1H), 3.16 (m, 2H), 2.92 (m, 2H), 2.66 (m, 2H), 1.92 (s, 9H), 1.88 (m, 3H), 1.34 (m, 6H). ^{13}C NMR (75 MHz, Methanol-d_4) δ 175.32, 172.96, 157.53, 154.11, 146.30, 137.95, 136.49, 128.74, 126.82, 125.56, 124.82, 124.57, 122.36, 119.73, 119.38, 118.55, 116.23, 112.21, 110.92, 80.62, 61.52, 57.32, 46.01, 37.35, 33.10, 31.49, 29.23, 28.60, 25.78, 23.69, 23.11, 22.06. HRMS [M + H]$^+$: 576.2728 (calculated for $[C_{32}H_{39}ClN_5O_3]^+$: 576.2736).

*14.1.5.10. Tert-butyl 1-(2-(6-chloro-1,2,3,4-tetrahydroacridin-9-ylamino)butylcarbamoyl)-2-(1H-indole-3-yl) ethylcarbamate (**49**).* Yield 91%. ^{1}H NMR (500 MHz, Methanol-d_4) δ 8.13 (d, J = 9.2 Hz, 1H), 7.66 (d, J = 2.2 Hz, 1H), 7.47 (dt, J = 7.7, 1.1 Hz, 1H), 7.39 (dd, J = 9.2, 2.2 Hz, 1H), 7.15 (d, J = 8.0 Hz, 1H), 7.07 (s, 1H), 6.84 (m, 2H), 4.29 (t, J = 6.9 Hz, 1H), 3.68 (m, 2H), 3.45 (m, 2H), 2.88 (m, 2H), 2.46 (s, 2H), 1.93 (s, 9H), 1.35 (s, 6H). ^{13}C NMR (126 MHz, Methanol-d_4) δ 171.98, 170.49, 157.15, 155.28, 151.59, 136.19, 133.52, 127.51, 126.02, 125.13, 123.93, 123.75, 120.94, 118.63, 118.25, 117.86, 115.23, 111.38, 110.41, 78.07, 59.92, 55.37, 47.66, 38.33, 32.61, 28.29, 28.10, 27.87, 24.94, 22.68, 22.51, 22.04, 20.93. HRMS [M + H]$^+$: 590.2889 (calculated for $[C_{33}H_{41}ClN_5O_3]^+$: 590.2893).

*14.1.5.11. Tert-butyl 1-(2-(6-chloro-1,2,3,4-tetrahydroacridin-9-ylamino)pentylcarbamoyl)-2-(1H-indole-3-yl) ethylcarbamate (**50**).* Yield 46%. ^{1}H NMR (500 MHz, DMSO-d_6) δ 10.76 (d, J = 2.3 Hz, 1H), 8.20 (d, J = 9.1 Hz, 1H), 7.79 (t, J = 5.7 Hz, 1H), 7.71 (dd, J = 2.3, 0.9 Hz, 1H), 7.53 (d, J = 7.9 Hz, 1H), 7.40 (m, 1H), 7.29 (d, J = 8.1 Hz, 1H), 7.09 (d, J = 2.3 Hz, 1H), 6.97 (m, 2H), 6.67 (d, J = 8.2 Hz, 1H), 4.11 (m, 1H), 3.50 (m, 2H), 3.01 (m, 3H), 2.87 (m, 3H), 2.65 (m, 2H), 1.78 (m, 4H), 1.75 (m, 2H), 1.58 (m, 2H), 1.34 (m, 2H), 1.28 (s, 9H). ^{13}C NMR (126 MHz, DMSO-d_6) δ 171.92, 171.63, 155.28, 152.36, 136.20, 134.19, 127.51, 126.37, 124.18, 124.02, 123.93, 123.75, 120.94, 118.62, 118.26, 117.24, 114.68, 111.39, 110.40, 78.08, 59.93, 55.38, 47.98, 38.50, 30.13, 28.85, 28.30, 28.09, 24.74, 23.65, 22.68, 22.32, 21.77, 20.93. HRMS [M + H]$^+$: 604.3045 (calculated for [$C_{34}H_{43}ClN_5O_3$]$^+$: 604.3049).

*14.1.5.12. Tert-butyl 1-(2-(6-chloro-1,2,3,4-tetrahydroacridin-9-ylamino)hexylcarbamoyl)-2-(1H-indole-3-yl) ethylcarbamate (**51**).* Yield 41%; mp 77.5–81.9 °C. ^{1}H NMR (300 MHz, Chloroform-d) δ 8.72 (m, 1H), 7.87 (m, 2H), 7.63 (d, J = 7.6 Hz, 1H), 7.26 (m, 1H), 7.11 (m, 2H), 7.01 (d, J = 2.3 Hz, 1H), 4.38 (m, 1H), 3.44 (t, J = 7.2 Hz, 2H), 3.07 (m, 6H), 2.65 (m, 3H), 1.89 (m, 5H), 1.55 (m, 2H), 1.41 (s, 9H), 1.21 (m, 4H). ^{13}C NMR (75 MHz, Chloroform-d) δ 171.57, 158.81, 155.41, 151.11, 147.32, 136.21, 134.30, 127.33, 126.65, 124.73, 124.28, 123.16, 122.07, 119.54, 118.81, 117.97, 115.38, 111.19, 110.50, 80.01, 55.28, 49.23, 39.11, 33.47, 31.41, 29.05, 28.53, 28.25, 26.31, 26.21, 24.42, 22.74, 22.41. HRMS [M + H]$^+$: 618.3209 (calculated for [$C_{35}H_{45}ClN_5O_3$]$^+$: 618.3206).

*14.1.5.13. Tert-butyl 1-(2-(6-chloro-1,2,3,4-tetrahydroacridin-9-ylamino)heptylcarbamoyl)-2-(1H-indole-3-yl) ethylcarbamate (**52**).* Yield 74%. ^{1}H NMR (500 MHz, Methanol-d_4) δ 8.08 (d, J = 9.1 Hz, 1H), 7.69 (d, J = 2.2 Hz, 1H), 7.53 (d, J = 7.9 Hz, 1H), 7.31 (dd, J = 9.2, 2.2 Hz, 1H), 7.27 (d, J = 8.1 Hz, 1H), 6.99 (m, 3H), 4.26 (m, 1H), 3.56 (m, 2H), 3.30 (m, 2H), 3.12 (m, 2H), 2.93 (m, 3H), 2.65 (m, 2H), 1.87 (m, 4H), 1.62 (m, 2H), 1.35 (s, 9H), 1.27 (m, 5H), 1.11 (m, 2H). ^{13}C NMR (126 MHz, Methanol-d_4) δ 174.57, 158.82, 157.46, 154.03, 147.18, 137.98, 136.22, 128.78, 126.90, 125.31, 125.24, 124.50, 122.33, 119.70, 119.38, 118.71, 116.06, 112.20, 110.97, 80.59, 61.52, 57.13, 40.23, 33.40, 32.02, 29.95, 29.89, 29.44, 28.63, 27.71, 27.53, 25.70, 23.74, 23.23, 22.05, 20.85. HRMS [M + H]$^+$: 632.3359 (calculated for [$C_{36}H_{47}ClN_5O_3$]$^+$: 632.3362).

*14.1.5.14. Tert-butyl 1-(2-(6-chloro-1,2,3,4-tetrahydroacridin-9-ylamino)octylcarbamoyl)-2-(1H-indole-3-yl) ethylcarbamate (**53**).* Yield 43%. ^{1}H NMR (500 MHz, Methanol-d_4) δ 8.14 (d, J = 9.1 Hz, 1H), 7.69 (d, J = 2.2 Hz, 1H), 7.53 (d, J = 7.9 Hz, 1H), 7.35 (dd, J = 9.1, 2.2 Hz, 1H), 7.27 (d, J = 8.1 Hz, 1H), 7.00 (m, 3H), 4.26 (m, 1H), 3.63 (m, 2H), 3.13 (m, 2H), 2.93 (m, 2H), 2.66 (m, 2H), 1.93 (m, 10H), 1.89 (m, 4H), 1.67 (m, 2H), 1.35 (s, 9H), 1.10 (m, 2H). ^{13}C NMR (126 MHz, Methanol-d_4) δ 174.58, 172.98, 157.66, 154.69, 146.01, 137.98, 136.89, 128.78, 127.21, 125.50, 124.50, 124.23, 122.33, 119.70, 119.37, 118.17, 115.64, 112.21, 110.98, 80.58, 61.52, 57.14, 40.28, 32.69, 31.91, 30.14, 30.09, 29.43, 28.63, 28.32, 27.70, 27.55, 25.53, 23.59, 22.98, 22.06, 20.85. HRMS [M + H]$^+$: 646.3510 (calculated for [$C_{37}H_{49}ClN_5O_3$]$^+$: 646.3519).

*14.1.5.15. Tert-butyl 1-(2-(1,2,3,4-tetrahydroacridin-9-ylamino)ethylcarbamoyl)-2-(1H-indole-3-yl) ethylcarbamate (**54**).* Yield 28%. ^{1}H NMR (500 MHz, Methanol-d_4) δ 8.04 (d, J = 8.6 Hz, 1H), 7.73 (m, 1H), 7.57 (m, 1H), 7.52 (d, J = 7.8 Hz, 1H), 7.37 (m, 1H), 7.24 (d, J = 8.1 Hz, 1H), 7.05 (s, 1H), 6.95 (m, 2H), 4.28 (m, 1H), 3.51 (m, 2H), 3.30 (m, 2H), 2.93 (t, J = 6.1 Hz, 2H), 2.62 (t, J = 6.2 Hz, 2H), 1.87 (m, 4H), 1.34 (s, 9H), 1.17 (m, 2H). ^{13}C NMR (126 MHz, Methanol-d_4) δ 176.35, 175.80, 157.82, 157.52, 153.59, 137.95, 130.41, 128.75, 126.57, 125.07, 124.72, 124.54, 122.37, 120.45, 119.75, 119.33, 116.33, 112.21, 110.83, 80.67, 57.20, 49.51, 41.16, 33.35, 29.20, 28.62, 25.85, 23.87, 23.33, 22.06, 20.85. HRMS [M + H]$^+$: 528.2972 (calculated for [$C_{31}H_{38}N_5O_3$]$^+$: 528.2970).

*14.1.5.16. Tert-butyl 1-(2-(1,2,3,4-tetrahydroacridin-9-ylamino)propylcarbamoyl)-2-(1H-indole-3-yl) ethylcarbamate (**55**).* Yield 23%; mp 88.3–92.7 °C. ^{1}H NMR (500 MHz, Methanol-d_4) δ 8.05 (d, J = 8.5 Hz, 1H), 7.74 (m, 1H), 7.54 (m, 2H), 7.36 (m, 1H), 7.26 (d, J = 8.1 Hz, 1H), 7.06 (s, 1H), 6.98 (m, 2H), 4.28 (m, 1H), 3.16 (m, 2H), 2.95 (t, J = 6.0 Hz, 2H), 2.69 (t, J = 5.9 Hz, 2H), 1.92 (m, 4H), 1.88 (m, 2H), 1.60 (m, 2H), 1.34 (s, 9H), 1.18 (m, 2H). ^{13}C NMR (126 MHz, Methanol-d_4) δ 175.18, 172.95, 158.45, 157.52, 153.39, 147.02, 137.97, 130.11, 128.77, 127.18, 125.02, 124.55, 122.38, 120.96, 119.74, 119.41, 116.74, 112.22, 110.96, 80.62, 61.51, 57.28, 46.10, 37.52, 33.71, 31.62, 28.61, 26.12, 23.97, 23.49, 22.06, 20.85. HRMS [M + H]$^+$: 542.3134 (calculated for [$C_{32}H_{40}N_5O_3$]$^+$: 542.3126).

*14.1.5.17. Tert-butyl 1-(2-(1,2,3,4-tetrahydroacridin-9-ylamino)butylcarbamoyl)-2-(1H-indole-3-yl) ethylcarbamate (**56**).* Yield 42%. ^{1}H NMR (500 MHz, Methanol-d_4) δ 8.02 (d, J = 8.5 Hz, 1H), 7.74 (dd, J = 8.5, 1.2 Hz, 1H), 7.52 (m, 2H), 7.33 (m, 1H), 7.26 (d, J = 8.0 Hz, 1H), 7.05 (s, 1H), 6.98 (m, 2H), 4.26 (m, 1H), 3.38 (m, 2H), 3.14 (m, 2H), 2.94 (t, J = 6.1 Hz, 2H), 2.67 (t, J = 5.8 Hz, 2H), 1.86 (m, 4H), 1.33 (m, 13H), 1.18 (s, 2H). ^{13}C NMR (126 MHz, Methanol-d_4) δ 174.65, 172.94, 159.10, 157.46, 153.03, 147.90, 137.98, 129.70, 128.82, 127.94, 124.73, 124.37, 122.37, 121.27, 119.74, 119.46, 116.80, 112.20, 110.98, 80.58, 61.51, 57.18, 39.95, 34.17, 29.39, 28.63, 28.32, 27.54, 26.10, 24.07, 23.66, 22.06, 20.85. HRMS [M + H]$^+$: 556.3275 (calculated for [$C_{33}H_{42}N_5O_3$]$^+$: 556.3283).

*14.1.5.18. Tert-butyl 1-(2-(1,2,3,4-tetrahydroacridin-9-ylamino)pentylcarbamoyl)-2-(1H-indole-3-yl) ethylcarbamate (**57**).* Yield 25%; mp 73.3–76.8 °C. ^{1}H NMR (300 MHz, Methanol-d_4) δ 8.04 (m, 1H), 7.75 (m, 1H), 7.52 (m, 2H), 7.33 (m, 1H), 7.24 (d, J = 7.9 Hz, 1H), 6.97 (m, 3H), 4.25 (m, 1H), 3.39 (m, 2H), 3.11 (m, 2H), 2.94 (m, 4H), 2.69 (m, 2H), 1.95 (m, 2H), 1.87 (m, 6H), 1.50 (m, 2H), 1.34 (s, 9H). ^{13}C NMR (75 MHz, Methanol-d_4) δ 174.58, 172.92, 159.07, 157.44, 153.17, 147.91, 137.96, 129.71, 128.79, 127.93, 124.70, 124.42, 122.35, 121.30, 119.71, 119.42, 116.78, 112.18, 110.96, 80.55, 61.50, 57.14, 40.14, 34.16, 31.91, 29.83, 29.42, 28.63, 26.09, 25.01, 24.07, 23.68, 22.06, 20.85. HRMS [M + H]$^+$: 570.3434 (calculated for [$C_{34}H_{44}N_5O_3$]$^+$: 570.3439).

*14.1.5.19. Tert-butyl 1-(2-(1,2,3,4-tetrahydroacridin-9-ylamino)hexylcarbamoyl)-2-(1H-indole-3-yl) ethylcarbamate (**58**).* Yield 25%. ^{1}H NMR (500 MHz, DMSO-d_6) δ 10.77 (s, 1H), 8.13 (d, J = 8.6 Hz, 1H), 7.75 (m, 1H), 7.70 (dd, J = 8.5, 1.2 Hz, 1H), 7.54 (m, 1H), 7.35 (m, 1H), 7.29 (d, J = 8.0 Hz, 1H), 7.09 (d, J = 2.3 Hz, 1H), 6.99 (m, 1H), 6.66 (d, J = 5.4 Hz, 6H), 4.11 (m, 1H), 3.43 (m, 2H), 3.00 (m, 2H), 2.89 (t, J = 6.2 Hz, 2H), 2.68 (t, J = 6.0 Hz, 2H), 2.49 (m, 2H), 1.79 (m, 4H), 1.75 (m, 6H), 1.53 (m, 2H), 1.28 (s, 9H). ^{13}C NMR (126 MHz, DMSO-d_6) δ 171.61, 170.49, 156.68, 155.25, 151.29, 136.19, 128.71, 127.52, 127.09, 123.71, 123.62, 123.50, 120.93, 119.74, 118.62, 118.26, 115.32, 111.37, 110.41, 78.06, 59.92, 55.35, 48.03, 38.56, 32.87, 30.67, 29.10, 28.29, 26.21, 26.16, 25.07, 22.67, 22.32, 20.92. HRMS [M + H]$^+$: 584.3593 (calculated for [$C_{35}H_{46}N_5O_3$]$^+$: 584.3596).

*14.1.5.20. Tert-butyl 1-(2-(1,2,3,4-tetrahydroacridin-9-ylamino)heptylcarbamoyl)-2-(1H-indole-3-yl) ethylcarbamate (**59**).* Yield 52%. ^{1}H NMR (500 MHz, Methanol-d_4) δ 8.08 (d, J = 8.6 Hz, 1H), 7.75 (m, 1H), 7.54 (m, 2H), 7.35 (m, 1H), 7.28 (d, J = 8.0 Hz, 1H), 7.00 (m, 3H), 4.26 (m, 1H), 3.51 (t, J = 7.2 Hz, 2H), 3.10 (m, 2H), 2.96 (m, 2H), 2.72 (m, 2H), 1.89 (m, 4H), 1.60 (m, 2H), 1.36 (s, 9H), 1.27 (m, 10H). ^{13}C NMR (126 MHz, Methanol-d_4) δ 174.55, 172.96, 158.90, 157.48, 153.40, 147.71, 138.01, 129.85, 128.82, 127.74, 124.73, 124.47, 122.36,

121.20, 119.73, 119.42, 116.66, 112.21, 111.00, 80.59, 61.52, 57.13, 40.27, 34.05, 33.06, 32.22, 30.74, 29.97, 29.46, 28.64, 27.80, 27.59, 26.10, 24.07, 23.66, 20.85. HRMS $[M + H]^+$: 598.3749 (calculated for $[C_{36}H_{48}N_5O_3]^+$: 598.3752).

*14.1.5.21. Tert-butyl 1-(2-(1,2,3,4-tetrahydroacridin-9-ylamino) octylcarbamoyl)-2-(1H-indole-3-yl) ethylcarbamate (**60**).* Yield 83%. ^{1}H NMR (500 MHz, DMSO-d_6) δ 10.78 (s, 1H), 8.33 (d, J = 8.7 Hz, 1H), 7.78 (m, 2H), 7.53 (m, 2H), 7.43 (d, J = 7.1 Hz, 1H), 7.29 (d, J = 8.0 Hz, 1H), 7.09 (d, J = 2.2 Hz, 1H), 6.98 (m, 1H), 6.68 (d, J = 8.3 Hz, 1H), 4.12 (m, 1H), 3.77 (m, 2H), 3.03 (m, 2H), 2.95 (m, 2H), 2.64 (m, 2H), 2.52 (m, 6H), 1.82 (m, 6H), 1.69 (m, 2H), 1.29 (s, 9H), 1.17 (m, 4H). ^{13}C NMR (126 MHz, DMSO-d_6) δ 171.85, 155.26, 151.50, 139.03, 136.19, 132.37, 127.51, 125.00, 124.25, 123.71, 120.92, 120.31, 118.60, 118.24, 116.18, 111.99, 111.87, 111.38, 110.41, 78.06, 55.36, 47.56, 45.92, 38.63, 36.64, 36.61, 30.05, 29.11, 28.75, 28.72, 28.30, 28.09, 26.29, 26.20, 24.16, 21.73, 20.73. HRMS $[M + H]^+$: 612.3901 (calculated for $[C_{37}H_{50}N_5O_3]^+$: 612.3903).

*14.1.5.22. Tert-butyl 1-(2-(6-chloro-1,2,3,4-tetrahydroacridin-9-ylamino)hexylcarbamoyl)-2-(1H-indole-3-yl) ethylcarbamate (**61**).* Yield 15%. 1H NMR (500 MHz, Methanol-d_4) δ 8.31 (d, J = 9.3 Hz, 1H), 7.82 (d, J = 8.4 Hz, 1H), 7.70 (d, J = 8.3 Hz, 1H), 7.66 (d, J = 2.2 Hz, 1H), 7.50 (m, 2H), 7.45 (m, 1H), 7.27 (d, J = 8.1 Hz, 1H), 7.05 (s, 1H), 6.98 (dt, J = 40.3, 7.4 Hz, 2H), 4.26 (t, J = 7.0 Hz, 1H), 3.86 (t, J = 7.3 Hz, 2H), 3.21–3.11 (m, 2H), 3.04 (m, 2H), 2.92 (t, J = 6.0 Hz, 2H), 2.61 (t, J = 5.8 Hz, 2H), 1.94 (m, 4H), 1.76 (m, 2H), 1.36 (s, 11H), 1.22 (m, 4H). 13C NMR (126 MHz, Methanol-d_4) δ 174.64, 157.62, 151.85, 140.40, 139.99, 137.92, 128.69, 127.90, 126.92, 126.69, 124.50, 122.30, 119.68, 119.31, 119.05, 118.57, 115.32, 113.23, 112.19, 111.49, 110.94, 80.61, 79.43, 57.16, 40.02, 39.99, 31.13, 29.91, 29.39, 29.22, 28.61, 27.12, 24.48, 22.76, 21.67. HRMS $[M + H]^+$: 618.3209 (calculated for $[C_{35}H_{45}ClN_5O_3]^+$: 618.3207).

*14.1.5.23. Tert-butyl 1-(2-(6-chloro-1,2,3,4-tetrahydroacridin-9-ylamino)hexylcarbamoyl)-2-(1H-indole-3-yl) ethylcarbamate (**62**).* Yield 60%. ^{1}H NMR (500 MHz, Methanol-d_4) δ 8.30 (d, J = 9.3 Hz, 1H), 7.68 (d, J = 8.3 Hz, 1H), 7.66 (d, J = 2.2 Hz, 1H), 7.53 (m, 2H), 7.42 (m, 1H), 7.26 (d, J = 8.1 Hz, 1H), 7.04 (s, 1H), 6.97 (dt, J = 40.8, 7.4 Hz, 2H), 4.26 (t, J = 7.0 Hz, 1H), 3.85 (t, J = 7.3 Hz, 2H), 3.16 (m, 2H), 3.06 (m, 2H), 2.91 (t, J = 6.0 Hz, 2H), 2.60 (t, J = 5.8 Hz, 2H), 1.92 (m, 4H), 1.76 (m, 2H), 1.36 (s, 11H), 1.24 (m, 4H). 13C NMR (126 MHz, Methanol-d_4) δ 174.63, 157.59, 151.83, 140.39, 139.95, 137.90, 128.69, 127.53, 126.69, 124.49, 122.29, 119.67, 119.04, 118.56, 115.30, 113.22, 112.18, 111.58, 110.93, 80.60, 57.16, 49.84, 40.13, 40.00, 31.12, 29.91, 29.38, 29.21, 28.61, 27.12, 24.46, 22.75, 21.66. HRMS $[M + H]^+$: 618.3209 (calculated for $[C_{35}H_{45}ClN_5O_3]^+$: 618.3205).

*14.1.5.24. N-(2-(7-methoxy-1,2,3,4-tetrahydroacridin-9-ylamino) ethyl-2-amino-3-(1H-indole-3-yl)propylamide dihydrochloride (**SK1024**).* Yield 99%; mp 97.1–99.2 °C. Purity: 98%. ^{1}H NMR (500 MHz, DMSO-d_6) δ 11.05 (d, J = 2.4 Hz, 1H), 9.29 (t, J = 5.6 Hz, 1H), 8.38 (d, J = 5.5 Hz, 3H), 7.96 (d, J = 9.2 Hz, 1H), 7.82 (d, J = 2.6 Hz, 1H), 7.62 (d, J = 7.9 Hz, 1H), 7.49 (dd, J = 9.2, 2.4 Hz, 1H), 7.28 (d, J = 8.2 Hz, 1H), 7.20 (d, J = 2.4 Hz, 1H), 6.94 (m, 2H), 3.93 (s, 3H), 3.37 (m, 2H), 3.11 (m, 2H), 2.99 (m, 2H), 2.71 (m, 2H), 2.49 (m, 2H), 1.77 (m, 5H). ^{13}C NMR (126 MHz, DMSO-d_6) δ 169.39, 156.85, 154.96, 150.05, 136.33, 132.63, 127.22, 124.91, 124.18, 121.16, 118.63, 118.47, 117.77, 111.51, 111.30, 107.09, 103.74, 56.53, 53.07, 45.97, 34.20, 28.08, 27.17, 25.10, 21.98, 20.41, 18.76. HRMS $[M + H]^+$: 458.2549 (calculated for $[C_{27}H_{32}N_5O_2]^+$: 458.2551).

*14.1.5.25. N-(2-(7-methoxy-1,2,3,4-tetrahydroacridin-9-ylamino) propyl-2-amino-3-(1H-indole-3-yl)propylamide dihydrochloride (**SK1025**).* Yield 61%; mp 97.2–101.4 °C. Purity: 99.9%. ^{1}H NMR (500 MHz, DMSO-d_6) δ 11.08 (d, J = 2.5 Hz, 1H), 9.06 (m, 1H), 8.35 (d, J = 5.2 Hz, 3H), 7.98 (d, J = 9.2 Hz, 2H), 7.84 (d, J = 2.6 Hz, 1H), 7.66 (d, J = 7.9 Hz, 1H), 7.49 (dd, J = 9.2, 2.4 Hz, 1H), 7.31 (d, J = 8.1 Hz, 1H), 7.23 (d, J = 2.4 Hz, 1H), 6.97 (m, 2H), 3.93 (m, 4H), 3.76 (m, 2H), 3.15 (m, 4H), 3.00 (m, 2H), 2.71 (m, 2H), 1.75 (m, 6H). ^{13}C NMR (126 MHz, DMSO-d_6) δ 168.87, 157.11, 155.12, 150.21, 136.62, 132.87, 127.53, 125.19, 124.36, 121.42, 121.25, 119.01, 118.74, 117.95, 111.78, 111.50, 107.50, 103.88, 56.76, 43.77, 36.05, 30.40, 28.32, 27.61, 25.33, 23.06, 22.21, 20.70. HRMS $[M + H]^+$: 472.2702 (calculated for $[C_{28}H_{34}N_5O_2]^+$: 472.2708).

*14.1.5.26. N-(2-(7-methoxy-1,2,3,4-tetrahydroacridin-9-ylamino) butyl-2-amino-3-(1H-indole-3-yl)propylamide dihydrochloride (**SK1026**).* Yield 96%. Purity: 99%. ^{1}H NMR (500 MHz, Methanol-d_4) δ 7.75 (dd, J = 9.2, 1.7 Hz, 1H), 7.65 (t, J = 2.2 Hz, 1H), 7.60 (dt, J = 7.3, 1.2 Hz, 1H), 7.49 (dt, J = 4.7, 2.0 Hz, 2H), 7.21 (d, J = 1.8 Hz, 1H), 7.00 (m, 2H), 4.08 (m, 1H), 3.95 (s, 3H), 3.81 (t, J = 7.2 Hz, 2H), 3.20 (m, 2H), 2.99 (m, 2H), 2.73 (m, 2H), 1.92 (m, 6H), 1.61 (m, 2H), 1.40 (m, 2H). ^{13}C NMR (126 MHz, Methanol-d_4) δ 170.01, 158.64, 157.04, 150.75, 138.06, 134.40, 128.41, 125.63, 125.40, 122.67, 121.79, 120.09, 119.34, 118.73, 112.90, 112.46, 108.12, 104.95, 56.78, 55.25, 48.06, 40.01, 29.26, 29.10, 28.81, 27.14, 25.77, 23.18, 21.84. HRMS $[M + H]^+$: 486.2682 (calculated for $[C_{29}H_{36}N_5O_2]^+$: 486.2864).

*14.1.5.27. N-(2-(7-methoxy-1,2,3,4-tetrahydroacridin-9-ylamino) pentyl-2-amino-3-(1H-indole-3-yl)propylamide dihydrochloride (**SK1027**).* Yield 73%; mp 155.0–157.7 °C. Purity: 99.9%. ^{1}H NMR (500 MHz, DMSO-d_6) δ 11.13 (d, J = 2.5 Hz, 1H), 8.75 (t, J = 5.6 Hz, 1H), 8.32 (d, J = 5.5 Hz, 3H), 7.97 (d, J = 9.2 Hz, 1H), 7.84 (d, J = 2.6 Hz, 1H), 7.64 (d, J = 7.9 Hz, 1H), 7.51 (s, 2H), 7.30 (d, J = 2.7 Hz, 3H), 7.20 (d, J = 2.4 Hz, 1H), 6.97 (m, 2H), 3.92 (s, 3H), 3.75 (m, 2H), 3.10 (m, 3H), 2.99 (m, 3H), 2.70 (m, 2H), 2.49 (m, 3H), 1.78 (m, 4H), 1.60 (m, 2H), 1.35 (m, 2H). ^{13}C NMR (126 MHz, DMSO-d_6) δ 169.39, 156.85, 154.96, 150.05, 136.33, 132.63, 127.22, 124.91, 124.18, 121.16, 118.63, 118.47, 117.77, 111.51, 111.30, 107.09, 103.74, 56.53, 56.21, 53.07, 45.97, 40.20, 39.20, 34.20, 28.08, 27.17, 25.10, 21.98, 20.41, 18.76. HRMS $[M + H]^+$: 500.3021 (calculated for $[C_{30}H_{38}N_5O_2]^+$: 500.3021).

*14.1.5.28. N-(2-(7-methoxy-1,2,3,4-tetrahydroacridin-9-ylamino) hexyl-2-amino-3-(1H-indole-3-yl)propylamide dihydrochloride (**SK1028**).* Yield 99%; mp 132.4–135.6 °C. Purity: 96%. ^{1}H NMR (500 MHz, Methanol-d_4) δ 7.73 (d, J = 9.2 Hz, 1H), 7.64 (d, J = 2.4 Hz, 1H), 7.59 (d, J = 7.8 Hz, 1H), 7.47 (dd, J = 9.1, 2.3 Hz, 1H), 7.32 (d, J = 8.0 Hz, 1H), 7.19 (s, 1H), 7.01 (m, 2H), 4.07 (t, J = 7.3 Hz, 1H), 3.95 (s, 3H), 3.87 (t, J = 7.2 Hz, 2H), 3.30 (m, 2H), 3.18 (m, 2H), 2.99 (m, 2H), 2.73 (m, 2H), 1.91 (m, 4H), 1.74 (t, J = 7.5 Hz, 2H), 1.31 (m, 4H), 1.17 (m, 2H). ^{13}C NMR (126 MHz, Methanol-d_4) δ 169.87, 158.54, 157.06, 150.60, 138.05, 134.41, 128.36, 125.51, 122.67, 121.76, 120.08, 119.23, 118.60, 112.78, 112.48, 108.09, 104.93, 56.68, 55.20, 53.83, 40.44, 31.81, 29.73, 29.23, 28.82, 27.38, 27.31, 25.67, 23.15, 21.85, 21.66. HRMS $[M + H]^+$: 514.3176 (calculated for $[C_{31}H_{40}N_5O_2]^+$: 514.3177).

*14.1.5.29. N-(2-(7-methoxy-1,2,3,4-tetrahydroacridin-9-ylamino) heptyl-2-amino-3-(1H-indole-3-yl)propylamide dihydrochloride (**SK1029**).* Yield 85%; mp 125.1–128.9 °C. Purity: 96%. ^{1}H NMR (500 MHz, DMSO-d_6) δ 11.11 (d, J = 2.5 Hz, 1H), 8.61 (s, 1H), 8.30 (d, J = 5.3 Hz, 3H), 7.98 (d, J = 9.2 Hz, 1H), 7.81 (d, J = 2.5 Hz, 1H), 7.63 (d, J = 7.9 Hz, 1H), 7.50 (dd, J = 9.2, 2.5 Hz, 1H), 7.33 (d, J = 8.1 Hz, 1H), 7.20 (d, J = 2.4 Hz, 1H), 6.99 (m, 2H), 3.92 (s, 3H), 3.78 (m, 2H), 3.18 (m, 2H), 3.01 (m, 3H), 2.69 (m, 3H), 1.78 (m, 5H), 1.67 (m, 2H), 1.22 (m, 6H), 1.12 (m, 2H). ^{13}C NMR (126 MHz, DMSO-d_6) δ 168.24, 156.66, 154.92, 149.78, 136.35, 132.74, 127.31, 124.85, 123.95, 121.14, 120.98, 118.70, 118.46, 117.46, 111.54, 110.97, 107.25, 103.90, 56.31,

53.05, 46.63, 38.84, 30.50, 28.69, 28.47, 28.01, 27.43, 26.32, 26.17, 24.95, 21.92, 20.47. HRMS [M + H]$^+$: 528.3335 (calculated for [$C_{32}H_{42}N_5O_2$]$^+$: 528.3334).

*14.1.5.30. N-(2-(7-methoxy-1,2,3,4-tetrahydroacridin-9-ylamino) octyl-2-amino-3-(1H-indole-3-yl)propylamide dihydrochloride (**S-K1030**).* Yield 79%; mp 163.5–166.2 °C. Purity: 97%. ^{1}H NMR (500 MHz, Methanol-d_4) δ 7.75 (d, J = 9.2 Hz, 1H), 7.65 (d, J = 2.4 Hz, 1H), 7.60 (d, J = 7.9 Hz, 1H), 7.49 (m, 1H), 7.33 (d, J = 8.1 Hz, 1H), 7.19 (s, 1H), 7.03 (m, 2H), 4.06 (t, J = 7.5 Hz, 1H), 3.95 (s, 3H), 3.89 (t, J = 7.2 Hz, 2H), 3.18 (m, 2H), 3.00 (m, 4H), 2.73 (m, 2H), 1.92 (m, 4H), 1.79 (m, 2H), 1.39 (m, 2H), 1.25 (m, 8H). ^{13}C NMR (126 MHz, Methanol-d_4) δ 169.85, 158.55, 157.14, 150.61, 138.08, 134.47, 128.37, 125.52, 125.37, 122.71, 121.79, 120.14, 119.21, 118.61, 112.83, 112.51, 108.10, 104.98, 58.31, 56.64, 55.23, 40.62, 31.94, 30.14, 30.11, 29.82, 29.24, 28.84, 27.67, 25.62, 23.15, 21.87, 21.35. HRMS [M + H]$^+$: 542.3483 (calculated for [$C_{33}H_{44}N_5O_2$]$^+$: 542.3490).

*14.1.5.31. N-(2-(6-chloro-1,2,3,4-tetrahydroacridin-9-ylamino)ethyl-2-amino-3-(1H-indole-3-yl)propylamide dihydrochloride (**S-K1031**).* Yield 56%; mp 65.1–68.5 °C. Purity: 97%. ^{1}H NMR (300 MHz, D_2O) δ 7.63 (d, J = 9.4 Hz, 1H), 7.35 (d, J = 2.1 Hz, 1H), 7.14 (m, 3H), 6.72 (d, J = 7.9 Hz, 1H), 6.26 (m, 1H), 3.51 (m, 2H), 3.29 (m, 2H), 2.67 (dt, J = 7.9, 4.1 Hz, 2H), 2.01 (m, 6H), 1.67 (m, 2H). ^{13}C NMR (75 MHz, D_2O) δ 171.34, 154.92, 150.15, 138.59, 138.43, 135.68, 127.25, 126.83, 125.54, 121.66, 119.30, 117.90, 117.77, 113.93, 111.98, 111.28, 105.97, 53.73, 39.50, 30.83, 30.20, 28.23, 26.55, 23.06, 21.77. HRMS [M + H]$^+$: 462.2052 (calculated for [$C_{26}H_{29}ClN_5O$]$^+$: 462.2056).

*14.1.5.32. N-(2-(6-chloro-1,2,3,4-tetrahydroacridin-9-ylamino)propyl-2-amino-3-(1H-indole-3-yl)propylamide dihydrochloride (**S-K1032**).* Yield 53%; mp 82.2–85.3 °C. Purity: 98%. ^{1}H NMR (500 MHz, D_2O) δ 7.56 (d, J = 9.3 Hz, 1H), 7.32 (d, J = 2.1 Hz, 1H), 7.18 (m, 3H), 6.83 (d, J = 8.0 Hz, 1H), 6.62 (m, 2H), 4.13 (m, 1H), 3.17 (m, 2H), 3.11 (m, 2H), 2.74 (m, 2H), 2.22 (m, 4H), 1.81 (m, 4H), 1.41 (m, 2H). ^{13}C NMR (126 MHz, D_2O) δ 169.05, 154.72, 149.89, 137.89, 135.32, 126.42, 124.95, 124.50, 124.46, 121.18, 121.06, 118.62, 117.57, 117.30, 112.87, 111.51, 110.91, 106.10, 53.90, 44.63, 36.37, 30.23, 28.68, 27.66, 26.53, 22.85, 21.02. HRMS [M + H]$^+$: 476.2210 (calculated for [$C_{27}H_{31}ClN_5O$]$^+$: 476.2212).

*14.1.5.33. N-(2-(6-chloro-1,2,3,4-tetrahydroacridin-9-ylamino)butyl-2-amino-3-(1H-indole-3-yl)propylamide dihydrochloride (**S-K1033**).* Yield 83%; mp 88.5–91.7 °C. Purity: 97%. ^{1}H NMR (500 MHz, DMSO-d_6) δ 11.09 (d, J = 2.3 Hz, 1H), 8.75 (t, J = 5.6 Hz, 1H), 8.44 (d, J = 9.3 Hz, 1H), 8.30 (d, J = 5.5 Hz, 3H), 8.11 (d, J = 2.2 Hz, 1H), 8.01 (s, 1H), 7.63 (d, J = 7.9 Hz, 1H), 7.56 (dd, J = 9.3, 2.2 Hz, 1H), 7.30 (m, 1H), 7.21 (d, J = 2.3 Hz, 1H), 7.01 (dd, J = 8.2, 6.9 Hz, 1H), 6.93 (m, 1H), 3.94 (m, 1H), 3.77 (m, 2H), 3.12 (m, 3H), 3.00 (m, 1H), 2.98 (m, 2H), 2.49 (m, 2H), 1.79 (m, 4H), 1.62 (m, 2H), 1.37 (m, 2H). ^{13}C NMR (126 MHz, DMSO-d_6) δ 168.38, 155.55, 151.21, 138.80, 137.09, 136.33, 127.84, 127.26, 125.38, 124.87, 121.13, 118.69, 118.46, 118.03, 114.30, 111.70, 111.50, 107.23, 53.06, 46.89, 38.32, 34.19, 28.07, 27.43, 25.88, 24.21, 22.67, 21.54. HRMS [M + H]$^+$: 490.2367 (calculated for [$C_{28}H_{33}ClN_5O$]$^+$: 490.2369).

*14.1.5.34. N-(2-(6-chloro-1,2,3,4-tetrahydroacridin-9-ylamino)pentyl-2-amino-3-(1H-indole-3-yl)propylamide dihydrochloride (**S-K1034**).* Yield 74%; mp 83.4–87.8 °C. Purity: 98%. ^{1}H NMR (500 MHz, DMSO-d_6) δ 11.12 (d, J = 2.4 Hz, 1H), 8.69 (t, J = 5.6 Hz, 1H), 8.45 (d, J = 9.3 Hz, 1H), 8.31 (d, J = 5.5 Hz, 3H), 8.12 (d, J = 2.2 Hz, 1H), 8.05 (s, 1H), 7.63 (d, J = 7.9 Hz, 1H), 7.56 (dd, J = 9.2, 2.2 Hz, 1H), 7.44 (m, 1H), 7.30 (m, 2H), 7.20 (d, J = 2.4 Hz, 1H), 6.97 (m, 2H), 3.94 (m, 1H), 3.78 (m, 2H), 3.13 (m, 3H), 2.98 (m, 3H), 2.63 (m, 2H), 1.78 (m, 4H), 1.67 (m, 2H), 1.33 (m, 2H), 1.22 (m, 2H). ^{13}C NMR (126 MHz, DMSO-d_6) δ 168.31, 155.53, 151.40, 138.86, 137.10, 136.36, 127.89, 127.30, 125.39, 124.87, 121.15, 118.73, 118.49, 118.05, 114.27, 111.67, 111.55, 107.26, 56.21, 53.06, 47.26, 34.21, 29.54, 28.36, 28.07, 27.46, 23.54, 21.54, 20.35. HRMS [M + H]$^+$: 504.2524 (calculated for [$C_{29}H_{35}ClN_5O$]$^+$: 504.2525).

*14.1.5.35. N-(2-(6-chloro-1,2,3,4-tetrahydroacridin-9-ylamino)hexyl-2-amino-3-(1H-indole-3-yl)propylamide dihydrochloride (**S-K1035**).* Yield 75%; mp 141.1–143.5 °C. Purity: 99.9%. ^{1}H NMR (500 MHz, DMSO-d_6) δ 11.12 (d, J = 2.5 Hz, 1H), 8.65 (t, J = 5.6 Hz, 1H), 8.46 (d, J = 9.2 Hz, 1H), 8.32 (d, J = 5.5 Hz, 3H), 8.15 (d, J = 2.2 Hz, 1H), 7.62 (d, J = 7.9 Hz, 1H), 7.55 (dd, J = 9.2, 2.2 Hz, 1H), 7.20 (d, J = 2.4 Hz, 1H), 6.97 (m, 2H), 3.95 (m, 1H), 3.80 (m, 2H), 3.17 (t, J = 6.3 Hz, 2H), 2.99 (m, 4H), 2.63 (m, 2H), 1.79 (m, 4H), 1.66 (m, 2H), 1.22 (m, 6H). ^{13}C NMR (126 MHz, DMSO-d_6) δ 168.23, 155.49, 151.17, 138.82, 137.04, 136.32, 127.80, 127.29, 125.33, 124.79, 121.09, 118.68, 118.43, 118.02, 114.29, 111.62, 111.50, 107.24, 56.16, 53.03, 47.16, 29.78, 28.63, 28.05, 27.38, 25.97, 25.87, 24.20, 22.66, 21.53, 20.34. HRMS [M + H]$^+$: 518.2681 (calculated for [$C_{30}H_{37}ClN_5O$]$^+$: 518.2682).

*14.1.5.36. N-(2-(6-chloro-1,2,3,4-tetrahydroacridin-9-ylamino)heptyl-2-amino-3-(1H-indole-3-yl)propylamide dihydrochloride (**S-K1036**).* Yield 84%; mp 121.8–125.9 °C. Purity: 96%. ^{1}H NMR (500 MHz, DMSO-d_6) δ 10.82 (d, J = 2.3 Hz, 1H), 8.39 (d, J = 9.3 Hz, 1H), 8.01 (d, J = 2.2 Hz, 1H), 7.89 (s, 1H), 7.82 (t, J = 5.7 Hz, 1H), 7.55 (m, 2H), 7.29 (d, J = 8.1 Hz, 1H), 7.08 (d, J = 2.3 Hz, 1H), 6.97 (m, 2H), 6.68 (d, J = 8.2 Hz, 1H), 4.12 (m, 1H), 3,81 (m, 2H), 3.67 (m, 2H), 3.00 (m, 4H), 2.60 (m, 2H), 1.79 (m, 4H), 1.70 (m, 2H), 1.28 (s, 8H). ^{13}C NMR (126 MHz, DMSO-d_6) δ 171.87, 155.58, 155.25, 151.10, 138.80, 137.18, 136.17, 127.74, 125.34, 123.70, 120.88, 118.58, 118.20, 114.20, 111.66, 111.37, 110.36, 78.04, 55.39, 48.75, 47.43, 29.81, 29.02, 28.44, 26.24, 26.17, 23.97, 22.66, 21.46, 20.34. HRMS [M + H]$^+$: 532.2829 (calculated for [$C_{31}H_{39}ClN_5O$]$^+$: 532.2838).

*14.1.5.37. N-(2-(6-chloro-1,2,3,4-tetrahydroacridin-9-ylamino)octyl-2-amino-3-(1H-indole-3-yl)propylamide dihydrochloride (**S-K1037**).* Yield 76%; mp 151.9–154.3 °C. Purity: 95%. ^{1}H NMR (500 MHz, Methanol-d_4) δ 8.36 (d, J = 9.2 Hz, 1H), 7.82 (d, J = 2.2 Hz, 1H), 7.59 (d, J = 7.9 Hz, 1H), 7.51 (m, 2H), 7.32 (m, 1H), 7.01 (m, 2H), 4.08 (t, J = 7.3 Hz, 1H), 3.91 (t, J = 7.3 Hz, 2H), 3.18 (m, 2H), 2.99 (m, 3H), 2.66 (m, 3H), 1.93 (m, 4H), 1.81 (m, 2H), 1.40 (m, 2H), 1.27 (m, 6H), 1.13 (m, 2H). 13C NMR (126 MHz, DMSO-d_6) δ 168.28, 155.62, 151.21, 138.89, 137.15, 136.39, 127.84, 127.34, 125.38, 124.89, 121.20, 118.72, 118.51, 118.10, 114.34, 111.71, 111.57, 107.28, 67.19, 53.10, 47.41, 34.36, 31.52, 29.88, 28.76, 28.11, 27.48, 27.06, 24.17, 22.46, 21.57, 20.40. HRMS [M + H]$^+$: 546.2991 (calculated for [$C_{32}H_{41}ClN_5O$]$^+$: 546.2995).

*14.1.5.38. N-(2-(1,2,3,4-tetrahydroacridin-9-ylamino)ethyl-2-amino-3-(1H-indole-3-yl)propylamide dihydrochloride (**S-K1038**).* Yield 87%; mp 192.4–195.3 °C. Purity: 96%. ^{1}H NMR (300 MHz, DMSO-d_6) δ 14.25 (s, 1H), 11.06 (d, J = 2.5 Hz, 1H), 9.36 (t, J = 5.6 Hz, 1H), 8.44 (d, J = 9.2 Hz, 2H), 8.02 (dd, J = 8.6, 1.2 Hz, 1H), 7.83 (m, 2H), 7.55 (m, 2H), 7.23 (m, 2H), 6.90 (m, 2H), 4.26 (m, 2H), 3.99 (m, 1H), 3.85 (m, 2H), 3.13 (m, 2H), 2.98 (m, 2H), 2.59 (m, 2H), 1.78 (m, 4H). 13C NMR (75 MHz, DMSO-d_6) δ 169.65, 155.74, 150.68, 138.05, 136.28, 132.65, 127.22, 125.42, 125.20, 124.92, 121.12, 119.26, 118.60, 118.46, 115.64, 111.48, 111.42, 107.05, 56.19, 53.04, 46.96, 34.17, 28.07, 27.14, 24.09, 21.66. HRMS [M + H]$^+$: 428.2442 (calculated for [$C_{26}H_{30}N_5O$]$^+$: 428.2445).

*14.1.5.39. N-(2-(1,2,3,4-tetrahydroacridin-9-ylamino)propyl-2-amino-3-(1H-indole-3-yl)propylamide dihydrochloride (**S-K1039**).* Yield 92%; mp 148.8–152.0 °C. Purity: 99.9%. ^{1}H NMR (500 MHz,

Methanol-d_4) δ 8.28 (d, J = 8.7 Hz, 1H), 7.81 (d, J = 4.0 Hz, 2H), 7.54 (m, 2H), 7.23 (d, J = 8.0 Hz, 1H), 7.10 (s, 1H), 6.94 (m, 2H), 4.28 (m, 1H), 3.18 (m, 2H), 3.02 (m, 2H), 2.68 (m, 2H), 1.94 (m, 8H), 1.80 (m, 2H). ^{13}C NMR (126 MHz, Methanol-d_4) δ 175.48, 157.91, 151.69, 139.64, 137.92, 133.98, 128.76, 126.44, 126.36, 124.68, 122.30, 120.12, 119.69, 119.40, 117.05, 112.95, 112.26, 110.85, 57.42, 45.69, 37.07, 31.27, 29.36, 28.64, 25.02, 23.01, 21.83. HRMS [M + H]$^+$: 442.2597 (calculated for $[C_{27}H_{32}N_5O]^+$: 442.2602).

*14.1.5.40. N-(2-(1,2,3,4-tetrahydroacridin-9-ylamino)butyl-2-amino-3-(1H-indole-3-yl)propylamide dihydrochloride (**S-K1040**).* Yield 53%; mp 76.3–81.0 °C. Purity: 98%. ^{1}H NMR (500 MHz, DMSO-d_6) δ 10.78 (d, J = 2.4 Hz, 1H), 8.10 (d, J = 8.8 Hz, 1H), 7.83 (t, J = 5.7 Hz, 1H), 7.69 (dd, J = 8.3, 1.2 Hz, 1H), 7.55 (d, J = 7.9 Hz, 1H), 7.50 (ddd, J = 8.2, 6.7, 1.2 Hz, 1H), 7.32 (m, 2H), 7.10 (d, J = 2.3 Hz, 1H), 6.99 (m, 2H), 6.67 (d, J = 8.3 Hz, 1H), 4.12 (m, 1H), 3.02 (m, 2H), 2.88 (m, 2H), 2.70 (m, 2H), 1.79 (m, 4H), 1.50 (m, 2H), 1.38 (m, 2H), 1.29 (m, 4H). ^{13}C NMR (126 MHz, DMSO-d_6) δ 171.92, 157.91, 155.26, 150.51, 146.89, 136.19, 128.25, 127.52, 123.74, 123.40, 123.23, 120.93, 120.31, 118.65, 118.25, 115.87, 111.37, 110.42, 78.05, 55.34, 47.83, 38.43, 33.57, 28.30, 26.64, 25.22, 22.90, 22.57. HRMS [M + H]$^+$: 456.2747 (calculated for $[C_{28}H_{34}N_5O]^+$: 456.2758).

*14.1.5.41. N-(2-(1,2,3,4-tetrahydroacridin-9-ylamino)pentyl-2-amino-3-(1H-indole-3-yl)propylamide dihydrochloride (**S-K1041**).* Yield 83%; mp 118.5–121.1 °C. Purity: 95%. ^{1}H NMR (300 MHz, D_2O) δ (ppm) 7.73 (d, J = 8.6 Hz, 1H), 7.60 (m, 1H), 7.27 (m, 2H), 7.14 (m, 1H), 7.04 (m, 2H), 6.69 (m, 2H), 4.08 (m, 1H), 3.65 (m, 2H), 3.37 (m, 2H), 3.03 (m, 2H), 2.44 (m, 2H), 2.22 (m, 4H), 1.65 (m, 4H), 1.41 (m, 2H), 0.95 (m, 2H). ^{13}C NMR (75 MHz, D_2O) δ 168.82, 154.52, 148.87, 136.93, 135.46, 132.25, 126.23, 124.58, 124.51, 124.38, 121.14, 118.60, 118.18, 117.53, 114.21, 111.05, 110.34, 105.77, 57.28, 53.42, 46.97, 39.06, 30.10, 29.26, 27.11, 26.77, 22.93, 20.92, 19.80. HRMS [M + H]$^+$: 470.2910 (calculated for $[C_{29}H_{36}N_5O]^+$: 470.2915).

*14.1.5.42. N-(2-(1,2,3,4-tetrahydroacridin-9-ylamino)hexyl-2-amino-3-(1H-indole-3-yl)propylamide dihydrochloride (**S-K1042**).* Yield 63%; mp 148.7–150.8 °C. Purity: 97%. ^{1}H NMR (300 MHz, Methanol-d_4) δ 8.36 (d, J = 8.7 Hz, 1H), 7.80 (m, 2H), 7.58 (m, 2H), 7.32 (m, 1H), 7.19 (s, 1H), 7.00 (m, 2H), 4.09 (m, 1H), 3.90 (t, J = 7.3 Hz, 2H), 3.30 (m, 2H), 2.99 (m, 2H), 2.68 (m, 2H), 2.16 (m, 4H), 1.93 (m, 4H), 1.76 (m, 2H), 1.31 (m, 4H). ^{13}C NMR (75 MHz, Methanol-d_4) δ 169.86, 157.77, 151.51, 139.63, 138.02, 133.97, 128.37, 126.48, 126.30, 125.53, 122.64, 120.09, 120.06, 119.27, 116.94, 112.71, 112.47, 108.08, 58.30, 55.18, 40.40, 31.33, 29.69, 27.28, 27.23, 24.97, 22.95, 21.80, 20.82, 20.79. HRMS [M + H]$^+$: 484.3066 (calculated for $[C_{30}H_{38}N_5O]^+$: 484.3017).

*14.1.5.43. N-(2-(1,2,3,4-tetrahydroacridin-9-ylamino)heptyl-2-amino-3-(1H-indole-3-yl)propylamide dihydrochloride (**S-K1043**).* Yield 38%; mp 148.7–150.8 °C. Purity: 98%. ^{1}H NMR (500 MHz, D_2O) δ 7.78 (m, 1H), 7.55 (m, 1H), 7.24 (m, 2H), 7.11 (m, 2H), 6.94 (m, 1H), 6.76 (m, 2H), 3.96 (m, 1H), 3.50 (m, 2H), 2.95 (m, 2H), 2.49 (m, 2H), 2.11 (m, 2H), 1.63 (m, 4H), 1.55 (m, 2H), 1.19 (m, 2H), 1.08 (m, 8H). ^{13}C NMR (126 MHz, D_2O) δ 169.03, 157.77, 155.03, 149.12, 137.35, 135.75, 132.42, 126.25, 124.69, 124.54, 121.57, 118.93, 118.48, 117.55, 114.48, 111.41, 110.68, 105.89, 57.40, 53.55, 47.31, 39.30, 29.45, 27.56, 27.45, 27.04, 25.43, 25.40, 22.79, 21.11, 20.04. HRMS [M + H]$^+$: 498.3225 (calculated for $[C_{31}H_{40}N_5O]^+$: 498.3228).

*14.1.5.44. N-(2-(1,2,3,4-tetrahydroacridin-9-ylamino)octyl-2-amino-3-(1H-indole-3-yl)propylamide dihydrochloride (**S-K1044**).* Yield 83%. Purity: 95%. ^{1}H NMR (500 MHz, DMSO-d_6) δ 14.20 (s, 1H), 11.09 (s, 1H), 8.43 (d, J = 8.6 Hz, 1H), 8.03 (d, J = 8.4 Hz, 1H), 7.83 (m, 1H), 7.58 (m, 2H), 7.32 (d, J = 8.1 Hz, 1H), 7.21 (s, 1H), 6.99 (m, 2H), 3.94 (m, 1H), 3.83 (m, 2H), 3.17 (m, 2H), 3.02 (m, 2H), 2.66 (m, 2H), 1.81 (m, 4H), 1.70 (m, 2H), 1.20 (m, 10H). ^{13}C NMR (126 MHz, DMSO-d_6) δ 168.23, 155.80, 150.76, 138.06, 136.35, 132.69, 127.33, 125.25, 125.17, 124.86, 121.14, 119.30, 118.69, 118.47, 115.73, 111.54, 111.21, 107.26, 53.06, 52.57, 47.30, 36.65, 34.22, 29.99, 28.78, 28.72, 28.67, 28.07, 27.42, 26.36, 24.25, 21.67. HRMS [M + H]$^+$: 512.3378 (calculated for $[C_{32}H_{42}N_5O]^+$: 512.3384).

*14.1.5.45. N-(2-(6-chloro-1,2,3,4-tetrahydroacridin-9-ylamino)hexyl-2-amino-3-(1H-indole-3-yl)propylamide dihydrochloride (**R-K1035**).* Yield 90%; mp 257.2–260.5 °C. Purity: 95%. ^{1}H NMR (500 MHz, Methanol-d_4) δ 8.37 (d, J = 9.2 Hz, 1H), 7.77 (d, J = 2.1 Hz, 1H), 7.59 (d, J = 7.9 Hz, 1H), 7.54 (dd, J = 9.2, 2.1 Hz, 1H), 7.34 (d, J = 8.1 Hz, 1H), 7.20 (s, 1H), 7.03 (m, 2H), 4.08 (t, J = 7.3 Hz, 1H), 3.91 (t, J = 7.3 Hz, 2H), 3.32 (m, 2H), 3.21 (m, 2H), 2.98 (t, J = 5.9 Hz, 2H), 2.66 (m, 2H), 1.94 (m, 6H), 1.79 (m, 2H), 1.36 (m, 4H). ^{13}C NMR (126 MHz, Methanol-d_4) δ 169.87, 157.65, 152.00, 140.41, 140.00, 138.08, 128.72, 128.34, 126.75, 125.49, 122.71, 120.11, 119.19, 119.11, 115.36, 113.24, 112.49, 108.09, 58.31, 55.20, 40.43, 31.18, 29.74, 29.30, 28.87, 27.32, 27.25, 24.77, 22.84, 21.73. HRMS [M + H]$^+$: 518.2681 (calculated for $[C_{30}H_{37}ClN_5O]^+$: 518.2683).

*14.1.5.46. N-(2-(6-chloro-1,2,3,4-tetrahydroacridin-9-ylamino)hexyl-2-amino-3-(1H-indole-3-yl)propylamide dihydrochloride (**rac-K1035**).* Yield 97%; mp 227.3–229.9 °C. Purity: 99%. ^{1}H NMR (500 MHz, Methanol-d_4) δ 8.36 (d, J = 9.2 Hz, 1H), 7.77 (d, J = 2.0 Hz, 1H), 7.59 (dt, J = 7.9, 0.9 Hz, 1H), 7.54 (dd, J = 9.2, 2.1 Hz, 1H), 7.34 (dt, J = 8.1, 0.8 Hz, 1H), 7.20 (s, 1H), 7.03 (m, 2H), 4.08 (t, J = 7.3 Hz, 1H), 3.90 (t, J = 7.3 Hz, 2H), 3.32 (m, 2H), 3.21 (ddd, J = 17.1, 14.0, 7.1 Hz, 2H), 2.98 (t, J = 6.0 Hz, 2H), 2.67 (t, J = 5.9 Hz, 3H), 1.95 (m, 6H), 1.79 (m, 2H), 1.36 (m, 4H). ^{13}C NMR (126 MHz, Methanol-d_4) δ 169.86, 157.62, 151.98, 140.38, 139.97, 138.07, 128.71, 128.33, 126.73, 125.49, 122.70, 120.10, 119.19, 119.10, 115.35, 113.23, 112.48, 108.08, 58.30, 55.19, 40.43, 31.18, 29.73, 29.30, 28.86, 27.31, 27.24, 24.77, 22.83, 21.72. HRMS [M + H]$^+$: 518.2681 (calculated for $[C_{30}H_{37}ClN_5O]^+$: 518.2685).

15. Inhibition of human AChE and BChE

The AChE and BChE inhibitory activities of the tested compounds were determined using modified Ellman's method [62]. Human recombinant acetylcholinesterase (*h*AChE; EC 3.1.1.7), human plasmatic butyrylcholinesterase (*h*BChE; EC 3.1.1.8), 5,5′-dithiobis(2-nitrobenzoic acid) (Ellman's reagent, DTNB), phosphate buffer solution (PBS, pH 7.4), acetylthiocholine (ATCh), and butyrylthiocholine (BTCh) were purchased from Sigma-Aldrich (Prague, Czech Republic). For measuring purposes – polystyrene Nunc 96-well microplates with flat bottom shape (ThermoFisher Scientific, USA) were utilized. All of the assays were carried out in 0.1 M KH_2PO_4/K_2HPO_4 buffer, pH 7.4. Enzyme solutions were prepared at an activity 2.0 units·mL^{-1} in 2 mL aliquots. The assay medium (100 μL) consisted of 40 μL of 0.1 M PBS (pH 7.4), 20 μL of 0.01 M DTNB, 10 μL of enzyme, and 20 μL of 0.01 M substrate (ATCh or BTCh iodide solution). Assayed solutions with inhibitors (10 μL, 10^{-3} – 10^{-9} M) were preincubated with *h*AChE or *h*BChE for 5 min. The reaction was started by addition of 20 μL of substrate. The enzyme activity was determined by measuring the increase in absorbance at 412 nm at 37 °C in 2 min intervals using a Multimode microplate reader Synergy 2 (Vermont, USA). Each concentration was assayed in triplicate. The obtained data were used to compute the percentage of inhibition (I; Equation (1)):

$$I = \left(1 - \frac{\Delta A_i}{\Delta A_0}\right) \times 100 \quad [\%] \tag{1}$$

ΔA_i indicates absorbance change provided by the cholinesterase exposed to AChE inhibitors. ΔA_0 indicates absorbance change caused by the intact cholinesterase (phosphate buffer was used instead of the AChE inhibitor solution). Inhibition potency of tested compounds was expressed as the IC_{50} value (the concentration of inhibitor, which causes 50% cholinesterase inhibition). All calculations were performed using Microsoft Excel software (Redmont, WA, USA) and GraphPad Prism version 5.02 for Windows (GraphPad Software, San Diego, CA) (www.graphpad.com).

15.1. Propidium displacement studies

The affinity of selected inhibitors for the peripheral binding site of *Ee*AChE (type VI-S, Sigma-Aldrich, Milano, Italy) was tested using propidium iodide (P) (Sigma-Aldrich, Milano, Italy), a known specific PAS ligand, following the method proposed by Taylor et al. [72,73]. The complexation of propidium iodide and AChE [72] determines a shift in the excitation wavelength [72]. A stock solution (4 mM) of ***S*-K1035** was prepared in methanol. *Ee*AChE (2 μM) was first incubated with 8 μM propidium iodide in 1 mM Tris-HCl, pH 8.0. In the back titration experiments of the propidium-AChE complex by ***S*-K1035**, aliquots of the inhibitor (8–56 μM) were added gradually and fluorescence emission was monitored at 635 nm upon excitation at 535 nm. Blanks containing propidium alone, inhibitor plus propidium and *Ee*AChE alone were prepared and fluorescence emission was determined. Experiments were carried out at room temperature using a Jasco 6200 spectrofluorometer (Cremella, Italy) and a 0.5 mL quartz cuvette. Raw data were processed following the method by Taylor and Lappi [73] to estimate K_D values assuming a dissociation constant value for propidium for *Ee*AChE equals to 0.7 μM [74].

15.2. Inhibition of AChE-induced $A\beta_{40}$ aggregation [90].

$A\beta_{40}$, supplied as trifluoroacetate salt, was purchased from Bachem AG (Bubendorf, Switzerland). $A\beta_{40}$ (2 mg mL^{-1}) was dissolved in 1,1,1,3,3,3-hexafluoro-2-propanol (HFIP) and lyophilized and redissolved in DMSO to achieve a concentration of 2.3 mM. Stock solutions of tested inhibitors were prepared in methanol (1.5–2 mM) and diluted in the assay buffer. Aliquots of 2 μL $A\beta_{40}$ peptide in DMSO were incubated in 0.215 M sodium phosphate buffer (pH 8.0) at a final concentration of 230 μM for 24 h. For co-incubation experiments aliquots (16 μL) of *h*AChE (final concentration of 2.30 μM, $A\beta$/AChE molar ratio 100:1) and AChE in the presence of 2 μL of the tested inhibitor (final inhibitor concentration of 100 μM) in 0.215 M sodium phosphate buffer solution (pH 8.0) were added. Blanks containing $A\beta_{40}$ alone, *h*AChE alone, and $A\beta_{40}$ plus tested inhibitors in 0.215 M sodium phosphate buffer (pH 8.0) were prepared. The final volume of each vial was 20 μL. Each assay was run in duplicate. To quantify amyloid fibril formation, the thioflavin T fluorescence method was then applied [108]. Due to β-sheet conformation, the fluorescence intensities were monitored for 300 s at $\lambda_{em} = 490$ nm ($\lambda_{exc} = 446$ nm). We calculate the percentage of inhibition of the AChE-induced aggregation due to the presence of tested compound.

15.3. Inhibition of $A\beta_{42}$ self-aggregation

As reported in a previously published protocol [88], HFIP pretreated $A\beta_{42}$ samples (Bachem AG) were first solubilized with a CH_3CN/0.3 mM Na_2CO_3/250 mM NaOH (48.4:48.4:3.2) mixture to obtain a 500 μM solution. Experiments were performed by incubating the peptide in 10 mM phosphate buffer (pH = 8.0) containing 10 mM NaCl, at 30 °C for 24 h (final $A\beta$ concentration 50 μM) with and without inhibitor (50 μM, $A\beta$/inhibitor = 1/1). Blanks containing the tested inhibitors were also prepared and measured. To quantify amyloid fibrils formation, the thioflavin T fluorescence method was used [108]. After incubation, samples were diluted to a final volume of 2.0 mL with 50 mM glycine–NaOH buffer (pH 8.5) containing 1.5 μM thioflavin T. A 300-second-time scan of fluorescence intensity was carried out ($\lambda_{exc} = 446$ nm; $\lambda_{em} = 490$ nm, FP-6200 fluorometer, Jasco Europe), and values at plateau were averaged after subtracting the background fluorescence of 1.5 μM thioflavin T solution. The fluorescence intensities were compared and the percentual inhibition due to the presence of the inhibitor was calculated by the following formula: $100 - (IF_i/IF_o \times 100)$ where IF_i and IF_o are the fluorescence intensities obtained for $A\beta_{42}$ in the presence and absence of inhibitor, respectively.

16. Determination of *in vitro* blood-brain barrier permeation

The parallel artificial membrane permeation assay (PAMPA) was used based on the reported protocol [95,96]. The filter membrane of the donor plate was coated with polar brain lipid (PBL, Avanti Polar Lipids, Ins., USA) in dodecane (4 μL of 20 mg mL^{-1} PBL in dodecane) and the acceptor well was filled with 300 μL of the PBS buffer (V_A; pH = 7.4)). Tested compounds were dissolved first in DMSO and the resulting solution was subsequently mixed with PBS (pH = 7.4) to reach the final concentration of 100 μM in the donor well. Concentration of DMSO did not exceed 0.5% (V/V) in the donor solution. A volume of 300 μL of the donor solution was added to the donor wells (V_D) and the donor filter plate was carefully put on the acceptor plate so that coated membrane was "in touch" with both the donor solution and the acceptor buffer. The test compound diffused from the donor well through the lipid membrane (area = 0.28 cm^2) to the acceptor well. The concentration of the drug in both the donor and the acceptor wells was assessed after 3, 4, 5 and 6 h of incubation in quadruplicate using the UV plate reader Synergy HT (Biotek, Vermont, USA) at the maximum absorption wavelength of each compound. The concentration of the compounds was calculated from the standard curve and expressed as permeability (P_e) according equation (2) [97,109]:

$$\log P_e = \log\left\{C \times -ln\left(1 - \frac{[drug]_{acceptor}}{[drug]_{equilibrium}}\right)\right\} \text{ where } C = \left(\frac{V_D \times V_A}{(V_D + V_A) \times Area \times time}\right) \tag{2}$$

where, $[drug]_{acceptor}$ is the concentration of the drug in the acceptor compartment in the certain time and $[drug]_{equilibrium}$ is the concentration of the drug in theoretical equilibrium i.e. after dilution of the drug between donor and acceptor compartment.

17. In vitro effects of compounds on the activity of nitric oxide synthase

All evaluated compounds were dissolved in redistilled water. Compounds ***S*-K1024**, ***S*-K1040**, ***S*-K1044** were also sonicated. Basic 1 mM stock solutions were stored at 8 °C for no longer than one month. Estimations of the activity of nitric oxide synthase (nNOS) were performed on purified cortical homogenates from a total of 5 male Wistar rats aged 3–5 months. A mixture of the cortexes was homogenized (1:10) in homogenisation buffer (1 mM EGTA, 1 mM dithiothreitol, 20 mM HEPES, 0.32 M sucrose, 14.6 μM pepstatin, 21 μM leupeptin, pH = 7.4), centrifuged at 1200 g for 10 min at 4 °C,

and the resulting aliquots of supernatants (2 mg mL^{-1} of proteins) were stored at −20 °C until assayed. Compounds (final concentrations in the incubation mixtures equaled 46 nM–68 μM) and supernatants were added to the reaction buffer (homogenisation buffer containing also 200 μM ß-nicotinamide adenine dinucleotide phosphate, 50 μM tetrahydrobiopterin and 2.3 μM [14C]arginine (PerkinElmer, USA) and incubated for 30 min at 37 °C. All samples contained also 1 μM $CaCl_2$ and some of them 1 mM spermidine (Merck, Prague, Czech Republic). The reaction was terminated by adding a stop buffer (30 mM HEPES, 3 mM EDTA, pH = 5.5) and by rapid cooling. DOWEX 50WX8-200 (Sigma-Aldrich) was used to separate citrulline from arginine, in accordance with our previous study [110].

18. *In vivo* studies

18.1. Animals

Male Wistar rats (10–12 week old) were obtained from Velaz (Prague, Czech Republic) and housed in groups of 4–6 in an accredited animal facility. Animals were kept in a controlled holding environment with a 12 h day-night cycle, access to standard rodent diet (Cerea Corp., Czech Republic) and water *ad libitum*. The time of acclimatization was at least 14 days prior to all experimental procedures. The use of animals was approved by the Ethics Committee of the Faculty of Military Health Sciences (Hradec Kralove, Czech Republic). All procedures involving animals were in accordance with contemporary legislation.

18.2. Assessment of maximum tolerated dose

The acute toxicity of ***S*-K1035** was evaluated by the assessment of MTD ($mg \cdot kg^{-1}$). Male Wistar Rats (body weight 313–370 g) were randomly assigned to experimental groups consisting of two males per one applied dose of ***S*-K1035**. Several doses were administered to identify MTD, the starting dose being 50 mg kg^{-1}. ***S*-K1035** was administered *via* i.p. injection in standardized volume of 1 mL kg^{-1}.

Treated rats were extensively observed for signs of toxicity during first two hours; then periodically for 48 h. Clinical signs, such as cardiovascular, respiratory and nervous system disability, weight loss or reduction of food consumption were monitoring according to Laboratory Animal Science Association (UK) guidelines. Severity of symptoms was classified as mild, moderate and substantial [111]. If category of substantial severity was achieved within 48 h, animals were immediately euthanized by CO_2 and a lower dose was selected for the further group. Similarly, if there was a severe adverse effect or death occurring within few minutes after administration to the first animal in the group, the other animal was not treated and lower dose were selected as well. Another lower/higher dose followed previous dose after 48 h, depending on severity of symptoms. All animals surviving 48 h were euthanized by CO_2 and subjected to basic macroscopic necropsy. Necropsy was also performed in the case of mortality, examining signs of macroscopic organ toxicity.

19. Behavioral studies

19.1. Animals

Thirty adult male Wistar rats (9–12 weeks old, 370–500 g), obtained from the Institute of Physiology Czech Academy of Sciences, accredited breeding colony, were used for described experiments. The rats were housed in pairs in transparent plastic cages (20 × 25 × 40 cm) in an air-conditioned animal room (temperature: 22 ± 1 °C, humidity: 50–60%, lights on: 06:00–18:00 h). Water and standard laboratory food were available *ad libitum*. After an acclimatization period in the animal room at the Institute of Physiology, Czech Academy of Sciences, the rats were habituated to human manipulations by handling (two days, 10 min per day). The behavioral experiments were conducted in the light phase of the day. All experiments were conducted in accordance with the guidelines of the European Union directive 2010/63/EU and approved by the Animal Care and Use Committee of the Institute of Physiology Czech Academy of Sciences and by the Central Committee of the Czech Academy of Sciences. The Institute of Physiology Czech Academy of Sciences possesses the National Institutes of Health Statement of Compliance with Standards for Humane Care and Use of Laboratory Animals.

19.2. Surgery

Surgical preparation was performed under 2% isoflurane anesthesia (Abbot Laboratories, Chicago, USA). Rats were placed in a stereotaxic frame (TSE Systems), eyes were covered by medical petroleum jelly (Vaseline®, Unilever, Rotterdam, Netherland) and hairs and scalp were removed. Rats were implanted with guide cannulas in both cerebral ventricles at the coordinates relative to Bregma: AP = −0.80 mm; ML = 1.5 mm; DV = 3.5 mm from skull surface [112]. The cannulas were fixed to the skull with two stainless steel screws and dental cement. After surgery animals had free access to food and water containing analgesics. Seven days after the surgery rats started the Morris water maze evaluation.

19.3. Drug application

***S*-K1035** was prepared according to the described chemical synthesis. The purity of ***S*-K1035** was >99% (HPLC detected). ***S*-K1035** was dissolved in sterile saline (0.9% NaCl) for a desired concentration of 10 and 100 nM. The freshly prepared solution was sonicated (20 min), fractioned on low volume aliquots (20 μL) and frozen at −20 °C.

Scopolamine hydrobromide (referred to as scopolamine or SCOP in group names, Sigma-Aldrich, 5 mg kg^{-1}) was dissolved in sterile saline one day before the experiment and stored in cold dark environment. As control, sterile saline (SAL) was used.

The drugs were applied on the MWM day 4. Each rat was pseudo-randomly assigned into one of five treatment groups (N = 6): (1) SAL i.c.v. + SAL i.p.; (2) SAL i.c.v. + SCOP i.p.; (3) ***S*-K1035** 100 nM i.c.v. + SAL i.p.; (4) ***S*-K1035** 10 nM i.c.v. + SCOP i.p.; (5) ***S*-K1035** 100 nM i.c.v. + SCOP i.p. Each rat received one bilateral intracerebroventricular (i.c.v., 60 min prior to MWM testing, ***S*-K1035** or saline) and one intraperitoneal (i.p., 20 min prior to MWM testing, scopolamine or saline) injection.

***S*-K1035** or NaCl was applied into the cerebral ventricles by an infusion pump (TSE Systems, Bad Homburg, Germany) with a constant flow rate 0.5 μL min^{-1}; and a total volume 1 μL in each injection. The internal cannula was removed 1 min after the end of the infusion. The volume of i.p. injections was 1 mL kg^{-1}.

19.4. Morris water maze (MWM)

The MWM apparatus consisted of a blue plastic circular pool (180 cm in diameter) with a circular platform (10 cm in diameter, submerged 1 cm below the water surface, transparent plastic). The pool was filled with water (23–24 °C, 28 cm deep) colored by a small amount of a non-toxic grey color. MWM task designed by Jackons and Soliman was modified and used [105]. The MWM was conducted during four consecutive days. The rats were trained to find the hidden platform, the position of which was constant (in the center of the NW quadrant). Every testing day each rat underwent

four swims from different starting points (N, S, W, E; their order was selected randomly and it was different each day). Animals were released into the water facing the wall of the pool. The trial stopped when the rat found the platform. If the rat did not find the platform in 60 s, it was gently guided to the platform by the experimenter. The drugs were applied only on day 4.

Rats were tracked during the experiment with a camera situated above the maze and connected to a digital tracking system (Tracker, Biosignal Group, New York, USA). The acquired data were stored for an off-line analysis using Carousel Maze Manager 0.4.0 (https://github.com/bahniks/CM_Manager_0_4_0).

19.5. Measured parameters and statistics

Following parameters were analyzed: distance moved (m), escape latency (s), average distance from the platform (cm), and time in the target sector (percentage of time spent swimming in the 90° sector with the platform in the center). These parameters were analyzed for every swim of day 3 and day 4 MWM and mean values were calculated for these days. The mean performance of a group on MWM day 3 (group's baseline, without drugs) and the mean performance of the same group on day 4 (with drugs) were compared using Mann-Whitney nonparametric test (GraphPad Prism 5.02). This analysis was done for all MWM parameters studied. In addition, performances of day 3 of all groups were compared by ANOVA and Tukey post hoc test (GraphPad Prism 5.02) to find out whether there are any differences in group baseline. This was done for all MWM parameters studied.

Accession codes

Atomic coordinates and structure factor amplitudes of the *Tc*AChE – ***S*-K1035** complex have been deposited in the Brookhaven Protein Data Bank under the PDB ID code 5NUU, *h*BChE – ***S*-K1035** complex under PDB entry 6I0B and *h*BChE – ***R*-K1035** complex under PDB entry 6I0C. Authors will release atomic coordinates and experimental data upon article publication.

Abbreviations

ACh, acetylcholine; AChE, acetylcholinesterase; AChEIs, acetylcholinesterase inhibitors; ATCh, acetylthiocholine; ALT, alanine aminotransferase; AD, Alzheimer's disease; Aβ, amyloid-β; APP, amyloid precursor protein; AST, aspartate aminotransferase; BOP, benzotriazol-1-yloxytris(dimethylamino)phosphonium hexafluorophosphate; BBB, blood-brain barrier; BCh, butyrylcholine; BChE, butyrylcholinesterase; BTCh, butyrylthiocholine; Boc_2O, di-*tert*-butyl dicarbonate; CAS, catalytic anionic site; CNS, central nervous system; COSY, correlation spectroscopy; CHO-K1, chinese hamster ovary; DMSO, dimethylsulfoxide; DEPT, distortionless enhancement by polarization transfer; DTNB, 5,5'-dithiobis(2-nitrobenzoic acid); ECD, electronic circular dischroism; FDA, Food and Drug Administration; HMBC, heteronuclear multiple-bond correlation; HPLC, high-performance liquid chromatography; HSQC, heteronuclear single-quantum correlation; HFIP, 1,1,1,3,3,3-hexafluoro-2-propanol; *h*AChE, human aetylcholinesterase; *h*BChE, human butyrylcholinesterase; HepG2, human liver carcinoma cell line; 5-HT, serotonin; 6-Cl-THA, 6-chlorotacrine; ChE, cholinesterase; ChEIs, cholinesterase inhibitors; IC, inhibitory concentration; i.c.v., intracerebroventricular; i.m., intramuscular; i.p., intraperitoneal; LC-HRMS, liquid-chromatography-high resolution mass spectrometry; MTT, 3-(4,5-dimethylthiazol-2-yl)-2,5-diphenyl tetrazolium bromide; MTD, maximum tolerated dose; 7-MEOTA, 7-methoxytacrine; MTDLs, multi-target directed ligands; MWM, Morris water maze, *L*-NMMA, N^G-monomethyl-L-arginine; NQ, naphthoquinone; nNOS, neuronal nitric oxide synthase; NO, nitric oxide; 7-NI, 7-nitroindozale; NMR, nuclear magnetic resonance; PAMPA, parallel artificial membrane permeation assay; PAINS, pan assay interference compounds; PAS, peripheral anionic site; P_e, permeability; SAL, saline; SCOP, scopolamine; SI, selectivity index; THA, tacrine; ThT, thioflavin T; TLC, thin layer chromatography; *Tc*AChE; *Torpedo californica* acetylcholinesterase; TEA; triethylamine; Trp, tryptophan.

Notes

The authors declare no competing financial interest.

Acknowledgement

This work was supported by Ministry of Health of the Czech Republic, grant nr. 15-30954A, by the grant of Ministry of Defence of the Czech Republic – "Long-term organization development plan Medical Aspects of Weapon of Mass Destruction of the Faculty of Military Health Sciences, University of Defence", by the Czech Science Foundation. nr. 17-05292S, and by European Regional Development Fund: Project "PharmaBrain" (no. CZ.02.1.01/0.0/0.0/16_025/0007444). Authors are also grateful to the ELETTRA XRD-1 and ESRF ID29 beamline staff in Trieste (Italy) and Grenoble (France) for their assistance during the data collection. X.B., A-J.G. and F.N. were supported by the Direction Générale de l'Armement (DGA) and Service de Santé des Armées (SSA), grant nr. PDH-2-NRBC-3-C-3201. This work is based upon work from COST Action CA15135.

Appendix A. Supplementary data

Supplementary data to this article can be found online at https://doi.org/10.1016/j.ejmech.2019.02.021.

References

[1] L. Piazzi, A. Rampa, A. Bisi, S. Gobbi, F. Belluti, A. Cavalli, M. Bartolini, V. Andrisano, P. Valenti, M. Recanatini, 3-(4-[[Benzyl(methyl)amino]methyl] phenyl)-6,7-dimethoxy-2H-2-chromenone (AP2238) inhibits both acetylcholinesterase and acetylcholinesterase-induced beta-amyloid aggregation: a dual function lead for Alzheimer's disease therapy, J. Med. Chem. 46 (2003) 2279–2282, https://doi.org/10.1021/jm0340602.

[2] P.D. Sloane, S. Zimmerman, C. Suchindran, P. Reed, L. Wang, M. Boustani, S. Sudha, The public health impact of Alzheimer's disease, 2000-2050: potential implication of treatment advances, Annu. Rev. Public Health 23 (2002) 213–231, https://doi.org/10.1146/annurev.publhealth.23.100901.140525.

[3] V. Tumiatti, A. Minarini, M.L. Bolognesi, A. Milelli, M. Rosini, C. Melchiorre, Tacrine derivatives and Alzheimer's disease, Curr. Med. Chem. 17 (2010) 1825–1838.

[4] E. Scarpini, P. Scheltens, H. Feldman, Treatment of Alzheimer's disease: current status and new perspectives, Lancet Neurol. 2 (2003) 539–547.

[5] J.B. Paulson, M. Ramsden, C. Forster, M.A. Sherman, E. McGowan, K.H. Ashe, Amyloid plaque and neurofibrillary tangle pathology in a regulatable mouse model of Alzheimer's disease, Am. J. Pathol. 173 (2008) 762–772, https://doi.org/10.2353/ajpath.2008.080175.

[6] H.W. Querfurth, F.M. LaFerla, Alzheimer's disease, N. Engl. J. Med. 362 (2010) 329–344, https://doi.org/10.1056/NEJMra0909142.

[7] D.J. Selkoe, Alzheimer's disease: genes, proteins, and therapy, Physiol. Rev. 81 (2001) 741–766.

[8] R.T. Bartus, R.L. Dean, B. Beer, A.S. Lippa, The cholinergic hypothesis of geriatric memory dysfunction, Science 217 (1982) 408–414.

[9] D. Muñoz-Torrero, Acetylcholinesterase inhibitors as disease-modifying therapies for Alzheimer's disease, Curr. Med. Chem. 15 (2008) 2433–2455.

[10] J. Birks, Cholinesterase inhibitors for Alzheimer's disease, Cochrane Database Syst. Rev. (2006) CD005593, https://doi.org/10.1002/14651858.CD005593.

[11] N.C. Inestrosa, A. Alvarez, C.A. Pérez, R.D. Moreno, M. Vicente, C. Linker, O.I. Casanueva, C. Soto, J. Garrido, Acetylcholinesterase accelerates assembly of amyloid-beta-peptides into Alzheimer's fibrils: possible role of the peripheral site of the enzyme, Neuron 16 (1996) 881–891.

[12] A. Alvarez, C. Opazo, R. Alarcón, J. Garrido, N.C. Inestrosa, Acetylcholinesterase promotes the aggregation of amyloid-beta-peptide fragments by forming a complex with the growing fibrils, J. Mol. Biol. 272 (1997) 348–361,

https://doi.org/10.1006/jmbi.1997.1245.
[13] F.J. Muñoz, N.C. Inestrosa, Neurotoxicity of acetylcholinesterase amyloid beta-peptide aggregates is dependent on the type of Abeta peptide and the AChE concentration present in the complexes, FEBS Lett. 450 (1999) 205–209.
[14] J.L. Sussman, M. Harel, F. Frolow, C. Oefner, A. Goldman, L. Toker, I. Silman, Atomic structure of acetylcholinesterase from Torpedo californica: a prototypic acetylcholine-binding protein, Science 253 (1991) 872–879.
[15] X. Chen, L. Fang, J. Liu, C.-G. Zhan, Reaction pathway and free energy profiles for butyrylcholinesterase-catalyzed hydrolysis of acetylthiocholine, Biochemistry (Mosc.) 51 (2012) 1297–1305, https://doi.org/10.1021/bi201786s.
[16] C. Geula, M.M. Mesulam, Cholinesterases and the pathology of Alzheimer disease, Alzheimers Dis. Assoc. Disord. 9 (Suppl 2) (1995) 23–28.
[17] D.J. Selkoe, J. Hardy, The amyloid hypothesis of Alzheimer's disease at 25 years, EMBO Mol. Med. 8 (2016) 595–608, https://doi.org/10.15252/emmm.201606210.
[18] M.S. Wolfe, J. De Los Angeles, D.D. Miller, W. Xia, D.J. Selkoe, Are presenilins intramembrane-cleaving proteases? Implications for the molecular mechanism of Alzheimer's disease, Biochemistry (Mosc.). 38 (1999) 11223–11230, https://doi.org/10.1021/bi991080q.
[19] S. Paul, S. Planque, Y. Nishiyama, Beneficial catalytic immunity to abeta peptide, Rejuvenation Res. 13 (2010) 179–187, https://doi.org/10.1089/rej.2009.0958.
[20] J. Hardy, D.J. Selkoe, The amyloid hypothesis of Alzheimer's disease: progress and problems on the road to therapeutics, Science 297 (2002) 353–356, https://doi.org/10.1126/science.1072994.
[21] S.H. Barage, K.D. Sonawane, Amyloid cascade hypothesis: pathogenesis and therapeutic strategies in Alzheimer's disease, Neuropeptides 52 (2015) 1–18, https://doi.org/10.1016/j.npep.2015.06.008.
[22] F. Zemek, L. Drtinova, E. Nepovimova, V. Sepsova, J. Korabecny, J. Klimes, K. Kuca, Outcomes of Alzheimer's disease therapy with acetylcholinesterase inhibitors and memantine, Expert Opin. Drug Saf. 13 (2014) 759–774, https://doi.org/10.1517/14740338.2014.914168.
[23] A.V. Terry, J.J. Buccafusco, The cholinergic hypothesis of age and Alzheimer's disease-related cognitive deficits: recent challenges and their implications for novel drug development, J. Pharmacol. Exp. Therapeut. 306 (2003) 821–827, https://doi.org/10.1124/jpet.102.041616.
[24] W.K. Summers, A.L. Koehler, G.M. Marsh, K. Tachiki, A. Kling, Long-term hepatotoxicity of tacrine, Lancet Lond. Engl. 1 (1989) 729.
[25] W.K. Summers, Tacrine (THA, Cognex(R)), J. Alzheimers Dis. JAD. 2 (2000) 85–93.
[26] O. Soukup, D. Jun, J. Zdarova-Karasova, J. Patocka, K. Musilek, J. Korabecny, J. Krusek, M. Kaniakova, V. Sepsova, J. Mandikova, F. Trejtnar, M. Pohanka, L. Drtinova, M. Pavlik, G. Tobin, K. Kuca, A resurrection of 7-MEOTA: a comparison with tacrine, Curr. Alzheimer Res. 10 (2013) 893–906.
[27] M. Recanatini, A. Cavalli, F. Belluti, L. Piazzi, A. Rampa, A. Bisi, S. Gobbi, P. Valenti, V. Andrisano, M. Bartolini, V. Cavrini, SAR of 9-amino-1,2,3,4-tetrahydroacridine-based acetylcholinesterase inhibitors: synthesis, enzyme inhibitory activity, QSAR, and structure-based CoMFA of tacrine analogues, J. Med. Chem. 43 (2000) 2007–2018.
[28] J. Misik, E. Nepovimova, J. Pejchal, J. Kassa, J. Korabecny, O. Soukup, Cholinesterase inhibitor 6-chlorotacrine - in vivo toxicological profile and behavioural effects, Curr. Alzheimer Res. 15 (2018) 552–560, https://doi.org/10.2174/1567205015666171212105412.
[29] K. Spilovska, J. Korabecny, E. Nepovimova, R. Dolezal, E. Mezeiova, O. Soukup, K. Kuca, Multitarget tacrine hybrids with neuroprotective properties to confront Alzheimer's disease, Curr. Top. Med. Chem. 17 (2017) 1006–1026. https://doi.org/10.2174/1568026605666160927152728.
[30] M.C. Carreiras, E. Mendes, M.J. Perry, A.P. Francisco, J. Marco-Contelles, The multifactorial nature of Alzheimer's disease for developing potential therapeutics, Curr. Top. Med. Chem. 13 (2013) 1745–1770.
[31] K. Spilovska, J. Korabecny, E. Nepovimova, R. Dolezal, E. Mezeiova, O. Soukup, K. Kuca, Multitarget tacrine hybrids with neuroprotective properties to confront Alzheimer's disease, Curr. Top. Med. Chem. 17 (2017) 1006–1026, https://doi.org/10.2174/1568026605666160927152728.
[32] E. Simoni, M. Bartolini, I.F. Abu, A. Blockley, C. Gotti, G. Bottegoni, R. Caporaso, C. Bergamini, V. Andrisano, A. Cavalli, I.R. Mellor, A. Minarini, M. Rosini, Multitarget drug design strategy in Alzheimer's disease: focus on cholinergic transmission and amyloid-β aggregation, Future Med. Chem. 9 (2017) 953–963, https://doi.org/10.4155/fmc-2017-0039.
[33] R.R. Ramsay, M.R. Popovic-Nikolic, K. Nikolic, E. Uliassi, M.L. Bolognesi, A perspective on multi-target drug discovery and design for complex diseases, Clin. Transl. Med. 7 (2018) 3, https://doi.org/10.1186/s40169-017-0181-2.
[34] J. Li, Z. Lu, L. Xu, Q. Wang, Z. Zhang, J. Fang, Neuroprotective effects of bis(7)-tacrine in a rat model of pressure-induced retinal ischemia, Cell Biochem. Biophys. 68 (2014) 275–282, https://doi.org/10.1007/s12013-013-9707-4.
[35] Y.P. Pang, P. Quiram, T. Jelacic, F. Hong, S. Brimijoin, Highly potent, selective, and low cost bis-tetrahydroaminacrine inhibitors of acetylcholinesterase. Steps toward novel drugs for treating Alzheimer's disease, J. Biol. Chem. 271 (1996) 23646–23649.
[36] W. Li, J. Xue, C. Niu, H. Fu, C.S.C. Lam, J. Luo, H.H.N. Chan, H. Xue, K.K.W. Kan, N.T.K. Lee, C. Li, Y. Pang, M. Li, K.W.K. Tsim, H. Jiang, K. Chen, X. Li, Y. Han, Synergistic neuroprotection by bis(7)-tacrine via concurrent blockade of N-methyl-D-aspartate receptors and neuronal nitric-oxide synthase, Mol. Pharmacol. 71 (2007) 1258–1267, https://doi.org/10.1124/mol.106.029108.
[37] S.A. Lipton, Paradigm shift in NMDA receptor antagonist drug development: molecular mechanism of uncompetitive inhibition by memantine in the treatment of Alzheimer's disease and other neurologic disorders, J. Alzheimers Dis. JAD. 6 (2004) S61–S74.
[38] M. Rosini, E. Simoni, R. Caporaso, A. Minarini, Multitarget strategies in Alzheimer's disease: benefits and challenges on the road to therapeutics, Future Med. Chem. 8 (2016) 697–711, https://doi.org/10.4155/fmc-2016-0003.
[39] N. Guzior, A. Wieckowska, D. Panek, B. Malawska, Recent development of multifunctional agents as potential drug candidates for the treatment of Alzheimer's disease, Curr. Med. Chem. 22 (2015) 373–404.
[40] F. Prati, A. De Simone, P. Bisignano, A. Armirotti, M. Summa, D. Pizzirani, R. Scarpelli, D.I. Perez, V. Andrisano, A. Perez-Castillo, B. Monti, F. Massenzio, L. Polito, M. Racchi, A.D. Favia, G. Bottegoni, A. Martinez, M.L. Bolognesi, A. Cavalli, Multitarget drug discovery for Alzheimer's disease: triazinones as BACE-1 and GSK-3β inhibitors, Angew Chem. Int. Ed. Engl. 54 (2015) 1578–1582, https://doi.org/10.1002/anie.201410456.
[41] J. Korabecny, R. Dolezal, P. Cabelova, A. Horova, E. Hruba, J. Ricny, L. Sedlacek, E. Nepovimova, K. Spilovska, M. Andrs, K. Musilek, V. Opletalova, V. Sepsova, D. Ripova, K. Kuca, 7-MEOTA-donepezil like compounds as cholinesterase inhibitors: synthesis, pharmacological evaluation, molecular modeling and QSAR studies, Eur. J. Med. Chem. 82 (2014) 426–438, https://doi.org/10.1016/j.ejmech.2014.05.066.
[42] S. Hamulakova, L. Janovec, M. Hrabinova, K. Spilovska, J. Korabecny, P. Kristian, K. Kuca, J. Imrich, Synthesis and biological evaluation of novel tacrine derivatives and tacrine-coumarin hybrids as cholinesterase inhibitors, J. Med. Chem. 57 (2014) 7073–7084, https://doi.org/10.1021/jm5008648.
[43] J.-S. Lan, S.-S. Xie, S.-Y. Li, L.-F. Pan, X.-B. Wang, L.-Y. Kong, Design, synthesis and evaluation of novel tacrine-(β-carboline) hybrids as multifunctional agents for the treatment of Alzheimer's disease, Bioorg. Med. Chem. 22 (2014) 6089–6104, https://doi.org/10.1016/j.bmc.2014.08.035.
[44] P. Muñoz-Ruiz, L. Rubio, E. García-Palomero, I. Dorronsoro, M. del Monte-Millán, R. Valenzuela, P. Usán, C. de Austria, M. Bartolini, V. Andrisano, A. Bidon-Chanal, M. Orozco, F.J. Luque, M. Medina, A. Martínez, Design, synthesis, and biological evaluation of dual binding site acetylcholinesterase inhibitors: new disease-modifying agents for Alzheimer's disease, J. Med. Chem. 48 (2005) 7223–7233, https://doi.org/10.1021/jm0503289.
[45] V. Hepnarova, J. Korabecny, L. Matouskova, P. Jost, L. Muckova, M. Hrabinova, N. Vykoukalova, M. Kerhartova, T. Kucera, R. Dolezal, E. Nepovimova, K. Spilovska, E. Mezeiova, N.L. Pham, D. Jun, F. Staud, D. Kaping, K. Kuca, O. Soukup, The concept of hybrid molecules of tacrine and benzyl quinolone carboxylic acid (BQCA) as multifunctional agents for Alzheimer's disease, Eur. J. Med. Chem. 150 (2018) 292–306, https://doi.org/10.1016/j.ejmech.2018.02.083.
[46] M.I. Rodríguez-Franco, M.I. Fernández-Bachiller, C. Pérez, B. Hernández-Ledesma, B. Bartolomé, Novel tacrine-melatonin hybrids as dual-acting drugs for Alzheimer disease, with improved acetylcholinesterase inhibitory and antioxidant properties, J. Med. Chem. 49 (2006) 459–462, https://doi.org/10.1021/jm050746d.
[47] M.I. Fernández-Bachiller, C. Pérez, N.E. Campillo, J.A. Páez, G.C. González-Muñoz, P. Usán, E. García-Palomero, M.G. López, M. Villarroya, A.G. García, A. Martínez, M.I. Rodríguez-Franco, Tacrine-melatonin hybrids as multifunctional agents for Alzheimer's disease, with cholinergic, antioxidant, and neuroprotective properties, ChemMedChem 4 (2009) 828–841, https://doi.org/10.1002/cmdc.200800414.
[48] R. Scherzer-Attali, R. Shaltiel-Karyo, Y.H. Adalist, D. Segal, E. Gazit, Generic inhibition of amyloidogenic proteins by two naphthoquinone-tryptophan hybrid molecules, Proteins 80 (2012) 1962–1973, https://doi.org/10.1002/prot.24080.
[49] M. Frenkel-Pinter, S. Tal, R. Scherzer-Attali, M. Abu-Hussien, I. Alyagor, T. Eisenbaum, E. Gazit, D. Segal, Cl-NQTrp alleviates tauopathy symptoms in a model organism through the inhibition of tau aggregation-engendered toxicity, Neurodegener. Dis. 17 (2016) 73–82, https://doi.org/10.1159/000448518.
[50] S. Butini, E. Guarino, G. Campiani, M. Brindisi, S.S. Coccone, I. Fiorini, E. Novellino, T. Belinskaya, A. Saxena, S. Gemma, Tacrine based human cholinesterase inhibitors: synthesis of peptidic-tethered derivatives and their effect on potency and selectivity, Bioorg. Med. Chem. Lett 18 (2008) 5213–5216, https://doi.org/10.1016/j.bmcl.2008.08.076.
[51] E. Nepovimova, E. Uliassi, J. Korabecny, L.E. Peña-Altamira, S. Samez, A. Pesaresi, G.E. Garcia, M. Bartolini, V. Andrisano, C. Bergamini, R. Fato, D. Lamba, M. Roberti, K. Kuca, B. Monti, M.L. Bolognesi, Multitarget drug design strategy: quinone-tacrine hybrids designed to block amyloid-β aggregation and to exert anticholinesterase and antioxidant effects, J. Med. Chem. 57 (2014) 8576–8589, https://doi.org/10.1021/jm5010804.
[52] H.M. van der Stelt, L.M. Broersen, B. Olivier, H.G.M. Westenberg, Effects of dietary tryptophan variations on extracellular serotonin in the dorsal hippocampus of rats, Psychopharmacology (Berl.) 172 (2004) 137–144, https://doi.org/10.1007/s00213-003-1632-6.
[53] R.J. Porter, B.S. Lunn, L.L. Walker, J.M. Gray, C.G. Ballard, J.T. O'Brien, Cognitive deficit induced by acute tryptophan depletion in patients with Alzheimer's disease, Am. J. Psychiatry 157 (2000) 638–640, https://doi.org/10.1176/appi.ajp.157.4.638.

[54] T.A. Jenkins, J.J. Elliott, T.C. Ardis, M. Cahir, G.P. Reynolds, R. Bell, S.J. Cooper, Tryptophan depletion impairs object-recognition memory in the rat: reversal by risperidone, Behav. Brain Res. 208 (2010) 479–483, https://doi.org/10.1016/j.bbr.2009.12.030.

[55] A.P. Pawar, K.F. Dubay, J. Zurdo, F. Chiti, M. Vendruscolo, C.M. Dobson, Prediction of "aggregation-prone" and "aggregation-susceptible" regions in proteins associated with neurodegenerative diseases, J. Mol. Biol. 350 (2005) 379–392, https://doi.org/10.1016/j.jmb.2005.04.016.

[56] R. Scherzer-Attali, R. Pellarin, M. Convertino, A. Frydman-Marom, N. Egoz-Matia, S. Peled, M. Levy-Sakin, D.E. Shalev, A. Caflisch, E. Gazit, D. Segal, Complete phenotypic recovery of an Alzheimer's disease model by a quinone-tryptophan hybrid aggregation inhibitor, PLoS One 5 (2010), e11101, https://doi.org/10.1371/journal.pone.0011101.

[57] T. Zhang, W. Xu, Y. Mu, P. Derreumaux, Atomic and dynamic insights into the beneficial effect of the 1,4-naphthoquinon-2-yl-L-tryptophan inhibitor on Alzheimer's Aβ1-42 dimer in terms of aggregation and toxicity, ACS Chem. Neurosci. 5 (2014) 148–159, https://doi.org/10.1021/cn400197x.

[58] M.-K. Hu, L.-J. Wu, G. Hsiao, M.-H. Yen, Homodimeric tacrine congeners as acetylcholinesterase inhibitors, J. Med. Chem. 45 (2002) 2277–2282.

[59] K. Spilovska, J. Korabecny, J. Kral, A. Horova, K. Musilek, O. Soukup, L. Drtinova, Z. Gazova, K. Siposova, K. Kuca, 7-Methoxytacrine-Adamantylamine heterodimers as cholinesterase inhibitors in Alzheimer's disease treatment — synthesis, biological evaluation and molecular modeling studies, Molecules 18 (2013) 2397–2418, https://doi.org/10.3390/molecules18022397.

[60] J. Korabecny, M. Andrs, E. Nepovimova, R. Dolezal, K. Babkova, A. Horova, D. Malinak, E. Mezeiova, L. Gorecki, V. Sepsova, M. Hrabinova, O. Soukup, D. Jun, K. Kuca, 7-Methoxytacrine-p-Anisidine hybrids as novel dual binding site acetylcholinesterase inhibitors for Alzheimer's disease treatment, Mol. Basel Switz. 20 (2015) 22084–22101, https://doi.org/10.3390/molecules201219836.

[61] H. Franzén, L. Grehn, U. Ragnarsson, Synthesis, properties, and use of Nin-Boc-tryptophan derivatives, J. Chem. Soc., Chem. Commun. (1984) 1699–1700, https://doi.org/10.1039/C39840001699.

[62] G.L. Ellman, K.D. Courtney, V. Andres, R.M. Feather-Stone, A new and rapid colorimetric determination of acetylcholinesterase activity, Biochem. Pharmacol. 7 (1961) 88–95.

[63] M. Pohanka, D. Jun, K. Kuca, Improvement of acetylcholinesterase-based assay for organophosphates in way of identification by reactivators, Talanta 77 (2008) 451–454, https://doi.org/10.1016/j.talanta.2008.06.007.

[64] K. Spilovska, J. Korabecny, A. Horova, K. Musilek, E. Nepovimova, L. Drtinova, Z. Gazova, K. Siposova, R. Dolezal, D. Jun, K. Kuca, Design, synthesis and in vitro testing of 7-methoxytacrine-amantadine analogues: a novel cholinesterase inhibitors for the treatment of Alzheimer's disease, Med. Chem. Res. 24 (2015) 2645–2655, https://doi.org/10.1007/s00044-015-1316-x.

[65] E. Nepovimova, J. Korabecny, R. Dolezal, K. Babkova, A. Ondrejicek, D. Jun, V. Sepsova, A. Horova, M. Hrabinova, O. Soukup, N. Bukum, P. Jost, L. Muckova, J. Kassa, D. Malinak, M. Andrs, K. Kuca, Tacrine-trolox hybrids: a novel class of centrally active, nonhepatotoxic multi-target-directed ligands exerting anticholinesterase and antioxidant activities with low in vivo toxicity, J. Med. Chem. 58 (2015) 8985–9003, https://doi.org/10.1021/acs.jmedchem.5b01325.

[66] J. Jeřábek, E. Uliassi, L. Guidotti, J. Korábečný, O. Soukup, V. Sepsova, M. Hrabinova, K. Kuča, M. Bartolini, L.E. Peña-Altamira, S. Petralla, B. Monti, M. Roberti, M.L. Bolognesi, Tacrine-resveratrol fused hybrids as multi-target-directed ligands against Alzheimer's disease, Eur. J. Med. Chem. 127 (2017) 250–262, https://doi.org/10.1016/j.ejmech.2016.12.048.

[67] M. Harel, J.L. Sussman, E. Krejci, S. Bon, P. Chanal, J. Massoulié, I. Silman, Conversion of acetylcholinesterase to butyrylcholinesterase: modeling and mutagenesis, Proc. Natl. Acad. Sci. U.S.A. 89 (1992) 10827–10831.

[68] C.-G. Zhan, F. Zheng, D.W. Landry, Fundamental reaction mechanism for cocaine hydrolysis in human butyrylcholinesterase, J. Am. Chem. Soc. 125 (2003) 2462–2474, https://doi.org/10.1021/ja020850+.

[69] X. Barril, S.G. Kalko, M. Orozco, F.J. Luque, Rational design of reversible acetylcholinesterase inhibitors, Mini Rev. Med. Chem. 2 (2002) 27–36.

[70] S. Darvesh, D.A. Hopkins, C. Geula, Neurobiology of butyrylcholinesterase, Nat. Rev. Neurosci. 4 (2003) 131–138, https://doi.org/10.1038/nrn1035.

[71] N.H. Greig, T. Utsuki, D.K. Ingram, Y. Wang, G. Pepeu, C. Scali, Q.-S. Yu, J. Mamczarz, H.W. Holloway, T. Giordano, D. Chen, K. Furukawa, K. Sambamurti, A. Brossi, D.K. Lahiri, Selective butyrylcholinesterase inhibition elevates brain acetylcholine, augments learning and lowers Alzheimer beta-amyloid peptide in rodent, Proc. Natl. Acad. Sci. U.S.A. 102 (2005) 17213–17218, https://doi.org/10.1073/pnas.0508575102.

[72] P. Taylor, J. Lwebuga-Mukasa, S. Lappi, J. Rademacher, Propidium—a fluorescence probe for a peripheral anionic site on acetylcholinesterase, Mol. Pharmacol. 10 (1974) 703–708.

[73] P. Taylor, S. Lappi, Interaction of fluorescence probes with acetylcholinesterase. The site and specificity of propidium binding, Biochemistry (Mosc.) 14 (1975) 1989–1997.

[74] N. Nunes-Tavares, A. Nery da Matta, C.M. Batista e Silva, G.M.N. Araújo, S.R.W. Louro, A. Hassón-Voloch, Inhibition of acetylcholinesterase from Electrophorus electricus (L.) by tricyclic antidepressants, Int. J. Biochem. Cell Biol. 34 (2002) 1071–1079.

[75] H. Dvir, D.M. Wong, M. Harel, X. Barril, M. Orozco, F.J. Luque, D. Muñoz-Torrero, P. Camps, T.L. Rosenberry, I. Silman, J.L. Sussman, 3D structure of Torpedo californica acetylcholinesterase complexed with huprine X at 2.1 A resolution: kinetic and molecular dynamic correlates, Biochemistry (Mosc.) 41 (2002) 2970–2981.

[76] X. Zha, D. Lamba, L. Zhang, Y. Lou, C. Xu, D. Kang, L. Chen, Y. Xu, L. Zhang, A. De Simone, S. Samez, A. Pesaresi, J. Stojan, M.G. Lopez, J. Egea, V. Andrisano, M. Bartolini, Novel tacrine-benzofuran hybrids as potent multitarget-directed ligands for the treatment of Alzheimer's disease: design, synthesis, biological evaluation, and X-ray crystallography, J. Med. Chem. 59 (2016) 114–131, https://doi.org/10.1021/acs.jmedchem.5b01119.

[77] J.P. Colletier, B. Sanson, F. Nachon, E. Gabellieri, C. Fattorusso, G. Campiani, M. Weik, Conformational flexibility in the peripheral site of Torpedo californica acetylcholinesterase revealed by the complex structure with a bifunctional inhibitor, J. Am. Chem. Soc. 128 (2006) 4526–4527, https://doi.org/10.1021/ja058683b.

[78] M. Harel, I. Schalk, L. Ehret-Sabatier, F. Bouet, M. Goeldner, C. Hirth, P.H. Axelsen, I. Silman, J.L. Sussman, Quaternary ligand binding to aromatic residues in the active-site gorge of acetylcholinesterase, Proc. Natl. Acad. Sci. U.S.A. 90 (1993) 9031–9035.

[79] E.H. Rydberg, B. Brumshtein, H.M. Greenblatt, D.M. Wong, D. Shaya, L.D. Williams, P.R. Carlier, Y.-P. Pang, I. Silman, J.L. Sussman, Complexes of alkylene-linked tacrine dimers with Torpedo californica acetylcholinesterase: binding of Bis5-tacrine produces a dramatic rearrangement in the active-site gorge, J. Med. Chem. 49 (2006) 5491–5500, https://doi.org/10.1021/jm060164b.

[80] M.C. Desai, P.F. Thadeio, C.A. Lipinski, D.R. Liston, R.W. Spencer, I.H. Williams, Physical parameters for brian uptake: optimizing log P, log D and pKa of T H A, Bioorg. Med. Chem. Lett 1 (1991) 411–414, https://doi.org/10.1016/S0960-894X(00)80267-X.

[81] W.D. Mallender, T. Szegletes, T.L. Rosenberry, Acetylthiocholine binds to asp74 at the peripheral site of human acetylcholinesterase as the first step in the catalytic pathway, Biochemistry (Mosc.) 39 (2000) 7753–7763.

[82] L. Gremer, D. Schölzel, C. Schenk, E. Reinartz, J. Labahn, R.B.G. Ravelli, M. Tusche, C. Lopez-Iglesias, W. Hoyer, H. Heise, D. Willbold, G.F. Schröder, Fibril structure of amyloid-β(1-42) by cryo-electron microscopy, Science 358 (2017) 116–119, https://doi.org/10.1126/science.aao2825.

[83] A.P. Pawar, K.F. Dubay, J. Zurdo, F. Chiti, M. Vendruscolo, C.M. Dobson, Prediction of "aggregation-prone" and "aggregation-susceptible" regions in proteins associated with neurodegenerative diseases, J. Mol. Biol. 350 (2005) 379–392, https://doi.org/10.1016/j.jmb.2005.04.016.

[84] R. Azriel, E. Gazit, Analysis of the minimal amyloid-forming fragment of the islet amyloid polypeptide. An experimental support for the key role of the phenylalanine residue in amyloid formation, J. Biol. Chem. 276 (2001) 34156–34161, https://doi.org/10.1074/jbc.M102883200.

[85] E. Gazit, A possible role for pi-stacking in the self-assembly of amyloid fibrils, FASEB J. Off. Publ. Fed. Am. Soc. Exp. Biol. 16 (2002) 77–83, https://doi.org/10.1096/fj.01-0442hyp.

[86] O.S. Makin, E. Atkins, P. Sikorski, J. Johansson, L.C. Serpell, Molecular basis for amyloid fibril formation and stability, Proc. Natl. Acad. Sci. U.S.A. 102 (2005) 315–320, https://doi.org/10.1073/pnas.0406847102.

[87] A. Frydman-Marom, M. Rechter, I. Shefler, Y. Bram, D.E. Shalev, E. Gazit, Cognitive-performance recovery of Alzheimer's disease model mice by modulation of early soluble amyloidal assemblies, Angew Chem. Int. Ed. Engl. 48 (2009) 1981–1986, https://doi.org/10.1002/anie.200802123.

[88] M. Bartolini, C. Bertucci, M.L. Bolognesi, A. Cavalli, C. Melchiorre, V. Andrisano, Insight into the kinetic of amyloid beta (1-42) peptide self-aggregation: elucidation of inhibitors' mechanism of action, Chembiochem Eur. J. Chem. Biol. 8 (2007) 2152–2161, https://doi.org/10.1002/cbic.200700427.

[89] M. Bartolini, M. Naldi, J. Fiori, F. Valle, F. Biscarini, D.V. Nicolau, V. Andrisano, Kinetic characterization of amyloid-beta 1-42 aggregation with a multimethodological approach, Anal. Biochem. 414 (2011) 215–225, https://doi.org/10.1016/j.ab.2011.03.020.

[90] M. Bartolini, C. Bertucci, V. Cavrini, V. Andrisano, beta-Amyloid aggregation induced by human acetylcholinesterase: inhibition studies, Biochem. Pharmacol. 65 (2003) 407–416.

[91] A.E. Reyes, M.A. Chacón, M.C. Dinamarca, W. Cerpa, C. Morgan, N.C. Inestrosa, Acetylcholinesterase-Abeta complexes are more toxic than Abeta fibrils in rat hippocampus: effect on rat beta-amyloid aggregation, laminin expression, reactive astrocytosis, and neuronal cell loss, Am. J. Pathol. 164 (2004) 2163–2174.

[92] A.E. Reyes, D.R. Perez, A. Alvarez, J. Garrido, M.K. Gentry, B.P. Doctor, N.C. Inestrosa, A monoclonal antibody against acetylcholinesterase inhibits the formation of amyloid fibrils induced by the enzyme, Biochem. Biophys. Res. Commun. 232 (1997) 652–655, https://doi.org/10.1006/bbrc.1997.6357.

[93] M.L. Bolognesi, R. Banzi, M. Bartolini, A. Cavalli, A. Tarozzi, V. Andrisano, A. Minarini, M. Rosini, V. Tumiatti, C. Bergamini, R. Fato, G. Lenaz, P. Hrelia, A. Cattaneo, M. Recanatini, C. Melchiorre, Novel class of quinone-bearing polyamines as multi-target-directed ligands to combat Alzheimer's disease, J. Med. Chem. 50 (2007) 4882–4897, https://doi.org/10.1021/jm070559a.

[94] M.L. Bolognesi, M. Bartolini, F. Mancini, G. Chiriano, L. Ceccarini, M. Rosini, A. Milelli, V. Tumiatti, V. Andrisano, C. Melchiorre, Bis(7)-tacrine derivatives as multitarget-directed ligands: focus on anticholinesterase and antiamyloid activities, ChemMedChem 5 (2010) 1215–1220, https://doi.org/10.1002/cmdc.201000086.

[95] L. Di, E.H. Kerns, K. Fan, O.J. McConnell, G.T. Carter, High throughput artificial membrane permeability assay for blood-brain barrier, Eur. J. Med. Chem. 38 (2003) 223–232.
[96] L.F.N. Lemes, G. de Andrade Ramos, A.S. de Oliveira, F.M.R. da Silva, G. de Castro Couto, M. da Silva Boni, M.J.R. Guimarães, I.N.O. Souza, M. Bartolini, V. Andrisano, P.C. do Nascimento Nogueira, E.R. Silveira, G.D. Brand, O. Soukup, J. Korábečný, N.C. Romeiro, N.G. Castro, M.L. Bolognesi, L.A.S. Romeiro, Cardanol-derived AChE inhibitors: towards the development of dual binding derivatives for Alzheimer's disease, Eur. J. Med. Chem. 108 (2016) 687–700, https://doi.org/10.1016/j.ejmech.2015.12.024.
[97] F. Wohnsland, B. Faller, High-throughput permeability pH profile and high-throughput alkane/water log P with artificial membranes, J. Med. Chem. 44 (2001) 923–930.
[98] T.L. Riss, R.A. Moravec, A.L. Niles, S. Duellman, H.A. Benink, T.J. Worzella, L. Minor, Cell viability assays, in: G.S. Sittampalam, N.P. Coussens, K. Brimacombe, A. Grossman, M. Arkin, D. Auld, C. Austin, J. Baell, B. Bejcek, J.M.M. Caaveiro, T.D.Y. Chung, J.L. Dahlin, V. Devanaryan, T.L. Foley, M. Glicksman, M.D. Hall, J.V. Haas, J. Inglese, P.W. Iversen, S.D. Kahl, S.C. Kales, M. Lal-Nag, Z. Li, J. McGee, O. McManus, T. Riss, O.J. Trask, J.R. Weidner, M.J. Wildey, M. Xia, X. Xu (Eds.), Assay Guid. Man., Eli Lilly & Company and the National Center for Advancing Translational Sciences, Bethesda (MD), 2004. http://www.ncbi.nlm.nih.gov/books/NBK144065/. (Accessed 17 September 2018).
[99] J. Patocka, D. Jun, K. Kuca, Possible role of hydroxylated metabolites of tacrine in drug toxicity and therapy of Alzheimer's disease, Curr. Drug Metabol. 9 (2008) 332–335.
[100] F.J. Jiménez-Jiménez, H. Alonso-Navarro, M.T. Herrero, E. García-Martín, J.A.G. Agúndez, An update on the role of nitric oxide in the neurodegenerative processes of Parkinson's disease, Curr. Med. Chem. 23 (2016) 2666–2679.
[101] C. Volbracht, J. van Beek, C. Zhu, K. Blomgren, M. Leist, Neuroprotective properties of memantine in different in vitro and in vivo models of excitotoxicity, Eur. J. Neurosci. 23 (2006) 2611–2622, https://doi.org/10.1111/j.1460-9568.2006.04787.x.
[102] W. Li, J. Xue, C. Niu, H. Fu, C.S.C. Lam, J. Luo, H.H.N. Chan, H. Xue, K.K.W. Kan, N.T.K. Lee, C. Li, Y. Pang, M. Li, K.W.K. Tsim, H. Jiang, K. Chen, X. Li, Y. Han, Synergistic neuroprotection by bis(7)-tacrine via concurrent blockade of N-methyl-D-aspartate receptors and neuronal nitric-oxide synthase, Mol. Pharmacol. 71 (2007) 1258–1267, https://doi.org/10.1124/mol.106.029108.
[103] L. Dejmek, 7-MEOTA, 1990, pp. 126–129 (n.d.).
[104] R.A. Lenz, J.D. Baker, C. Locke, L.E. Rueter, E.G. Mohler, K. Wesnes, W. Abi-Saab, M.D. Saltarelli, The scopolamine model as a pharmacodynamic marker in early drug development, Psychopharmacology (Berl.) 220 (2012) 97–107, https://doi.org/10.1007/s00213-011-2456-4.
[105] J.J. Jackson, M.R. Soliman, Effects of tacrine (THA) on spatial reference memory and cholinergic enzymes in specific rat brain regions, Life Sci. 58 (1996) 47–54.
[106] A.M. Janas, S.C. Cunningham, K.B. Duffy, B.D. Devan, N.H. Greig, H.W. Holloway, Q.-S. Yu, A.L. Markowska, D.K. Ingram, E.L. Spangler, The cholinesterase inhibitor, phenserine, improves Morris water maze performance of scopolamine-treated rats, Life Sci. 76 (2005) 1073–1081, https://doi.org/10.1016/j.lfs.2004.06.028.
[107] J.B. Baell, G.A. Holloway, New substructure filters for removal of Pan assay interference compounds (PAINS) from screening libraries and for their exclusion in bioassays, J. Med. Chem. 53 (2010) 2719–2740, https://doi.org/10.1021/jm901137j.
[108] H. Naiki, K. Higuchi, K. Nakakuki, T. Takeda, Kinetic analysis of amyloid fibril polymerization in vitro, Lab. Investig. J. Tech. Methods Pathol. 65 (1991) 104–110.
[109] K. Sugano, H. Hamada, M. Machida, H. Ushio, High throughput prediction of oral absorption: improvement of the composition of the lipid solution used in parallel artificial membrane permeation assay, J. Biomol. Screen 6 (2001) 189–196, https://doi.org/10.1089/108705701300362728.
[110] J. Fang, R.B. Silverman, A cellular model for screening neuronal nitric oxide synthase inhibitors, Anal. Biochem. 390 (2009) 74–78, https://doi.org/10.1016/j.ab.2009.04.004.
[111] Guidance on Dose Level Selection for Regulatory General Toxicology Studies for Pharmaceuticals, (n.d.). https://www.norecopa.no/3r-guide/guidance-on-dose-level-selection-for-regulatory-general-toxicology-studies-for-pharmaceuticals (accessed June 22, 2018).
[112] B. Seyer, V. Pham, A.L. Albiston, S.Y. Chai, Cannula implantation into the lateral ventricle does not adversely affect recognition or spatial working memory, Neurosci. Lett. 628 (2016) 171–178, https://doi.org/10.1016/j.neulet.2016.06.034.

Biochemical Pharmacology 186 (2021) 114460

Contents lists available at ScienceDirect

Biochemical Pharmacology

journal homepage: www.elsevier.com/locate/biochempharm

7-phenoxytacrine is a dually acting drug with neuroprotective efficacy *in vivo*

Martina Kaniakova [a,b], Jan Korabecny [c,d], Kristina Holubova [a,e], Lenka Kleteckova [a,e], Marketa Chvojkova [a,e], Kristina Hakenova [e], Lukas Prchal [c], Martin Novak [c,f], Rafael Dolezal [c], Vendula Hepnarova [d], Barbora Svobodova [c,d], Tomas Kucera [d], Katarina Lichnerova [a,b], Barbora Krausova [b], Martin Horak [a,b,*], Karel Vales [a,e,*], Ondrej Soukup [c,*]

[a] Institute of Physiology of the Czech Academy of Sciences, Videnska 1083, 14220 Prague 4, Czech Republic
[b] Institute of Experimental Medicine of the Czech Academy of Sciences, Videnska 1083, 14220 Prague 4, Czech Republic
[c] Biomedical Research Center, University Hospital Hradec Kralove, Sokolska 581, 500 05 Hradec Kralove, Czech Republic
[d] Department of Toxicology and Military Pharmacy, Faculty of Military Health Sciences, University of Defence, Trebesska 1575, 500 01 Hradec Kralove, Czech Republic
[e] National Institute of Mental Health, Topolová 748, 250 67 Klecany, Czech Republic
[f] Department of Pharmaceutical Chemistry and Pharmaceutical Analysis, Faculty of Pharmacy, Charles University, Akademika Heyrovskeho 1203, 500 05 Hradec Kralove, Czech Republic

ARTICLE INFO

Keywords:
Behavioral experiment
Electrophysiology
Glutamate receptor
Mutation
Ion channel
Acetylcholinesterase

ABSTRACT

N-methyl-D-aspartaterecepro receptor (NMDARs) are a subclass of glutamate receptors, which play an essential role in excitatory neurotransmission, but their excessive overactivation by glutamate leads to excitotoxicity. NMDARs are hence a valid pharmacological target for the treatment of neurodegenerative disorders; however, novel drugs targeting NMDARs are often associated with specific psychotic side effects and abuse potential. Motivated by currently available treatment against neurodegenerative diseases involving the inhibitors of acetylcholinesterase (AChE) and NMDARs, administered also in combination, we developed a dually-acting compound 7-phenoxytacrine (7-PhO-THA) and evaluated its neuropsychopharmacological and drug-like properties for potential therapeutic use. Indeed, we have confirmed the dual potency of 7-PhO-THA, i.e. potent and balanced inhibition of both AChE and NMDARs. We discovered that it selectively inhibits the GluN1/GluN2B subtype of NMDARs via an ifenprodil-binding site, in addition to its voltage-dependent inhibitory effect at both GluN1/GluN2A and GluN1/GluN2B subtypes of NMDARs. Furthermore, whereas NMDA-induced lesion of the dorsal hippocampus confirmed potent anti-excitotoxic and neuroprotective efficacy, behavioral observations showed also a cholinergic component manifesting mainly in decreased hyperlocomotion. From the point of view of behavioral side effects, 7-PhO-THA managed to avoid these, notably those analogous to symptoms of schizophrenia. Thus, CNS availability and the overall behavioral profile are promising for subsequent investigation of therapeutic use.

1. Introduction

N-methyl-D-aspartate receptors (NMDARs) are a subclass of glutamate receptors playing an essential role in synaptic plasticity and excitatory neurotransmission [1,2]. However, they are often associated with their excessive activation, known as "excitotoxicity" and are also implicated in many disorders of the central nervous system (CNS), such as Alzheimer's disease (AD), Parkinson's disease, Huntington's disease, brain ischemia or multiple sclerosis [3]. Thus, NMDARs are a suitable target for the treatment of such CNS syndromes via the development of novel drugs with known mechanisms of action and known affinity to different NMDAR subtypes.

Most NMDARs are heterotetramers composed of the GluN1 and GluN2A-D subunits (GluN1/GluN2 type). They are activated by agonists

* Corresponding authors at: Department of Neurochemistry, Institute of Experimental Medicine of the Czech Academy of Sciences, Videnska 1083, 14220 Prague 4, Czech Republic (M. Horak); Center for Transfer Technologies and Applied Research of NIMH, National Institute of Mental Health, Topolova 748, 25067 Klecany, Czech Republic (K. Vales); Biomedical Research Center, University Hospital Hradec Kralove, Sokolska 581, 50005, Hradec Kralove, Czech Republic (O. Soukup).
E-mail addresses: martin.horak@iem.cas.cz (M. Horak), karel.vales@nudz.cz (K. Vales), ondrej.soukup@fnhk.cz (O. Soukup).

https://doi.org/10.1016/j.bcp.2021.114460
Received 20 December 2020; Received in revised form 29 January 2021; Accepted 29 January 2021
Available online 8 February 2021

of the glutamate binding site within the GluN2 subunit, and by co-agonists of the glycine-binding site within the GluN1 subunit [2]. GluN2A and GluN2B subunits are the most common GluN2 subunits expressed in the forebrain of postnatal animals [2,4]. All GluN subunits share the same membrane topology, namely an extracellular N-terminus comprising the amino terminal domain (ATD) and part of the ligand-binding domain, followed by four membrane domains (M1 - M4) with an ion channel formed by M2 and M3, and an intracellular C-terminus. The extracellular and membrane domain regions of the NMDARs are targets of many different inhibitory compounds, including those acting by competitive, allosteric and/or open-channel block mechanisms.

Many different allosteric inhibitors of NMDARs have been previously described, including a set of compounds acting via the ifenprodil-binding site within the GluN1/GluN2B receptors [5-7]. The major motivation in these studies was that it has been shown that the specific inhibitors of the GluN1/GluN2B receptors may decrease the negative effects of excitotoxicity [8] and ischemia [6]. Furthermore, it has been hypothesized that the particularly low expression levels of the GluN1/GluN2B type of NMDARs in the cerebellum may enhance the therapeutic action of GluN1/GluN2B-selective compounds while limiting their side effects [9]. However, human clinical trials with GluN1/GluN2B-selective compounds so far have not yielded satisfactory results, and clinical use has been restrained due to observed side effects similar to those of phencyclidine, raising concerns of abuse potential [10,11].

With respect to the open-channel blockers of NMDARs, it has been shown that ketamine shows hallucinogenic properties [12]; memantine is used for AD treatment; and dizocilpine (MK-801) is used in a pharmacologically-induced model of schizophrenia [13]. Indeed, the open-channel blockers differ in the precise mechanism of inhibitory action (namely "foot-in-the-door", "partial-trapping" or "trapping" mechanisms). However, it is not clear if the mechanism of inhibitory action affects the pharmacological manifestations of the open-channel blockers [14,15], but in any case, it seems likely that the open-channel blockers which do not interfere with normal synaptic transmission provide the best therapeutic profile [16].

1,2,3,4-tetrahydro-9-aminoacridine (tacrine; THA) was the first FDA approved drug for AD treatment, indirectly stimulating the cholinergic system via inhibition of acetylcholinesterase (AChE). However, the underlying mechanism is more complex and seems to involve interaction with other targets [17]. Our previous study on the effect of THA and its derivatives on NMDARs revealed an interesting voltage-dependent mechanism of action at the NMDARs, which together with AChE inhibition may explain the beneficial effect on symptoms of AD [14]. However, THA was later withdrawn from the market due to its hepatotoxicity and other side effects [18]. Subsequently, to avoid the hepatotoxic effect of THA, the 7-methoxy derivative of THA (7-MEOTA) was developed as a pharmacologically similar compound [19,20]. 7-MEOTA passed clinical trial stage I and stage II, with recommendation for stage III, [21], however further development was stopped. We have recently shown that 7-MEOTA is CNS permeable and a potent "foot-in-the-door" blocker of NMDARs, exerting neuroprotective efficacy *in vivo* with no behavioral side effects [15]. However, as a drawback of its dual action (i.e. inhibition of AChE and NMDARs), 7-MEOTA is characterized by i) a higher selectivity towards GluN2A subunit containing NMDARs; and ii) preferential inhibition of NMDARs ($IC_{50} = 3$ μM for GluN1/GluN2A type [15]) rather than AChE ($IC_{50} = 15$ μM [19]).

One of the major paradigms of modern multi-target directed ligand strategy, which aims to develop novel drugs capable of hitting at least two different levels of disease pathophysiology, is that the affinity of a drug to the targets is balanced [22]. One frequently cited approach is the simultaneous blockade of AChE and NMDARs [23-25]. However, so called "hybrid compounds", linking two distinct pharmacophores by a carbon chain or by other types of chains, usually do not exhibit drug-like properties, displaying deficiencies such as water insolubility, off-targeting, and low permeability to the brain. Therefore, reducing the size of the molecule while preserving its multi-targeting character seems to be the most promising approach.

Motivated by the beneficial effect of 7-MEOTA, we focused on the development of a derivative of THA showing even better pharmacological properties. We have developed 7-phenoxytacrine (7-PhO-THA) and examined its inhibitory effect on AChE using Ellman's assay and on various types of recombinant NMDARs by electrophysiology. In addition, we assessed its basic pharmacokinetic parameters, its neuroprotective activity in a model of NMDA-induced lesion of the rat dorsal hippocampus, and its effect on the hyperlocomotion induced by the administration of MK-801 in rats. Together, our experimental data showed that 7-PhO-THA is a promising compound which acts beneficially at both glutamatergic and cholinergic systems, with favorable *in vivo* characteristics, and with potential for use in the treatment of neurodegenerative diseases and other disorders associated with glutamatergic excitotoxicity.

2. Materials and methods

2.1. Chemical synthesis of 7-PhO-THA

All chemical reagents used were purchased from Sigma-Aldrich (Prague, Czech Republic). Organic solvents for synthesis were obtained from Penta Chemicals Co (Prague, Czech Republic). The reactions were monitored by thin layer chromatography (TLC) on aluminium plates precoated with silica gel 60 F254 (Merck, Prague, Czech Republic) and visualized by UV 254. Melting points were determined using microheating stage PHMK 05 (VEB Kombinant Nagema, Radebeul, Germany) and are uncorrected. Uncalibrated purity was ascertained by ultra-high-performance liquid chromatography (UHPLC) using a reverse phase C18 chromatographic column with UV detection at wavelength 254 nm. The final compound exhibited purity of 99.8%. Nuclear magnetic resonance (NMR) spectra were recorded on a Varian S500 spectrometer (operating at 500 MHz for ^{1}H and 126 MHz for ^{13}C; Varian Comp. Palo Alto, USA). For ^{1}H δ are given in parts per million (ppm) relative to $CDCl_3$ ($\delta = 7.26$), CD_3OD ($\delta = 3.31$) or DMSO-d_6 ($\delta = 2.50$), and for ^{13}C relative to $CDCl_3$ ($\delta = 77.00$), CD_3OD ($\delta = 49.05$) or DMSO-d_6 ($\delta = 39.52$). Spin multiplicities are given as s (singlet), bs (broad singlet), d (doublet), dd (doublet of doublets), t (triplet), or m (multiplet) and coupling constants (*J*) are reported in Hertz (Hz). High-resolution mass spectra (HRMS) were determined by Q Exactive Plus hybrid quadrupole-orbitrap spectrometer.

2.1.1. 7-phenoxy-1,2,3,4,9,10-hexahydroacridin-9-one (1)

4-Phenoxyaniline (5.00 g; 26.99 mmol), ethyl 2-oxocyclohexane-1-carboxylate (5.05 g; 29.69 mmol) and *p*-toluenesulfonic acid monohydrate (0.15 g; cat.) were dissolved in toluene (150 ml) and heated at 150 °C under Dean-Stark trap overnight to collect water. The reaction mixture was cooled to room temperature and the solvent evaporated under reduced pressure. Diphenyl ether (80 mL) was added and the reaction mixture heated for 2 h at 230–240 °C using a Dean-Stark apparatus. After cooling to room temperature, 100 mL of hexane was slowly added, observing the precipitation of intermediate **1**. The product was collected by filtration and washed with hexane (2 × 100 mL) to give the title compound as a yellow solid (6.70 g; 85% yield). The compound was immediately used without further purification in the next step. Chemical structure and purity were verified by HPLC/HRMS: HRMS $[M + H]^+$: 292.1324 (calculated for $[C_{19}H_{18}NO_2]^+$: 292.1293); HPLC purity 95.4%.

2.1.2. 9-chloro-7-phenoxy-1,2,3,4-tetrahydroacridine (2)

Intermediate **1** (6.70 g; 22.99 mmol) was put into a 250 mL round-bottom boiling flask and cooled to 0 °C. $POCl_3$ (31.73 g; 0.21 mol) was added dropwise over 15 min with vigorous stirring. The reaction mixture was cooled for another 15 min and then heated at reflux (130 °C) for 1 h. $POCl_3$ was then removed by distillation under reduced pressure. The organic residue was dissolved in dichloromethane (150

ml) and poured into a beaker containing 200 g of drifting ice and 100 ml of concentrated ammonia solution (25% aqueous solution). The mixture was then stirred for 1 h at room temperature with slow spontaneous ice melting, with more drifting ice added as necessary to control the exothermic reaction. The organic layer was washed with water (150 mL) and brine (150 mL), and dried with anhydrous sodium sulphate. Solvent was removed under reduced pressure and the crude mixture purified using column chromatography with petroleum ether: ethyl acetate (4:1) as mobile phase to obtain compound **2** as a yellowish oil (6.77 g; 95%)

^{1}H NMR (500 MHz, Chloroform-*d*) δ 7.95 (d, J = 9.1 Hz, 1H), 7.63 (d, J = 2.7 Hz, 1H), 7.40 (dd, J = 9.1, 2.7 Hz, 1H), 7.38 – 7.33 (m, 2H), 7.18 – 7.12 (m, 1H), 7.10 – 7.05 (m, 2H), 3.14 – 3.03 (m, 2H), 2.99 – 2.89 (m, 2H), 1.97 – 1.83 (m, 4H); ^{13}C (126 MHz, Chloroform-*d*) δ 157.88, 156.62, 155.41, 143.42, 140.21, 130.58, 129.80, 129.11, 126.16, 123.69, 122.77, 119.07, 109.87, 33.85, 27.42, 22.56, 22.48; HRMS $[M + H]^+$: 311.0894 (calculated for $[C_{19}H_{17}ClNO]^+$: 311.0891); HPLC purity 97.3%.

2.1.3. 7-phenoxy-1,2,3,4-tetrahydroacridin-9-amine hydrochloride (7-PhO-THA)

Compound **2** (6.75 g; 21.79 mmol) and phenol (18.94 g; 0.20 mol) were placed into a two-necked 250 mL round-bottom flask and heated to 180 °C. On reaching 180 °C, the reaction mixture was continuously bubbled with ammonia gas for 2 h. The progress of the reaction was monitored with TLC (hexane: ethyl acetate = 1:1). After the reaction was complete, the mixture was cooled to room temperature, diluted with dichloromethane (150 mL), and washed with 2 M NaOH solution (2 × 150 mL), water (100 mL), and brine (100 mL). The organic layer was dried with anhydrous sodium sulphate and the solvent removed by distillation under reduced pressure. The crude reaction mixture was purified using silica gel column chromatography, eluting with hexane: ethyl acetate (95:5 → 90:10). 7-PhO-THA was obtained as a yellow amorphous solid which was then converted to its salt using a 1 M solution of hydrochloric acid in methanol (5.55 g; 78%).

m.p. 142.5–143.8 °C; ^{1}H NMR (500 MHz, DMSO-d_6) δ 8.24 (d, J = 2.2 Hz, 1H), 8.05 (d, J = 9.2 Hz, 1H), 7.64 – 7.54 (m, 1H), 7.41 (tt, J = 7.4, 1.1 Hz, 2H), 7.16 (tt, J = 7.4, 1.1 Hz, 1H), 7.08 – 6.97 (m, 2H), 3.06 – 2.95 (m, 2H), 2.57 – 2.51 (m, 2H), 1.89 – 1.75 (m, 4H); ^{13}C NMR (126 MHz, DMSO-d_6) δ 157.02, 154.79, 153.48, 150.91, 134.01, 130.34, 126.15, 123.79, 121.66, 118.22, 116.11, 112.02, 109.13, 27.81, 22.82, 21.22, 20.68; HRMS $[M + H]^+$: 291.1484 (calculated for $[C_{19}H_{19}N_2O]^+$: 291.1453); HPLC purity: 99.8%

2.2. In vitro anti-cholinesterase assay

The inhibitory activity of 7-PhO-THA and all the reference drugs against human recombinant AChE (hAChE, E.C. 3.1.1.7, purchased from Sigma-Aldrich, Prague, Czech Republic) and human plasmatic butyrylcholinesterase (hBChE, E.C. 3.1.1.8, purchased from Sigma-Aldrich, Prague, Czech Republic) were assessed using modified Ellman's method [26]. Results are expressed as IC_{50} values (the concentration of the compound that cause reduction by 50% of cholinesterase (ChE) activity). The other compounds used – phosphate buffer solution (PBS, pH = 7.4), 5,5′-dithio-bis(2-nitrobenzoic) acid (Ellman's reagent, DTNB), acetylthiocholine (ATCh) and butyrylthiocholine (BTCh) – were also commercially available and were purchased from Sigma-Aldrich (Prague, Czech Republic). For the assessment, 96-well polystyrene microplates (ThermoFisher Scientific, Waltham, MA, USA) were used. Solutions of the corresponding enzyme in PBS were prepared up to a final activity of 0.002 U/μl. The assay medium consisted of either hAChE or hBChE (10 μl), DTNB (20 μl of 0.01 M solution) and PBS (40 μl of 0.10 M solution). Solutions of the tested compounds (10 μl of different concentrations) were pre-incubated for 5 min in the assay medium, then addition of substrate solution (20 μl of 0.01 M ATCh or BTCh iodide solution) started the reaction. The absorbance was measured at 412 nm using a Multimode microplate reader Synergy 2 (BioTek Inc., Winooski, VT, USA). For calculation of the percentage inhibition of activity (I), the following formula was used:

$$I = \left(1 - \frac{\Delta A_i}{\Delta A_0}\right) \times 100[\%]$$

where ΔA_i indicates the absorbance change provided in the presence of inhibitor, and ΔA_0 indicates the absorbance change when a solution of PBS was added instead of a solution of inhibitor (absence of inhibitor). Software Microsoft Excel 10 (Microsoft Corporation, Redmont, WA, USA) and GraphPad Prism version 5.02 for Windows (GraphPad Software, San Diego, CA, USA) were used for evaluation of the statistical data.

2.3. Molecular biology

The cDNA vectors for expression of rat versions of GluN1-1a, GluN2A and GluN2B subunits have been described previously [27,28]. GluN1-ΔATD, GluN2A-ΔATD and GluN2B-ΔATD constructs with 354 amino acids of the ATDs deleted (32 to 386) were either introduced previously (GluN1-ΔATD, GluN2B-ΔATD) or were generated (GluN2A-ΔATD) as described [29]. The GluN1-Y109C construct was generated by site-directed mutagenesis using an established approach and was verified by DNA sequencing.

2.4. Mammalian cell culture and transfection

Human embryonic kidney 293 (HEK293) cells were kept in Opti-MEM I medium containing 5% foetal bovine serum (FBS; v/v) and transfected with cDNA constructs carrying the GluN subunits and green fluorescent protein using Lipofectamine 2000 (Thermo Fisher Scientific), according to protocol described previously [27,28]. For the experiment, the cells were trypsinised, re-suspended in Opti-MEM I containing 1% FBS, 20 mM $MgCl_2$, 1 mM D,L-2-amino-5-phosphonopentanoic acid, and 3 mM kynurenic acid (to inhibit excessive activation of NMDARs during cell culturing) and plated on poly-L-lysine-coated glass coverslips. Experiments were performed within 24–48 h after transfection.

2.5. Electrophysiology

Whole-cell patch-clamp recordings using HEK293 cells were performed using an Axopatch 200B patch-clamp amplifier (Molecular Devices, San Jose, California, USA), combined with a microprocessor-controlled multi-barrel rapid perfusion system with a time constant for solution exchange around the cell of ~20 ms [28]. Glass patch pipettes of 3–6 MΩ tip resistance were produced by the model P-97 horizontal micropipette puller (Sutter Instrument Co, Novato, California, USA). The extracellular solution (ECS) contained (in mM): 160 NaCl, 2.5 KCl, 10 HEPES, 10 glucose, 0.2 EDTA, and 0.7 $CaCl_2$ (pH adjusted to 7.3 with NaOH). The intracellular recording solution contained (in mM): 125 gluconic acid, 15 CsCl, 5 BAPTA, 10 HEPES, 3 $MgCl_2$, 0.5 $CaCl_2$, and 2 ATP-Mg salt (pH adjusted to 7.2 with CsOH) (all reagents from Sigma Aldrich, Czech Republic). Currents were filtered at 2 kHz with an eight-pole low-pass Bessel filter and digitized at 5 kHz with a Digidata 1322A using pClamp 9 software (Molecular Devices, San Jose, California, USA). A stock solution of 7-PhO-THA (10 mM) was prepared fresh before each experiment by dissolving in dimethyl sulfoxide (DMSO). The final concentration of DMSO was 1% (v/v) in all control and tested ECS. All experiments were performed at room temperature. The inhibition curves for 7-PhO-THA at the NMDARs were obtained using *Equation 1*:

$I = 1/(1 + ([7\text{-PhO-THA}]/IC_{50})^h)$

where [7-PhO-THA] is the 7-PhO-THA concentration, IC_{50} is the concentration of 7-PhO-THA that produces a 50% inhibition of agonist-evoked current, and h is the apparent Hill coefficient. Data were statistically analyzed by Student's t-test (the level of significance was set to p

< 0.05) using SigmaStat 3.5 (Systat Software Inc., San Jose, California).

2.6. Docking study

The structure of GluN1-GluN2B ATD was obtained from RCSB Protein Data Bank – PDB ID: 5EWM [5]. Receptor structure was prepared by the DockPrep function of UCSF Chimera (version 1.4) and converted to pdbqt-files by AutodockTools (v. 1.5.6) [30,31]. Flexible residues selection was made spherically in the region around the binding cavity of EVT-101 [5]. Three-dimensional structures of ligands were built by Open Babel (v. 2.3.1), then minimized by Avogadro (v 1.1.0), and converted to pdbqt-file format using AutodockTools [32]. The docking calculations were made by using Autodock Vina (v. 1.1.2) with exhaustiveness of 8 [33]. Calculation was repeated 20 times and the best-scored result was selected for manual inspection. The enzyme-ligand interaction visualization interactions was prepared using the PyMOL Molecular Graphics System, Version 2.0 (Schrödinger, LLC, Mannheim, Germany). The 2D diagram was created with Dassault Systèmes BIOVIA, Discovery Studio Visualizer, v 17.2.0.16349 (San Diego: Dassault Systèmes, 2016).

2.7. In vivo pharmacokinetic study

All the animal experiments were performed after approval of the local Ethical Committee.

Solvents and other common chemicals were purchased from Sigma-Aldrich (Prague, Czech Republic). Solvents for chromatographic procedures were supplied in LC-MS grade. 6chlorotacrine (6-Cl-THA) was synthesized *de novo* at the same department and used as the internal standard.

48 male Wistar rats (2–3 months, 200–300 g, Velaz Ltd., Czech Republic) were injected i.p. with 7-PhO-THA at a dose of 24 $mg{\cdot}kg^{-1}$. Rats (6 animals per group) were sacrificed at different intervals of 10, 20, 40, 60, 90, 180, 240 min, and 24 h after administration, and several animals were used for zero time or blank control. The rats were then bled out and plasma and brains were collected from each animal. Plasma was heparinized and centrifuged; brains were perfused with saline and kept at −80 °C in a freezer prior to sample preparation and assessment.

Brains were weighed and PBS in ratio 1:4 was added. The brains were subsequently homogenised by T-25 Ultra Turrax disperser (IKA, Staufen, Germany), ultrasonicated by UP 50H needle homogeniser (Hielscher, Teltow, Germany), and stored at 80 °C prior to the next step.

Either plasma (180 μl) or brain homogenate was spiked with 10 μl of internal standard (IS; 6-Cl-THA in methanol), so that the final concentration was 100 $\mu g{\cdot}ml^{-1}$, the sample was then alkalized with 100 μl of 20% (w/w) sodium hydroxide, and 1600 μl of dichloromethane added. The samples were then shaken for 2 h and centrifuged. The lower layer was transferred to a 2 ml Eppendorf microtube and evaporated in a CentriVap concentrator (Labconco Corporation, Kansas City, USA). Dried samples were resuspended in 50 μl of 10% (v/v) DMSO. Samples for calibration were prepared by spiking 190 μl of plasma or brain homogenate from blank animals with either 10 μl of 7-PhO-THA solution in methanol (final concentrations from 0.1 to 500 $\mu g{\cdot}ml^{-1}$) or 10 μl of IS (final concentration 0.5 $\mu g{\cdot}ml^{1}$); they were then extracted as described above.

Compound levels in plasma and brain homogenate were measured by UHPLC with UV detection and mass spectrometry (MS) detection. Analysis was performed using a Dionex UltiMate 3000 RS UHPLC chromatograph, consisting of a high-pressure RS pump module, RS autosampler module, RS column compartment module, and RS variable wavelength detector controlled by Chromeleon 6.80 (SR13, build 3967) software (Thermo Scientific, Waltham, USA). The mass spectrometer used was Q Exactive Plus Orbitrap controlled by Thermo Xcalibur (version 3.1.66.10.) software (Thermo Scientific) with heated electrospray ionization.

Data were obtained by the reverse phase gradient elution method with mobile phase A: 0.1% (v/v) formic acid in ultrapure water, prepared by Barnstead Smart2Pure 3 UV/UF apparatus (resistance 18.2 MΩ.cm at 25 °C, Thermo Scientific); and mobile phase B: 0.1% (v/v) formic acid in LC-MS grade acetonitrile. The mobile phase flow was set to 0.4 $ml{\cdot}min^{-1}$ and the gradient protocol was as follows: elution started with 10% B isocratic flow for 3 min, followed by the gradient flow of 10% B to 100% over 7 min; flow was then 100% B isocratic for 2 min; the flow then returned to 10% B isocratic flow, equilibrating for 3 min. The column used was C18 Phenomenex Kinetex (3.0 × 150 mm; 2.6 μm; 100 Å; Phenomenex, Japan), heated to 35 °C. The injection volume was 5 μl. UV spectra were measured at wavelength 254 nm. The chromatograph was connected to the MS by heated electrospray ion source with the following settings: spray voltage 3.5 kV; capillary temperature: 262 °C; sheath gas: 40 arbitrary units; auxiliary gas: 12.5 arbitrary units; spare gas: 3 arbitrary units; probe heater temperature: 350 °C; max spray current: 100 μA; S-lens RF Level: 50. MS detection was performed on the total ion current in the scan range 200–300 m/z with the following settings: resolution 70 000; AGC target 5e6; maximum ion trapping time 200 ms. Substances were identified according to their high-resolution mass to charge ratio, which was 233.0841 for 6-Cl-THA (IS) and 291.1491 for 7-PhO-THA. The retention time for 6-Cl-THA (IS) was 6.5 min and for 7-PhO-THA was 7.2 min. The calibration range of standard samples was prepared by dissolution of 7-PhO-THA and 6ClTHA in methanol. Calibration was linear across its 10 pointrange from 0.1 to 100 $\mu g{\cdot}ml^{-1}$. Calculations were performed using GraphPad Prism 6.05 and Microsoft Excel 2010 with PK solver extension [34].

2.8. Behavioral experiments

2.8.1. Animals and drugs

Adult male Wistar rats (3–4 months, 360–450 g) were used for the behavioral experiments. The rats were obtained from Velaz Ltd. and accommodated in the animal facility in The National Institute of Mental Health. They were housed in pairs in transparent plastic boxes (23 × 38 × 23 cm) in an air-conditioned animal room (temperature: 22 ± 1 °C; humidity: 50–60%) with a 12-h light cycle (lights on at 6:00), and with free access to food and water. All experiments were performed in the light phase of the day after a week-long acclimatization period. Experiments were conducted in accordance with the guidelines of European Union directive 2010/63/EU and approved by the Animal Care and Use Committee which possesses the National Institutes of Health Statement of Compliance with Standards for Humane Care and Use of Laboratory Animals.

7-PhO-THA was dissolved in 5% DMSO and redistilled water. Doses of 5 $mg.kg^{-1}$ and 10 $mg.kg^{-1}$ were prepared. As control, the solution of 5% DMSO and redistilled water was used. MK-801 was dissolved in saline and administered at doses of 0.1 $mg.kg^{-1}$ and 0.3 $mg.kg^{-1}$, and saline was used as control. All rats received two i.p. injections – 7-PhO-THA (or DMSO) and MK-801 (or saline). The injection volume was 1 ml. kg^{-1}.

The rats were randomly assigned into one of six experimental groups classified according to the treatment: NaCl + DMSO, NaCl + 7-PhO-THA (5 $mg.kg^{-1}$), NaCl + 7-PhO-THA (10 $mg.kg^{-1}$), MK-801 + DMSO, MK-801 + 7-PhO-THA (5 $mg.kg^{-1}$), MK-801 + 7-PhO-THA (10 $mg.kg^{-1}$). The dose of MK-801 was 0.3 $mg.kg^{-1}$ in the open field test (OF) and 0.1 $mg.kg^{-1}$ in the elevated plus maze test (EPM). The drugs were applied *i.p.*, 30 min before the experiments. The experiments were statistically analyzed in GraphPad Prism 5.0 by two-way ANOVA with phenotype (NaCl/MK-801) and treatment (7-PhO-THA/DMSO) as independent factors. Outliers were excluded from the analysis. When appropriate, Bonferroni post-hoc correction was applied. In the graphs data are shown as mean + S.E.M. and the level of significance was set at $p < 0.05$.

2.8.2. Open field (OF)

A black plastic square (80 × 80 cm) OF apparatus was used. The rat was placed in a corner of the OF apparatus and its position was

monitored by EthoVision software (Noldus, Netherlands) for 10 min. Subsequently, the total path moved was analyzed by EthoVision software. The number n of animals per group was as follows: $n = 8$ animals in groups NaCl + DMSO, NaCl + 7-PhO-THA (10 mg.kg^{-1}), MK-801 + DMSO, MK-801 + 7-PhO-THA (10 mg.kg^{-1}) and $n = 6$ animals in groups NaCl + 7-PhO-THA (5 mg.kg^{-1}) and MK-801 + 7-PhO-THA (5 mg.kg^{-1}).

2.8.3. Elevated plus maze (EPM)

A plus-shaped EPM apparatus with two open and two closed (wall 35 cm high) arms was used (each arm length 40 cm, width 15 cm, elevated 47 cm above the floor). It was made of black plastic. The rat was placed in the center of the apparatus facing a closed arm. Its position was monitored by EthoVision software for 10 min. Subsequently, time spent in the open arms of the EPM and total path moved were analyzed by EthoVision software. The number of animals in each group was $n = 8$.

2.9. NMDA-induced lesion in rats

Experiments were conducted in accordance with the guidelines of the European Union directive 2010/63/EU and approved by the Animal Care and Use Committee which possesses the National Institutes of Health Statement of Compliance with Standards for Humane Care and Use of Laboratory Animals.

Adult male Wistar rats (250–350 g) were used for experiments to assess the neuroprotective activity of 7-PhO-THA. The rats were kept in a controlled environment as described above in section 2.8.1. NMDA was dissolved in sterile 10 mM PBS to a final concentration of 25 mM. 7-PhO-THA was diluted in sterile 0.9% physiological saline solution containing 3% DMSO to a final concentration of 30 μM. Memantine was diluted in sterile 0.9% physiological saline to a final concentration of 30 μM. The solutions containing NMDA at 25 mM and 7-PhO-THA / memantine at 30 μM were mixed thoroughly in a 1:1 ratio. Surgery was performed under 2.0–2.5% isoflurane anesthesia (Abbot Laboratories, Chicago, USA) with initial anesthesia of 3.5% isoflurane. The animals were mounted onto the stereotaxic apparatus (TSE Systems, Bad Homburg, Germany), medical petroleum jelly (Vaseline®, Unilever, London, United Kingdom) was used to cover the eyes, hair was shaved from the area, and the scalp was incised. The hole for the infusion application was drilled unilaterally at coordinates −4.0 mm AP and 2.5 mm ML relative to the bregma point according to the rat brain atlas of Paxinos and Watson (2004). A Hamilton syringe (No. 7635–01, Hamilton, Nevada, USA) was placed into the right dorsal hippocampus (DV = 4.6 mm). A pump (model 540,310 plus; TSE Systems, Bad Homburg, Germany) was used for mixed solutions infusion at a constant flow rate of 0.25 μl.min^{-1} to a total volume of the mixed solutions of 2 μl.

The control group of animals received a mixed solution of NMDA (25 mM) and sterile saline, and the second group received a mixed solution of 10 mM PBS and sterile saline. A total $n = 27$ animals were used for the experiment: $n = 7$ animals in each of the groups PBS + NaCl, NMDA + NaCl, and NMDA + memantine; and $n = 6$ animals in the group NMDA + 7-PhO-THA. After the surgery, the animals had free access to food and water containing analgesics. 24 h after the application, the rats were euthanized by overdose by the anesthetics Narketan (ketamine, 100 mg.ml^{-1}) and Rometar (xylazine, 20 mg.ml^{-1}), and were transcardially perfused with 4% paraformaldehyde (PFA). Then, the brains were post-fixed in 4% PFA for 24 h and subsequently cryoprotected in gradually increasing concentrations of sucrose solution (10, 20 and 30%). Brain slices were done in the coronal plane (50 μm, 1-in-5 series); all sections were collected and stored at −20 °C in the cryoprotective buffer solution. The slices were used for the evaluation of damage in the hippocampus using the Fluoro Jade B (FJB) method [35]. The hippocampal damage was scored in the following hippocampal regions: granular cell layer of the dentate gyrus lower part (DGl), the granular cell layer of the dentate gyrus higher part (DGh), the hilus, CA3, and CA1, as described previously [15,36]. Scores ranged from 0 to 4 according to the percentage of the area damaged: 0: 0–5%; 1: 6–25%; 2: 26–50%; 3: 51–75%; 4: >75% damaged. 17 – 20 slices were evaluated for each hippocampus.

3. Results

3.1. Synthesis

7-PhO-THA was prepared in three-step chemical synthesis according to the previously described method [37]. The procedure is outlined in Fig. 1. The initial step involved cyclocondensation of 4-phenoxyaniline with ethyl 2-oxocyclohexane-1-carboxylate to obtain 7-phenoxy-1,2,3,4,9,10-hexahydroacridin-9-one (**1**). Compound **1** was than chlorinated with $POCl_3$ to yield 9-chloro-7-phenoxy-1,2,3,4-tetrahydroacridine (**2**) almost quantitatively (95%). The final step introduced a primary amino-group under nucleophilic substitution conditions in phenol resulting in 7-PhO-THA base, which after the treatment with 1 M solution of hydrochloric acid solution formed the hydrochloride salt in good overall yield (63%).

3.2. In vitro anti-cholinesterase assay

Modified Ellman's method was applied to assess the inhibitory potency of 7-PhO-THA and its parent compounds. 7-PhO-THA showed moderate and non-selective potency towards hAChE and hBChE. Although being almost 3-orders of magnitude less potent than donepezil [38], the affinity was higher than in the case of 7–MEOTA. Furthermore, balanced and moderate activity is beneficial in the case of a suggested multi-target directed mechanism of action. The inhibitory potency is summarized in Table 1.

3.3. Mechanism of action of 7-PhO-THA at NMDARs

Our recent data showed that both THA and 7-MEOTA are "foot-in-the-door" open-channel blockers of the NMDARs [15]. Here, we aimed to examine the mechanism of inhibition by 7-PhO-THA at GluN1/GluN2A and GluN1/GluN2B receptors (at the responses induced by a saturating concentration of 1 mM glutamate and 50 μM glycine). We measured the dose–response curves for the inhibitory effect of 7-PhO-THA (0.3–100 μM) at membrane potentials of −60 mV, −20 mV and +40 mV (Fig. 2A-D). These experiments showed that i) 7-PhO-THA inhibited GluN1/GluN2A receptors, but not GluN1/GluN2B receptors, in a voltage-dependent manner, and ii) 7-PhO-THA exhibited profoundly lower IC_{50} values at the GluN1/GluN2B receptors compared with the GluN1/GluN2A receptors (Table 2; $p < 0.001$ for all tested membrane potentials; Student's *t*-test). These data indicate that 7-PhO-THA inhibits the GluN1/GluN2B receptors by a different mechanism of action compared with the GluN1/GluN2A receptors.

There are many GluN1/GluN2B receptor-specific pharmacological compounds which act via an ifenprodil-binding site present within the ATDs of the GluN subunits [2,5]. In the next set of experiments, we aimed to examine if 7-PhO-THA acts via the ifenprodil-binding site within the GluN1/GluN2B receptors. Therefore, we co-expressed GluN1/GluN2B receptors lacking the ATDs (GluN1-ΔATD/GluN2B-ΔATD receptors) in the HEK293 cells and examined the inhibitory effect of 7-PhO-THA using the same approach as above. In this experiment, we observed that 7-PhO-THA inhibited the GluN1-ΔATD/GluN2B-ΔATD receptors both in a voltage-dependent manner, and with similar IC_{50} value to the GluN1/GluN2A receptors (Fig. 2EG; Table 2). Furthermore, the GluN1/GluN2A receptors lacking the ATDs (GluN1-ΔATD/GluN2A-ΔATD receptors) did not exhibit an altered IC_{50} value for 7-PhO-THA at a membrane potential of −60 mV when compared with the wild-type GluN1/GluN2A receptors (Fig. 2H,I; Table 2; $p = 0.867$; Student's *t*-test). All of these findings are compatible with our hypothesis that 7-PhO-THA acts via the ifenprodil-binding site within the GluN1/GluN2B receptors. A previous study showed that the GluN1-Y109 residue is critical for the inhibitory effect of the specific inhibitors at the

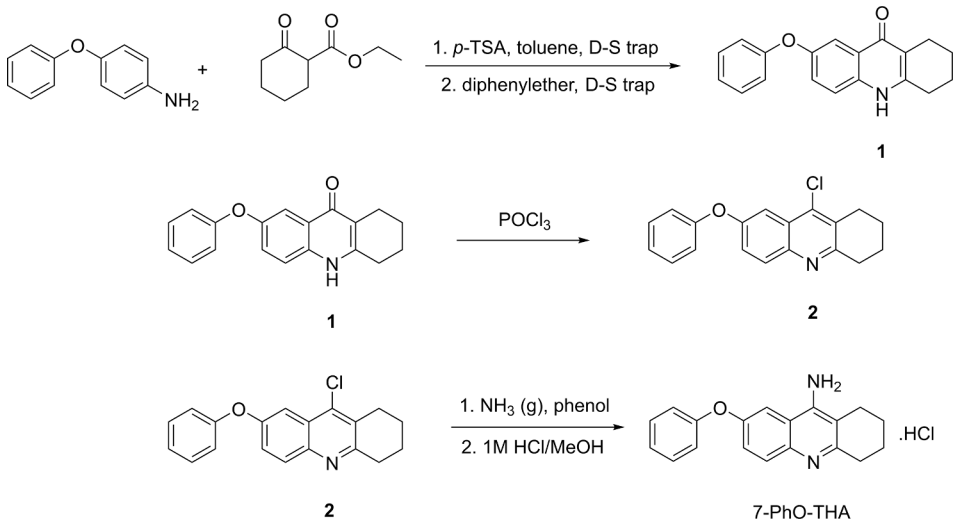

Fig. 1. Three-step chemical synthesis of 7-PhO-THA. For detailed conditions see Materials and Methods.

Table 1
In vitro anti-cholinesterase activity of 7-PhO-THA, THA and 7-MEOTA.

Compound	*h*AChE IC_{50} ± S.E.M. (μM)	*h*BChE IC_{50} ± S.E.M. (μM)
7-PhO-THA	2.40 ± 1.8	4.9 ± 3.3
THA	0.32 ± 0.01	0.22 ± 0.01
7-MEOTA	15.0 ± 2.4	21.0 ± 3.4

GluN1/GluN2B receptors [5]. Therefore, we examined the inhibitory effect of 7-PhO-THA at the GluN1-Y109C/GluN2B receptors expressed in the HEK293 cells. Indeed, 7-PhO-THA exhibited a similar IC_{50} value for inhibition at the GluN1-Y109C/GluN2B receptors at a membrane potential of −60 mV when compared with the GluN1-ΔATD/GluN2B-ΔATD receptors (Fig. 2J,K; Table 2; p = 1.000; Student's *t*-test). Together, we conclude that 7-PhO-THA potently inhibits the GluN1/GluN2B receptors via an ifenprodil-binding site, in addition to its voltage-dependent inhibitory effect at both GluN1/GluN2A and GluN1/GluN2B receptors. Thus, the 7-PhO-THA has a unique mechanism of action at the NMDARs when compared with THA and 7-MEOTA.

3.4. Docking studies

To investigate the binding pattern of 7-PhO-THA at the NMDAR, we performed molecular modeling simulation at the ATDs of GluN1 and GluN2B subunits. Initially, we selected a suitable crystallographic template deposited under PDB entry 5EWM from Protein Data Bank (2.76 Å resolution) [39]. This model was previously used for docking of EVT-101, a potent and highly selective GluN2B antagonist [40]. Our top-scored docking pose for 7-PhO-THA (-11.8 kcal/mol) nested the ligand into the cavity more resembling complex of the ifenprodil-GluN2B rather than of EVT-101-GluN2B (Fig. 3). Indeed, the 1,2,3,4-tetrahydroacridine core of 7-PhO-THA is anchored via several distinct hydrophobic interactions. Among them, the GluN1(Phe113, Ile133) and GluN2B(Glu106, Gln110, Phe176) residues enabled van der Waals interaction, the GluN1(Phe113) residue displayed a T-shaped π-π interaction at 3.8 Å distance, and the GluN1(Leu135) residue established π-alkyl/alkyl-alkyl attractive intermolecular forces. More importantly, the 7-phenoxy appendage of 7-PhO-THA binds to the same cavity as the 4-benzylpiperidine residue of ifenprodil or the 5-[3-(difluormethyl)-4-fluorphenyl] residue of EVT-101 [39]. Having said that, the 7-phenoxy moiety of 7-PhO-THA revealed favorable albeit distorted π-π interactions to GluN2B(Phe114) (5.3 Å; distance measured from ring-to-ring center) and GluN1(Tyr109) (4.9 Å) residues. Other key mediators, GluN1(Thr110) and GluN2B(Ile111) residues, orchestrated further hydrophobic contact. It has been previously shown that ifenprodil, a potent and selective GluN1/GluN2B receptor antagonist, occupies a heteromeric interface of the so-called phenylethanolamine binding site between GluN1 ATD upper lobe and GluN2B lower lobe [41]. The binding patterns of EVT-101 and ifenprodil differ slightly from each other. Specifically, EVT-101, unlike ifenprodil, makes minimal contact with the GluN2B ATD lower lobe [5]. Taking into consideration our results obtained herein, we presume that 7-PhO-THA adopts occupancy in the binding pocket more closely resembling the ifenprodil arrangement in the crystal structure of the GluN1-GluN2B ATD interface.

3.5. Pharmakokinetics of 7-PhO-THA

Pharmacokinetic experiments were performed on rats by injecting i.p. 24 $mg \cdot kg^{-1}$ of 7-PhO-THA, which in a separate experiment (data not shown) was found to be a tolerated dose, and its concentration levels were measured in the plasma and brain tissue by UHPLC-MS at time points of 0, 10, 20, 40, 60, 90, 180, 240 min, and 24 h (a group of 6 animals per each time point). Time profiles of plasma and brain tissue levels of 7-PhO-THA are shown in Fig. 4 and basic pharmacokinetic parameters are summarized in Table 3. The maximal concentration of 7-PhO-THA in both tissues was reached in our experiment in 20^{th} minute after administration. Plasma concentrations are about 3 times higher than those found in brain tissue. The half-life in both tissues was approximately 50 min. After 24 h, detectable concentrations (0.39 $\mu g \cdot ml^{-1}$) were found only in the brain tissue.

3.6. Behavioral assessment

In the OF test we investigated the effect of 7-PhO-THA on locomotion and whether 7-PhO-THA can alleviate the hyperlocomotion caused by MK-801 (0.3 $mg \cdot kg^{-1}$). Analysis of the path moved in OF showed a statistically significant effect of treatment with 7-PhO-THA ($F(2, 38) = 7.90$, $p = 0.0013$; two-way ANOVA) and change of phenotype caused by application of MK-801 ($F(1, 38) = 59.07$, $p < 0.0001$; two-way ANOVA). As expected, MK-801 caused hyperlocomotion, which is seen as an analogue of positive symptoms of schizophrenia. The path moved by the group treated with MK-801 + 7-PhO-THA (10 $mg \cdot kg^{-1}$) was significantly shorter than the path moved by the group MK-801 + DMSO ($p < 0.001$; two-way ANOVA with Bonferroni post-hoc test), suggesting that 7-PhO-THA at a dose of 10, but not 5 $mg \cdot kg^{-1}$, alleviated the MK-801-induced hyperlocomotion. In NaCl-treated animals, 7-PhO-THA did not significantly influence the path moved (Fig. 5).

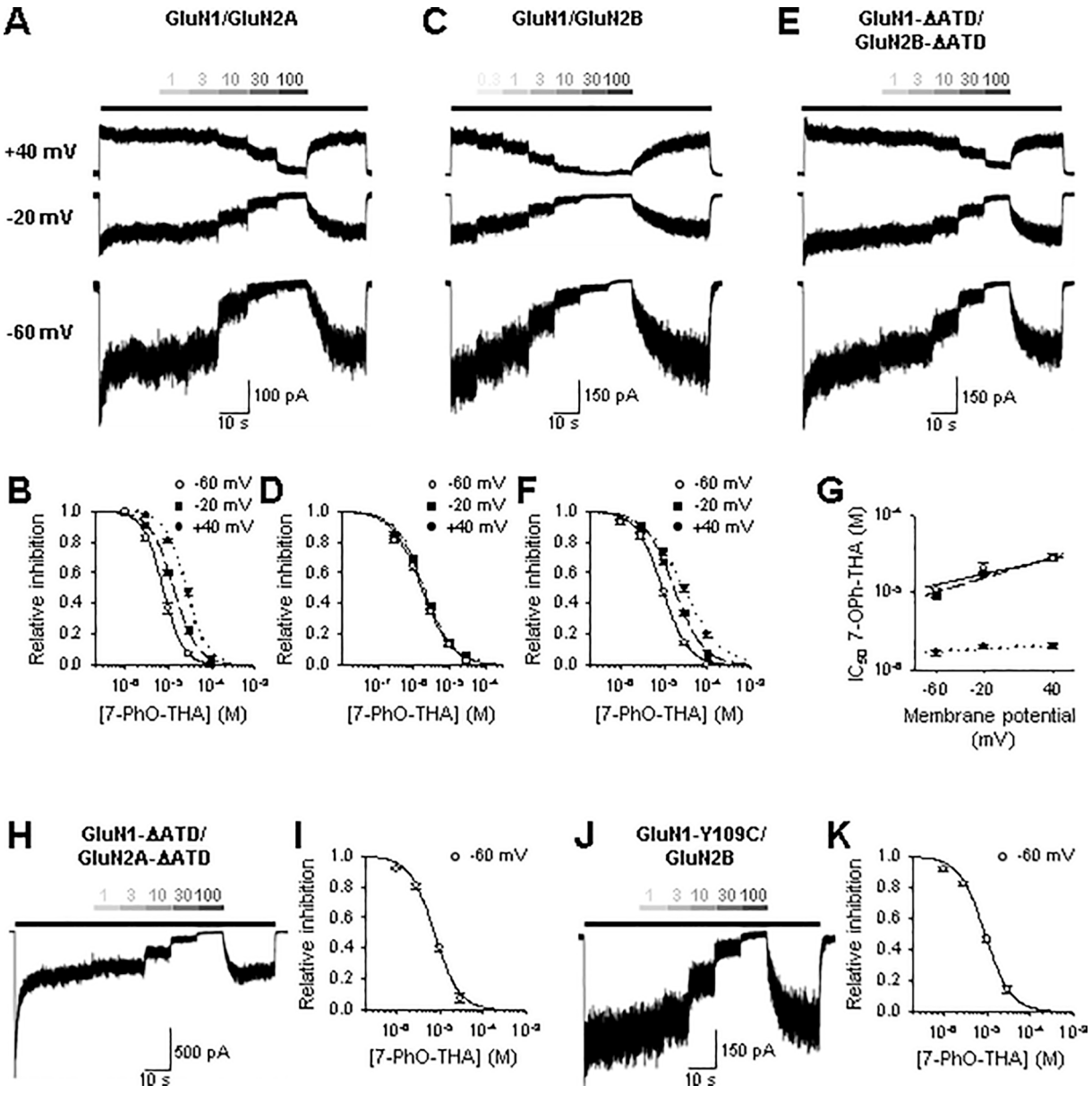

Fig. 2. 7-PhO-THA differently inhibits the GluN1/GluN2A and GluN1/GluN2B types of NMDARs. (A, C, E, H, J) Representative current traces recorded at indicated membrane potentials from HEK293 cells transfected with GluN1/GluN2 receptors, to measure dose–response relationship for the effect of 7-PhO-THA. Current traces were induced by fast application of 1 mM glutamate and 50 μM glycine (black bar); concentrations of 7-PhO-THA are shown in the micromolar range (grey bars). (B, D, F, I, K) Dose-response curves for the effect of 7-PhO-THA were obtained by fitting the experimental data from HEK293 cells transfected with the GluN1/GluN2 receptors using *Equation 1*. The obtained IC_{50} values and Hill coefficients are summarized in the Tab. 2. (G) Graph shows the relationship of the IC_{50} values determined for the inhibitory effect of 7-PhO-THA at the indicated GluN1/GluN2 receptors at three different membrane potentials (−60, −20, +40 mV).

In the EPM test we tested the potential anxiolytic effect of 7-PhO-THA and its possible interaction with the effect of MK-801. Analysis of the time spent in the open arms of EPM revealed a significant effect of MK-801 treatment ($F(1, 39) = 6.845$, $p = 0.0126$; two-way ANOVA), manifested as increased time spent in the open arms. Conversely, administration of 7-PhO-THA (either alone or combined with MK-801 at a dose of 0.1 $mg.kg^{1}$) did not significantly change the time spent in the open arms of the EPM ($F(2, 39) = 1.30$, $p = 0.2829$; two-way ANOVA), despite the fact that we observed an increasing trend towards spending more time in the open arms of the EPM when we applied 7-PhO-THA to MK-801-treated groups (Fig. 6A). Analysis of the distance moved in the EPM revealed a significant effect of MK-801 application ($F(1, 42) = 17.26$, $p = 0.0002$; two-way ANOVA) and treatment with 7-PhO-THA ($F(2, 42) = 8.108$, $p = 0.0011$; two-way ANOVA) on locomotor activity. At higher dose, 7-PhO-THA significantly attenuated the hyperlocomotion caused by administration of MK-801 ($p < 0.05$; two-way ANOVA with Bonferroni post-hoc test; Fig. 6B). These results are consistent with the results from OF and confirm the safety of administration of 7-PhO-THA without undesirable psychotomimetic side effects, and when combined with MK-801, with a non-significant tendency to anxiolytic manifestation.

3.7. Neuroprotective effect of 7-PhO-THA on NMDA-induced hippocampal lesion

NMDA-induced lesion of the dorsal hippocampus leads to over-activation of NMDARs and long-lasting well-described degeneration of glutamatergic neurons [42] in all evaluated areas (DGl, DGh, hilus, CA3, and CA1), and is therefore widely used for the animal model of excito-toxicity [43]. Our experiments were focused on the potential

Table 2
Parameters of dose–response relationship of 7-PhO-THA at recombinant NMDARs expressed in HEK293 cells.

Receptor	7-PhO-THA								
	−60 mV			−20 mV			+40 mV		
	IC_{50} (μM)	*h*	*n*	IC_{50} (μM)	*h*	*n*	IC_{50} (μM)	*h*	*n*
GluN1/GluN2B	1.7 ± 0.1	1.1 ± 0.1	14	2.0 ± 0.1	1.1 ± 0.1	8	2.0 ± 0.1	1.1 ± 0.1	10
GluN1/GluN2A	7.4 ± 0.5	1.9 ± 0.1	6	13.2 ± 0.9	1.6 ± 0.1	6	26.3 ± 1.3	1.7 ± 0.1	5
GluN1-ΔATD/GluN2B-ΔATD	9.0 ± 0.6	1.5 ± 0.1	9	17.3 ± 1.1	1.3 ± 0.1	5	27.9 ± 2.7	1.0 ± 0.0	5
GluN1-ΔATD/GluN2A-ΔATD	7.5 ± 0.3	1.5 ± 0.1	6	–	–	–	–	–	–
GluN1-Y109C/GluN2B	9.0 ± 0.4	1.5 ± 0.1	9	–	–	–	–	–	–

The experimental data were fitted by *Equation 1*; the resulting values of IC_{50}, Hill coefficients (*h*) and numbers of analyzed cells (*n*) for indicated membrane potentials are shown. Data shown as mean ± S.E.M.

neuroprotective effect of 7-PhO-THA in this animal model, and its effect was compared to that of memantine. We infused 25 mM NMDA and 30 μM 7-PhO-THA or memantine into the rat dorsal hippocampus and analyzed the severity of damage of FJB-positive cells in the selected parts of the hippocampus. In control animals (PBS + NaCl) we observed only minimal damage in the location around the injection-affected area. Our analysis revealed a significant neuroprotective effect of 7-PhO-THA ($p < 0.05$ vs. NMDA + NaCl; one-way ANOVA; Fig. 7) which reduced the total score of NMDA-induced lesion, in contrast to that of memantine. Significant neuroprotective effect of 7-PhO-THA was observed in the DGl, hilus, and CA3 parts of the afflicted hippocampus (Table 4). On the other hand, co-administration of NMDA with clinically used memantine did not result in any significant difference in comparison to NMDA-treated rats.

4. Discussion

Ionotropic glutamate receptors, and especially NMDARs, are key players in the excitatory system within the whole CNS. While NMDARs are essential for cognitive processes and memory function, these receptors are also implicated in heterogeneous neuropathology of various CNS diseases such as AD, Parkinson's disease, multiple sclerosis etc. Over-activation of NMDARs leads to excitotoxic damage of nervous tissue.

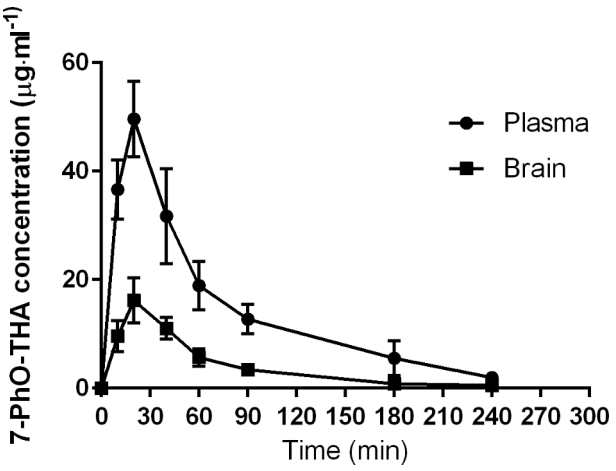

Fig. 4. The pharmacokinetics of 7-PhO-THA in the rat brain and plasma. In the graph are depicted the changes in concentration of 7-PhO-THA over time in rat plasma and brain tissue after i.p. application of 7-PhO-THA (24 $mg \cdot kg^{-1}$). Data shown as mean ± S.D., $n = 6$ per group.

Table 3
Basic kinetic parameters after i.p. administration of 7-PhO-THA (24 $mg \cdot kg^{-1}$).

Parameter[a]	Units	Plasma	Brain
$t_{1/2}$	min	54.46	51.23
t_{max}	min	20.00	20.00
C_{max}	$\mu g \cdot ml^{-1}$	49.60	16.20
AUC	$\mu g \cdot ml^{-1} \cdot min$	3454.11	981.88
MRT	min	77.36	67.20

[a] $t_{1/2}$ half-life, t_{max} time of maximal concentration, C_{max} maximal concentration, *AUC* area under curve, *MRT* mean residence time.

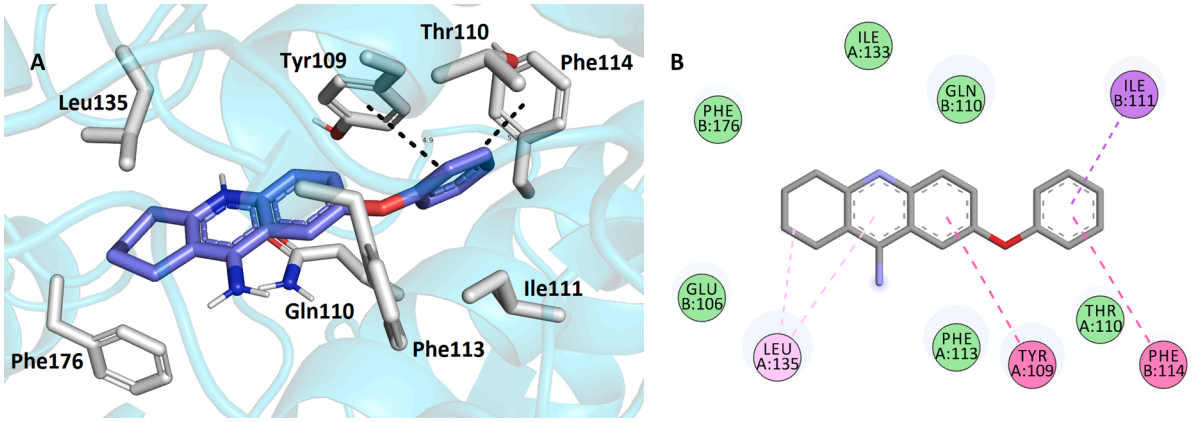

Fig. 3. Top-scored docking pose of 7-PhO-THA at the GluN1-GluN2B ATD interface (PDB ID: 5EWM). Close-up views are presented as three-dimensional (A) and two-dimensional (B) diagrams, respectively. Generally, in (A), 7-PhO-THA is shown as dark blue carbon sticks, important amino acid residues are in grey, and the rest of GluN1 and GluN2B ATDs as light-blue ribbon. Dashed lines in (A) and (B) represent crucial attractive interactions. In (B), amino acid residues marked as A corresponds to GluN1 ATD, and B corresponds to GluN2B ATD. Figure (A) was created with The PyMOL Molecular Graphics System (Version 2.0 Schrödinger, LLC). Figure (B) was rendered with Dassault Systèmes BIOVIA, Discovery Studio Visualizer (v 17.2.0.16349, San Diego: Dassault Systèmes, 2016). (For interpretation of the references to colour in this figure legend, the reader is referred to the web version of this article.)

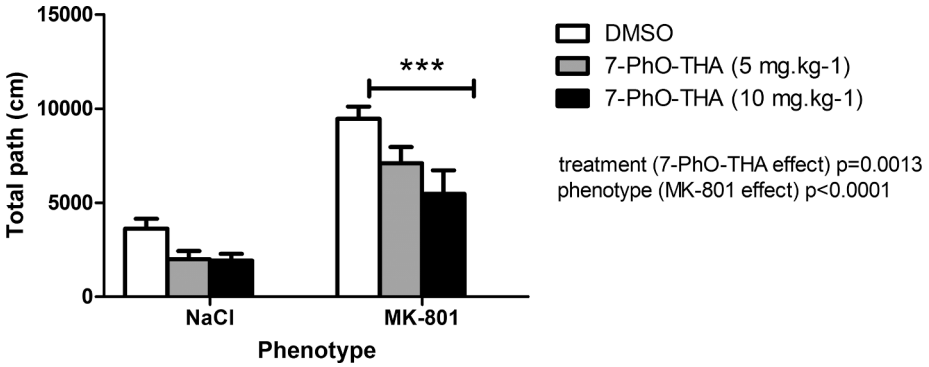

Fig. 5. Effect of 7-PhO-THA on locomotor activity in OF. Bar graph represents total path in cm walked in OF by rats with two kinds of phenotypes – rats were injected either with NaCl or MK-801 (0.3 mg.kg^{-1}). Both groups were then treated either with DMSO as control (white bars) or 7-PhO-THA at the dose of 5 (grey bars) or 10 mg.kg^{-1} (black bars); *** $p < 0.001$.

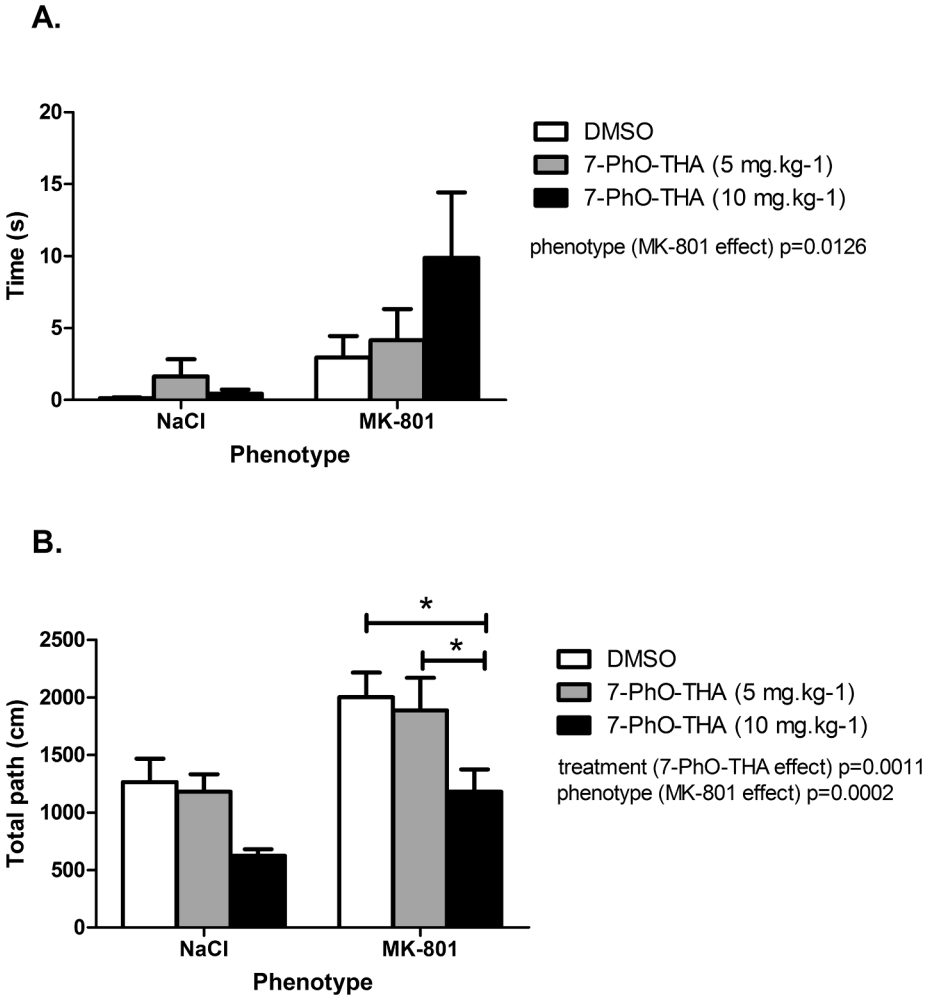

Fig. 6. Effect of 7-PhO-THA on anxiety and activity behavior in EPM. Bar graphs represent (A) total time spent in open arms of EPM and (B) total path in cm walked in EPM by rats with two kinds of phenotypes – rats were injected either with NaCl or MK-801 (0.1 mg.kg^{-1}). Both groups were then treated either with DMSO as control (white bars) or 7-PhO-THA at the dose of 5 (grey bars) or 10 mg.kg^{-1} (black bars); * $p < 0.05$.

Our electrophysiological data showed that 7-PhO-THA potently inhibits (with IC_{50} ~ 2 μM) the GluN1/GluN2B receptors in a voltage-independent manner and, furthermore, we confirmed the docking-study findings which suggested that the inhibitory effect is primarily mediated via the ifenprodil-binding site located in the ATD of the GluN1/GluN2B receptors. In addition, we revealed that GluN1/GluN2B receptors lacking the ATD as well as the wild-type GluN1/GluN2A receptors are inhibited by 7-PhO-THA in a voltage-dependent manner with slightly reduced potency (IC_{50} ~ 10 μM at −60 mV). Thus, 7-PhO-THA acts as a unique subunit-dependent inhibitory compound at the NMDARs.

Given the fact that excessive activation of the GluN1/GluN2B receptors is often associated in the literature with excitotoxicity-induced neurodegeneration [8,44-46], we examined the effect of 7-PhO-THA

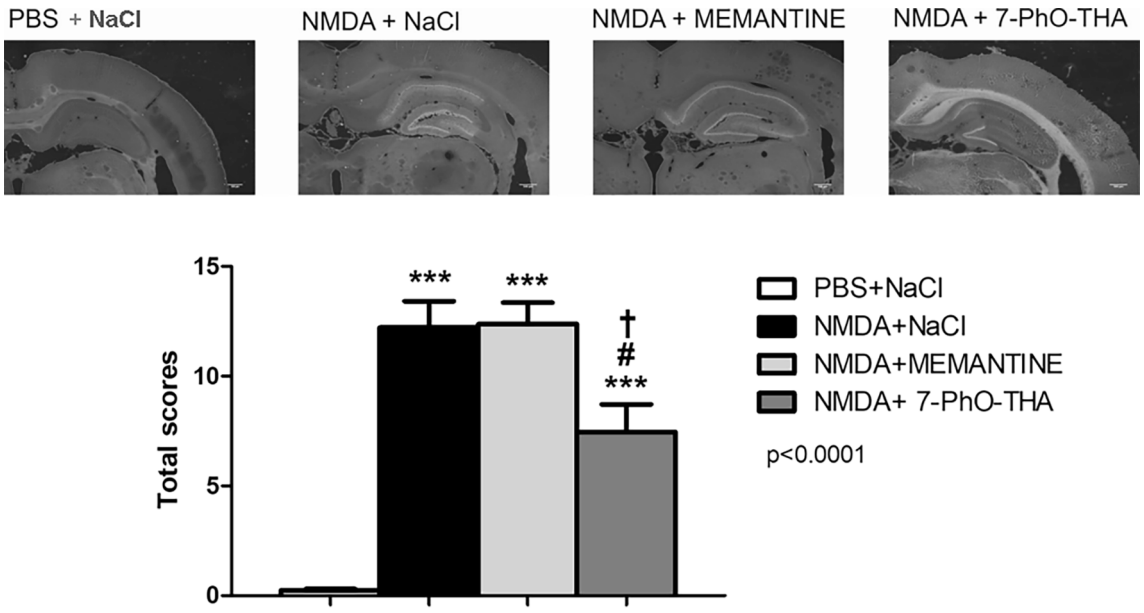

Fig. 7. 7-PhO-THA demonstrates neuroprotective activity in animal model of excitotoxicity. Total damage score of the dorsal hippocampus in case of NMDA-induced lesion was determined as described in Methods ($n \geq 6$; one-way ANOVA followed by Bonferroni post-hoc test, $p < 0.001$; *** $p < 0.001$ vs. PBS + NaCl; # $p < 0.05$ vs. NMDA + NaCl; † $p < 0.05$ vs. NMDA + memantine).

Table 4
Neuroprotective effect of 7-PhO-THA in a model of NMDA-induced lesion of rat dorsal hippocampus.

Treatment	Hippocampal regions[a]				
	DGl	DGh	hilus	CA3	CA1
PBS + NaCl	0.05 ± 0.03	0.05 ± 0.02	0.11 ± 0.03	0.02 ± 0.02	0.03 ± 0.02
NMDA + NaCl	3.12 ± 0.15***	1.93 ± 0.44**	2.89 ± 0.32***	2.36 ± 0.07***	1.92 ± 0.50***
NMDA + memantine	3.28 ± 0.11***	1.91 ± 0.31**	3.20 ± 0.21***	2.40 ± 0.20***	1.60 ± 0.40*
NMDA + 7-PhO-THA	2.71 ± 0.11***##	1.25 ± 0.34	1.28 ± 0.34*###	1.22 ± 0.42**##	1.00 ± 0.36
one-way ANOVA[b]	$p < 0.0001$	$p = 0.0008$	$p < 0.0001$	$p < 0.0001$	$p = 0.0062$

[a] Evaluated hippocampal regions: granular cell layer of the dentate gyrus lower part (DGl), granular cell layer of the dentate gyrus higher part (DGh), hilus, CA1, and CA3. Scoring: 0: 0–5% of the area is damaged; score 1: 6–25% of the area is damaged; score 2: 26–50% of the area is damaged; score 3: 51–75% of the area is damaged; score 4:>75% of the area is damaged. Data shown as mean ± S.E.M.

[b] To evaluate the neuroprotective effect of 7-PhO-THA in different hippocampal regions we performed one-way ANOVA (for each region separately; obtained p values are provided in the last row) with Tukey post-hoc test (* $p < 0.05$, ** $p < 0.01$, *** $p < 0.001$ vs. PBS + NaCl; ## $p < 0.05$, ### $p < 0.001$ vs. NMDA + NaCl). 1/5 of the hippocampus (17–21 slices) was evaluated for each rat brain; $n \geq 7$ animals were used for each condition. Data are shown as mean ± S.E.M.

in a model of NMDA-induced lesions in the rat hippocampus. We observed that 7-PhO-THA was effective in protecting the brain tissue around the area of NMDA application, which is in agreement with our electrophysiological data (see below). Thus, 7-PhO-THA belongs to a group of GluN1/GluN2B receptor selective compounds which are considered to be suitable candidates for the treatment of neurodegenerative conditions including ischemia [7]. However, 7-PhO-THA also acts at the GluN1/GluN2A receptors, likely as an open-channel blocker because of the observed voltage-dependency of the inhibition. Using the same experimental setup as in previously published work on 7-MEOTA [15] we anticipate, that also 7-PhO-THA directly competes with other open channel blockers like MK-801 at both GluN1/GluN2A and GluN1/GluN2B receptors (see below). In addition, our data confirmed that 7-PhO-THA, similarly to its parent THA, acts on the cholinergic system as an indirect cholinomimetic via inhibition of both AChE and BChE. Notably, the observed *in vitro* inhibitory potency expressed as IC_{50} for both NMDARs and AChE are within the same range, which is important for "multitargeting", as balanced affinities ensure interaction with all presumed targets [22]. Taking together all our *in vitro* findings, we concluded that 7-PhO-THA is a promising compound with a unique mechanism of action at both the glutamatergic and cholinergic systems.

In contrast to previously published studies on the 7-MEOTA [15], currently investigated 7-PhO-THA is 6-times more effective inhibitor of AChE with balanced activities on the cholinergic and the glutamatergic system (IC_{50}(AChE) = 2.4 μM; IC_{50}(BChE) = 4.9 μM; IC_{50}(GluN1/GluN2B) = 1.7 μM). Furthermore, we showed that 7-PhO-THA binds to the ifenprodil-binding site, which determines its selectivity towards GluN1/GluN2B. This finding is of high importance as selective GluN1/GluN2B antagonists are considered as promising tool to target the neurodegenerative diseases [47].

In the next phase, we focused on evidence of the *in vivo* efficacy of 7-PhO-THA. Since the fundamental limitation of all known NMDAR inhibitors is the risk of behavioral changes and induction of psychotomimetic behavior, manifested as hyperlocomotion in laboratory rodents, we first studied the effect of 7-PhO-THA on the behavior of the intact rats. At the same time, we studied the effect of 7-PhO-THA on schizophrenia-like behavior induced by the application of MK-801, an open channel blocker of NMDARs. Finally, we turned attention to evaluation of the effect of 7-PhO-THA in animal models of neurodegeneration, specifically using a pharmacological model of NMDA-induced lesion of the dorsal hippocampus [42].

In behavioral experiments we investigated the effect of 7-PhO-THA

on spontaneous activity and anxiety in OF and EPM, respectively. We found that administration of 7-PhO-THA alone did not increase the locomotor activity of animals in both types of behavioral tests, suggesting a low risk of psychotomimetic side effects. We further employed a pharmacological model of schizophrenia, induced by administration of MK-801, in order to investigate whether the effect of 7-PhO-THA is mediated via the interaction with NMDARs. MK-801 administration led to significant behavioral alterations in both OF and EPM, consistently with the literature [48].

NMDAR antagonists are known for their anxiolytic effect represented in lab animals by increased time spent in the open arms in the EPM task (Wiley, Cristello et al. 1995). However, our experiments showed that administration of 7-PhO-THA alone did not influence the anxiety of the animals. Application of 7-PhO-THA to MK-801-treated animals resulted in a mild but insignificant anxiolytic effect. It has been shown that ifenprodil and MK-801 both showed an anxiolytic profile in EPM. This anxiolytic effect of ifenprodil was accompanied by an increase in locomotion as reflected in an increase of total arm entries. Therefore the increased open arm time might be the result of increased locomotion [48]. However, co-administration of ifenprodil with MK-801 prevented the anxiolytic effect of MK-801 [48], in contrast to our results with 7-PhO-THA, which also acts via the ifenprodil binding site. The reasons for this difference in effect between ifenprodil and 7-PhO-THA are not completely clear; however the other mechanism of action of 7-PhO-THA (i.e. AChE inhibition) must be taken into consideration. The effect of AChE inhibitors on anxiety is complex. The effect of cholinergic tone on anxiety-like behavior may depend on levels of stress, its duration and severity and the baseline acetylcholine levels [49,50]. Thus AChEI administration may trigger an anxiogenic as well as anxiolytic response [51,52].

MK-801-induced hyperlocomotion in OF was reduced by 7-PhO-THA co-administration. This effect was dose-dependent: administration of 7-PhO-THA at a dose of 10 $mg.kg^{-1}$, but not 5 $mg.kg^{-1}$, was able to significantly attenuate the hyperlocomotion induced by MK-801. Results of the analysis of locomotor activity in EPM corroborated the results from the OF – only the higher dose of 7-PhO-THA decreased MK-801-induced hyperlocomotion. However, in OF short intermittent episodes of ataxia were occasionally seen in some animals of all three groups treated with MK-801. Despite the fact that these ataxia episodes were not quantified systematically and subjected to statistical analysis, the hyperlocomotion-ameliorating effect of 7-PhO-THA should be interpreted cautiously, as involvement of motoric alterations induced by the MK-801 and 7-PhO-THA co-application in OF cannot be excluded.

Our behavioral data further indicate that the effect of 7-PhO-THA treatment could be mediated also through the cholinergic system. Administration of AChE inhibitors may decrease the motor activity in rats and mice. While physostigmine, donepezil and THA decreased locomotion in the OF task, galantamine had no significant effect on locomotion [53,54]. As a consequence of the AChE inhibition, cholinergic transmission is increased, resulting in greater activation of the autonomic nervous system [55], which could have a negative impact on locomotor activity. In addition, cholinergic activity in the striatum might be enhanced by treatment with AChE inhibitors affecting extrapyramidal motor function which leads to bradykinesia [56]. Thus, enhancement of central and peripheral cholinergic transmission might collectively contribute to the suppression of voluntary motor activity.

Correspondingly, in animals treated with 7-PhO-THA alone we observed a tendency to decreased locomotor activity in OF, although it did not achieve statistical significance. Moreover, certain AChE inhibitors such as physostigmine can reverse the hyperlocomotion and some other behavioral alterations induced by MK-801 [54]. Taken together with our results from OF, these facts further support the idea that 7-PhO-THA, although also being an NMDAR antagonist, exerts its behavioral outcome more profoundly through the inhibition of AChE. The 7-PhO-THA-induced decrease of the MK-801-induced hyperlocomotion in both OF and EPM tasks might be a result of complex interactions with cholinergic and glutamatergic systems.

Finally, we focused on comparison of the potential neuroprotective effect of 7-PhO-THA with clinically used memantine on a permanent lesion of the dorsal hippocampus. Our results demonstrated that unilateral NMDA-lesion induced extensive damage to nervous tissue in all evaluated hippocampal structures which is in agreement with our previous observations [42]. Co-administration of NMDA and 7-PhO-THA significantly reduced development of neurodegeneration in afflicted dorsal hippocampus. In our experimental arrangement, memantine did not exhibit any neuroprotective effect despite its positive effects having been demonstrated in other animal models and clinical studies [57-59]. This discrepancy could be explained by the different dose of memantine and the different animal model or approach used. However, the ineffectiveness of memantine in our experimental model is consistent with the results from our previous work focused on neuroprotective activity of 7-MEOTA [15].

In general, GluN1/GluN2 selective compounds are a very attractive research area with possible clinical application. Special attention is paid to selective inhibitors of GluN2B-containing NMDARs due to their involvement in excitotoxic cell death [47]. It has been reported that GluN2B selective inhibitors (i.e. ifenprodil, eliprodil, and traxoprodil) did not cause neurological side effects typical for other NMDAR antagonists, and their application in animal models has provided impressive results. For example, application of eliprodil in the case of a bilateral carotid artery occlusion and middle cerebral artery occlusion led to a reduction of infarct volume and neurodegeneration [60]. Moreover, administration of GluN1/GluN2B-selective eliprodil had a positive effect in a model of retinal excitotoxicity, caused by direct injection of NMDA into the vitreous, as well as in the model of traumatic brain damage, compared to the unselective NMDAR open channel blocker MK-801 [61,62]. Traxoprodil also demonstrated a neuroprotective effect in animal models of ischemia-like middle cerebral artery occlusion and traumatic brain injury [63,64]. Moreover, traxoprodil potentiates the antidepressant-effect of certain antidepressant drugs [64]. However, neither traxoprodil nor eliprodil was able to demonstrate a positive effect in clinical trials despite their good tolerability [64,65]. Thus, 7-PhO-THA represents a novel compound with dual effect that has potential to be beneficial in the treatment of above-mentioned disorders and neurodenegerative diseases. The main advantage of 7-PhO-THA is its lack of the undesirable behavioral side effects typical for strong NMDAR inhibitors acting as competitive antagonists or open channel blockers. Finally, it appears that the dual effect of 7-PhO-THA on both glutamatergic and cholinergic systems is a promising pharmacological tool as both biological targets clearly contribute desirable pharmacological effect. It surpasses previously studied 7-MEOTA thanks to its higher efficacy in inhibition of cholinesterases, balanced activities on the cholinergic and glutamatergic system and selectivity towards GluN1/GluN2B.

In conclusion we have shown the dual potency of 7-PhO-THA, namely potent and balanced inhibition of both AChE and NMDARs. 7-PhO-THA selectively inhibits GluN1/GluN2B receptors via an ifenprodil-binding site, in addition to its voltage-dependent inhibitory effect at both GluN1/GluN2A and GluN1/GluN2B receptors. Whereas the NMDA-induced lesion of the dorsal hippocampus confirmed potent anti-excitotoxic and neuroprotective efficacy, behavioral observations showed a prevailing cholinergic component manifesting mainly in decreased hyperlocomotion. On the other hand, 7-PhO-THA managed to avoid behavioral side effects that are perceived as analogous to symptoms of schizophrenia. Finally, CNS availability and the overall behavioral profile are promising for subsequent investigation of therapeutic effects after systemic administration.

CRediT authorship contribution statement

Martina Kaniakova: Investigation, Writing - original draft. **Jan Korabecny:** Supervision, Writing - review & editing. **Kristina**

Holubova: Investigation, Formal analysis, Writing - original draft. **Lenka Kleteckova:** Investigation. **Marketa Chvojkova:** Investigation, Formal analysis, Writing - original draft. **Kristina Hakenova:** Investigation. **Lukas Prchal:** Investigation, Writing - original draft. **Martin Novak:** . **Rafael Dolezal:** . **Vendula Hepnarova:** . **Barbora Svobodova:** . **Tomas Kucera:** . **Katarina Lichnerova:** . **Barbora Krausova:** . **Martin Horak:** Supervision, Conceptualization, Writing - review & editing. **Karel Vales:** Supervision, Conceptualization, Writing - review & editing. **Ondrej Soukup:** Supervision, Conceptualization, Writing - review & editing.

Declaration of Competing Interest

The authors declare that they have no known competing financial interests or personal relationships that could have appeared to influence the work reported in this paper.

Acknowledgements

This work has was supported by the grant of Czech Science Foundation (no. 20-12047S); by Ministry of Education, Youth and Sports of Czech Republic (ERDF/ESF project PharmaBrain no. CZ.02.1.01/0.0/0.0/16_025/0007444; OPPK BrainView no. CZ.2.16/3.1.00/21544 and by Charles University (SVV 260 547). B.S. acknowledges the support of specific project no. SV/FVZ2019/01 (Faculty of Military Health Sciences, University of Defence).

The authors are grateful to Ian McColl MD, PhD for assistance with the manuscript and declare that author(s) are entirely responsible for the scientific content of the paper.

References

[1] M. Horak, R.S. Petralia, M. Kaniakova, N. Sans, ER to synapse trafficking of NMDA receptors, Front. Cell. Neurosci. 8 (2014) 394.
[2] S.F. Traynelis, L.P. Wollmuth, C.J. McBain, F.S. Menniti, K.M. Vance, K.K. Ogden, K.B. Hansen, H. Yuan, S.J. Myers, R. Dingledine, Glutamate receptor ion channels: structure, regulation, and function, Pharmacol. Rev. 62 (3) (2010) 405–496.
[3] S. Bleich, K. Römer, J. Wiltfang, J. Kornhuber, Glutamate and the glutamate receptor system: a target for drug action, Int. J. Geriatr. Psychiatry 18 (S1) (2003) S33–S40.
[4] A. Sanz-Clemente, R.A. Nicoll, K.W. Roche, Diversity in NMDA Receptor Composition: Many Regulators, Many Consequences, Neuroscientist (2012).
[5] D. Stroebel, D.L. Buhl, J.D. Knafels, P.K. Chanda, M. Green, S. Sciabola, L. Mony, P. Paoletti, J. Pandit, A Novel Binding Mode Reveals Two Distinct Classes of NMDA Receptor GluN2B-selective Antagonists, Mol. Pharmacol. 89 (5) (2016) 541–551.
[6] M.C. Regan, Z. Zhu, H. Yuan, S.J. Myers, D.S. Menaldino, Y.A. Tahirovic, D. C. Liotta, S.F. Traynelis, H. Furukawa, Structural elements of a pH-sensitive inhibitor binding site in NMDA receptors, Nat. Commun. 10 (1) (2019) 321.
[7] H. Yuan, S.J. Myers, G. Wells, K.L. Nicholson, S.A. Swanger, P. Lyuboslavsky, Y. A. Tahirovic, D.S. Menaldino, T. Ganesh, L.J. Wilson, Context-dependent GluN2B-selective inhibitors of NMDA receptor function are neuroprotective with minimal side effects, Neuron 85 (6) (2015) 1305–1318.
[8] E.S. Vizi, M. Kisfali, T. Lőrincz, Role of nonsynaptic GluN2B-containing NMDA receptors in excitotoxicity: evidence that fluoxetine selectively inhibits these receptors and may have neuroprotective effects, Brain Res. Bull. 93 (2013) 32–38.
[9] H. Chaffey, P.L. Chazot, NMDA receptor subtypes: Structure, function and therapeutics, Curr. Anaesth. Crit. Care 19 (4) (2008) 183–201.
[10] K.L. Strong, Y. Jing, A.R. Prosser, S.F. Traynelis, D.C. Liotta, NMDA receptor modulators: an updated patent review (2013–2014), Expert. Opin. Ther. Pat. 24 (12) (2014) 1349–1366.
[11] K.L. Nicholson, R.S. Mansbach, F.S. Menniti, R.L. Balster, The phencyclidine-like discriminative stimulus effects and reinforcing properties of the NR2B-selective N-methyl-D-aspartate antagonist CP-101 606 in rats and rhesus monkeys, Behav. Pharmacol. 18 (8) (2007) 731–743.
[12] K. Wolff, A.R. Winstock, Ketamine : from medicine to misuse, CNS Drugs 20 (3) (2006) 199–218.
[13] P. Andine, N. Widermark, R. Axelsson, G. Nyberg, U. Olofsson, E. Martensson, M. Sandberg, Characterization of MK-801-induced behavior as a putative rat model of psychosis, J. Pharmacol. Exp. Ther. 290 (3) (1999) 1393–1408.
[14] M. Horak, K. Holubova, E. Nepovimova, J. Krusek, M. Kaniakova, J. Korabecny, L. Vyklicky, K. Kuca, A. Stuchlik, J. Ricny, K. Vales, O. Soukup, The pharmacology of tacrine at N-methyl-d-aspartate receptors, Prog. Neuropsychopharmacol. Biol. Psychiatry 75 (2017) 54–62.
[15] M. Kaniakova, L. Kleteckova, K. Lichnerova, K. Holubova, K. Skrenkova, M. Korinek, J. Krusek, T. Smejkalova, J. Korabecny, K. Vales, 7-Methoxyderivative of tacrine is a 'foot-in-the-door'open-channel blocker of GluN1/GluN2 and GluN1/GluN3 NMDA receptors with neuroprotective activity in vivo, Neuropharmacology (2018).
[16] V. Vyklicky, M. Korinek, T. Smejkalova, A. Balik, B. Krausova, M. Kaniakova, K. Lichnerova, J. Cerny, J. Krusek, I. Dittert, Structure, function, and pharmacology of NMDA receptor channels, Physiol. Res. 63 (2014).
[17] A. Adem, Putative mechanisms of action of tacrine in Alzheimer's disease, Acta Neurol. Scand. Suppl. 139 (1992) 69–74.
[18] P.B. Watkins, H.J. Zimmerman, M.J. Knapp, S.I. Gracon, K.W. Lewis, Hepatotoxic effects of tacrine administration in patients with Alzheimer's disease, JAMA 271 (13) (1994) 992–998.
[19] O. Soukup, D. Jun, J. Zdarova-Karasova, J. Patocka, K. Musilek, J. Korabecny, J. Krusek, M. Kaniakova, V. Sepsova, J. Mandikova, F. Trejtnar, M. Pohanka, L. Drtinova, M. Pavlik, G. Tobin, K. Kuca, A resurrection of 7-MEOTA: a comparison with tacrine, Curr. Alzheimer Res. 10 (8) (2013) 893–906.
[20] J. Patocka, D. Jun, K. Kuca, Possible role of hydroxylated metabolites of tacrine in drug toxicity and therapy of Alzheimer's disease, Curr. Drug Metab. 9 (4) (2008) 332–335.
[21] R.J. Sram, Overeni ucinnosti MTX pri psychiatrickych onemocnenich, Psychiatricke Centrum Praha (1990).
[22] C.J. Van der Schyf, The use of multi-target drugs in the treatment of neurodegenerative diseases, Expert Rev. Clin. Pharmacol. 4 (3) (2011) 293–298.
[23] M. Rosini, E. Simoni, A. Minarini, C. Melchiorre, Multi-target design strategies in the context of Alzheimer's disease: acetylcholinesterase inhibition and NMDA receptor antagonism as the driving forces, Neurochem. Res. 39 (10) (2014) 1914–1923.
[24] E. Simoni, S. Daniele, G. Bottegoni, D. Pizzirani, M.L. Trincavelli, L. Goldoni, G. Tarozzo, A. Reggiani, C. Martini, D. Piomelli, Combining galantamine and memantine in multitargeted, new chemical entities potentially useful in Alzheimer's disease, J. Med. Chem. 55 (22) (2012) 9708–9721.
[25] Z. Gazova, O. Soukup, V. Sepsova, K. Siposova, L. Drtinova, P. Jost, K. Spilovska, J. Korabecny, E. Nepovimova, D. Fedunova, M. Horak, M. Kaniakova, Z.J. Wang, A. K. Hamouda, K. Kuca, Multi-target-directed therapeutic potential of 7-methoxytacrine-adamantylamine heterodimers in the Alzheimer's disease treatment, Biochimica Et Biophysica Acta-Molecular Basis of Disease 1863 (2) (2017) 607–619.
[26] G.L. Ellman, K.D. Courtney, V. Andres, R.M. Featherstone, A New and Rapid Colorimetric Determination of Acetylcholinesterase Activity, Biochem. Pharmacol. 7 (2) (1961) 88.
[27] K. Lichnerova, M. Kaniakova, S.P. Park, K. Skrenkova, Y.X. Wang, R.S. Petralia, Y. H. Suh, M. Horak, Two N-glycosylation Sites in the GluN1 Subunit Are Essential for Releasing N-methyl-d-aspartate (NMDA) Receptors from the Endoplasmic Reticulum, J. Biol. Chem. 290 (30) (2015) 18379–18390.
[28] M. Kaniakova, K. Lichnerova, K. Skrenkova, L. Vyklicky, M. Horak, Biochemical and electrophysiological characterization of N-glycans on NMDA receptor subunits, J. Neurochem. 138 (4) (2016) 546–556.
[29] V. Vyklicky, B. Krausova, J. Cerny, A. Balik, M. Zapotocky, M. Novotny, K. Lichnerova, T. Smejkalova, M. Kaniakova, M. Korinek, M. Petrovic, P. Kacer, M. Horak, H. Chodounska, L. Vyklicky, Block of NMDA receptor channels by endogenous neurosteroids: implications for the agonist induced conformational states of the channel vestibule, Sci. Rep. 5 (2015) 10935.
[30] G.M. Morris, R. Huey, W. Lindstrom, M.F. Sanner, R.K. Belew, D.S. Goodsell, A. J. Olson, AutoDock4 and AutoDockTools4: Automated docking with selective receptor flexibility, J. Comput. Chem. 30 (16) (2009) 2785–2791.
[31] E.F. Pettersen, T.D. Goddard, C.C. Huang, G.S. Couch, D.M. Greenblatt, E.C. Meng, T.E. Ferrin, UCSF chimera - A visualization system for exploratory research and analysis, J. Comput. Chem. 25 (13) (2004) 1605–1612.
[32] N.M. O'Boyle, M. Banck, C.A. James, C. Morley, T. Vandermeersch, G. R. Hutchison, Open Babel: An open chemical toolbox, J. Cheminform. 3 (1) (2011) 33.
[33] O. Trott, A.J. Olson, AutoDock Vina: improving the speed and accuracy of docking with a new scoring function, efficient optimization, and multithreading, J. Comput. Chem. 31 (2) (2010) 455–461.
[34] Y. Zhang, M. Huo, J. Zhou, S. Xie, PKSolver: An add-in program for pharmacokinetic and pharmacodynamic data analysis in Microsoft Excel, Comput. Methods Programs Biomed. 99 (3) (2010) 306–314.
[35] L.C. Schmued, C. Albertson, W. Slikker Jr, Fluoro-Jade: a novel fluorochrome for the sensitive and reliable histochemical localization of neuronal degeneration, Brain Res. 751 (1) (1997) 37–46.
[36] L. Kleteckova, G. Tsenov, H. Kubova, A. Stuchlik, K. Vales, Neuroprotective effect of the 3alpha5beta-pregnanolone glutamate treatment in the model of focal cerebral ischemia in immature rats, Neurosci. Lett. 564 (2014) 11–15.
[37] J. Korabecny, R. Dolezal, P. Cabelova, A. Horova, E. Hruba, J. Ricny, L. Sedlacek, E. Nepovimova, K. Spilovska, M. Andrs, 7-MEOTA–donepezil like compounds as cholinesterase inhibitors: Synthesis, pharmacological evaluation, molecular modeling and QSAR studies, Eur. J. Med. Chem. 82 (2014) 426–438.
[38] H. Ogura, T. Kosasa, Y. Kuriya, Y. Yamanishi, Comparison of inhibitory activities of donepezil and other cholinesterase inhibitors on acetylcholinesterase and butyrylcholinesterase in vitro, Methods Find. Exp. Clin. Pharmacol. 22 (8) (2000) 609–613.
[39] D. Stroebel, D.L. Buhl, J.D. Knafels, P.K. Chanda, M. Green, S. Sciabola, L. Mony, P. Paoletti, J. Pandit, A novel binding mode reveals two distinct classes of NMDA receptor GluN2B-selective antagonists, Molecular Pharmacology (2016) mol. 115.103036.
[40] A. Fernandes, T. Wojcik, P. Baireddy, R. Pieschl, A. Newton, Y. Tian, Y. Hong, L. Bristow, Y.-W. Li, Inhibition of in vivo [3H] MK-801 binding by NMDA receptor

open channel blockers and GluN2B antagonists in rats and mice, Eur. J. Pharmacol. 766 (2015) 1–8.
[41] E. Karakas, N. Simorowski, H. Furukawa, Subunit arrangement and phenylethanolamine binding in GluN1/GluN2B NMDA receptors, Nature 475 (7355) (2011) 249.
[42] L. Rambousek, L. Kleteckova, A. Kubesova, D. Jirak, K. Vales, J.-M. Fritschy, Rat intra-hippocampal NMDA infusion induces cell-specific damage and changes in expression of NMDA and GABAA receptor subunits, Neuropharmacology 105 (2016) 594–606.
[43] L. Rambousek, V. Bubenikova-Valesova, P. Kacer, K. Syslova, J. Kenney, K. Holubova, V. Najmanova, P. Zach, J. Svoboda, A. Stuchlik, Cellular and behavioural effects of a new steroidal inhibitor of the N-methyl-d-aspartate receptor 3α5β-pregnanolone glutamate, Neuropharmacology 61 (1–2) (2011) 61–68.
[44] G.E. Hardingham, K.Q. Do, Linking early-life NMDAR hypofunction and oxidative stress in schizophrenia pathogenesis, Nat. Rev. Neurosci. 17 (2) (2016) 125–134.
[45] M.M. Vieira, J. Schmidt, J.S. Ferreira, K. She, S. Oku, M. Mele, A.E. Santos, C. B. Duarte, A.M. Craig, A.L. Carvalho, Multiple domains in the C-terminus of NMDA receptor GluN2B subunit contribute to neuronal death following in vitro ischemia, Neurobiol. Dis. 89 (2016) 223–234.
[46] X. Zhou, Q. Ding, Z. Chen, H. Yun, H. Wang, Involvement of GluN2A and GluN2B in synaptic and extrasynaptic NMDA receptor function and neuronal excitotoxicity, J. Biol. Chem. jbc. M113 (2013), 482000.
[47] M.-A. Martel, T.J. Ryan, K.F. Bell, J.H. Fowler, A. McMahon, B. Al-Mubarak, N. H. Komiyama, K. Horsburgh, P.C. Kind, S.G. Grant, The subtype of GluN2 C-terminal domain determines the response to excitotoxic insults, Neuron 74 (3) (2012) 543–556.
[48] C. Fraser, M. Cooke, A. Fisher, I. Thompson, T. Stone, Interactions between ifenprodil and dizocilpine on mouse behaviour in models of anxiety and working memory, Eur. Neuropsychopharmacol. 6 (4) (1996) 311–316.
[49] M.J. Higley, M.R. Picciotto, Neuromodulation by acetylcholine: examples from schizophrenia and depression, Curr. Opin. Neurobiol. 29 (2014) 88–95.
[50] Y.S. Mineur, A. Obayemi, M.B. Wigestrand, G.M. Fote, C.A. Calarco, A.M. Li, M. R. Picciotto, Cholinergic signaling in the hippocampus regulates social stress resilience and anxiety-and depression-like behavior, Proc. Natl. Acad. Sci. U.S.A. 110 (9) (2013) 3573–3578.
[51] K. Martinowich, R.J. Schloesser, Y. Lu, D.V. Jimenez, D. Paredes, J.S. Greene, N. H. Greig, H.K. Manji, B. Lu, Roles of p75NTR, Long-term depression, and cholinergic transmission in anxiety and acute stress coping, Biol. Psychiatry 71 (1) (2012) 75–83.
[52] M. Papp, P. Gruca, M. Lason-Tyburkiewicz, P. Willner, Antidepressant, anxiolytic and procognitive effects of subacute and chronic ketamine in the chronic mild stress model of depression, Behav. Pharmacol. 28 (1) (2017) 1–8.
[53] D. Carriero, G. Outslay, A. Mayorga, J. Aberman, G. Gianutsos, Salamone, JD, Motor dysfunction produced by tacrine administration in rats, Pharmacol. Biochem. Behav. 58 (4) (1997) 851–858.
[54] J.G. Csernansky, M. Martin, R. Shah, A. Bertchume, J. Colvin, H. Dong, Cholinesterase inhibitors ameliorate behavioral deficits induced by MK-801 in mice, Neuropsychopharmacology 30 (12) (2005) 2135.
[55] H. Umegaki, O. Khookhor, The response of the autonomic nervous system to the cholinesterase inhibitor, donepezil, Neuroendocrinol. Lett. 34 (5) (2013) 383–387.
[56] B.R. Ott, M.C. Lannon, Exacerbation of parkinsonism by tacrine, Clin. Neuropharmacol. 15 (4) (1992) 322–325.
[57] H.S. Chen, S.A. Lipton, Mechanism of memantine block of NMDA-activated channels in rat retinal ganglion cells: uncompetitive antagonism, J. Physiol. 499 (Pt 1) (1997) 27–46.
[58] H.S. Chen, J.W. Pellegrini, S.K. Aggarwal, S.Z. Lei, S. Warach, F.E. Jensen, S. A. Lipton, Open-channel block of N-methyl-D-aspartate (NMDA) responses by memantine: therapeutic advantage against NMDA receptor-mediated neurotoxicity, J. Neurosci. 12 (11) (1992) 4427–4436.
[59] J.-M. Orgogozo, A.-S. Rigaud, A. Stöffler, H.-J. Möbius, F. Forette, Efficacy and safety of memantine in patients with mild to moderate vascular dementia: a randomized, placebo-controlled trial (MMM 300), Stroke 33 (7) (2002) 1834–1839.
[60] C.P. Bath, L.N. Farrell, J. Gilmore, M.A. Ward, C.A. Hicks, M.J. O'Neill, D. Bleakman, The effects of ifenprodil and eliprodil on voltage-dependent Ca2+ channels and in gerbil global cerebral ischaemia, Eur. J. Pharmacol. 299 (1–3) (1996) 103–112.
[61] M.A. Kapin, R. Doshi, B. Scatton, L.M. DeSantis, M.L. Chandler, Neuroprotective effects of eliprodil in retinal excitotoxicity and ischemia, Invest. Ophthalmol. Vis. Sci. 40 (6) (1999) 1177–1182.
[62] S. Toulmond, A. Serrano, J. Benavides, B. Scatton, Prevention by eliprodil (SL 82.0715) of traumatic brain damage in the rat. Existence of a large (18h) therapeutic window, Brain Res. 620 (1) (1993) 32–41.
[63] X. Di, R. Bullock, J. Watson, P. Fatouros, B. Chenard, F. White, F. Corwin, Effect of CP101, 606, a novel NR2B subunit antagonist of the N-methyl-D-aspartate receptor, on the volume of ischemic brain damage and cytotoxic brain edema after middle cerebral artery occlusion in the feline brain, Stroke 28 (11) (1997) 2244–2251.
[64] E. Tsuchida, M. Rice, R. Bullock, The Neuroprotective Effect of the Forebrain-S elective NMD A Antagonist CP101, 606 upon Focal Ischemic Brain Damage Caused by Acute Subdural Hematoma in the Rat, J. Neurotrauma 14 (6) (1997) 409–417.
[65] R.E. Merchant, M.R. Bullock, C.A. Carmack, A.K. Shah, K.D. Wilner, G. Ko, S. A. Williams, A double-blind, placebo-controlled study of the safety, tolerability and pharmacokinetics of CP-101,606 in patients with a mild or moderate traumatic brain injury, Ann. N. Y. Acad. Sci. 890 (1) (1999) 42–50.

European Journal of Medicinal Chemistry 219 (2021) 113434

Contents lists available at ScienceDirect

European Journal of Medicinal Chemistry

journal homepage: http://www.elsevier.com/locate/ejmech

Structure-activity relationships of dually-acting acetylcholinesterase inhibitors derived from tacrine on *N*-methyl-D-Aspartate receptors

Lukas Gorecki [a, 1], Anna Misiachna [b, c, d, 1], Jiri Damborsky [e, f], Rafael Dolezal [a], Jan Korabecny [a], Lada Cejkova [g], Kristina Hakenova [g], Marketa Chvojkova [g], Jana Zdarova Karasova [h], Lukas Prchal [a], Martin Novak [a, i], Marharyta Kolcheva [b, c], Stepan Kortus [b, c], Karel Vales [g], Martin Horak [b, c, *], Ondrej Soukup [a, **]

[a] *Biomedical Research Center, University Hospital Hradec Kralove, Sokolska 581, 500 05, Hradec Kralove, Czech Republic*
[b] *Institute of Experimental Medicine of the Czech Academy of Sciences, Videnska 1083, 14220, Prague 4, Czech Republic*
[c] *Institute of Physiology of the Czech Academy of Sciences, Videnska 1083, 14220, Prague 4, Czech Republic*
[d] *Department of Physiology, Faculty of Science, Charles University in Prague, Albertov 6, 12843, Prague 2, Czech Republic*
[e] *Loschmidt Laboratories, Department of Experimental Biology and RECETOX, Masaryk University, Kamenice 5/A4, 625 00, Brno, Czech Republic*
[f] *International Centre for Clinical Research, St. Anne's University Hospital, Pekarska 53, 656 91 Brno, Czech Republic*
[g] *National Institute of Mental Health, Topolová 748, 250 67, Klecany, Czech Republic*
[h] *Department of Toxicology and Military Pharmacy, Faculty of Military Health Sciences, University of Defence, Trebesska 1575, 500 01, Hradec Kralove, Czech Republic*
[i] *Department of Pharmaceutical Chemistry and Pharmaceutical Analysis, Faculty of Pharmacy in Hradec Kralove, Charles University, Heyrovskeho, 1203, Hradec Kralove, Czech Republic*

ARTICLE INFO

Article history:
Received 19 February 2021
Received in revised form
29 March 2021
Accepted 31 March 2021
Available online 20 April 2021

Keywords:
QSAR
Acetylcholinesterase
Electrophysiology
Glutamate receptor
Ion channel
Pharmacology
in vivo
Tacrine

ABSTRACT

Tacrine is a classic drug whose efficacy against neurodegenerative diseases is still shrouded in mystery. It seems that besides its inhibitory effect on cholinesterases, the clinical benefit is co-determined by NMDAR-antagonizing activity. Our previous data showed that the direct inhibitory effect of tacrine, as well as its 7-methoxy derivative (7-MEOTA), is ensured via a "foot-in-the-door" open-channel blockage, and that interestingly both tacrine and 7-MEOTA are slightly more potent at the GluN1/GluN2A receptors when compared with the GluN1/GluN2B receptors. Here, we report that in a series of 30 novel tacrine derivatives, designed for assessment of structure-activity relationship, blocking efficacy differs among different compounds and receptors using electrophysiology with HEK293 cells expressing the defined types of NMDARs. Selected compounds (**4** and **5**) potently inhibited both GluN1/GluN2A and GluN1/GluN2B receptors; other compounds (**7** and **23**) more effectively inhibited the GluN1/GluN2B receptors; or the GluN1/GluN2A receptors (**21** and **28**). QSAR study revealed statistically significant model for the data obtained for inhibition of GluN1/Glu2B at −60 mV expressed as IC_{50} values, and for relative inhibition of GluN1/Glu2A at +40 mV caused by a concentration of 100 μM. The models can be utilized for a ligand-based virtual screening to detect potential candidates for inhibition of GluN1/Glu2A and/or GluN1/Glu2B subtypes. Using *in vivo* experiments in rats we observed that unlike MK-801, the tested novel compounds did not induce hyperlocomotion in open field, and also did not impair prepulse inhibition of startle response, suggesting minimal induction of psychotomimetic side effects. We conclude that tacrine derivatives are promising compounds since they are centrally available subtype-specific inhibitors of the NMDARs without detrimental behavioral side-effects.

* Corresponding author. Department of Neurochemistry, Institute of Experimental Medicine of the Czech Academy of Sciences, Videnska 1083, 14220, Prague 4, Czech Republic.
** Corresponding author. Biomedical Research Centre, University Hospital Hradec Kralove, Sokolska 581, 50005, Hradec Kralove, Czech Republic.
E-mail addresses: martin.horak@iem.cas.cz (M. Horak), ondrej.soukup@fnhk.cz (O. Soukup).
[1] L.G.. and A.M. contributed equally.

https://doi.org/10.1016/j.ejmech.2021.113434

1. Introduction

The so-called multitarget-directed ligand (MTDL) paradigm has been widely applied in the last decade to find novel drug candidates against Alzheimer's disease (AD) [1–4]. However, this approach seems to be limited by oversimplified design of novel drug candidates combining pharmacophores with incompatible mechanisms of action, or by reason of irrelevance in the context of disease progression in time [5]. Another limitation is associated with the fact that simple *linking* of the two pharmacophores usually leads to lower drug-likeness, and hence *fused* or *merged* strategies are more preferred [5]. Since AD is currently treated by acetylcholinesterase inhibitors (AChEI) and memantine, an antagonist of *N*-methyl-D-aspartate receptors (NMDAR), a combination of such drugs makes sense, given the fact that impairment of both cholinergic and glutamatergic neurotransmission occurs simultaneously, i.e. in the latter stage of the disease. Hence, Namzaric, a fixed dose combination of donepezil and memantine, was approved by the FDA in 2014 [6].

The dual concept applying inhibition of both AChE and NMDAR based on a *linking* MTDL approach was first pioneered by Simoni et al. who linked galantamine and memantine by a six-membered carbon chain to deliver memagal as a lead structure [7]. It was followed by an *in vivo* study of the shorter-tethered analogue ARN14140, which demonstrated efficacy in preventing cognitive impairment and in its neuroprotective potential [8]. In other research, tacrine-based hybrids with memantine were prepared and evaluated for their *in vitro* affinity towards NMDAR [9,10], and later neuroprotective efficacy was confirmed in the NMDA-induced lesion rat model for the 6-chlorotacrine − memantine hybrid [11]. Notably, the concomitant effect of NMDAR-antagonism and AChE inhibition was established for huperzine-A, a compound approved for AD treatment in China. However, despite high expectations, its dually-acting derivatives [12] together with bis(7)-tacrine [bis(7)-cognitin] [13] have never reached clinical trials.

We have recently summarized that tacrine itself possesses both direct and indirect effects on glutamatergic neurons. Indirect beneficial effect may involve inhibition of Ca^{2+}-activated potassium channels, which prevents membrane repolarization and thus leads to prolonged NMDAR activation and long-term potentiation [14]. Interestingly, the direct effect of tacrine, as well as its 7-methoxy derivative (7-MEOTA), is implemented by inhibition of NMDAR via a "foot-in-the-door" open-channel block, with affinity in the case of 7-MEOTA comparable to that of memantine [15]. We also found that the IC_{50} values for tacrine and 7-MEOTA exhibit the following GluN2 subunit-dependent pattern: GluN1/GluN2A < GluN1/GluN2B < GluN1/GluN2C = GluN1/GluN2D. Interestingly, 7-MEOTA significantly surpassed the neuroprotective effect of both tacrine and memantine in the NMDA-induced lesion rat model, which supports a potential clinical impact [15].

In summary, we hypothesize that the clinical efficacy of tacrine is also co-determined by the NMDAR-antagonizing activity. Thus, compounds structurally related to tacrine can be considered as true MTDLs, and tacrine's structural simplicity ensures its drug-likeness, in contrast to MTDLs created by the *linked* approach. From this standpoint, different tacrine substitutions will deliver various effects on both AChE and NMDAR. In particular, effects on the latter offer a novel approach, and tuning the efficacy and selectivity to different subtypes of NMDARs represents an interesting opportunity in the field of NMDAR antagonists. It is of note that specific inhibitors of GluN1/GluN2B receptors are of interest for their suppression of the negative effects of excitotoxicity [16] and ischemia [17]. Moreover, it has been anticipated that low expression levels of GluN1/GluN2B receptors in the cerebellum may prevent their side effects [18].

The aim of this study was to develop novel tacrine derivatives with dual effect on cholinesterases and NMDAR, specifically with preference towards GluN1/GluN2A and/or GluN1/GluN2B receptors. Specifically, we synthesized a series of 30 tacrine derivatives and investigated their inhibitory potency towards human recombinant AChE (hAChE) and human plasmatic butyrylcholinesterase (hBChE), and their ability to block GluN1/GluN2A and GluN1/GluN2B receptors at negative and positive membrane potentials. These experiments were followed by analyses of quantitative structure-activity relationships (QSAR) which to the best of our knowledge was performed for the first time ever for tacrine-based compounds. In addition, to follow the potential clinical application of such dually-acting compounds, we have selected the six most promising candidates with more or less balanced activities and characterized them for their ability to cross the blood-brain barrier and for their safety *in vivo*, since a major concern for NMDAR ligands is their psychotomimetic side effects.

2. Design

Tacrine (Fig. 1) was the driving motif in the design of novel compounds (**1**–**30**). The critical features in the design of the novel compounds were invested in their basic physicochemical properties as defined by both bioavailability rules (Lipinski rule of 5) [19] and central accessibility (blood-brain barrier score; BBB score) (Table S1) [20]. Physicochemical characteristics are extremely important in drug development, particularly for CNS disorders. Indeed, previous attempts to amalgamate both NMDAR and cholinesterase inhibition properties into one molecule were mostly associated with poor drug-likeness of the final hybrid. 7-MEOTA-adamantylamines [9,10], 6-chlorotacrine-memantine [11], galantamine-memantines [7], benzohomoadamantane-chlorotacrines [21], and amantadine-carbazoles/tetrahydrocarbazoles [22,23], all constructed by the *linking* approach, are a few such examples of developed families possessing dual action against NMDAR and cholinesterases. The translation of their promising *in vitro* properties into *in vivo* conditions was hampered by i) imbalance of their affinities to the relevant targets (NMDAR, hAChE, hBChE); ii) a complicated drug administration protocol not suitable for long-term use in the animal/human (e.g. ARN14140 was injected intracerebroventricularly) [8]; and iii) limited solubility of the drug (e.g. 7-MEOTA-adamantylamine heterodimers) [10]. While the first issue can be addressed by tuning the affinities via structural modifications, the latter two are constrained by their physicochemical properties. Hence, in our study, all the compounds fulfill the criteria to become both CNS and orally available (Table S1). From the chemistry standpoint, we pursued a fundamental structure-activity relationship (SAR) consequent to structural modifications in two regions: i) the substitution by electron-withdrawing and/or electron-donating groups on the aromatic moiety of the basic tacrine scaffold. We have selected distinct positions of derivatization, most of them with the intention to avoid formation of toxic tacrine metabolite, i.e. 7-hydroxytacrine, as reported for hepatotoxic tacrine [24]; and ii) the size of the cycloalkyl moiety attached to the aromatic region, specifically cyclopentane, cyclohexane and cycloheptane rings. There have been numerous studies describing the SAR with respect to hAChE inhibition in tacrine congeners, and a few publications with quantitative evaluation [25–28]. However, the effect of tacrine derivatives on the NMDAR has never been systematically studied.

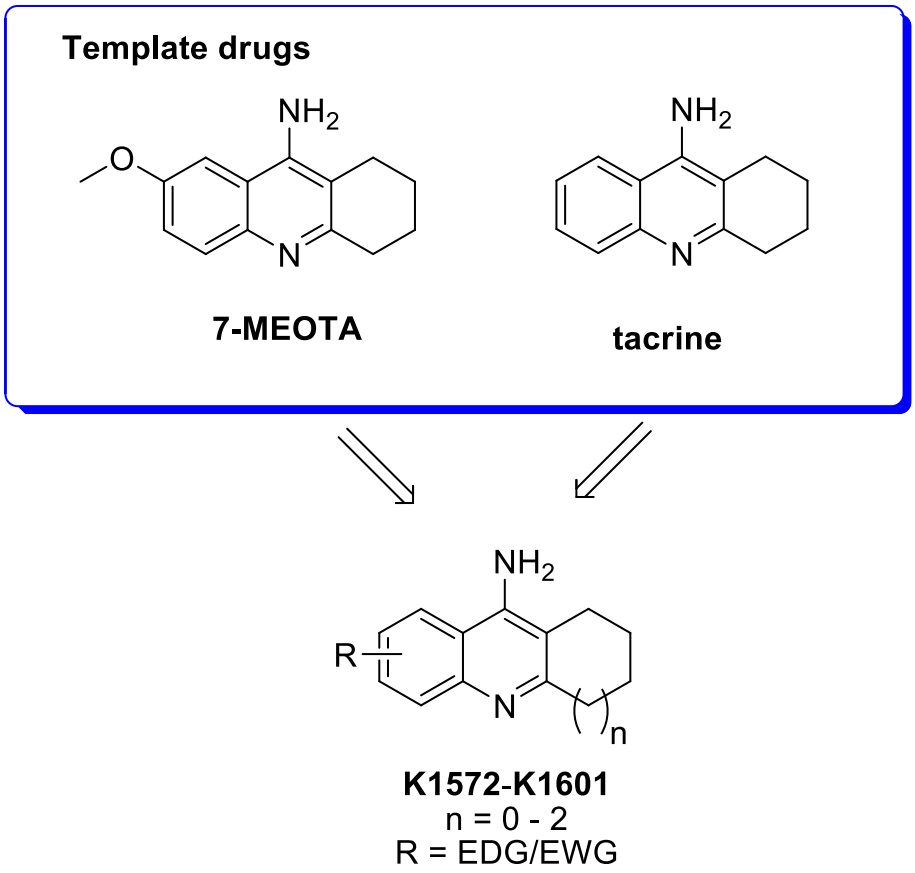

Fig. 1. Design considerations for novel tacrine derivatives **K1572**–**K1601** possessing dual AChE and NMDAR antagonism properties with tacrine and 7-MEOTA as template drugs.

3. Results and discussion

3.1. Chemistry

A highly efficient one-step procedure was applied for the synthesis of **1**–**30** (Scheme 1). The crucial aspect in the synthesis was the commercial availability of starting material, namely 2-aminobenzonitrile. The Lewis acid (LA) catalysed Friedländer type condensation for tacrine formation is well established in the literature. The overnight reflux reaction in 1,2-dichloroethane with excellent yields (72%–95%) has been recently described [29]. Another approach, a solvent-free reaction under standard conditions at 130 °C, leads to the desired product with poor to good yields (20%–60%) [25].

In our case, we applied microwave (MW) irradiation to speed up the reaction [30]. Indeed, the full conversion was completed in less than 10 min. Moreover, the solvent-free reaction exhibited mostly excellent yields over 80%. We also found that not all LAs were equally efficient. In some cases, $ZnCl_2$ led to no reaction at all.

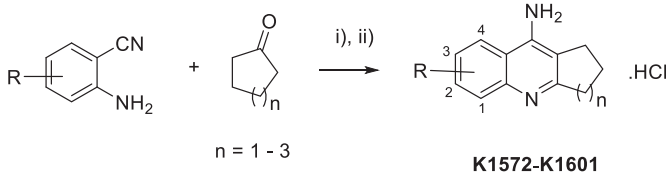

Scheme 1. The reaction of 2-aminobenzonitrile with cyclic ketone leading to the final tacrine derivatives. $ZnCl_2$ or $AlCl_3$ were used as LAs in the Friedländer type condensation. Reagents and conditions: i) LA; MW; 10 min; 150 °C; ii) MeOH; HCl (25% in H_2O), RT.

Generally, in the case of the reaction with cyclopentanone, stronger LAs had to be used. In contrast, $AlCl_3$ always yielded a complete reaction. All the tacrines were converted into their corresponding hydrochloride salts. Compounds were analyzed by a combination of ^1H NMR and ^{13}C NMR spectra, and their identity was confirmed by HRMS. All of them exhibited purity ≥97%.

3.2. In vitro anti-cholinesterase assay

Modified Ellman's method was applied to assess the inhibitory potency of the novel compounds [31]. The inhibitory potencies of all newly developed compounds are summarized in Table 1. hAChE inhibition is still regarded as crucial in the symptomatic therapy of AD, but it has to be pointed out that hAChE levels decrease with the disease progression, whereas those of hBChE remain stable or become slightly elevated as a compensatory mechanism for the loss of neuronal hAChE activity [32]. For these reasons, we have established the inhibition activity against both hAChE and hBChE. Except for **19**, all the compounds were effective inhibitors of both hAChE and hBChE in a two-digit nanomolar to two-digit micromolar range, with IC_{50} values ranging respectively from 33 nM (**20**) to 22.5 μM (**3**), and from 62 nM (**20**) to 89.9 μM (**15**). With respect to the size of the saturated rings, compounds bearing five- and six-membered rings exhibited slightly increased selectivity towards AChE. Seven-membered congeners showed less profound selectivity; although, hBChE selectivity was rather observed. This accords with the larger hBChE cavity compared to the narrow hAChE gorge, such that larger derivatives should be better accommodated by the hBChE enzyme [33]. 3-Fluoro derivatives (**16**–**18**) were more potent than 3-chloro derivatives (**7**–**9**), and those in turn exceeded

Table 1
Inhibitory effect of tacrine derivatives at AChE, BChE and recombinant NMDAR expressed in HEK293 cells.

compound	n	R	GluN1/GluN2A		GluN1/GluN2B		ChE		
			IC_{50} ± SEM (μM) (−60 mV)	RI (+40 mV) at 100 μM (%)*	IC_{50} ± SEM (μM) (−60 mV)*	RI (+40 mV) at 100 μM (%)	*h*AChE IC_{50} ± SEM (μM)	*h*BChE IC_{50} ± SEM (μM)	SI (*h*BChE/*h*AChE)
K1572 (**1**)	1	3-CH_3	20.46 ± 1.21	30.78 ± 2.03	19.78 ± 2.84	53.74 ± 2.35	10.0 ± 1.0	23.7 ± 2.37	2.37
K1573 (**2**)	2	3-CH_3	12.28 ± 1.56	18.54 ± 2.08	13.18 ± 0.91	78.41 ± 2.99	15.5 ± 1.4	13.7 ± 0.4	0.88
K1574 (**3**)	3	3-CH_3	27.12 ± 1.97	40.09 ± 2.45	16.58 ± 1.30	50.94 ± 2.69	22.5 ± 1.6	10.6 ± 0.4	0.47
K1575* (**4**)	1	3-Br	6.31 ± 0.27	75.31 ± 1.85	8.24 ± 0.80	93.22 ± 2.38	5.69 ± 0.28	16.9 ± 1.5	3.03
K1576* (**5**)	2	3-Br	6.93 ± 1.03	79.33 ± 2.65	8.32 ± 0.97	90.95 ± 3.27	4.79 ± 0.02	20.8 ± 1.2	4.34
K1577 (**6**)	3	3-Br	13.84 ± 1.25	57.72 ± 4.02	11.81 ± 1.37	91.58 ± 4.02	13.8 ± 0.6	15.1 ± 1.1	1.09
K1578* (**7**)	1	3-Cl	21.01 ± 0.71	56.49 ± 2.26	8.69 ± 0.60	78.73 ± 4.65	1.58 ± 0.05	6.88 ± 0.65	4.35
K1579 (**8**)	2	3-Cl	14.79 ± 1.22	47.53 ± 2.31	9.82 ± 1.28	86.54 ± 1.88	1.94 ± 0.07	6.72 ± 0.54	3.46
K1580 (**9**)	3	3-Cl	20.23 ± 1.74	43.05 ± 2.03	12.00 ± 1.00	88.46 ± 2.94	8.60 ± 0.47	10.3 ± 0.7	1.19
K1581 (**10**)	1	1,3-diCl	14.63 ± 2.04	33.54 ± 3.58	21.45 ± 1.75	49.11 ± 5.88	13.1 ± 1.0	17.9 ± 0.1	1.36
K1582 (**11**)	2	1,3-diCl	23.99 ± 1.92	38.24 ± 4.28	37.09 ± 4.77	42.96 ± 6.56	4.34 ± 0.31	14.8 ± 0.4	3.41
K1583 (**12**)	3	1,3-diCl	20.03 ± 2.03	38.53 ± 5.32	37.86 ± 3.71	43.94 ± 3.78	9.04 ± 0.49	23.8 ± 1.0	2.63
K1584 (**13**)	1	1,3-diBr	10.24 ± 1.38	55.69 ± 2.27	17.11 ± 1.12	43.34 ± 1.98	15.1 ± 1.0	34% at 100 μM	n/a
K1585 (**14**)	2	1,3-diBr	15.55 ± 1.62	67.65 ± 5.27	18.70 ± 0.94	40.35 ± 3.24	5.18 ± 0.3	32.0 ± 1.1	6.17
K1586 (**15**)	3	1,3-diBr	21.52 ± 0.97	80.65 ± 3.16	26.92 ± 5.03	17.32 ± 3.44	15.1 ± 1.4	89.9 ± 7.2	5.95
K1587 (**16**)	1	3-F	27.96 ± 2.16	28.69 ± 1.15	30.32 ± 1.88	38.40 ± 0.87	0.662 ± 0.02	1.91 ± 0.1	2.88
K1588 (**17**)	2	3-F	15.44 ± 1.68	41.93 ± 2.09	21.27 ± 1.35	46.77 ± 0.66	0.978 ± 0.051	0.751 ± 0.032	0.77
K1589 (**18**)	3	3-F	14.47 ± 0.82	38.47 ± 1.61	19.81 ± 1.22	56.01 ± 1.39	0.624 ± 0.025	0.569 ± 0.022	0.911
K1590 (**19**)	1	4-Cl	27.02 ± 2.94	24.48 ± 2.91	44.88 ± 5.00	23.83 ± 3.22	6% at 100 μM	6% at 100 μM	n/a
K1591 (**20**)	2	4-Cl	19.61 ± 0.91	34.97 ± 1.40	23.72 ± 1.89	28.96 ± 1.26	0.0334 ± 0.0014	0.062 ± 0.003	1.85
K1592* (**21**)	3	4-Cl	7.29 ± 0.57	46.73 ± 3.49	22.07 ± 1.11	37.95 ± 5.26	0.223 ± 0.006	0.311 ± 0.016	1.39
K1593 (**22**)	1	2-CH_3	7.68 ± 0.79	53.56 ± 1.36	15.59 ± 1.28	62.98 ± 3.07	0.347 ± 0.013	8.44 ± 0.49	24.3
K1594* (**23**)	2	2-CH_3	17.05 ± 1.59	51.33 ± 1.44	7.83 ± 0.34	72.00 ± 2.89	0.072 ± 0.003	2.90 ± 0.08	40.2
K1595 (**24**)	3	2-CH_3	15.19 ± 1.47	50.05 ± 3.98	9.29 ± 0.54	58.86 ± 5.59	0.104 ± 0.004	1.00 ± 0.03	9.16
K1596 (**25**)	1	4-CH_3	21.92 ± 2.18	22.04 ± 2.84	16.55 ± 2.28	37.43 ± 1.76	0.415 ± 0.028	0.471 ± 0.011	1.13
K1597 (**26**)	2	4-CH_3	18.48 ± 1.72	40.48 ± 2.16	14.21 ± 0.89	43.06 ± 8.61	0.125 ± 0.007	0.495 ± 0.017	3.96
K1598 (**27**)	3	4-CH_3	12.55 ± 1.48	54.29 ± 1.95	17.44 ± 1.43	49.04 ± 6.16	0.255 ± 0.011	0.107 ± 0.006	0.42
K1599* (**28**)	1	3-OCH_3	4.16 ± 0.37	66.12 ± 1.88	14.56 ± 1.37	52.05 ± 1.55	8.22 ± 0.35	10.6 ± 0.3	1.23
K1600 (=7-MEOTA) (**29**)	2	3-OCH_3	5.05 ± 0.62	77.59 ± 1.52	7.24 ± 0.34	68.84 ± 1.50	10.0 ± 1.0	17.6 ± 0.8	1.76
K1601 (**30**)	3	3-OCH_3	20.02 ± 1.29	53.58 ± 2.76	7.67 ± 1.22	69.17 ± 3.59	17.6 ± 0.7	4.41 ± 0.34	0.25
tacrine[1]	–	–	9.1 ± 0.5	Table 2	19.7 ± 1.8	Table 2	0.32 ± 0.013	0.08 ± 0.001	0.25

the activity of 3-bromotacrines (**4**–**6**). Addition of another halogen into the 1-position decreased the affinity compared to single halogen-substituted analogues, with 1,3-dibromo compounds (**13**–**15**) being the least active in the whole series. 4-Substituted derivatives revealed inhibition potency increment in the following order: 4-chloro (**20**–**21**) > 3-chloro (**7**–**9**) derivatives; however, the 4-chloro substituted compound **19** with a five-membered ring exhibited almost no activity for both ChE. A similar trend in substituent positioning was observed in methyl derivatives, where 2-substitution (**22**–**24**) was superior to 4-substitution (**25**–**27**) and 3-substitution (**1**–**3**), the latter being the least effective towards hAChE. On the other hand, 4-methyl derivatives (**25**–**27**) were more active than 2-methyl (**22**–**24**) in the case of hBChE inhibition. The compounds with a 3-methoxy group showed only moderate albeit balanced affinity towards both enzymes. Noteworthy, the study by Recanatini and colleagues highlighted 6-chlorotacrine as the most hAChE active tacrine derivative from the series with single-digit nanomolar IC_{50} value (IC_{50} = 9.9 ± 0.3 nM). Other aryl substitutions at the aliphatic six-membered tacrine derivatives ring diminished the activity, except for some amino-substitutions by heptyl or, more preferably, by benzyl appendages [25]. Such observations have also been well documented by us in the family of *N*-alkyl-substituted 7-methoxytacrine derivatives, pointing out that the attachment of aliphatic alkyl chains improve the hAChE potency [34].

Interestingly, several compounds (**20**, **21**, **23**, **24**, **26**, and **27**) were shown to be more effective in hAChE inhibition than the parent tacrine, although none of the novel compounds surpassed tacrine's hBChE inhibition. Notably, **20** was the most potent ChE inhibitor tested (hAChE IC_{50} = 0.033 ± 0.001 μM; BChE IC_{50} = 0.062 ± 0.003 μM).

3.3. Interaction with NMDAR

Next, we aimed to examine the inhibitory effect of the new derivatives at the most common types of NMDARs in the adult human forebrain, GluN1/GluN2A and GluN1/GluN2B [35], as expressed in HEK293 cells. As we needed to screen a large set of novel derivatives with these two NMDAR types, we initially examined each compound using three different concentrations (1, 10, 100 μM) at two membrane potentials (−60 mV, +40 mV, Table 1); we did not examine concentrations >100 μM, due to physiological irrelevance and due to the fact that some compounds exhibited limited solubility when dissolved in the extracellular recording solution (ECS). Consistently with our previous data [15], we observed that at membrane potential −60 mV, 7-MEOTA is slightly more potent at the GluN1/GluN2A receptors when compared to the GluN1/GluN2B receptors (IC_{50} values: ~5 versus

~7 μM). Interestingly, the novel compounds exhibited IC_{50} values ranging from ~4 μM to ~45 μM at both the GluN1/GluN2A receptors and GluN1/GluN2B receptors, and we observed that in most cases there is no preference for the GluN1/GluN2A receptors over the GluN1/GluN2B receptors (Table 1). Notably, the reference drug memantine showed the IC_{50} value of 1.34 ± 0.08 and 0.78 ± 0.09 on GluN1/GluN2A and GluN1/GluN2B respectively [36]. With respect to our measurements at membrane potential 40 mV, we indeed observed, consistently with our previous data [15], that tacrine and its derivatives exhibited reduced inhibitory effect at both NMDAR types (Table 1). Due to the lower inhibitory activity and the screening nature of our investigation at this stage (only three concentrations were tested), we expressed the inhibitory effect of each compound at this membrane potential as the relative inhibition (RI (40 mV)). Similarly to our conclusion at negative membrane potential, RI (40 mV) values exhibited no clear preference for the GluN1/GluN2A receptors over the GluN1/GluN2B (Table 1). Nevertheless, to investigate the structure-activity relationship of tacrine derivatives on both types of NMDAR we performed QSAR analysis. Moreover, based on the results obtained from ChE/NMDA evaluation we selected 6 compounds (**4**, **5**, **7**, **21**, **23** and **28**) with the most interesting properties for detailed evaluation of NMDAR properties and for *in vivo* tests. Specifically, we selected **4** and **5** for their relatively similar affinity towards all studied targets and **7** for its approximately 10-fold higher affinity toward ChE over the GluN1/GluN2B subtype. Furthermore, we chose **21** as a non-selective submicromolar ChE inhibitor, **23** as selective AChE inhibitor with the preference of GluN1/GluN2B subtype and **28** as a compound with the preference of GluN1/GluN2A subtype.

The experimental data obtained from the electrophysiological measurements with three concentrations of each compound (1, 10, 100 μM) were fitted by Equation (2) (see the methods section); the resulting values of IC_{50}, Hill coefficient (h), and numbers of analyzed cells (n) recorded at membrane potential of −60 mV were obtained. IC_{50} (in μM) values and relative inhibition values (RI (+40 mV)) calculated for the measurements at membrane potential +40 mV are shown. Data are shown as mean ± SEM (standard error of the mean). Experimental details (h coefficient and n) are listed in Table S2. *Compounds selected for detailed assessment where IC_{50} ± SEM value was established in addition to RI at 100 μM (Table 2). [1] The data obtained from Ref. [15].

3.4. Quantitative structure-activity relationships (QSAR)

Next, analyses of Quantitative Structure-Activity Relationships were carried out to understand how the biological effects depend on the structural properties of the studied molecules. Concerning the inhibitory potency towards the GluN1/Glu2A unit, the Partial Least Squares (PLS) analysis provided a statistically significant model correlating molecular descriptors and experimentally determined observables in the relative inhibition of these receptors evoked by 100 μM of the tested compound at +40 mV (2A-RI-40). The model uses four principal components and shows statistically significant coefficient of determination $R^2 = 0.89$ and cross-validated coefficient of determination $Q^2 = 0.79$ (Fig. S1). The 45 most significant variables contributing to explanation of experimental values are shown in the Variable Importance to Projections (VIP) plot (Fig. S2). Validation of the QSAR model for 2A-RI-40 activities by cross-validation and permutation testing is illustrated in SI (Fig. S3). This exhaustive test proved that the QSAR model loses its predictivity when the input data are randomly permuted.

The most influential molecular descriptors in this QSAR model, namely Mor15 m, GeomPetitj, GoemShapeI, BCUTs-1l, and MATS1p, belong among 3D or 2D topological indices weighted by certain distance, electronegativity or intrinsic state. Apart from these complex molecular descriptors, significant influence on the biological activity was exhibited also by lipophilicity (SlogP_VSA6), suggesting that more lipophilic compounds elicit stronger biological response, i.e., higher inhibitory potency towards the GluN1/Glu2A subunit.

Furthermore, PLS analysis provided also a statistically significant model correlating molecular descriptors and experimentally determined inhibitory potency on the GluN1/Glu2B unit at −60mV, expressed as the IC_{50} values (2B-IC50). The model uses four principal components and shows a significant coefficient of determination $R^2 = 0.89$ and cross-validated coefficient of determination $Q^2 = 0.73$ (Fig. S4). The 54 most significant variables contributing to explanation of experimental values are shown in the VIP plot (Fig. S5). The validation test of the QSAR model proving its high sensitivity to data mismatch is described in Fig. S6. According to the VIP values, the most influential molecular descriptors in this QSAR model are represented by BalabanJ, Xc-5d, MATS4pe, MDEC-33, and Xpc-5d, which are 2D/3D topological indices weighted by certain geometrical or electronic parameters. It was discovered in the plot of loadings for the two most significant principal components in the QSAR model that the molecular descriptors form several features and groups, suggesting intercorrelations among the descriptors.

However, the proposed QSAR models are applicable at the above-mentioned statistical level of significance only if all involved molecular descriptors are taken into consideration. Due to the high complexity of PLS based models, this QSAR can be utilized especially in a ligand-based virtual screening to select potential candidates for inhibition of GluN1/Glu2A and/or GluN1/Glu2B rather than for intuitive design of novel chemical structures with significant activity for the receptor. Further details on the selected descriptors may be found online (https://mordred-descriptor.github.io/documentation/master/descriptors.html).

In summary, both GluN1/GluN2A and GluN1/GluN2B receptors have a highly homologous amino acid composition in the ion channel region [35], which likely contains a binding site for the studied inhibitors [15]. Therefore, the significance of similar

Table 2
Dose-response relationships for inhibition of the selected tacrine derivatives at GluN1/GluN2A and GluN1/GluN2B receptors.

code name	GluN1/GluN2A		GluN1/GluN2B	
	IC_{50} ±SEM (−60 mV	IC_{50} ±SEM (+40 mV)	IC_{50} ±SEM (−60 mV	IC_{50} ±SEM (+40 mV)
29	4.70 ± 0.30	49.31 ± 1.97	7.24 ± 0.34	51.02 ± 2.99
4	6.12 ± 0.12	51.35 ± 1.77	6.98 ± 0.39	23.00 ± 1.27
5	6.58 ± 0.76	45.89 ± 3.23	7.80 ± 0.48	12.75 ± 1.36
7	22.56 ± 0.83	84.16 ± 5.75	9.39 ± 0.47	27.66 ± 1.11
23	21.55 ± 1.38	98.56 ± 5.06	8.03 ± 0.52	41.82 ± 2.74
21	7.66 ± 0.35	111.60 ± 5.32	26.14 ± 0.93	146.40 ± 10.86
28	5.16 ± 0.58	66.80 ± 4.30	16.06 ± 1.15	88.89 ± 4.66
tacrine[1]	9.1 ± 0.5	84.6 ± 1.6	19.7 ± 1.8	168.8 ± 9.3

molecular descriptors was expected when analyzing structure-activity relationships. Both models employ analogous descriptors (complex topological indexes) for the explanation of the biological activity. This is in accordance with the expected binding of studied molecules to the molecular pore, which will primarily depend on the size and conformational flexibility of studied inhibitors. The model constructed for the determined activities 2A-RI-40 additionally employs also the descriptor of lipophilicity (SlogP_VSA6). This descriptor's statistical importance suggests that hydrophobic interactions are the additional driving force for the binding of studied compounds to the receptor, besides the size and shape of the molecules captured by various topological complexes. In addition, different functional and pharmacological properties of GluN1/GluN2A and GluN1/GluN2B receptors, such as desensitization or open probability, may co-determine different sensitivity towards inhibitors [38]. Overall, the two models are highly similar in their composition as well as in their predictive power. Therefore, the individual models are specifically helpful for predictive purposes.

3.5. Detailed electrophysiological analysis of selected tacrine compounds at both GluN1/GluN2A and GluN1/GluN2B receptors

To pursue the pre-clinical aspect of our study, we selected the 6 most promising compounds which notwithstanding interaction with ChE: potently inhibited both GluN1/GluN2A and GluN1/GluN2B receptors (**4** and **5**); more potently inhibited the GluN1/GluN2B receptors (**7** and **23**); more potently inhibited the GluN1/GluN2A receptors (**21** and **28**) (see Table 1). Firstly, we used the same electrophysiological experimental approach as above, but with five different concentrations of tacrine derivatives (1, 3, 10, 30, 100 μM); we then obtained the respective IC_{50} values for each compound at two membrane potentials (−60 mV, +40 mV) at both NMDAR types (Table 2, Fig. 2) which corresponds well to the data shown in Table 1.

The electrophysiological data obtained using five concentrations of each compound (1, 3, 10, 30, 100 μM) from HEK293 cells expressing the indicated NMDARs were fitted by Equation (1); the resulting values of IC_{50} (in μM) recorded at membrane potentials of −60 mV or +40 mV are shown as the mean ± SEM (standard error of the mean). Experimental details (Hill's coefficient (*h*) and number of analyzed cell (n) are listed in Table S3). [1] The data obtained from Ref. [15].

3.6. Blood-brain barrier permeability

In compliance with RRR strategy for using laboratory animals, the blood-brain barrier permeability (BBB) was evaluated for six selected candidates first *in vitro* via the MDCK cell-based assay [39,40], and subsequently verified *in vivo* on a small number of mice. The cell-based assay predicted high BBB permeability, similar to that obtained for tacrine or donepezil (Table S4). *In vivo* pharmacokinetic experiments were performed on mice by injecting i.p. 5 mg kg^{-1} of the six selected candidates, and their concentration levels measured in the plasma and brain tissue by HPLC-MS at two time points, after 15 min and 60 min (a group of 3 animals per each time point). The plasma and brain distribution of the tested compounds at the two time intervals are shown in Table 3. It is obvious that all compounds are able to reach the brain, as in the case of the parent tacrine; however, in contrast they are relatively quickly excreted [41]. In the 15th minute the brain/plasma ratios were found to vary from 33% in the case of **21**−138% in the case of **28**. The brain/plasma ratio data suggests that **5** and **28** tend to accumulate in the brain [41,42], whereas compound **21** may be subject to some efflux mechanism. Such result confirms that although all the compounds are available in the CNS, levels at the 60th min interval in both plasma and brain suggest quick elimination from the organism.

3.7. Behavioral assessment of side effects

Besides their beneficial effects, NMDAR antagonists as well as AChEIs may possess side effects. Specifically, the use of numerous antagonists of NMDAR is limited by psychotomimetic effects [43−45], manifested in rodents as a behavioral syndrome including hyperlocomotion and deficits of sensorimotor gating [46−48]. On the other hand, behavioral side effects of AChEIs may involve suppression of locomotor activity [49,50]. Therefore, we assessed the acute effect of the six selected substances (**4, 5, 7, 21, 23** and **28**; 1 and 5 mg/kg, administered i.p. 15 min prior to the experiment) on spontaneous locomotor activity in open field, and prepulse inhibition of acoustic startle response in rats in order to investigate the risk of the aforementioned side effects. For comparison, the effects of 7-MEOTA (5 mg/kg) and the NMDAR non-competitive antagonist MK-801 are shown as well.

Analysis of distance moved in open field (1 mg/kg doses) revealed significant effect of treatment (ANOVA; $F(6, 37) = 6.269$, $P = 0.0001$). Compound **21** decreased locomotor activity ($P < 0.0001$ vs. DMSO; Bonferroni post hoc test; Fig. 3A). At a dose of 5 mg/kg, a significant effect of treatment was observed, too (Brown-Forsythe ANOVA; $F^*(8, 13.37) = 38.00$, $P < 0.0001$). Dunnett's T3 multiple comparisons test showed that the distance moved by the animals from groups **4, 5, 7, 21, 23** (5 mg/kg for all) was significantly lower than that of the control DMSO group ($P = 0.0194$, $P = 0.0374$, $P = 0.0001$, $P < 0.0001$ and $P = 0.0013$, respectively), while MK-801 (0.2 mg/kg), as expected, significantly increased the locomotion ($P = 0.0098$; Fig. 3B).

Next, we investigated the effect of the tested compounds on prepulse inhibition of acoustic startle response (% PPI). At a dose of 1 mg/kg, the compounds did not affect PPI (Fig. 3C). ANOVA of PPI for the compounds at a 5 mg/kg dose showed a significant effect of treatment ($F(8, 48) = 7.377$, $P < 0.0001$), with Bonferroni post hoc test revealing the expected deleterious effect of MK-801 (0.3 mg/kg, $P < 0.0001$ vs. DMSO; Fig. 3D). The results thus indicated that unlike MK-801, all the tested compounds at both doses were free of hyperlocomotion-inducing effects in open field, and they did not impair prepulse inhibition of startle response, suggesting low risk of induction of psychotomimetic side effects. This fact is of great importance, given that serious psychotomimetic effects represent a major limitation for the use of many NMDAR antagonists [45].

On the other hand, substances **4**, **5**, **7**, **21** and **23**, when administered at the higher dose, considerably suppressed locomotor activity in the open field. As AChEIs may suppress locomotor activity [49,50], we suggest that the observed effect may be at least partially exerted via inhibition of hAChE. It seems to be corroborated by the fact that **28** and 7-MEOTA, the only compounds which at a dose of 5 mg/kg did not decrease the locomotor activity, represent the least potent AChEIs of all the tested compounds. By contrast, hypolocomotion was most prominent in animals treated with **21** (5 mg/kg), a potent inhibitor of both AChE and BChE. Moreover, compound **21**, unlike the other compounds, decreased locomotion even at the lower tested dose (1 mg/kg). However, the *in vivo* mechanisms of action seem to be complex, and simultaneous involvement of other mechanisms in the hypolocomotion-inducing effect cannot be excluded, as the extent of suppression of locomotion does not appear to correspond exactly to the IC_{50} for hAChE. Compound **23**, the most potent inhibitor of hAChE, did not induce the most prominent locomotion-decreasing effect. Notably, **21** exerts about 10-fold more potent inhibition of BChE than **23**, perhaps explaining the more pronounced behavioral effect of **21** and suggesting that

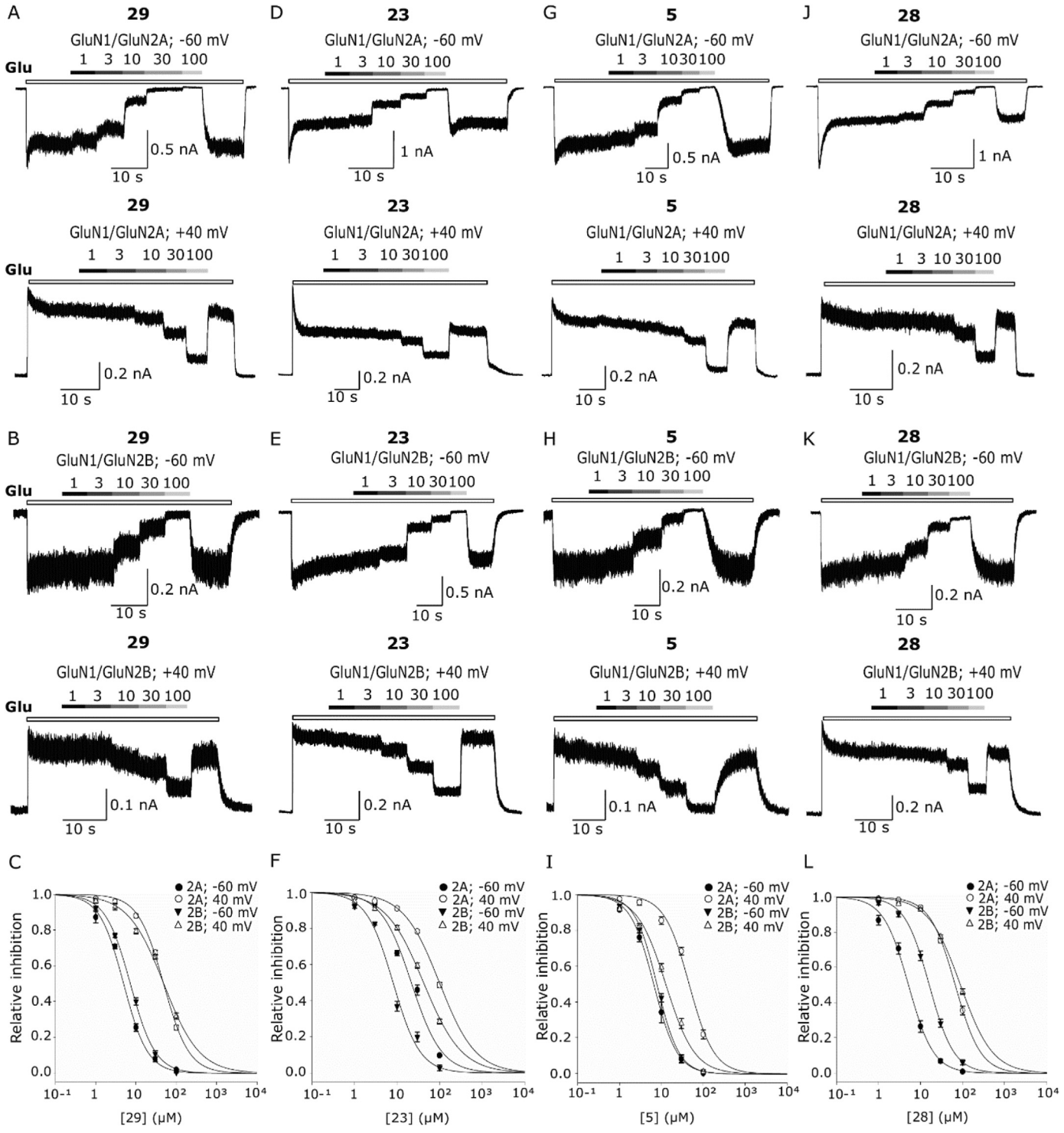

Fig. 2. The selected most potent derivatives of tacrine. Representative responses of tacrine's derivatives at membrane potentials of −60 mV and +40 mV from HEK293 cells transfected with GluN1/GluN2A (A,D,G,J) and GluN1/GluN2B (B,E,H,K) receptors; the identities of the derivatives are shown above each current trace with a concentration scale (1−100 μM) with co-application of 1 mM glutamate (Glu). Concentration-inhibition curves for **29** (C), **23** (F), **5** (I), **28** (L) were obtained by fitting the experimental data from GluN1/GluN2A and GluN1/GluN2B receptors at −60 and + 40 mV with Equation (1).

inhibition of BChE or the ratio of hBChE/hAChE inhibition might also play a role in the suppression of locomotor activity. These findings seem to be in accordance with these of Pan et al. [51], who compared the effect of tacrine and bis(7)-tacrine on locomotor activity, revealing that tacrine, despite its much less potent inhibition of AChE, decreased the locomotion more profoundly. Interestingly, tacrine and bis(7)-tacrine show different hBChE/hAChE IC_{50} ratios (0.41 and 99.38 respectively) [52], possibly explaining the locomotion-decreasing potential of tacrine and perhaps mirroring our situation with **21** and **23**. Correspondingly [4], suggest that higher selectivity towards hAChE may be associated with lower risk of certain side effects [53].

Table 3
In vivo availability of selected compounds in the plasma and brain (mice, dose 5 mg/kg), i.p.).

	Concentration (nM) 15th min		Concentration (nM) 60th min		Brain/plasma ratio (%; 15th min)
Compound	Plasma	Brain	Plasma	Brain	
4	2522	1176	154	116	47
5	1334	1376	170	218	103
7	1657	1003	389	173	61
21	2297	762	185	32	33
23	1304	731	87	251	56
29	1673	2315	207	326	138

In summary, the selected compounds were found to be free of psychotomimetic effects of NMDAR antagonists. The only observed side effect, manifested as suppression of locomotor activity and presented at the higher of the tested doses, may represent an expected side effect associated with the drugs' mechanism of action, and hopefully should not appreciably limit the potential use of the tested substances. These favorable findings justify future testing of their therapeutic *in vivo* effects.

4. Conclusions

In this work we have prepared a series of 30 novel tacrine derivatives designed for assessment of structure-activity relationships on the NMDARs. We have shown that, apart of the inhibitory activity towards cholinesterases, selected compounds (**4** and **5)** potently non-selectively inhibit both GluN1/GluN2A and GluN1/GluN2B receptors; compounds (**7** and **23)** more potently inhibited the GluN1/GluN2B receptors; compounds (**21** and **28**) more potently inhibited GluN1/GluN2A receptors. The QSAR analysis revealed significant correlation for data obtained for inhibition of GluN1/Glu2B at −60mV and for relative inhibition of GluN1/Glu2A at +40 mV respectively, which can be used in ligand-based virtual screening to detect potential NMDAR ligands. The most influential molecular descriptors were found the 3D or 2D weighted topological indices namely Mor15 m, GeomPetitj, GoemShapeI, BCUTs-1l, and MATS1p for the GluN1/Glu2A subunit and BalabanJ, Xc-5d, MATS4pe, MDEC-33, and Xpc-5d for the GluN1/Glu2B subunit. Apart from that, lipophilicity showed significant influence on the biological activity.

From the (pre-)clinical point of view, we observed in rats that the tested novel compounds did not induce hyperlocomotion, neither impaired the prepulse inhibition of startle response. Thus despite of proved CNS availability of this class of compounds absence of side-effects typical for blockers of NMDA receptors was observed. Thus, the data have indicated that tacrine derivatives are promising dual-acting compounds, which in addition to their anti-ChE effects, act as centrally available subtype-specific inhibitors of the NMDARs without negative behavioral side effects.

5. Experimental section

5.1. General synthetic methods

Column chromatography was performed using silica gel 100 at atmospheric pressure (70−230-mesh ASTM, Fluka, Prague, Czech Republic). Analytical thin-layer chromatography was carried out using plates coated with silica gel 60 with the fluorescent indicator F254 (Merck, Prague, Czech Republic). The thin-layer chromatography plates were visualized by exposure to ultraviolet light

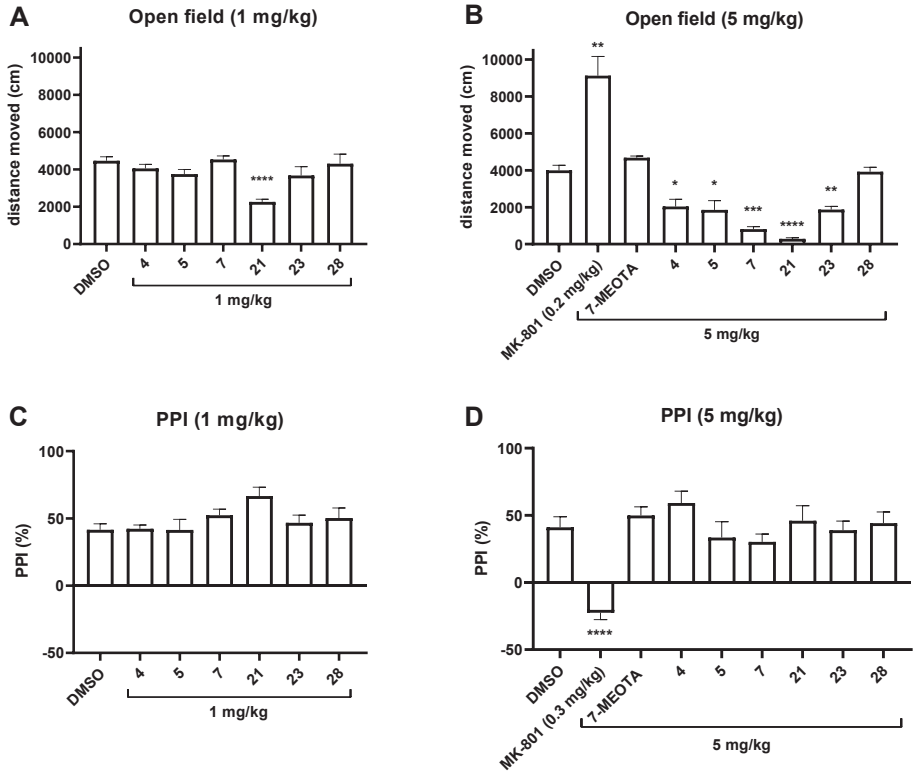

Fig. 3. Behavioral effects of compounds **4**, **5**, **7**, **21**, **23** and **28**. Graphs show distance moved in open field by rats treated with the tested compounds at doses of 1 mg/kg (A) and 5 mg/kg (B), and prepulse inhibition of acoustic startle response in rats treated with the compounds at doses of 1 mg/kg (C) and 5 mg/kg (D). *P < 0.05, **P < 0.01, ***P < 0.001 and ****P < 0.0001 compared to DMSO.

(254 nm) or using the detection reagents phosphomolybdic acid (PMA) and *p*-anisaldehyde (PERNOD). All the NMR spectra were recorded on a Varian S500 spectrometer (500 MHz for ^{1}H and 126 MHz for ^{13}C). Chemical shifts are reported in δ ppm referenced to residual solvent signals (for ^{1}H NMR and ^{13}C NMR: chloroform-*d* ($CDCl_3$; 7.26 (D) or 77.16 (C) ppm), methanol-d_4 (CD_3OD; 3.35, 4.78 (D), or 49.3 (C) ppm), or dimethylsulfoxide-d_6 (DMSO-d_6; 2.50 (D) or 39.7 (C) ppm). The chemicals were purchased from Sigma-Aldrich Co., LLC (Prague, Czech Republic) and were used without additional purification. A CEM Explorer SP 12 S was used for the MW-assisted reactions. The final compounds were analyzed by high performance liquid chromatography (HPLC) with mass spectrometric detection (MS) using a Dionex Ultimate 3000 RS UHPLC system coupled with a Q Exactive Plus Orbitrap mass spectrometer (Thermo Fisher Scientific, Bremen, Germany) to obtain high-resolution mass spectra (HRMS). Gradient LC analysis confirmed >97% purity.

5.2. Synthesis

5.2.1. General procedure for tacrine derivatives formation

The appropriately-substituted starting 2-amino-benzonitrile (1.0 eq); lewis acid (LA; 2.0 eq); and cyclopentanone, cyclohexanone, or cycloheptanone (2 mL) were challenged by MW irradiation for 10 min at 150 °C. The resulting solid was diluted with 2 M NaOH (3 mL) and dichloromethane (DCM) 2 mL and stirred for 30 min. The solution was diluted by another 2 M NaOH (20 mL) and washed three times with DCM (3 × 20 mL). The organic layers were collected, dried with anhydrous Na_2SO_4, and filtered, and the filtrate concentrated. The residue was purified by column chromatography to give the crude product as a base. The base was dissolved in MeOH (10 mL) and HCl (25% in H_2O; 1.5 mL) and stirred overnight. The solution was concentrated and dried to give crude hydrochloride product.

7-methyl-1*H*,2*H*,3*H*-cyclopenta[*b*]quinolin-9-amine hydrochloride (1): 2-amino-5-methylbenzonitrile (180 mg; 1.36 mmol); $AlCl_3$ (363 mg; 2.72 mmol). Purified by column chromatography using mobile phase DCM/MeOH/NH_4OH (7:1:0.1) to give the product as a brownish solid. Yield 83%; mp at 252 °C with decomposition.

^{1}H NMR (500 MHz, DMSO-d_6) δ 8.04 (s, 1H), 7.64 (d, J = 8.5 Hz, 1H), 7.47–7.39 (m, 1H), 7.06 (bs, 2H), 2.96 (t, J = 7.7 Hz, 2H), 2.81 (t, J = 7.3 Hz, 2H), 2.44 (s, 3H), 2.08 (p, J = 7.6 Hz, 2H). ^{13}C NMR (126 MHz, DMSO-d_6) δ 163.06, 148.31, 143.37, 132.99, 131.37, 125.08, 121.73, 116.91, 113.89, 33.55, 27.82, 22.30, 21.29. HRMS (HESI$^+$): [M+H]$^+$: calculated for $C_{13}H_{15}N_2^+$ (m/z): 199.1230; found: 199.1229. HPLC purity >99%.

7-methyl-1,2,3,4-tetrahydroacridin-9-amine hydrochloride (2): 2-amino-5-methylbenzonitrile (315 mg; 2.38 mmol); $ZnCl_2$ (648 mg; 4.76 mmol). Purified by column chromatography using mobile phase DCM/MeOH/NH_4OH (9:1:0.1) to give the product as a brownish solid. Yield 98%; mp 154 °C.

^{1}H NMR (500 MHz, CD_3OD) δ 7.81 (dd, J = 1.9, 1.0 Hz, 1H), 7.59 (d, J = 8.6 Hz, 1H), 7.40 (dd, J = 8.6, 1.8 Hz, 1H), 2.88 (t, J = 6.1 Hz, 2H), 2.58 (t, J = 6.2 Hz, 2H), 2.48 (s, 3H), 1.97–1.83 (m, 4H). ^{13}C NMR (126 MHz, CD_3OD) δ 156.99, 151.01, 144.28, 134.76, 132.35, 126.31, 121.47, 117.96, 110.54, 33.31, 24.51, 23.75, 23.63, 21.60. HRMS (HESI$^+$): [M+H]$^+$: calculated for $C_{14}H_{17}N_2^+$ (m/z): 213.1386; found: 213.1383. HPLC purity >99%.

2-methyl-6*H*,7*H*,8*H*,9*H*,10*H*-cyclohepta[b]quinolin-11-amine hydrochloride (3): 2-amino-5-methylbenzonitrile (180 mg; 1.36 mmol); $AlCl_3$ (363 mg; 2.72 mmol). Purified by column chromatography using mobile phase DCM/MeOH/NH_4OH (7:1:0.1) to give the product as a brownish solid. Yield 81%; mp 103 °C.

^{1}H NMR (500 MHz, DMSO-d_6) δ 7.99 (d, J = 1.7 Hz, 1H), 7.61 (d, J = 8.5 Hz, 1H), 7.40 (dd, J = 8.5, 1.8 Hz, 1H), 6.71 (bs, 2H), 3.04–2.95 (m, 2H), 2.83–2.76 (m, 2H), 2.44 (s, 3H), 1.79 (p, J = 6.3 Hz, 2H), 1.63 (p, J = 5.4 Hz, 2H), 1.55 (p, J = 5.6 Hz, 2H). ^{13}C NMR (126 MHz, DMSO-d_6) δ 161.79, 148.32, 142.30, 133.12, 130.90, 126.02, 121.68, 117.36, 114.29, 37.74, 31.64, 27.57, 26.56, 25.30, 21.41. HRMS (HESI$^+$): [M+H]$^+$: calculated for $C_{15}H_{19}N_2^+$ (m/z): 227.1543; found: 227.1543. HPLC purity >99%.

7-bromo-1*H*,2*H*,3*H*-cyclopenta[b]quinolin-9-amine hydrochloride (4): 2-amino-5-bromobenzonitrile (154 mg; 0.782 mmol); $ZnCl_2$ (213 mg; 1.563 mmol). Purified by column chromatography using mobile phase DCM/MeOH/NH_4OH (15:1:0.1) to give the product as an orange solid. Yield 77%; mp at 247 °C with decomposition.

^{1}H NMR (500 MHz, DMSO-d_6) δ 8.39 (d, J = 1.9 Hz, 1H), 7.65–7.54 (m, 2H), 6.53 (bs, 2H), 2.87 (t, J = 7.7 Hz, 2H), 2.80 (t, J = 7.3 Hz, 2H), 2.14–1.95 (m, 2H). ^{13}C NMR (126 MHz, DMSO-d_6) δ 167.45, 147.45, 145.58, 130.77, 130.67, 124.58, 119.17, 115.48, 114.34, 34.71, 27.82, 22.31. HRMS (HESI$^+$): [M+H]$^+$: calculated for $C_{12}H_{12}BrN_2^+$ (m/z): 263.0178; found: 263.0176. HPLC purity >99%.

7-bromo-1,2,3,4-tetrahydroacridin-9-amine hydrochloride (5): 2-amino-5-bromobenzonitrile (156 mg; 0.792 mmol); $ZnCl_2$ (216 mg; 1.58 mmol). Purified by column chromatography using mobile phase DCM/MeOH/NH_4OH (9:1:0.1) to give the product as a light orange solid. Yield 72%; mp at 274 °C with decomposition.

^{1}H NMR (500 MHz, DMSO-d_6) δ 8.42 (d, J = 1.8 Hz, 1H), 7.60–7.51 (m, 2H), 6.44 (bs, 2H), 2.80 (t, J = 6.0 Hz, 2H), 2.53 (t, J = 6.1 Hz, 2H), 1.86–1.74 (m, 4H). ^{13}C NMR (126 MHz, DMSO-d_6) δ 158.29, 147.61, 145.18, 130.98, 130.42, 124.43, 118.54, 115.44, 109.96, 33.71, 23.84, 22.67, 22.56. HRMS (HESI$^+$): [M+H]$^+$: calculated for $C_{13}H_{14}BrN_2^+$ (m/z): 277.0335; found: 277.0333. HPLC purity >99%.

2-bromo-6*H*,7*H*,8*H*,9*H*,10*H*-cyclohepta[b]quinolin-11-amine hydrochloride (6): 2-amino-5-bromobenzonitrile (155 mg; 0.787 mmol); $ZnCl_2$ (214 mg; 1.57 mmol). Purified by column chromatography using mobile phase DCM/MeOH/NH_4OH (9:1:0.1) to give the product as an orange solid. Yield 88%; mp at 231 °C with decomposition.

^{1}H NMR (500 MHz, DMSO-d_6) δ 8.44–8.32 (m, 1H), 7.57 (d, J = 2.0 Hz, 2H), 6.42 (bs, 2H), 2.99–2.89 (m, 2H), 2.81–2.74 (m, 2H), 1.78 (p, J = 5.9 Hz, 2H), 1.61 (p, J = 5.5 Hz, 2H), 1.54 (p, J = 5.6 Hz, 2H). ^{13}C NMR (126 MHz, DMSO-d_6) δ 164.92, 146.38, 145.06, 130.82, 130.71, 124.78, 119.45, 116.03, 115.11, 31.73, 27.75, 26.71, 25.48. HRMS (HESI$^+$): [M+H]$^+$: calculated for $C_{14}H_{16}BrN_2^+$ (m/z): 291.0491; found: 291.0488. HPLC purity >99%.

7-chloro-1*H*,2*H*,3*H*-cyclopenta[b]quinolin-9-amine hydrochloride (7): 2-amino-5-chlorobenzonitrile (173 mg; 1.134 mmol); $AlCl_3$ (302 mg; 2.27 mmol). Purified by column chromatography using mobile phase DCM/MeOH/NH_4OH (9:1:0.1) to give the product as a brownish solid. Yield 82%; mp at 266 °C with decomposition.

^{1}H NMR (500 MHz, DMSO-d_6) δ 8.25 (d, J = 2.4 Hz, 1H), 7.67 (d, J = 8.9 Hz, 1H), 7.47 (dd, J = 8.9, 2.3 Hz, 1H), 6.52 (bs, 2H), 2.88 (t, J = 7.7 Hz, 2H), 2.80 (t, J = 7.3 Hz, 2H), 2.10–1.97 (m, 2H). ^{13}C NMR (126 MHz, DMSO-d_6) δ 167.38, 147.27, 145.67, 130.47, 128.19, 127.18, 121.41, 118.55, 114.34, 34.68, 27.81, 22.33 HRMS (HESI$^+$): [M+H]$^+$: calculated for $C_{12}H_{12}ClN_2^+$ (m/z): 219.0684; found: 219.0681. HPLC purity >99%.

7-chloro-1,2,3,4-tetrahydroacridin-9-amine hydrochloride (8): 2-amino-5-chlorobenzonitrile (177 mg; 1.16 mmol); $AlCl_3$ (309 mg; 2.32 mmol). Purified by column chromatography using mobile phase DCM/MeOH/NH_4OH (9:1:0.1) to give the product as a brownish solid. Yield 66%; mp at 247 °C with decomposition.

^{1}H NMR (500 MHz, DMSO-d_6) δ 8.28 (d, J = 2.3 Hz, 1H), 7.62 (d, J = 8.9 Hz, 1H), 7.46 (dd, J = 9.0, 2.3 Hz, 1H), 6.42 (bs, 2H), 2.80 (t, J = 6.0 Hz, 2H), 2.53 (t, J = 6.1 Hz, 2H), 1.91–1.69 (m, 4H). ^{13}C NMR (126 MHz, DMSO-d_6) δ 158.22, 147.66, 145.07, 130.30, 128.40, 127.11,

121.22, 117.92, 109.94, 33.73, 23.85, 22.70, 22.58. HRMS (HESI$^+$): [M+H]$^+$: calculated for $C_{13}H_{14}ClN_2^+$ (*m*/*z*): 233.0840; found: 233.0837. HPLC purity >99%.

2-chloro-6*H*,7*H*,8*H*,9*H*,10*H*-cyclohepta[b]quinolin-11-amine hydrochloride (9): 2-amino-5-chlorobenzonitrile (181 mg; 1.186 mmol); $AlCl_3$ (316 mg; 1.372 mmol). Purified by column chromatography using mobile phase DCM/MeOH/NH_4OH (9:1:0.1) to give the product as a brownish solid. Yield 94%; mp at 253 °C with decomposition.

^{1}H NMR (500 MHz, DMSO-d_6) δ 8.25 (d, J = 2.4 Hz, 1H), 7.64 (d, J = 8.9 Hz, 1H), 7.47 (dd, J = 8.9, 2.3 Hz, 1H), 6.41 (bs, 2H), 3.01−2.91 (m, 2H), 2.84−2.73 (m, 2H), 1.78 (p, J = 5.8 Hz, 2H), 1.61 (p, J = 5.5 Hz, 2H), 1.54 (p, J = 5.5 Hz, 2H). ^{13}C NMR (126 MHz, DMSO-d_6) δ 164.83, 146.48, 144.89, 130.54, 128.25, 127.70, 121.62, 118.85, 115.11, 31.74, 27.76, 26.75, 25.50. HRMS (HESI$^+$): [M+H]$^+$: calculated for $C_{14}H_{16}ClN_2^+$ (*m*/*z*): 247.0997; found: 247.0995. HPLC purity >99%.

5,7-dichloro-1*H*,2*H*,3*H*-cyclopenta[b]quinolin-9-amine hydrochloride (10): 2-amino-3,5-dichlorobenzonitrile (148 mg; 0.79 mmol); $AlCl_3$ (211 mg; 1.58 mmol). Purified by column chromatography using mobile phase petroleum ether/ethyl acetate (PE/EA) (1:1) to give the product as a brownish solid. Yield 72%; mp at 222 °C with decomposition.

^{1}H NMR (500 MHz, DMSO-d_6) δ 8.27 (d, J = 2.3 Hz, 1H), 7.75 (d, J = 2.2 Hz, 1H), 6.70 (bs, 2H), 2.93 (t, J = 7.7 Hz, 2H), 2.81 (t, J = 7.3 Hz, 2H), 2.13−2.02 (m, 2H). ^{13}C NMR (126 MHz, DMSO-d_6) δ 168.07, 146.26, 143.49, 133.27, 128.02, 126.22, 120.99, 119.31, 115.38, 34.97, 27.86, 22.23. HRMS (HESI$^+$): [M+H]$^+$: calculated for $C_{12}H_{11}Cl_2N_2^+$ (*m*/*z*): 253.0294; found: 253.0291. HPLC purity >99%.

5,7-dichloro-1,2,3,4-tetrahydroacridin-9-amine hydrochloride (11): 2-amino-3,5-dichlorobenzonitrile (148 mg; 0.79 mmol); $AlCl_3$ (211 mg; 1.58 mmol). Purified by column chromatography using mobile phase PE/EA (2:1) to give the product as a brownish solid. Yield 86%; mp at 193 °C with decomposition.

^{1}H NMR (500 MHz, DMSO-d_6) δ 8.30 (d, J = 2.3 Hz, 1H), 7.74 (d, J = 2.2 Hz, 1H), 6.60 (bs, 2H), 2.87−2.82 (m, 2H), 2.53 (t, J = 6.0 Hz, 2H), 1.85−1.76 (m, 4H). ^{13}C NMR (126 MHz, DMSO-d_6) δ 158.97, 148.31, 141.25, 133.08, 128.12, 126.06, 120.83, 118.54, 111.02, 33.97, 23.89, 22.58, 22.38. HRMS (HESI$^+$): [M+H]$^+$: calculated for $C_{13}H_{13}Cl_2N_2^+$ (*m*/*z*): 267.0450; found: 267.0449. HPLC purity >96%.

2,4-dichloro-6*H*,7*H*,8*H*,9*H*,10*H*-cyclohepta[b]quinolin-11-amine hydrochloride (12): 2-amino-3,5-dichlorobenzonitrile (145 mg; 0.775 mmol); $AlCl_3$ (207 mg; 1.55 mmol). Purified by column chromatography using mobile phase PE/EA (2:1) to give the product as a brownish solid. Yield 96%; mp at 244 °C with decomposition.

^{1}H NMR (500 MHz, DMSO-d_6) δ 8.27 (d, J = 2.2 Hz, 1H), 7.75 (d, J = 2.2 Hz, 1H), 6.58 (bs, 2H), 3.05−2.96 (m, 2H), 2.84−2.75 (m, 2H), 1.85−1.74 (m, 2H), 1.66−1.58 (m, 2H), 1.58−1.51 (m, 2H). ^{13}C NMR (126 MHz, DMSO-d_6) δ 165.46, 147.13, 141.05, 133.35, 128.02, 126.71, 121.20, 119.52, 116.09, 39.48, 31.67, 27.52, 26.60, 25.49. HRMS (HESI$^+$): [M+H]$^+$: calculated for $C_{14}H_{15}Cl_2N_2^+$ (*m*/*z*): 281.0608; found: 281.0604. HPLC purity >99%.

5,7-dibromo-1*H*,2*H*,3*H*-cyclopenta[b]quinolin-9-amine hydrochloride (13): 2-amino-3,5-dibromobenzonitrile (167 mg; 0.605 mmol); $AlCl_3$ (161 mg; 1.21 mmol). Purified by column chromatography using mobile phase PE/EA (1:1) to give a product as a light orange solid. Yield 82%; mp at 153 °C with decomposition.

^{1}H NMR (500 MHz, DMSO-d_6) δ 8.45 (d, J = 2.1 Hz, 1H), 8.01 (d, J = 2.1 Hz, 1H), 6.71 (bs, 2H), 2.93 (t, J = 7.7 Hz, 2H), 2.82 (t, J = 7.3 Hz, 2H), 2.06 (p, J = 7.6 Hz, 2H). ^{13}C NMR (126 MHz, DMSO-d_6) δ 168.38, 146.15, 144.42, 133.59, 125.12, 124.77, 119.79, 115.37, 114.56, 35.03, 27.87, 22.24. HRMS (HESI$^+$): [M+H]$^+$: calculated for $C_{12}H_{11}Br_2N_2^+$ (*m*/*z*): 342.9263; found: 342.9259. HPLC purity >99%.

5,7-dibromo-1,2,3,4-tetrahydroacridin-9-amine hydrochloride (14): 2-amino-3,5-dibromobenzonitrile (170 mg; 0.616 mmol); $AlCl_3$ (164 mg; 1.232 mmol). Purified by column chromatography using mobile phase PE/EA (1:1) to give the product as a light orange solid. Yield 55%; mp at 203 °C with decomposition.

^{1}H NMR (500 MHz, DMSO-d_6) δ 8.48 (d, J = 2.1 Hz, 2H), 7.99 (d, J = 2.0 Hz, 1H), 6.61 (bs, 3H), 2.86−2.80 (m, 2H), 2.55−2.51 (m, 2H), 1.84−1.78 (m, 4H). ^{13}C NMR (126 MHz, DMSO-d_6) δ 159.27, 148.21, 142.14, 133.66, 125.05, 124.66, 118.99, 114.39, 111.00, 34.01, 23.88, 22.57, 22.38. HRMS (HESI$^+$): [M+H]$^+$: calculated for $C_{13}H_{13}Br_2N_2^+$ (*m*/*z*): 356.942; found: 356.9414. HPLC purity >97%.

2,4-dibromo-6*H*,7*H*,8*H*,9*H*,10*H*-cyclohepta[b]quinolin-11-amine hydrochloride (15): 2-amino-3,5-dibromobenzonitrile (167 mg; 0.605 mmol); $AlCl_3$ (161 mg; 1.21 mmol). Purified by column chromatography using mobile phase PE/EA (3:1) to give the product as a light orange solid. Yield 65%; mp at 142 °C decomposition.

^{1}H NMR (500 MHz, DMSO-d_6) δ 8.45 (d, J = 2.1 Hz, 1H), 8.00 (d, J = 1.9 Hz, 1H), 6.60 (bs, 2H), 3.04−2.96 (m, 2H), 2.82−2.76 (m, 2H), 1.83−1.76 (m, 2H), 1.66−1.59 (m, 2H), 1.59−1.51 (m, 2H). ^{13}C NMR (126 MHz, DMSO-d_6) δ 165.73, 147.06, 141.93, 133.58, 125.26, 125.01, 119.95, 116.06, 115.08, 31.67, 27.53, 26.58, 25.50. HRMS (HESI$^+$): [M+H]$^+$: calculated for $C_{14}H_{15}Br_2N_2^+$ (*m*/*z*): 370.9576; found: 370.9570. HPLC purity >99%.

7-fluoro-1*H*,2*H*,3*H*-cyclopenta[b]quinolin-9-amine hydrochloride (16): 2-amino-5-fluorobenzonitrile (122 mg; 0.896 mmol); $AlCl_3$ (239 mg; 1.79 mmol). Purified by column chromatography using mobile phase DCM/MeOH/NH_4OH (9:1:0.1) to give the product as a white solid. Yield 83%; mp at 185 °C with decomposition.

^{1}H NMR (500 MHz, DMSO-d_6) δ 7.97−7.88 (m, 1H), 7.76−7.66 (m, 1H), 7.45−7.31 (m, 1H), 6.40 (bs, 2H), 2.88 (t, J = 7.7 Hz, 2H), 2.80 (t, J = 7.3 Hz, 2H), 2.05 (p, J = 7.5 Hz, 2H). ^{13}C NMR (126 MHz, DMSO-d_6) δ 166.46, 166.44, 159.10, 157.20, 145.86, 145.84, 130.84, 130.77, 118.05, 117.98, 117.35, 117.15, 113.97, 106.14, 105.96, 34.57, 27.78, 22.43. HRMS (HESI$^+$): [M+H]$^+$: calculated for $C_{12}H_{12}FN_2^+$ (*m*/*z*): 203.0979; found: 203.0976. HPLC purity >99%.

7-fluoro-1,2,3,4-tetrahydroacridin-9-amine hydrochloride (17): 2-amino-5-fluorobenzonitrile (177 mg; 1.30 mmol); $AlCl_3$ (347 mg; 2.60 mmol). Purified by column chromatography using mobile phase DCM/MeOH/NH_4OH (9:1:0.1) to give the product as a white solid. Yield 77%; mp at 268 °C with decomposition.

^{1}H NMR (500 MHz, DMSO-d_6) δ 8.08−8.00 (m, 1H), 7.76−7.69 (m, 1H), 7.49−7.41 (m, 1H), 6.75 (bs, 2H), 2.83 (t, J = 5.9 Hz, 2H), 2.53 (t, J = 6.1 Hz, 2H), 1.85−1.75 (m, 4H). ^{13}C NMR (126 MHz, DMSO-d_6) δ 159.24, 157.33, 155.97, 149.41, 141.72, 128.92, 118.77, 118.57, 117.06, 109.49, 106.30, 106.12, 32.42, 23.64, 22.32. HRMS (HESI$^+$): [M+H]$^+$: calculated for $C_{13}H_{14}FN_2^+$ (*m*/*z*): 217.1136; found: 217.1135. HPLC purity >97%.

2-fluoro-6*H*,7*H*,8*H*,9*H*,10*H*-cyclohepta[b]quinolin-11-amine hydrochloride (18): 2-amino-5-fluorobenzonitrile (177 mg; 1.30 mmol); $AlCl_3$ (347 mg; 2.60 mmol). Purified by column chromatography using mobile phase DCM/MeOH/NH_4OH (9:1:0.1) to give the product as a white solid. Yield 98%; mp at 269 °C with decomposition.

^{1}H NMR (500 MHz, DMSO-d_6) δ 7.96−7.89 (m, 1H), 7.71−7.64 (m, 1H), 7.41−7.33 (m, 1H), 6.30 (bs, 2H), 3.01−2.91 (m, 2H), 2.84−2.74 (m, 2H), 1.86−1.74 (m, 2H), 1.65−1.50 (m, 4H). ^{13}C NMR (126 MHz, DMSO-d_6) δ 160.45, 158.51, 158.05, 153.95, 153.92, 133.87, 122.53, 122.46, 122.15, 121.95, 116.82, 116.74, 114.75, 108.60, 108.40, 32.79, 31.04, 26.23, 25.47, 24.59. HRMS (HESI$^+$): [M+H]$^+$: calculated for $C_{14}H_{16}FN_2^+$ (*m*/*z*): 231.1292; found: 231.1287. HPLC purity >99%.

8-chloro-1*H*,2*H*,3*H*-cyclopenta[b]quinolin-9-amine hydrochloride (19): 2-amino-6-chlorobenzonitrile (140 mg; 0.92 mmol); $AlCl_3$ (245 mg; 1.84 mmol). Purified by column chromatography

using mobile phase DCM/MeOH/NH_4OH (15:1:0.1) to give the product as a brownish solid. Yield 63%; mp at 253 °C with decomposition.

^{1}H NMR (500 MHz, DMSO-d_6) δ 7.65 (dd, J = 8.4, 1.4 Hz, 1H), 7.41 (dd, J = 8.4, 7.5 Hz, 1H), 7.33 (dd, J = 7.5, 1.4 Hz, 1H), 6.51 (bs, 2H), 2.90 (t, J = 7.8 Hz, 2H), 2.82−2.76 (m, 2H), 2.12−2.02 (m, 2H). ^{13}C NMR (126 MHz, DMSO-d_6) δ 166.75, 151.22, 146.28, 128.96, 128.27, 127.73, 125.83, 116.29, 114.60, 34.59, 28.15, 22.04. HRMS (HESI$^+$): [M+H]$^+$: calculated for $C_{12}H_{12}ClN_2^+$ (m/z): 219.0684; found: 219.0682. HPLC purity >98%.

8-chloro-1,2,3,4-tetrahydroacridin-9-amine hydrochloride (20): 2-amino-6-chlorobenzonitrile (135 mg; 0.885 mmol); $AlCl_3$ (236 mg; 1.77 mmol). Purified by column chromatography using mobile phase DCM/MeOH/NH_4OH (15:1:0.1) to give the product as a brownish solid. Yield 48%; mp at 252 °C with decomposition.

^{1}H NMR (500 MHz, DMSO-d_6) δ 7.61 (dd, J = 8.4, 1.4 Hz, 1H), 7.44−7.38 (m, 1H), 7.33 (dd, J = 7.5, 1.4 Hz, 1H), 6.53 (bs, 2H), 2.80 (t, J = 6.2 Hz, 2H), 2.49−2.46 (m, 2H), 1.87−1.75 (m, 4H). ^{13}C NMR (126 MHz, DMSO-d_6) δ 157.87, 148.60, 148.22, 128.68, 127.82, 127.52, 125.90, 113.89, 111.29, 33.47, 23.98, 22.51, 22.41. HRMS (HESI$^+$): [M+H]$^+$: calculated for $C_{13}H_{14}ClN_2^+$ (m/z): 233.0840; found: 233.0838. HPLC purity >99%.

1-chloro-6*H*,7*H*,8*H*,9*H*,10*H*-cyclohepta[b]quinolin-11-amine hydrochloride (21): 2-amino-6-chlorobenzonitrile (135 mg; 0.885 mmol); $AlCl_3$ (236 mg; 1.77 mmol). Purified by column chromatography using mobile phase DCM/MeOH/NH_4OH (15:1:0.1) to give the product as a brownish solid. Yield 89%; mp at 244 °C with decomposition.

^{1}H NMR (500 MHz, DMSO-d_6) δ 7.62 (s, 1H), 7.44−7.38 (m, 1H), 7.35 (dd, J = 7.5, 1.5 Hz, 1H), 6.59 (bs, 2H), 2.99−2.92 (m, 2H), 2.81−2.72 (m, 2H), 1.79 (t, J = 5.7 Hz, 2H), 1.65−1.52 (m, 4H). ^{13}C NMR (126 MHz, DMSO-d_6) δ 164.40, 148.64, 147.14, 129.09, 127.78, 127.76, 126.57, 116.44, 114.79, 39.01, 31.57, 27.37, 26.61, 25.35. HRMS (HESI$^+$): [M+H]$^+$: calculated for $C_{14}H_{16}ClN_2^+$ (m/z): 247.0997; found: 247.0994. HPLC purity >98%.

6-methyl-1*H*,2*H*,3*H*-cyclopenta[b]quinolin-9-amine hydrochloride (22): 2-amino-4-methylbenzonitrile (148 mg; 1.12 mmol); $AlCl_3$ (299 mg; 2.24 mmol). Purified by column chromatography using mobile phase DCM/MeOH/NH_4OH (9:1:0.1) to give the product as a brownish solid. Yield 83%; mp at 273 °C with decomposition.

^{1}H NMR (500 MHz, DMSO-d_6) δ 8.02 (d, J = 8.5 Hz, 1H), 7.45 (t, J = 1.4 Hz, 1H), 7.14 (dd, J = 8.5, 1.8 Hz, 1H), 6.49 (bs, 2H), 2.87 (t, J = 7.7 Hz, 2H), 2.78 (t, J = 7.4 Hz, 2H), 2.41 (s, 3H), 2.10−1.99 (m, 2H). ^{13}C NMR (126 MHz, DMSO-d_6) δ 166.02, 148.26, 146.68, 137.59, 126.95, 124.87, 122.10, 115.56, 112.98, 34.53, 27.73, 22.40, 21.33. HRMS (HESI$^+$): [M+H]$^+$: calculated for $C_{13}H_{15}N_2^+$ (m/z): 199.123; found: 199.1228. HPLC purity >99%.

6-methyl-1,2,3,4-tetrahydroacridin-9-amine hydrochloride (23): 2-amino-4-methylbenzonitrile (142 mg; 1.07 mmol); $AlCl_3$ (287 mg; 2.15 mmol). Purified by column chromatography using mobile phase DCM/MeOH/NH_4OH (9:1:0.1) to give the product as a brownish solid. Yield 77%; mp at 225 °C with decomposition.

^{1}H NMR (500 MHz, DMSO-d_6) δ 8.04 (d, J = 8.6 Hz, 1H), 7.43−7.38 (m, 1H), 7.12 (dd, J = 8.5, 1.8 Hz, 1H), 6.36 (bs, 2H), 2.80 (t, J = 6.0 Hz, 2H), 2.52 (t, J = 6.1 Hz, 2H), 2.40 (s, 3H), 1.85−1.74 (m, 4H). ^{13}C NMR (126 MHz, DMSO-d_6) δ 157.03, 148.53, 146.22, 137.63, 126.58, 124.89, 121.97, 115.09, 108.51, 33.41, 23.69, 22.75, 22.68, 21.37. HRMS (HESI$^+$): [M+H]$^+$: calculated for $C_{14}H_{17}N_2^+$ (m/z): 213.1386; found: 213.1384. HPLC purity >98%.

3-methyl-6*H*,7*H*,8*H*,9*H*,10*H*-cyclohepta[b]quinolin-11-amine hydrochloride (24): 2-amino-4-methylbenzonitrile (142 mg; 1.07 mmol); $AlCl_3$ (287 mg; 2.15 mmol). Purified by column chromatography using mobile phase DCM/MeOH/NH_4OH (5:1:0.1) to give the product as a brownish solid. Yield 99%; mp at 274 °C with decomposition.

^{1}H NMR (500 MHz, DMSO-d_6) δ 8.08 (d, J = 8.5 Hz, 1H), 7.52−7.44 (m, 1H), 7.20 (dd, J = 8.5, 1.8 Hz, 1H), 6.75 (bs, 2H), 3.02−2.95 (m, 2H), 2.83−2.74 (m, 2H), 2.42 (s, 3H), 1.79 (p, J = 5.9 Hz, 2H), 1.62 (p, J = 5.5 Hz, 2H), 1.55 (p, J = 5.7 Hz, 2H). ^{13}C NMR (126 MHz, DMSO-d_6) δ 162.56, 148.75, 144.21, 138.65, 125.84, 125.29, 122.57, 115.46, 113.79, 37.84, 31.67, 27.57, 26.55, 25.22, 21.32. HRMS (HESI$^+$): [M+H]$^+$: calculated for $C_{15}H_{19}N_2^+$ (m/z): 227.1543; found: 227.154. HPLC purity >99%.

8-methyl-1*H*,2*H*,3*H*-cyclopenta[b]quinolin-9-amine hydrochloride (25): 2-amino-6-methylbenzonitrile (158 mg; 1.196 mmol); $AlCl_3$ (319 mg; 2.39 mmol). Purified by column chromatography using mobile phase DCM/MeOH/NH_4OH (5:1:0.1) to give the product as a yellowish solid. Yield 58%; mp at 275 °C with decomposition.

^{1}H NMR (500 MHz, DMSO-d_6) δ 7.51 (dd, J = 8.4, 1.4 Hz, 1H), 7.31 (dd, J = 8.4, 7.0 Hz, 1H), 7.02 (d, J = 7.0 Hz, 1H), 5.88 (bs, 2H), 2.92−2.85 (m, 5H), 2.79 (t, J = 7.3 Hz, 2H), 2.05 (p, J = 7.6 Hz, 2H). ^{13}C NMR (126 MHz, DMSO-d_6) δ 165.19, 150.22, 148.36, 134.19, 127.49, 126.91, 126.24, 117.92, 115.72, 34.36, 28.03, 24.24, 22.20. HRMS (HESI$^+$): [M+H]$^+$: calculated for $C_{13}H_{15}N_2^+$ (m/z): 199.123; found: 199.1227. HPLC purity >99%.

8-methyl-1,2,3,4-tetrahydroacridin-9-amine hydrochloride (26): 2-amino-6-methylbenzonitrile (160 mg; 1.21 mmol); $AlCl_3$ (323 mg; 2.42 mmol). Purified by column chromatography using mobile phase DCM/MeOH/NH_4OH (9:1:0.1) to give the product as a yellowish solid. Yield 77%; mp at 240 °C with decomposition.

^{1}H NMR (500 MHz, CD_3OD) δ 7.57−7.53 (m, 1H), 7.50−7.45 (m, 1H), 7.20−7.16 (m, 1H), 2.94 (s, 3H), 2.90 (t, J = 6.2 Hz, 2H), 2.55 (t, J = 6.3 Hz, 2H), 1.99−1.87 (m, 4H). ^{13}C NMR (126 MHz, CD_3OD) δ 155.34, 155.06, 145.15, 135.86, 131.20, 128.97, 122.86, 117.54, 111.72, 31.63, 24.31, 24.27, 23.40, 22.91. HRMS (HESI$^+$): [M+H]$^+$: calculated for $C_{14}H_{17}N_2^+$ (m/z): 213.1386; found: 213.1384. HPLC purity >95%.

1-methyl-6*H*,7*H*,8*H*,9*H*,10*H*-cyclohepta[b]quinolin-11-amine hydrochloride (27): 2-amino-6-methylbenzonitrile (160 mg; 1.121 mmol); $AlCl_3$ (323 mg; 2.42 mmol). Purified by column chromatography using mobile phase DCM/MeOH/NH_4OH (7:1:0.1) to give the product as a yellowish solid. Yield 59%; mp at 235 °C with decomposition.

^{1}H NMR (500 MHz, DMSO-d_6) δ 7.50 (dd, J = 8.3, 1.4 Hz, 1H), 7.34 (dd, J = 8.4, 7.0 Hz, 1H), 7.07 (dt, J = 7.0, 1.2 Hz, 1H), 6.04 (bs, 2H), 3.00−2.93 (m, 2H), 2.89 (s, 3H), 2.81−2.74 (m, 2H), 1.83−1.76 (m, 2H), 1.63 (p, J = 5.7, 5.3 Hz, 2H), 1.56 (p, J = 5.7 Hz, 2H). ^{13}C NMR (126 MHz, DMSO-d_6) δ 162.27, 149.90, 146.76, 134.00, 127.93, 127.16, 125.97, 118.22, 115.87, 38.19, 31.60, 27.54, 26.62, 25.21, 24.26. HRMS (HESI$^+$): [M+H]$^+$: calculated for $C_{15}H_{19}N_2^+$ (m/z): 227.1543; found: 227.1539. HPLC purity >99%.

7-methoxy-1*H*,2*H*,3*H*-cyclopenta[b]quinolin-9-amine hydrochloride (28): 2-amino-5-methoxybenzonitrile (177 mg; 1.19 mmol); $AlCl_3$ (319 mg; 2.39 mmol). Purified by column chromatography using mobile phase DCM/MeOH/NH_4OH (9:1:0.1) to give the product as a white solid. Yield 60%; mp at 264 °C with decomposition.

^{1}H NMR (500 MHz, DMSO-d_6) δ 7.59 (d, J = 9.1 Hz, 1H), 7.49 (d, J = 2.8 Hz, 1H), 7.14 (dd, J = 9.1, 2.7 Hz, 1H), 6.30 (bs, 2H), 3.85 (s, 3H), 2.86 (t, J = 7.7 Hz, 2H), 2.80 (t, J = 7.3 Hz, 2H), 2.10−1.99 (m, 2H). ^{13}C NMR (126 MHz, DMSO-d_6) δ 164.15, 155.28, 145.52, 144.07, 129.58, 119.44, 118.05, 113.64, 101.55, 55.67, 34.35, 27.79, 22.50. HRMS (HESI$^+$): [M+H]$^+$: calculated for $C_{13}H_{15}ON_2^+$ (m/z): 215.1179; found: 215.1176. HPLC purity >99%.

7-methoxy-1,2,3,4-tetrahydroacridin-9-amine hydrochloride (29): 2-amino-5-methoxybenzonitrile (181 mg; 1.24 mmol); $AlCl_3$ (330 mg; 2.48 mmol). Purified by column chromatography using mobile phase DCM/MeOH/NH_4OH (9:1:0.1) to give the product as a yellowish solid. Yield 52%; mp 163 °C.

^{1}H NMR (500 MHz, DMSO-d_6) δ 7.60–7.53 (m, 2H), 7.20 (dd, J = 9.1, 2.7 Hz, 1H), 6.56 (bs, 2H), 3.86 (s, 3H), 2.81 (t, J = 6.0 Hz, 2H), 2.54 (t, J = 6.2 Hz, 2H), 1.85–1.76 (m, 4H). ^{13}C NMR (126 MHz, DMSO-d_6) δ 155.54, 154.03, 148.65, 140.37, 127.96, 120.80, 117.21, 109.12, 101.28, 55.80, 32.42, 23.71, 22.50. HRMS (HESI$^+$): [M+H]$^+$: calculated for $C_{14}H_{17}ON_2^+$ (m/z): 229.1335; found: 229.1331. HPLC purity >97%.

2-methoxy-6*H*,7*H*,8*H*,9*H*,10*H*-cyclohepta[b]quinolin-11-amine hydrochloride (30): 2-amino-5-methoxybenzonitrile (181 mg; 1.24 mmol); $AlCl_3$ (330 mg; 2.48 mmol). Purified by column chromatography using mobile phase DCM/MeOH/NH_4OH (7:1:0.1) to give the product as a yellowish solid. Yield 82%; mp 237 °C.

^{1}H NMR (500 MHz, DMSO-d_6) δ 7.64 (d, J = 9.1 Hz, 1H), 7.56 (d, J = 2.7 Hz, 1H), 7.23 (dd, J = 9.1, 2.6 Hz, 1H), 6.75 (bs, 2H), 3.87 (s, 3H), 3.02–2.94 (m, 2H), 2.85–2.77 (m, 2H), 1.80 (p, J = 5.9 Hz, 2H), 1.63 (p, J = 5.4 Hz, 2H), 1.57 (p, J = 5.5 Hz, 2H). ^{13}C NMR (126 MHz, DMSO-d_6) δ 160.14, 156.15, 156.15, 148.24, 139.03, 127.41, 120.78, 117.96, 114.38, 102.09, 55.91, 37.46, 31.62, 27.51, 26.56, 25.35. HRMS (HESI$^+$): [M+H]$^+$: calculated for $C_{14}H_{17}ON_2^+$ (m/z): 243.1492; found: 243.1488. HPLC purity >99%.

5.3. In vitro anti-cholinesterase assay

The inhibitory activity of 7-PhO-THA and all the standards against human recombinant AChE (hAChE, E.C. 3.1.1.7, purchased from Sigma-Aldrich, Prague, Czech Republic) and human plasmatic butyrylcholinesterase (hBChE, E.C. 3.1.1.8, purchased from Sigma-Aldrich, Prague, Czech Republic) were determined using the modified Ellman's method [31], according to previously published protocol [54]. The results are expressed as IC_{50} values (the concentration of the compound that is required to reduce 50% of cholinesterase (ChE) activity). For calculation of the percentage inhibition of activity (I) the following equation 1 was used:

$$I = \left(1 - \frac{\Delta A_i}{\Delta A_0}\right) \times 100\ [\%] \quad (1)$$

where ΔA_i indicates the absorbance change provided by adequate enzyme exposed to its corresponding inhibitor, and ΔA_0 indicates the absorbance change when a solution of PBS was added instead of a solution of inhibitor. Software Microsoft Excel 10 (Microsoft Corporation, Redmont, WA, USA) and GraphPad Prism version 5.02 for Windows (GraphPad Software, San Diego, CA, USA) were used for evaluation of the statistical data.

5.4. The cell culture and transfection with DNA vectors

The DNA vectors encoding the human versions of GluN1-1a (GluN1), GluN2A and GluN2B subunits as well as green fluorescent protein (GFP) have been described recently [55]. Human embryonic kidney 293 (HEK293) cells were cultured in Opti-MEM I media containing 5% fetal bovine serum (FBS; v/v; Thermo Fisher Scientific). The HEK293 cells were transfected in Opti-MEM I media containing a mixture of 0.6 μL of MATra-A Reagent (IBA) and 600 ng of DNA vectors carrying the GluN1, GluN2 and GFP (diluted in equal ratio), and were then placed on a magnet plate for 30 min [56]. After that, the HEK293 cells were trypsinised and grown in Opti-MEM I containing 1% FBS, 20 mM $MgCl_2$ and 3 mM kynurenic acid (to reduce excitotoxicity) on 35 mm glass coverslips. Electrophysiological recordings were performed at room temperature within 24–48 h after transfection.

5.5. Electrophysiology

Whole-cell patch-clamp recordings were performed using Axopatch 200B amplifiers (Molecular Devices), combined with WAS02 application systems [15,57]. The extracellular recording solution (ECS) had the following composition (in mM): 160 NaCl, 2.5 KCl, 10 HEPES, 10 glucose, 0.2 EDTA, and 0.7 $CaCl_2$ (pH adjusted to 7.3 with NaOH). In all experiments, the ECS contained the saturating concentration of co-agonist glycine (50 μM) and the NMDARs were activated by the saturating concentration of agonist glutamate (1 mM; Merck). The stock solutions of 7-MEOTA and its derivatives (10 mM) were prepared freshly before each experiment in dimethyl sulfoxide (DMSO; Merck) [15]. Glass pipettes with 5–7 MΩ tip resistance made using a P-1000 horizontal puller (Sutter Instrument Co.) were filled with the intracellular recording solution containing (in mM): 125 gluconic acid, 15 CsCl, 5 EGTA, 10 HEPES, 3 $MgCl_2$, 0.5 $CaCl_2$, and 2 ATP-Mg salt (pH adjusted to 7.2 with CsOH). The currents were filtered at 2 kHz with an eight-pole low-pass Bessel filter and digitized at 5 kHz with Digidata 1322A digitizers and pClamp 10 software (Molecular Devices). All recordings were performed at the indicated holding potentials (−60 or +40 mV). The dose-response inhibitory curves for 7-MEOTA and its derivatives were obtained using Equation (2).

$$I = 1/(1 + ([\text{compound}]/IC_{50})^h) \quad (2)$$

where IC_{50} is the concentration of tested compound that produces a 50% inhibition of agonist-evoked current, [compound] is the concentration of tested compounds, and h is the apparent Hill coefficient.

5.6. Quantitative structure activity relationship (QSAR)

Partial least squares projection to latent structures (PLS) analysis [58] was carried out for exploration of the relationships between the molecular and structural descriptors (X) and experimentally determined inhibitory activity towards NMDARs consisting of the GluN2A or GluN2B subunit respectively (y). Molecular and structure descriptors were calculated using the software tool MORDRED (Osaka University, Japan, https://mordred.phs.osaka-u.ac.jp/) [37]. PLS uses the correlation structure among the original variables and the variables are weighted together by the PLS weights to a small number of new latent variables. Auto-scaled and centered data were used in the PLS analysis. The importance of every descriptor in the model was accessed using the variable importance in the projection (VIP) parameter [59] and scores plots and loadings plots [60]. Validation was employed to assess the quality and validity of developed PLS models [61]. The validation was secured by a cross-validation routine and permutation testing. During the cross-validation procedure [59], parts of the y data are kept out of model development and predicted by the model, and compared with the actual values, providing cross-validated Q^2. This gives a more realistic value for the predictive power than the squared multiple regression coefficient R^2. In this study 1/7 of the compounds were deleted at each cross-validation round. In the permutation testing, the model is recalculated 999-times using a randomly re-ordered dependent variable. The statistical package SIMCA-P version 12 (Umetrics, Umea, Sweden) was used for statistical analyses.

5.7. Blood-brain barrier permeability prediction

The MDCK assay evaluates the ability of compounds to diffuse from the donor compartment through the MDCK's cell membrane into the acceptor compartment. The MDCK cells were seeded on a

polycarbonate membrane (area 1.12 cm^2) with 3 μm pores of the 12-well plates with 12 mm inserts. The tested compounds were dissolved in DMSO and then diluted with OptiMEM to reach the final concentrations (in the range 100 μM); the concentration of DMSO did not exceed 0.5% (v/v). 750 μL of the donor solution was added to the donor compartment (insert) and the same volume of OptiMEM was added into the acceptor. The concentration of the drug in both compartments was measured in triplicate by UV-VIS spectrophotometry after 1, 2, 4 and 6 h of incubation. The apparent permeability coefficient (Papp) was calculated from the concentrations ratio using equation (3). The tightness of the MDCK monolayer is assessed by the permeability of FITC (fluorescein isothiocyanate) at 0.4 mg/mL.

$$Papp = \frac{dC}{dt} * \frac{Vr}{(A * C0)} \quad (3)$$

where, A is area of the well/cell monolayer.

dC/dt is amount in the receiver compartment in given time
Vr is volume of the receiver compartment
C0 is the initial concentration of tested compounds

5.8. In vivo pharmacokinetic study

5.8.1. Animals

Adult male ICR mice (23–25 g) purchased from the Velaz breeding colony were used. The mice were housed in transparent plastic boxes in an air-conditioned animal room of Faculty of Military Health Sciences, Hradec Kralove, Czech Republic. The mice were kept under a 12:12 h light/dark cycle, with free access to food and water. All experiments were performed after a week-long acclimatization period. The experiments were conducted in accordance with the guidelines of the European Union directive 2010/63/EU and Act No246/1992 Coll. The handling of the experimental animals was done under the supervision of the Ethics Committee of the Faculty of Military Health Sciences, Czech Republic.

40 male mice (20–30 g, Velaz Ltd., Czech Republic) were injected i.p. with the tested compounds at a concentration of 5 mg kg^{-1} in 5% DMSO/saline mixture. Blood samples were collected under deep terminal anesthesia directly by cardiac puncture into heparinized 1.5 mL tubes at 15 and 60 min (3 animals per time interval). Four animals were used for zero time or blank control. The animals were perfused transcardially with saline solution (0.9% NaCl) for 5 min (1 mL/min) [62], and after the wash-out the skull was opened, and the brain carefully removed; brains were stored at −80 °C until analysis.

The brains were weighed PBS was added in the weight ratio 1:4. The brains were subsequently homogenised by T-25 Ultra Turrax disperser (IKA, Staufen, Germany), ultrasonicated by UP 50H needle homogeniser (Hielscher, Teltow, Germany), and stored at −80 °C prior to extraction.

5.8.2. Sample extraction

190 μL of brain homogenate or 95 μL of plasma was spiked with 10 μl (homogenate) or 5 μL (plasma) of internal standard (IS; 7-PhO-THA in methanol), so that the final concentration was 1 μM, the sample alkalized with 100 μL of 1 M sodium hydroxide, and 1000 μl of ethyl acetate was added. The samples were then vortexed (1200 RPM, Wizard Advanced IR Vortex Mixer, Velp Scientifica, Usmate, Italy) and centrifuged (12000 RPM, 5 min, Universal 320 R centrifuge, Hettich, Tuttlingen, Germany). 700 μL of supernatant was transferred to a microtube and evaporated to dryness in a CentriVap concentrator (Labconco Corporation, Kansas City, USA). Calibration samples were prepared by spiking 90 μl of blank plasma or 180 μL of blank brain homogenate with 5 μL (plasma) or 10 μL (homogenate) of the studied compounds dissolved in methanol (final concentrations range from 0.5 nM to 50 μM) and 5 or 10 μL of IS (7-PhO-THA in methanol, final concentration 1 μM), and then vortexing and extracting as above. Analysis samples were reconstituted in 100 μL of acetonitrile/water mixture 50/50 (v/v).

5.8.3. Liquid chromatography mass spectrometry

Solvents and other common chemicals were purchased from VWR (Stribrna Skalice, Czech Republic). Solvents for chromatographic procedures were supplied in LC-MS grade. 7-phenoxytacrine (7-PhO-THA) was synthesized *de novo* and used as the internal standard.

5.8.4. HPLC-MS instrumentation

The system used in this study was Dionex Ultimate 3000 UHPLC RS consisting of RS Pump, RS Column Compartment, RS Autosampler and Diode Array Detector controlled by Chromeleon (version 7.2.9. build 11323) software (Thermo Fisher Scientific, Germering, Germany) with Q Exactive Plus Orbitrap mass spectrometer with Thermo Xcalibur (version 3.1.66.10.) software (Thermo Fisher Scientific, Bremen, Germany). Detection was performed by mass spectrometry in positive mode. Settings of the heated electrospray source were: spray voltage 3.5 kV; capillary temperature 220 °C; sheath gas 55 arbitrary units; auxiliary gas 15 arbitrary units; spare gas 3 arbitrary units; probe heater temperature 220 °C; max spray current 100 μA; S-lens RF Level 50.

5.8.5. High-resolution mass spectrometry and purity

HRMS and sample purities were obtained by high performance liquid chromatography (HPLC) with the UV and mass spectrometry gradient method. A C18 column (Waters Atlantis dC18; 2.1 × 100mm; 3 μm, Waters, Wexford, Ireland) was used in this study. Mobile phase A was ultrapure water of ASTM I type (resistance 18.2 MΩ cm at 25 °C) prepared by Barnstead Smart2Pure 3 UV/UF apparatus (Thermo Fisher Scientific, Bremen, Germany) with 0.1% (v/v) formic acid; mobile phase B was acetonitrile with 0.1% (v/v) of formic acid. The flow was constant at 0.4 ml/min. The method started with 1 min of isocratic flow of 5% B, the concentration of B was then increased to 100% in 15 min and remained constant at 100% B for 1 min. The composition then reverted to 5% B and equilibrated for 5.5 min. The column was tempered to 27 °C. Samples were dissolved in methanol at a concentration of 1 mg/ml and sample injection was 1 μL. Purity was determined from UV spectra measured at wavelength 254 nm. HRMS was determined in total ion current spectra from the mass spectrometer in positive mode.

5.8.6. Pharmacokinetic study - HPLC-MS analysis

Compound levels in plasma and brain homogenate were measured by the above-mentioned UHPLC system with mass spectrometric detection. The results were obtained by gradient elution with reverse phase on a C18 column (Luna Omega Polar C18, 2.1 × 50 mm, 1.6 μm, Phenomenex, Torrance, California, USA) with SecurityGuard ULTRA Cartridge (C18, 2.1 μm, Phenomenex, Torrance, California, USA). The mobile phase was as above: water and acetonitrile with formic acid. Initially 5% B flowed for 0.2 min, and the composition then increased to 100% B in 3 min. After 0.5 min steady flow of 100% B the composition reverted to 5% B and equilibrated for 1.8 min. The total run time of the method was 5.5 min. Flow of the mobile phase was set to 0.5 ml/min and the column was tempered to 40 °C. The injection volume was 5 μL. Samples were analyzed by the previously-mentioned Orbitrap mass spectrometer in parallel reaction monitoring (PRM) positive

mode. Settings for each compound and internal standard are in Table 4. The calibration curves had 6 points, and for brain homogenates ranged from 5 nM to 1 μM and for plasma samples from 50 nM to 10 μM, and were linear in the measured range.

5.9. Behavioral experiments

5.9.1. Animals

Adult male Wistar rats (280–400 g, 2–3 months) purchased from the Velaz breeding colony were used. The rats were housed in pairs in transparent plastic boxes (50 × 25 × 25 cm) in an air-conditioned animal room of National Institute of Mental Health, Prague, Czech Republic. The rats were kept under a 12:12 h light/dark cycle, with free access to food and water. All experiments were performed in the light phase of the day after a week-long acclimatization period. The experiments were conducted in accordance with the guidelines of European Union directive 2010/63/EU and Act No. 246/1992 Coll. on the protection of animals against cruelty, and were approved by the Animal Care and Use Committee of the National Institute of Mental Health (reference number MZDR 51755/2018-4/OVZ).

5.9.2. Drugs

The rats were pseudo-randomly assigned to 16 experimental groups according to treatment: DMSO (control for the 1 mg/kg groups), **4** (1 mg/kg), **5** (1 mg/kg), **7** (1 mg/kg), **21** (1 mg/kg), **23** (1 mg/kg), **28** (1 mg/kg), DMSO (control for the 5 mg/kg groups), **4** (5 mg/kg), **5** (5 mg/kg), **7** (5 mg/kg), **21** (5 mg/kg), **23** (5 mg/kg), **28** (5 mg/kg), 7-MEOTA (5 mg/kg) and MK-801. The compounds were administered intraperitoneally 15 min before the behavioral testing, except for the comparator drugs MK-801 and 7-MEOTA, which were administered 30 min before the testing, based on our previous study [15]. For application of the compounds at a dose of 1 mg/kg, the compounds **5**, **7, 21, 23** and **28** were dissolved in a vehicle consisting of 5% dimethyl sulfoxide (DMSO) in physiological saline (drug concentration 1 mg/mL of vehicle) and administered at an injection volume of 1 mL/kg. For the dose of 5 mg/kg, the compounds **5**, **7, 21, 23**, **28** and 7-MEOTA were dissolved in the same vehicle (2 mg/mL of the vehicle) and then administered at an injection volume of 2.5 ml/kg. MK-801 ((+)-MK-801 hydrogen maleate, Sigma-Aldrich) was dissolved in the same vehicle and administered at an injection volume also of 2.5 mL/kg; the dose of MK-801 was 0.2 mg/kg for the open field and 0.3 mg/kg for the PPI experiment. Due to the suboptimal solubility of compound **4**, the solution vehicle for this contained the corresponding volume of distilled water instead of saline. Gentle heating was used during preparation of the solutions. Control animals (DMSO groups) received corresponding volumes of the vehicle (1 or 2.5 mL/kg).

5.9.3. Open field

The effect of the compounds on spontaneous locomotor activity in the open field was assessed. The experiments were performed in a black plastic square arena (80 × 80 cm), located in a separate room with defined light conditions (80 lx). The rat was placed in the center of the arena and then recorded for 10 min by a camera placed above the arena, connected to tracking software (EthoVision 14, Noldus, Netherlands). The arena was thoroughly cleaned between the animals. The dependent variable was the distance moved by the animal. The number of animals was 8 in the DMSO group (control for the 1 mg/kg groups; 1 mL/kg), 8 in MK-801 group and 6 in each other group.

5.9.4. Prepulse inhibition of acoustic startle response (PPI)

Next, the effect of the compounds on prepulse inhibition of acoustic startle response was tested. The experimental design was as previously described in Ref. [15].

The apparatus (SR-LAB, San Diego Instruments, CA, USA) consisted of a soundproof chamber, a piezoelectric accelerometer, a cylinder for animal placement and a loudspeaker. The animal was placed in a plexiglass cylinder (9 cm diameter, 17 cm length). The amplitudes of the startle response were detected by a piezoelectric accelerometer mounted below the cylinders and further analyzed. The background noise was set at 75 dB for the entire experiment. Habituation took place two days before the test session. Drug-free animals were exposed to 6 pulse stimuli alone (125 dB/40 ms) over white background noise after a 5-min acclimatization period. For the test sessions, the drug was administered to the animals 15 min before the test. After the 5-min acclimatization period the session began with 72 trials with variable inter-trial interval (ITI) of 4–20 s (mean ITI 12.27 s). Automatically randomized durations of ITIs ensured that the animal would not discern a pattern that could skew results. First, six pulse stimuli alone (125 dB/40 ms) were presented. Subsequently, 60 trials were presented in pseudo-random order: A) pulse alone 40 ms 125 dB; B) prepulse-pulse: 20 ms of two different intensities of prepulses 83 dB or 91 dB with a variable (30, 60 or 120 ms) inter-stimulus interval followed by a 125 dB pulse of 40 ms duration; C) no stimulus (60 ms). Finally, six pulse stimuli alone (125 dB/40 ms) were delivered again. PPI was calculated as the difference between the average values of the single pulse and prepulse-pulse trials and it was expressed as a percentage of PPI:

100-(mean response to prepulse-pulse trials/mean startle response to pulse alone trials)*100

The number of animals was 8 in the groups DMSO (control for the 5 mg/kg groups; 2.5 mL/kg), **28** 1 mg/kg, and **21** 5 mg/kg; and 6 animals in other groups.

5.9.5. Statistics

The data from open field (distance moved) and PPI (% PPI) were subjected to the following analyses in GraphPad Prism 8 (San Diego, USA). First, the data from each group was tested for outliers using Grubb's test. The tests detected two outliers in distance moved in

Table 4
Parameters for HPLC-MS analysis.

Compound	Parent ion	Normalised collision energy	Selected product ion	t_R (min)
4	263.01816	70	216.08891	2.70
5	277.03339	70	249.00175	2.80
7	219.06799	70	167.07271	2.65
21	247.09894	70	206.05989	2.85
23	213.13795	70	185,10680	2.75
28	215.11729	70	172.09897	2.65
7-PhO-THA (IS)	291.14853	70	230.10452	3.15

t_R, retention time; IS, internal standard.

open field (in groups **21** 5 mg/kg and 7-MEOTA 5 mg/kg) and one in % PPI (**21** 5 mg/kg). The outliers were excluded from further analyses. The data was evaluated using ANOVA (the effects of the drugs at a dose of 1 and 5 mg/kg analyzed separately), followed by Bonferroni's multiple comparisons test when appropriate. The data from open field (5 mg/kg doses) did not meet the assumption of homogeneity of variances for ANOVA (Bartlett's test), therefore Brown-Forsythe ANOVA with Dunnett's T3 multiple comparison test was used. The differences were considered significant at $P < 0.05$. The graphs show group means + S.E.M.; asterisks denote significant difference from the corresponding control group (DMSO): *$P < 0.05$, **$P < 0.01$, ***$P < 0.001$ and ****$P < 0.0001$.

Declaration of interest

The authors declare that they have no known competing financial interests or personal relationships that could have appeared to influence the work reported in this paper.

Declaration of competing interest

The authors declare that they have no known competing financial interests or personal relationships that could have appeared to influence the work reported in this paper.

Acknowledgements

Authors would like to thank the grant of Czech Science Foundation (no. 20-12047S, M.H.) to project TACR (no. TO01000078 O.S.) and European Regional Development Fund: Project "PharmaBrain" (no. CZ.CZ.02.1.01/0.0/0.0/16_025/0007444; K.V.) and Charles University (SVV 260547; M.N.). The authors are grateful to Jana Hatlapatkova for animal handling and Ian McColl MD, PhD for assistance with the manuscript.

Appendix A. Supplementary data

Supplementary data to this article can be found online at https://doi.org/10.1016/j.ejmech.2021.113434.

References

[1] R. Morphy, C. Kay, Z. Rankovic, From magic bullets to designed multiple ligands, Drug Discov. Today 9 (2004) 641–651.
[2] E. Proschak, H. Stark, D. Merk, Polypharmacology by design: a medicinal chemist's perspective on multitargeting compounds, J. Med. Chem. 62 (2018) 420–444.
[3] C. Albertini, A. Salerno, P. de Sena Murteira Pinheiro, M.L. Bolognesi, From combinations to multitarget-directed ligands: a continuum in Alzheimer's disease polypharmacology, Med. Res. Rev. (2020), https://doi.org/10.1002/med.21699.
[4] R. Morphy, Z. Rankovic, Designed multiple ligands. An emerging drug discovery paradigm, J. Med. Chem. 48 (2005) 6523–6543.
[5] O. Benek, J. Korabecny, O. Soukup, A perspective on multi-target drugs for alzheimer's disease, Trends Pharmacol. Sci. 41 (2020) 434–445.
[6] A. Calhoun, C. King, R. Khoury, G.T. Grossberg, An evaluation of memantine ER+ donepezil for the treatment of Alzheimer's disease, Expet Opin. Pharmacother. 19 (2018) 1711–1717.
[7] E. Simoni, S. Daniele, G. Bottegoni, D. Pizzirani, M.L. Trincavelli, L. Goldoni, G. Tarozzo, A. Reggiani, C. Martini, D. Piomelli, Combining galantamine and memantine in multitargeted, new chemical entities potentially useful in Alzheimer's disease, J. Med. Chem. 55 (2012) 9708–9721.
[8] A.M. Reggiani, E. Simoni, R. Caporaso, J. Meunier, E. Keller, T. Maurice, A. Minarini, M. Rosini, A. Cavalli, In vivo characterization of ARN14140, a memantine/galantamine-based multi-target compound for Alzheimer's disease, Sci. Rep. 6 (2016) 1–11.
[9] Z. Gazova, O. Soukup, V. Sepsova, K. Siposova, L. Drtinova, P. Jost, K. Spilovska, J. Korabecny, E. Nepovimova, D. Fedunova, M. Horak, M. Kaniakova, Z.J. Wang, A.K. Hamouda, K. Kuca, Multi-target-directed therapeutic potential of 7-methoxytacrine-adamantylamine heterodimers in the Alzheimer's disease treatment, Biochim. Biophys. Acta (BBA) - Mol. Basis Dis. 1863 (2017) 607–619.
[10] K. Spilovska, J. Korabecny, J. Kral, A. Horova, K. Musilek, O. Soukup, L. Drtinova, Z. Gazova, K. Siposova, K. Kuca, 7-Methoxytacrine-Adamantylamine heterodimers as cholinesterase inhibitors in alzheimer's disease treatment — synthesis, biological evaluation and molecular modeling studies, Molecules (2013) 2397–2418.
[11] M. Kaniakova, E. Nepovimova, L. Kleteckova, K. Skrenkova, K. Holubova, Z. Chrienova, V. Hepnarova, T. Kucera, T. Kobrlova, K. Vales, Combination of memantine and 6-chlorotacrine as novel multi-target compound against Alzheimer's disease, Curr. Alzheimer Res. 16 (2019) 821–833.
[12] J.-M. Zhang, G.-Y. Hu, Huperzine A, a nootropic alkaloid, inhibits N-methyl-D-aspartate-induced current in rat dissociated hippocampal neurons, Neuroscience 105 (2001) 663–669.
[13] Y.W. Liu, C.Y. Li, J.L. Luo, W.M. Li, H.J. Fu, Y.Z. Lao, L.J. Liu, Y.P. Pang, D.C. Chang, Z.W. Li, R.W. Peoples, Y.X. Ai, Y.F. Han, Bis(7)-tacrine prevents glutamate-induced excitotoxicity more potently than memantine by selectively inhibiting NMDA receptors, Biochem. Biophys. Res. Commun. 369 (2008) 1007–1011.
[14] M. Horak, K. Holubova, E. Nepovimova, J. Krusek, M. Kaniakova, J. Korabecny, L. Vyklicky, K. Kuca, A. Stuchlik, J. Ricny, K. Vales, O. Soukup, The pharmacology of tacrine at N-methyl-d-aspartate receptors, Prog. Neuro-Psychopharmacol. Biol. Psychiatry 75 (2017) 54–62.
[15] M. Kaniakova, L. Kleteckova, K. Lichnerova, K. Holubova, K. Skrenkova, M. Korinek, J. Krusek, T. Smejkalova, J. Korabecny, K. Vales, O. Soukup, M. Horak, 7-Methoxyderivative of tacrine is a 'foot-in-the-door'open-channel blocker of GluN1/GluN2 and GluN1/GluN3 NMDA receptors with neuroprotective activity in vivo, Neuropharmacology 140 (2018) 217–232.
[16] E.S. Vizi, M. Kisfali, T. Lőrincz, Role of nonsynaptic GluN2B-containing NMDA receptors in excitotoxicity: evidence that fluoxetine selectively inhibits these receptors and may have neuroprotective effects, Brain Res. Bull. 93 (2013) 32–38.
[17] M.C. Regan, Z. Zhu, H. Yuan, S.J. Myers, D.S. Menaldino, Y.A. Tahirovic, D.C. Liotta, S.F. Traynelis, H. Furukawa, Structural elements of a pH-sensitive inhibitor binding site in NMDA receptors, Nat. Commun. 10 (2019) 321.
[18] H. Chaffey, P.L. Chazot, NMDA receptor subtypes: structure, function and therapeutics, Curr. Anaesth. Crit. Care 19 (2008) 183–201.
[19] C.A. Lipinski, F. Lombardo, B.W. Dominy, P.J. Feeney, Experimental and computational approaches to estimate solubility and permeability in drug discovery and development settings, Adv. Drug Deliv. Rev. 23 (1997) 3–25.
[20] M. Gupta, H.J. Lee, C.J. Barden, D.F. Weaver, The blood–brain barrier (BBB) score, J. Med. Chem. 62 (2019) 9824–9836.
[21] F.J. Pérez-Areales, A.L. Turcu, M. Barniol-Xicota, C. Pont, D. Pivetta, A. Espargaró, M. Bartolini, A. De Simone, V. Andrisano, B. Pérez, A novel class of multitarget anti-Alzheimer benzohomoadamantane–chlorotacrine hybrids modulating cholinesterases and glutamate NMDA receptors, Eur. J. Med. Chem. 180 (2019) 613–626.
[22] C. Saturnino, D. Iacopetta, M.S. Sinicropi, C. Rosano, A. Caruso, A. Caporale, N. Marra, B. Marengo, M.A. Pronzato, O.I. Parisi, N-alkyl carbazole derivatives as new tools for Alzheimer's disease: preliminary studies, Molecules 19 (2014) 9307–9317.
[23] G. Marotta, F. Basagni, M. Rosini, A. Minarini, Memantine derivatives as multitarget agents in alzheimer's disease, Molecules 25 (2020) 4005.
[24] J. Patocka, D. Jun, K. Kuca, Possible role of hydroxylated metabolites of tacrine in drug toxicity and therapy of Alzheimer's disease, Curr. Drug Metabol. 9 (2008) 332–335.
[25] M. Recanatini, A. Cavalli, F. Belluti, L. Piazzi, A. Rampa, A. Bisi, S. Gobbi, P. Valenti, V. Andrisano, M. Bartolini, SAR of 9-amino-1, 2, 3, 4-tetrahydroacridine-based acetylcholinesterase inhibitors: synthesis, enzyme inhibitory activity, QSAR, and structure-based CoMFA of tacrine analogues, J. Med. Chem. 43 (2000) 2007–2018.
[26] D. dos Santos Pisoni, J.S. da Costa, D. Gamba, C.L. Petzhold, A.C. de Amorim Borges, M.A. Ceschi, P. Lunardi, C.A.S. Gonçalves, Synthesis and AChE inhibitory activity of new chiral tetrahydroacridine analogues from terpenic cyclanones, Eur. J. Med. Chem. 45 (2010) 526–535.
[27] K.Y. Wong, A.G. Mercader, L.M. Saavedra, B. Honarparvar, G.P. Romanelli, P.R. Duchowicz, QSAR analysis on tacrine-related acetylcholinesterase inhibitors, J. Biomed. Sci. 21 (2014) 84.
[28] M. Jung, J. Tak, Y. Lee, Y. Jung, Quantitative structure–activity relationship (QSAR) of tacrine derivatives against acetylcholinesterase (AChE) activity using variable selections, Bioorg. Med. Chem. Lett 17 (2007) 1082–1090.
[29] H. Boulebd, L. Ismaili, H. Martin, A. Bonet, M. Chioua, J. Marco Contelles, A. Belfaitah, New (benz) imidazolopyridino tacrines as nonhepatotoxic, cholinesterase inhibitors for Alzheimer disease, Future Med. Chem. 9 (2017) 723–729.
[30] L. Gorecki, L. Junova, T. Kucera, V. Hepnarova, L. Prchal, T. Kobrlova, L. Muckova, O. Soukup, J. Korabecny, Tacroximes: novel unique compounds for the recovery of organophosphorus-inhibited acetylcholinesterase, Future Med. Chem. 11 (2019) 2625–2634.
[31] G.L. Ellman, K.D. Courtney, V. Andres, R.M. Featherstone, A new and rapid colorimetric determination of acetylcholinesterase activity, Biochem. Pharmacol. 7 (1961) 88. &.
[32] N.H. Greig, D.K. Lahiri, K. Sambamurti, Butyrylcholinesterase: an important new target in Alzheimer's disease therapy, Int. Psychogeriatr. 14 (2002) 77.
[33] O. Lockridge, Review of human butyrylcholinesterase structure, function, genetic variants, history of use in the clinic, and potential therapeutic uses, Pharmacol. Ther. 148 (2015) 34–46.

[34] J. Korabecny, K. Musilek, O. Holas, J. Binder, F. Zemek, J. Marek, M. Pohanka, V. Opletalova, V. Dohnal, K. Kuca, Synthesis and in vitro evaluation of N-alkyl-7-methoxytacrine hydrochlorides as potential cholinesterase inhibitors in Alzheimer disease, Bioorg. Med. Chem. Lett 20 (2010) 6093–6095.
[35] S.F. Traynelis, L.P. Wollmuth, C.J. McBain, F.S. Menniti, K.M. Vance, K.K. Ogden, K.B. Hansen, H. Yuan, S.J. Myers, R. Dingledine, Glutamate receptor ion channels: structure, regulation, and function, Pharmacol. Rev. 62 (2010) 405–496.
[36] J. Konecny, A. Misiachna, M. Hrabinova, L. Pulkrabkova, M. Benkova, L. Prchal, T. Kucera, T. Kobrlova, V. Finger, M. Kolcheva, Pursuing the complexity of alzheimer's disease: discovery of fluoren-9-amines as selective butyrylcholinesterase inhibitors and N-Methyl-d-Aspartate receptor antagonists, Biomolecules 11 (2021) 3.
[37] H. Moriwaki, Y.-S. Tian, N. Kawashita, T. Takagi, Mordred: a molecular descriptor calculator, J. Cheminf. 10 (2018) 4.
[38] P. Paoletti, C. Bellone, Q. Zhou, NMDA receptor subunit diversity: impact on receptor properties, synaptic plasticity and disease, Nat. Rev. Neurosci. 14 (2013) 383–400.
[39] O. Soukup, J. Korabecny, D. Malinak, E. Nepovimova, N. Pham, K. Musilek, M. Hrabinova, V. Hepnarova, R. Dolezal, P. Pavek, In Vitro and in Silico Evaluation of Non-quaternary Reactivators of AChE as Antidotes of Organophosphorus Poisoning-A New Hope or a Blind Alley?, Medicinal Chemistry, Shariqah (United Arab Emirates)), 2018.
[40] P. Garberg, M. Ball, N. Borg, R. Cecchelli, L. Fenart, R. Hurst, T. Lindmark, A. Mabondzo, J. Nilsson, T. Raub, In vitro models for the blood–brain barrier, Toxicol. Vitro 19 (2005) 299–334.
[41] J. Zdarova Karasova, O. Soukup, J. Korabecny, M. Hroch, M. Krejciova, M. Hrabinova, J. Misik, L. Novotny, V. Hepnarova, K. Kuca, Tacrine and its 7-methoxy derivate; time-change concentration in plasma and brain tissue and basic toxicological profile in rats, Drug Chem. Toxicol. (2019) 1–8.
[42] W.P. McNally, W.F. Pool, M.W. Sinz, P. Dehart, D.F. Ortwine, C.C. Huang, T. Chang, T.F. Woolf, Distribution of tacrine and metabolites in rat brain and plasma after single-and multiple-dose regimens. Evidence for accumulation of tacrine in brain tissue, Drug Metabol. Dispos. 24 (1996) 628–633.
[43] J. Grotta, W. Clark, B. Coull, L.C. Pettigrew, B. Mackay, L.B. Goldstein, I. Meissner, D. Murphy, L. LaRue, Safety and tolerability of the glutamate antagonist CGS 19755 (selfotel) in patients with acute ischemic stroke: results of a phase IIa randomized trial, Stroke 26 (1995) 602–605.
[44] J.H. Krystal, L.P. Karper, J.P. Seibyl, G.K. Freeman, R. Delaney, J.D. Bremner, G.R. Heninger, M.B. Bowers, D.S. Charney, Subanesthetic effects of the noncompetitive NMDA antagonist, ketamine, in humans: psychotomimetic, perceptual, cognitive, and neuroendocrine responses, Arch. Gen. Psychiatr. 51 (1994) 199–214.
[45] K.W. Muir, K.R. Lees, Clinical experience with excitatory amino acid antagonist drugs, Stroke 26 (1995) 503–513.
[46] T. Bast, W. Zhang, J. Feldon, I.M. White, Effects of MK801 and neuroleptics on prepulse inhibition: re-examination in two strains of rats, Pharmacol. Biochem. Behav. 67 (2000) 647–658.
[47] M. Chatterjee, S. Ganguly, M. Srivastava, G. Palit, Effect of 'chronic'versus 'acute'ketamine administration and its 'withdrawal'effect on behavioural alterations in mice: implications for experimental psychosis, Behav. Brain Res. 216 (2011) 247–254.
[48] D. Manahan-Vaughan, D. von Haebler, C. Winter, G. Juckel, U. Heinemann, A single application of MK801 causes symptoms of acute psychosis, deficits in spatial memory, and impairment of synaptic plasticity in rats, Hippocampus 18 (2008) 125–134.
[49] D. Carriero, G. Outslay, A. Mayorga, J. Aberman, G. Gianutsos, J.D. Salamone, Motor dysfunction produced by tacrine administration in rats, Pharmacol. Biochem. Behav. 58 (1997) 851–858.
[50] J.G. Csernansky, M. Martin, R. Shah, A. Bertchume, J. Colvin, H. Dong, Cholinesterase inhibitors ameliorate behavioral deficits induced by MK-801 in mice, Neuropsychopharmacology 30 (2005) 2135.
[51] S.-Y. Pan, Z.-L. Yu, C.-J. Xiang, H. Dong, H.-Y. Fang, K.-M. Ko, Comparison studies of tacrine and bis (7)-tacrine on the suppression of scopolamine-induced behavioral changes and inhibition of acetylcholinesterase in mice, Pharmacology 83 (2009) 294–300.
[52] H. Wang, P.R. Carlier, W.L. Ho, D.C. Wu, N.T.K. Lee, C.P. Li, Y.P. Pang, Y.F. Han, Effects of bis (7)-tacrine, a novel anti-Alzheimer's agent, on rat brain AChE, Neuroreport 10 (1999) 789–793.
[53] D.R. Liston, J.A. Nielsen, A. Villalobos, D. Chapin, S.B. Jones, S.T. Hubbard, I.A. Shalaby, A. Ramirez, D. Nason, W.F. White, Pharmacology of selective acetylcholinesterase inhibitors: implications for use in Alzheimer's disease, Eur. J. Pharmacol. 486 (2004) 9–17.
[54] K. Chalupova, J. Korabecny, M. Bartolini, B. Monti, D. Lamba, R. Caliandro, A. Pesaresi, X. Brazzolotto, A.J. Gastellier, F. Nachon, J. Pejchal, M. Jarosova, V. Hepnarova, D. Jun, M. Hrabinova, R. Dolezal, J.Z. Karasova, M. Mzik, Z. Kristofikova, J. Misik, L. Muckova, P. Jost, O. Soukup, M. Benkova, V. Setnicka, L. Habartova, M. Chvojkova, L. Kleteckova, K. Vales, E. Mezeiova, E. Uliassi, M. Valis, E. Nepovimova, M.L. Bolognesi, K. Kuca, Novel tacrine-tryptophan hybrids: multi-target directed ligands as potential treatment for Alzheimer's disease, Eur. J. Med. Chem. 168 (2019) 491–514.
[55] K. Skrenkova, J.-m. Song, S. Kortus, M. Kolcheva, J. Netolicky, K. Hemelikova, M. Kaniakova, B.H. Krausova, T. Kucera, J. Korabecny, The pathogenic S688Y mutation in the ligand-binding domain of the GluN1 subunit regulates the properties of NMDA receptors, Sci. Rep. 10 (2020) 1–15.
[56] M. Kaniakova, K. Lichnerova, L. Vyklicky, M. Horak, Single amino acid residue in the M4 domain of GluN1 subunit regulates the surface delivery of NMDA receptors, J. Neurochem. 123 (2012) 385–395.
[57] M. Kaniakova, J. Korabecny, K. Holubova, L. Kleteckova, M. Chvojkova, K. Hakenova, L. Prchal, M. Novak, R. Dolezal, V. Hepnarova, 7-phenoxytacrine is a dually acting drug with neuroprotective efficacy in vivo, Biochem. Pharmacol. (2021) 114460.
[58] A. Höskuldsson, PLS regression methods, J. Chemom. 2 (1988) 211–228.
[59] S. Wold, E. Johansson, M. Cocchi, PLS: Partial Least Squares Projections to Latent Structures, 1993.
[60] S. Wold, W.J. Dunn III, Multivariate quantitative structure-activity relationships (QSAR): conditions for their applicability, J. Chem. Inf. Comput. Sci. 23 (1983) 6–13.
[61] S. Wold, Validation of QSAR's, Quant. Struct.-Act. Relat. 10 (1991) 191–193.
[62] J.Z. Karasova, V. Hepnarova, R. Andrys, M. Lisa, P. Jost, L. Muckova, J. Pejchal, D. Herman, D. Jun, J. Kassa, Encapsulation of oxime K027 into cucurbit [7] uril: in vivo evaluation of safety, absorption, brain distribution and reactivation effectiveness, Toxicol. Lett. 320 (2020) 64–72.